KAHRAMAMARAŞ SÜTÇÜ İMAM
ÜNİVERSİTESİ

e-ISSN 1309-1751

Mühendislik Bilimleri Dergisi
Journal of Engineering Sciences

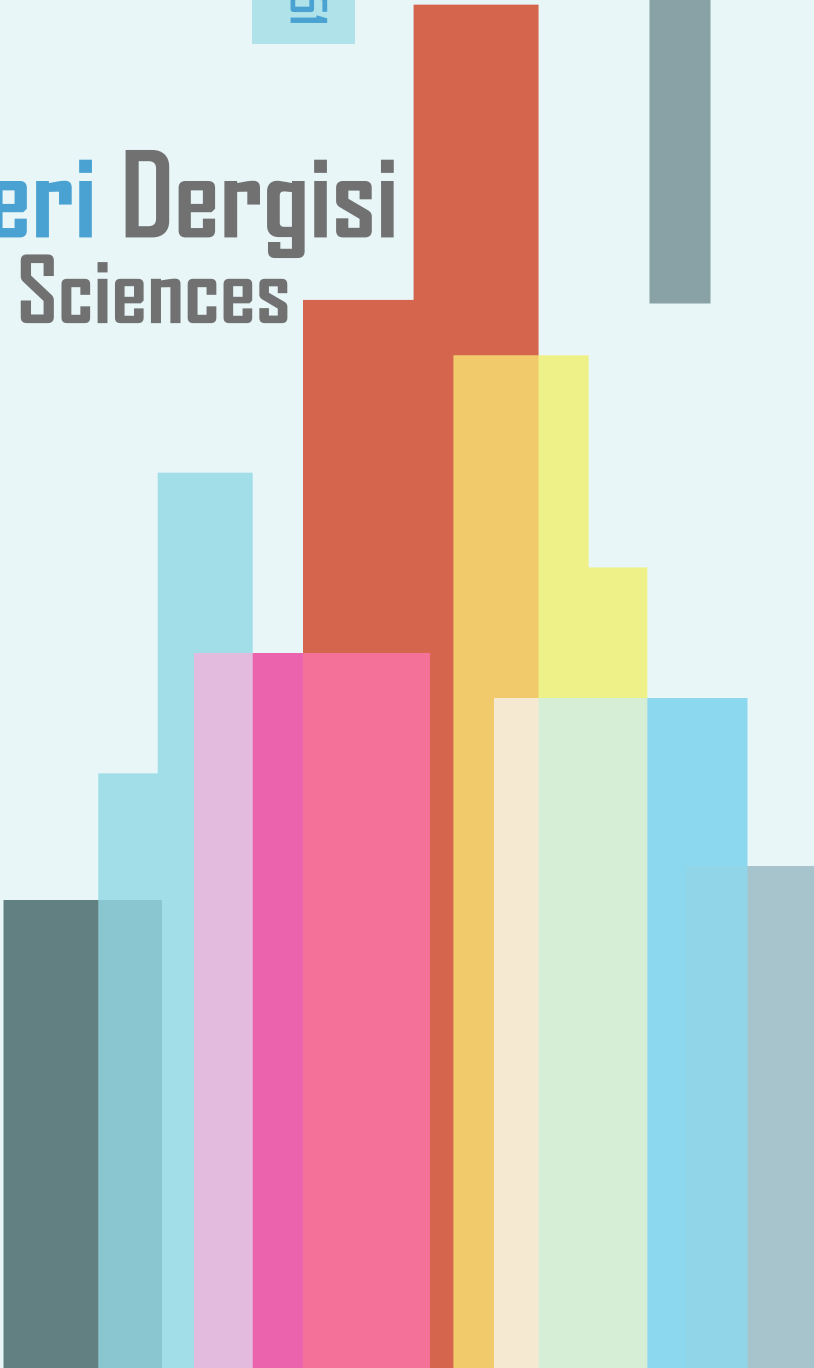

2019
ÖZEL SAYI / SPECIAL ISSUE
CILT / VOLUME : 22

e-ISSN 1309-1751

Kahramanmaraş Sütçü İmam University
Journal of Engineering Sciences

Yazışma Adresi / Corresponding Address

**Kahramanmaraş Sütçü İmam Üniversitesi
Mühendislik Bilimleri Dergisi
46050, Onikişubat/Kahramanmaraş
TÜRKİYE**

E - Posta

jes@ksu.edu.tr

Web

http://jes.ksu.edu.tr/

**Bu dergi hakemli olup yılda 4 kez yayınlanır.
This journal is peer - reviewed and published 4 issues per year.**

Cilt / Volume : 22 Özel Sayı / Special Issue Yıl / Year : 2019

e-ISSN 1309-1751

Kahramanmaraş Sütçü İmam University
Journal of Engineering Sciences

Sahibi / Owner

Prof.Dr. Niyazi CAN
KSU Rector

Baş Editör / Editor in Chief

Prof. Dr. Hüseyin TEMİZ
htemiz@ksu.edu.tr

Baş Editör Yardımcısı / Vice Editor in Chief

Assist. Prof. Dr. Ö. Fatih KEÇECİOĞLU
fkececioglu@ksu.edu.tr

Editörler / Editors

Prof. Dr. Ahmet Serdar YILMAZ
Electrical and Electronics Eng.
asyilmaz@ksu.edu.tr
Prof. Dr. Ahmet KAYA
Mechanical Eng.
kaya38@ksu.edu.tr
Assist. Prof. Dr. Hasan BADEM
Computer Eng.
hbadem@ksu.edu.tr
Prof.Dr. Özlem TURGAY
Food Eng.
ozlem@ksu.edu.tr

Prof. Dr. Ahmet ALKAN
Electrical and Electronics Eng.
aalkan@ksu.edu.tr
Assist. Prof. Dr. Beril ÖZÇELİK
Mechanical Eng.
bozcelik@ksu.edu.tr
Assist.Prof.Dr. Yakup CUCİ
Environmental Eng.
cuci@ksu.edu.tr
Prof. Dr. Fatih MENGELOĞLU
Landscape Arc.
fmengelo@ksu.edu.tr

Prof. Dr. Mehmet ÜNSAL
Civil Eng.
munsal@ksu.edu.tr
Assoc. Prof.Dr. Tamer RIZAOĞLU
Geological Eng.
tamer@ksu.edu.tr
Assoc.Prof.Dr. Suat ÇETİNER
Textile Eng.
suatcetiner@ksu.edu.tr
Lecturer Ahmet GANİ
Technical Editor
agani@ksu.edu.tr

Danışma Kurulu / Advisory Board

Prof. Dr. Cetin Kaya KOC
Dep. of Computer Eng. Univ Of
Cal. Santa Barbara. USA
koc@cs.ucsb.edu

Prof. Dr. Ayhan ÖZDEMİR
Dep. of Elect. & Elcn Eng.
Sakarya Univ. Sakarya,
TURKEY
aozdemir@sakarya.edu.tr

Prof. Dr. Hüseyin AKILLI
Dep. of Mechanical Eng. ÇU Univ.
Adana, TURKEY
hakilli@cu.edu.tr

Prof. Dr. Mehmet KORÜREK
Dep. Of Elcn & Comm Eng. İTU
Univ. İstanbul. TURKEY
korurek@itu.edu.tr

Prof. Dr. Yasemin KORKMAZ
Dep. of Textile Eng.
KSU Univ. TURKEY
ykorkmaz@ksu.edu.tr

Prof. Dr. Ahmet PINARBAŞI
Dep. of Mechanical Eng.
Alanya Alaaddin Keykubat
Univ. Antalya, TURKEY
apinarbasi@alanya.edu.tr

Prof. Dr. S. Serhat ŞEKER
Dep. Of Elect. Eng.
İTU Univ. İstanbul. TURKEY
sekers@itu.edu.tr

Prof. Dr. Şerafettin EREL
Dep. of Elect. & Elcn Eng.
YBU Univ. Ankara, TURKEY
serel@ybu.edu.tr

Assoc. Prof. Dr. Mustafa ONAT
Dep. of Computer Eng. Marmara
Univ. İstan. TURKEY
monat@marmara.edu.tr

Prof. Dr. Eyüp DEBİK
Dep. of Environmential Eng.
Yıldız Technical Univ. İstanbul.
TURKEY
debik@yildiz.edu.tr

Prof. Dr. Fan MIZI
Dep. of Civil Eng.
Brunel Univ.Uxbridge,UK
mizi.fan@brunel.ac.uk

Prof. Dr. A. Fevzi BABA
Dep. of Elect. & Elcn. Eng.
Marmara Univ. İst., TURKEY
fbaba@marmara.edu.tr

Dr. Amit CHAUDHRY
Dep. of Microelectronics Panjab
Univ, Chandigarh , India
amit_chaudhry01@yahoo.com

Assist. Prof. Dr. Nazmi EKREN
Dep. of Elect. & Elcn. Eng.
Marmara Univ. İstanbul,
TURKEY
nekren@marmara.edu.tr

Prof. Dr. Mustafa YAZICI
Dep. of Physics Education. KSU
Univ. K.Maras. TURKEY
yazici@ksu.edu.tr

Prof. Dr. Selim AY
Dep. Of Elect. Eng.
YTU Univ. İstanbul. TURKEY
selimay@yildiz.edu.tr

Prof. Dr. Musa GÖĞEBAKAN
Dep. of Physics KSU Univ.
K.Maras, TURKEY
gogebakan@ksu.edu.tr

Prof. Dr. Murat PALA
Dep. of Civil Eng. Adıyaman Univ.
Adıyaman. TURKEY
pala@adiyaman.edu.tr

Prof. Dr. İ.Taner OKUMUŞ
Dep. of Computer Eng
KSU Univ. K.Maraş. TURKEY
iokumus@ksu.edu.tr

Cilt / Volume : 22 Özel Sayı / Special Issue Yıl / Year : 2019

e-ISSN 1309-1751

Kahramanmaraş Sütçü İmam University
Journal of Engineering Sciences

İÇİNDEKİLER

Cilt / Volume : 22 Özel Sayı / Special Issue Yıl / Year : 2019

e-ISSN 1309-1751

Kahramanmaraş Sütçü İmam University
Journal of Engineering Sciences

İÇİNDEKİLER

Cilt / Volume : 22 Özel Sayı / Special Issue Yıl / Year : 2019

KSÜ Mühendislik Bilimleri Dergisi, 22, Özel Sayı, 2019 KSU J Eng Sci, 22, Special Issue, 2019
Uluslararası İleri Mühendislik Teknolojileri Sempozyumu (ISADET) Özel Sayısı
International Symposium on Advanced Engineering Technologies (ISADET) Symposium Special Issue
Araştırma Makalesi Research Article

Kahramanmaras Sutcu Imam University
Journal of Engineering Sciences

Geliş Tarihi : 18.07.2019 Received Date : 18.07.2019
Kabul Tarihi : 14.10.2019 Accepted Date : 14.10.2019

FORMATION AND COMPARISON OF RARE EARTH ELEMENT (REE) GEOCHEMISTRY OF MALATYA FLUORITE DEPOSITS

MALATYA FLORİT YATAKLARININ OLUŞUMU VE NADİR TOPRAK ELEMENT (NTE) JEOKİMYASININ KARŞILAŞTIRILMASI

Yusuf URAS [1*], *Cihan YALÇIN* [2], *Merve PAKSOY* [1]

[1] Kahramanmaraş Sütçü İmam Üniversitesi, Jeoloji Mühendisliği Bölümü, Kahramanmaraş, Türkiye
[2]Sanayi ve Teknoloji Bakanlığı, Burdur İl Müdürlüğü, Burdur, Türkiye

*Sorumlu Yazar / Corresponding Author: yuras@ksu.edu.tr

ABSTRACT

The fluorite deposits in Malatya (Turkey) region are observed in Yeşilyurt and Kuluncak districts. Yesilyurt fluorites are observed as vein type along the plane of unconformity between metamorphic rocks on hydrothermal phase. Kuluncak fluorites are observed in the contacts of alkaline syenites and marbles as vein type which the mineralization occured in the pegmatitic phase as shown on Tb/La-Tb/Ca diagram. Yeşilyurt fluorites are seen in purple, dark purple and blackish colors and Kuluncak is blue to purple. When the geochemical characteristics of the Malatya fluorites are taken into comparison, the Yeşilyurt region has 12.2-35.8% F values and Kuluncak has 15, 03-25, 42%. The REE contents of Kuluncak fluorites are richer than Yeşilyurt fluorites as well as in Sr contents. In the $(La/Yb)_N$-$(Tb/Yb)_N$ diagram the Yeşilyurt fall into the field of New Mexico, however the Kuluncak fluorites fall into the field of Akdağmadeni. The fluorite deposites are compared on $(Eu/Eu^*)_n$–$(La/Yb)_n$ and Sc–ΣREE, $(Tb/Yb)_n$–$(La/Yb)_n$ diagrams. The Yeşilyurt fluorites display a distribution similar to the Buyukkizilcik (Kahramanmaras) fluorites but Kuluncak fluorites spread in large areas. The normalized-REE compositions of the Malatya fluorites exhibit enrichment in LREEs compared to the HREEs. In the light of all the data obtained, it can be concluded that the geochemical properties and formation of Malatya fluorites are different from each other.

Keywords: Fluorite, Hydrothermal, Pegmatitic phase, REE, Malatya.

ÖZET

Malatya’daki (Türkiye) florit yatakları Yeşilyurt ve Kuluncak bölgelerinde bulunmaktadır. Yeşilyurt floritleri, hidrotermal evrede metamorfik kayaçlar arasındaki uyumsuzluk düzlemi boyunca damar tipi olarak görülmektedir. Kuluncak floritleri ise Tb/La-Tb/Ca diyagramında gösterildiği gibi, pegmatitik evrede oluşmakta ve alkali siyenit ve mermer dokanağında damar tipi şeklinde görülmektedir. Yeşilyurt floritleri mor, koyu mor ve siyahımsı renklerde, Kuluncak floritleri ise maviden mora kadar farklı renklerde görülmektedir. Malatya bölgesinde farklı lokasyonlarda gözlenen floritlerin jeokimyasal özellikleri karşılaştırıldığında; Yeşilyurt bölgesindeki F % 21,2-35,8 değerlerinde; Kuluncak bölgesinde ise F % 15,03- 25,42 arasındadır. Kuluncak floritlerinin nadir toprak element (NTE) ve Sr içeriği, Yeşilyurt floritlerininkinden daha zengindir. $(La/Yb)_N$-$(Tb/Yb)_N$ diyagramlarında Yeşilyurt floritleri New Mexico alanına düşerken, Kuluncak floritleri Akdağmadeni floritleri ile aynı alandadır. Florit yataklarının $(Eu/Eu^*)_n$–$(La/Yb)_n$ ve Sc–ΣNTE, $(Tb/Yb)_n$–$(La/Yb)_n$ diyagramlarında karşılaştırmaları yapılmıştır. Yeşilyurt floritleri Büyükkızılcık (Kahramanmaraş) floritlerine benzer bir dağılım sergilerken, Kuluncak floritleri geniş alanlara yayılmıştır. Malatya floritlerinin normalize edilmiş Nadir Toprak Element (NTE) bileşimlerine göre, hafif nadir toprak elementlerinin ağır nadir toprak elementlerine göre zenginleştiği görülmektedir. Elde edilen tüm veriler ışığında Malatya floritlerinin Jeokimyasal özellikleri ve oluşumlarının birbirlerinden farklı olduğu sonucuna varılabilir.

Anahtar Kelimeler: Florit, Hidrotermal, Pegmatitik evre, NTE, Malatya.

INTRODUCTION

Ketin (1966) classified the orogenic belts of Turkey into 4 different classes as Pontides, Anatolides, Taurides and Border folds. In Malatya (Figure 1) where is the tectonic location on Eastern Taurus Orogenic region, Doğanşehir, Malatya, Doğanyol and Pütürge consists of Precambrian-Paleozoic and Mesozoic aged gneiss, amphibolite, marble and schists (MTA, 2009). Miocene-Pliocene aged volcanic rocks are located in the north of Hekimhan-Arguvan (Atabey, 2015). Upper Cretaceous ophiolites, Cretaceous limestones, Eocene volcanoclastic and sedimentary rocks and Miocene-Pliocene lacustrine, evaporitic sedimentary rocks are located in different locations (Perinçek and Kozlu, 1984; Atabey, 2015). The fluorite veins which developed in Malatya region have been studied by Revan and Genç (2003) in Yeşilyurt and Özgenç and Kibici (1994). Altuncu (2009) stated that the Yeşilyurt fluorites are poor in terms of REE and the trace element association is in the form of F+Ba+Si+Au. Kuluncak stated that the fluorite bed is formed as vein fillings and irregular veins in contact with syenite limestone due to alkali magmatism in the region. It also states that the formation of fluorite forms at the pegmatitic stage (Altuncu, 2009). Depending on the type of rare earth element-rich rocks fluorite deposits in Turkey are divided into three classes: (i) carbonatite, (ii) alkaline igneous rocks, and (iii) limestone (Altuncu, 2009). Öztürk et al. (2019) reported that these deposits developed in relation to post-collision magmatism and that ore-forming fluids were fed from other sources.The aim of this study is comparing the formation and REE geochemistry of Malatya fluorites.

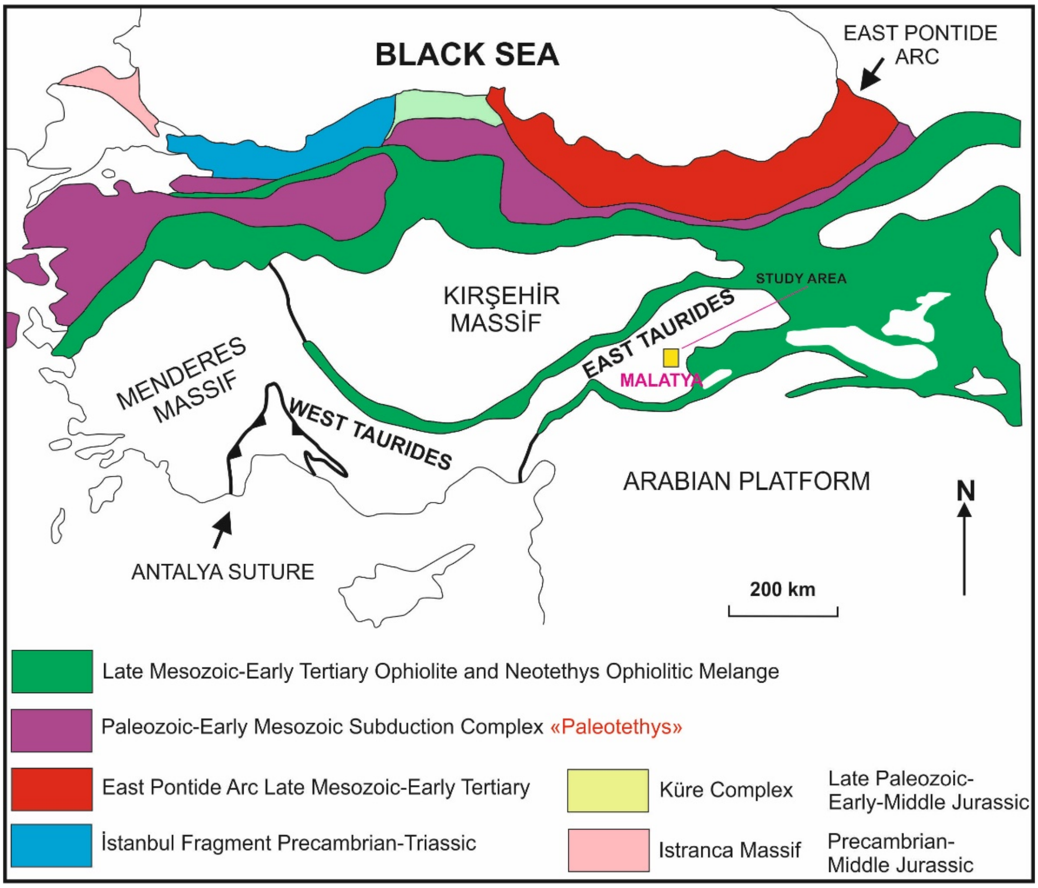

Figure 1. Location of the study area on the tectonic units of Turkey (Quoted as modified from Şengör et al., 1982)

Geological Settings

The Yeşilyurt fluorites were formed (Fig 2) along the discordance plane between the Devonian-Carboniferous aged Kalecik marbles and the Permian aged Düzağaç schists are located at the west and south of Kuz Tepe (Fig 2) (Revan, 2003). Mineralized zone has a geometry which is parallel to the discordance plane and which continues by thinning towards the sides (Fig 3). Faults with NW-SE orientation are generally observed in the area of examination. It is considered that these broken faults, which are observed systematically, are effective in mineralization. Fluorite mineralization occurred as the hot waters circulating around the fault lines transferred the mineralized solutions and discharged those into suitable areas. Observation of mineralization in the schist and limestone discordance plane occurred as the solutions moving in faults and cracks encountered impermeable schists and left their solutions in this discordance plane.

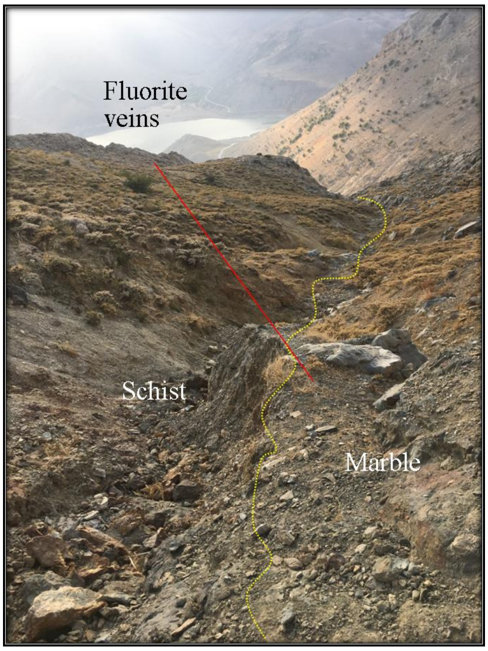

Figure 2. Location of fluorite mineralization on western part of Kuz Tepe

The Kuluncak fluorites are related to the syenite-limestone contact (Fig 4) in the region (Özgenç, 1999). Altuncu (2009) stated that the Kuluncak fluorite deposit is formed as vein fillings and irregular veins in contact with syenite limestone due to alkali magmatism in the region. In fluid inclusion studies Altuncu (2009) reported that the homogenization temperature (Th) is above 580°C on average. Fluorite mineralization in the study area is located in Aşılık Pınarı, Ardıçlı Tepe and Alibeyli (Fig 5).

The Yeşilyurt Fluorites are observed in purple, light purple and blackish colours (Fig 6) but the Kuluncak fluorites are purple (Fig 7).

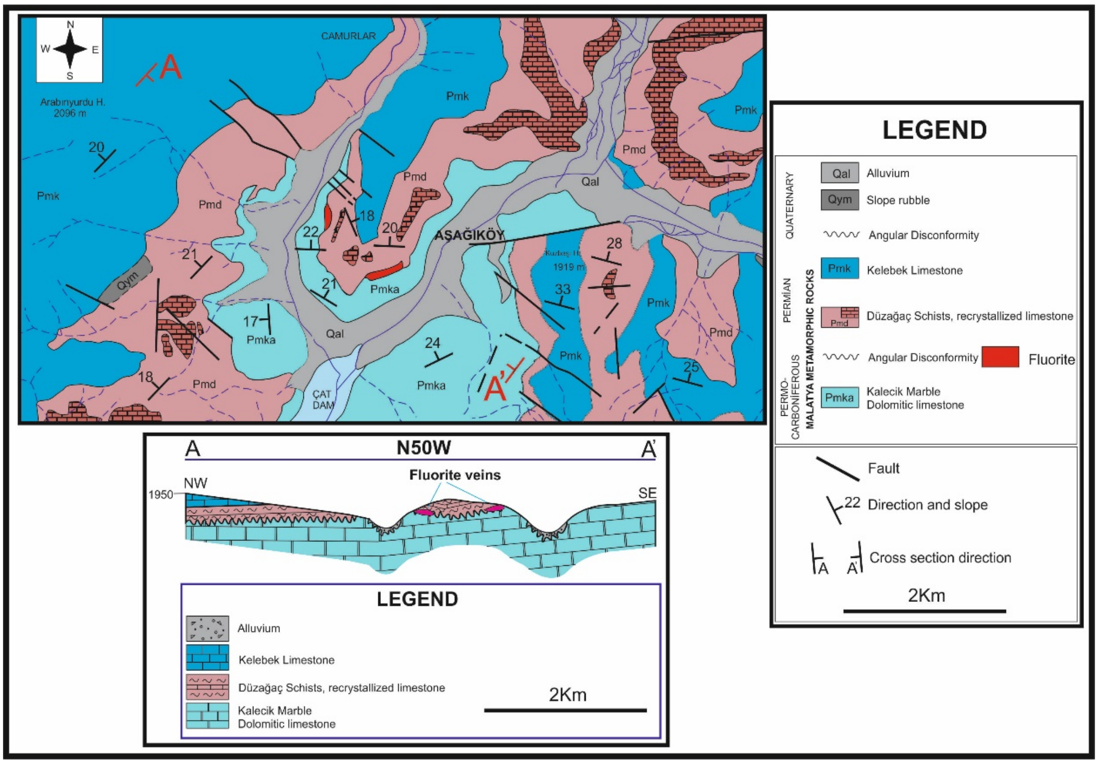

Figure 3. Geological map of the Aşağıköy (Yeşilyurt-Malatya) area and the geological cross section with NW-SE orientation (Modified from Revan, 2003)

Figure 4. General view of quarries with fluorite mineralizations

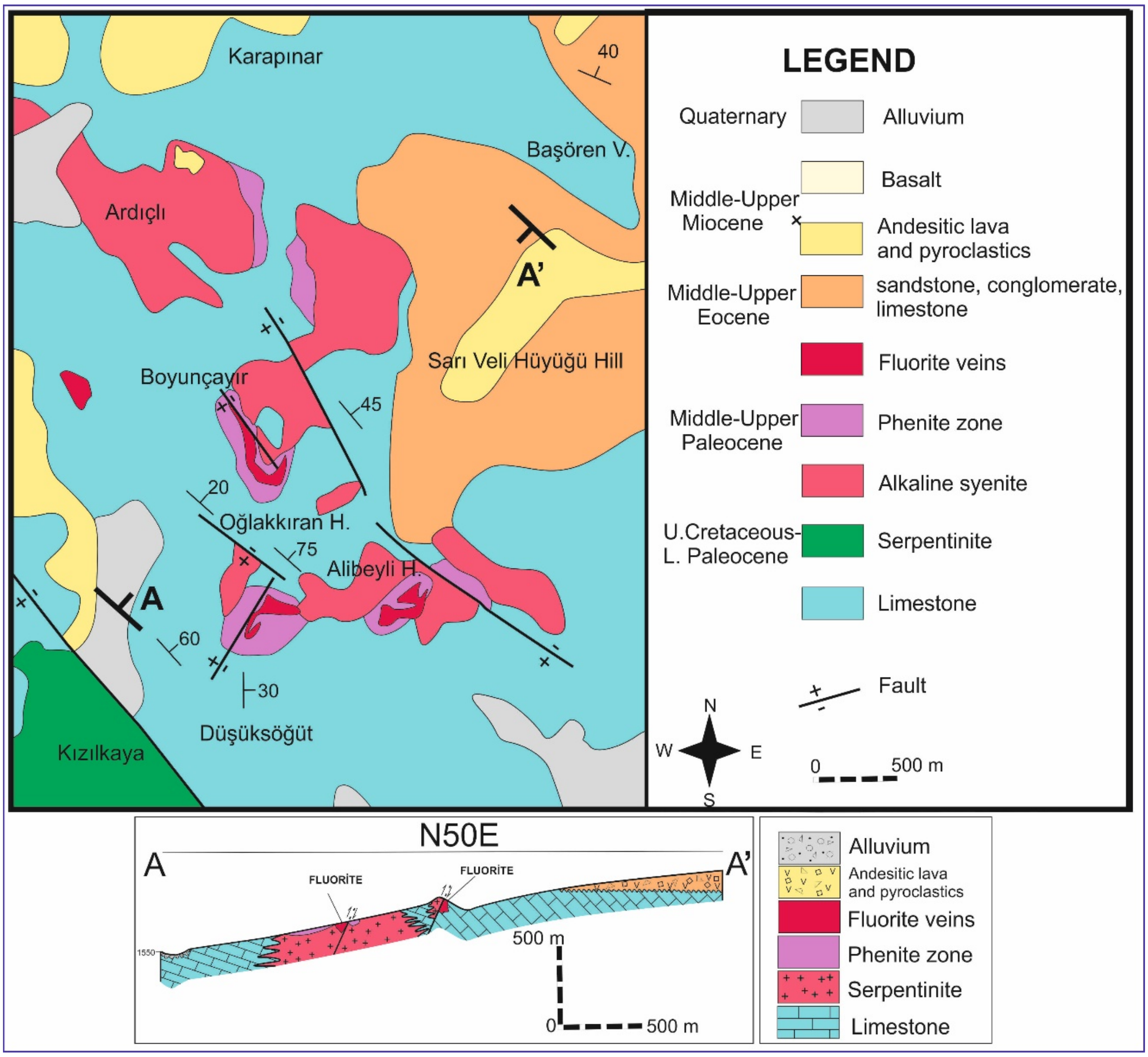

Figure 5. Geological map of the Kuluncak area and the geological cross section with NE-SW orientation (Modified from Özgenç, 1999)

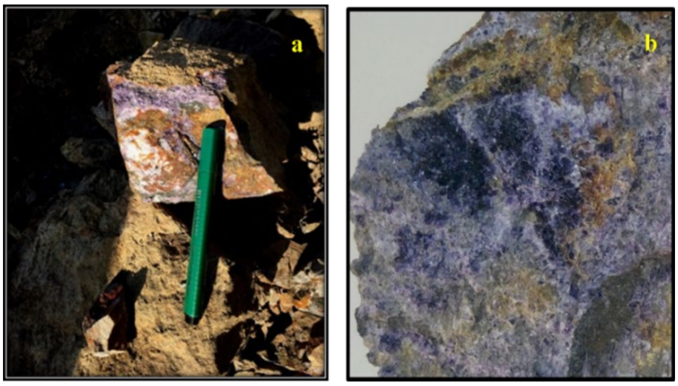

Figure 6. Appearances of purple fluorites in the Yeşilyurt district

Figure 7. Appearances of purple fluorites in the Kuluncak district

METHOD

Rare earth elements are used as a geological indicator in order to reveal the genesis of rocks and ore deposits. The determination of the geotectonic environment of magmatic melts is of importance in terms of revealing the origins and learning the data related to the crystallization conditions. The fluorite samples taken from Yeşilyurt and Kuluncak (Malatya) region were fractured in the geochemistry laboratory of Kahramanmaraş Sütçü İmam University and separated by their colours in the form of pure crystals. The fluorite samples were sorted separately as pure fluorite and decomposed fluorite. Selected crystals are grounded in agate mortar, packaged as 5-grams 20 samples were sent to Acme Laboratories (Vancouver–Canada) and their rare earth element analyses are performed using LİBO_2 fusion, ICP-MS method.

RESULTS AND DISCUSSION

REE Geochemistry

The rare earth element contents of the Yeşilyurt fluorites present a poor content which are similar contents were observed in Feke fluorites (Uras, 2002) and in Büyükkızılcık fluorites (Uras and Çalışkan, 2014) but Kuluncak fluorites present a very rich content also Sr % F values change between 12.2-35.8 (Table 1) in Yeşilyurt and 15,03-25,42 (Table 2) in Kuluncak district. The rare earth element contents of Yeşilyurt fluorites range from 0.02 to 25.8 ppm (Table 1) and the rare earth element contents of Kuluncak fluorites vary between 0.11 and 789.5 ppm (Table 2). A total of 10 fluorite samples contain 369,64 ppm of rare earth elements in Yeşilyurt (Table 1). Total amount of rare earth elements of Kuluncak fluorites varies between 167.01-1188.82 ppm (Table 2).

Terbium (Tb) and Lanthanum (La) are subjected to extensive disaggregation during the formation of fluorite. For this reason, the formation environment and the degree of disaggregation of the mineral are determined by evaluating Tb/La and Tb/Ca ratios (Schneider et al. 1975, Möller et al. 1976; Möller and Morteani, 1983). The Yeşilyurt fluorites fall in the hydrothermal origin field and Kuluncak in the pegmatitic origin field in the Tb/Ca vs. Tb/La diagram (Figure 8).

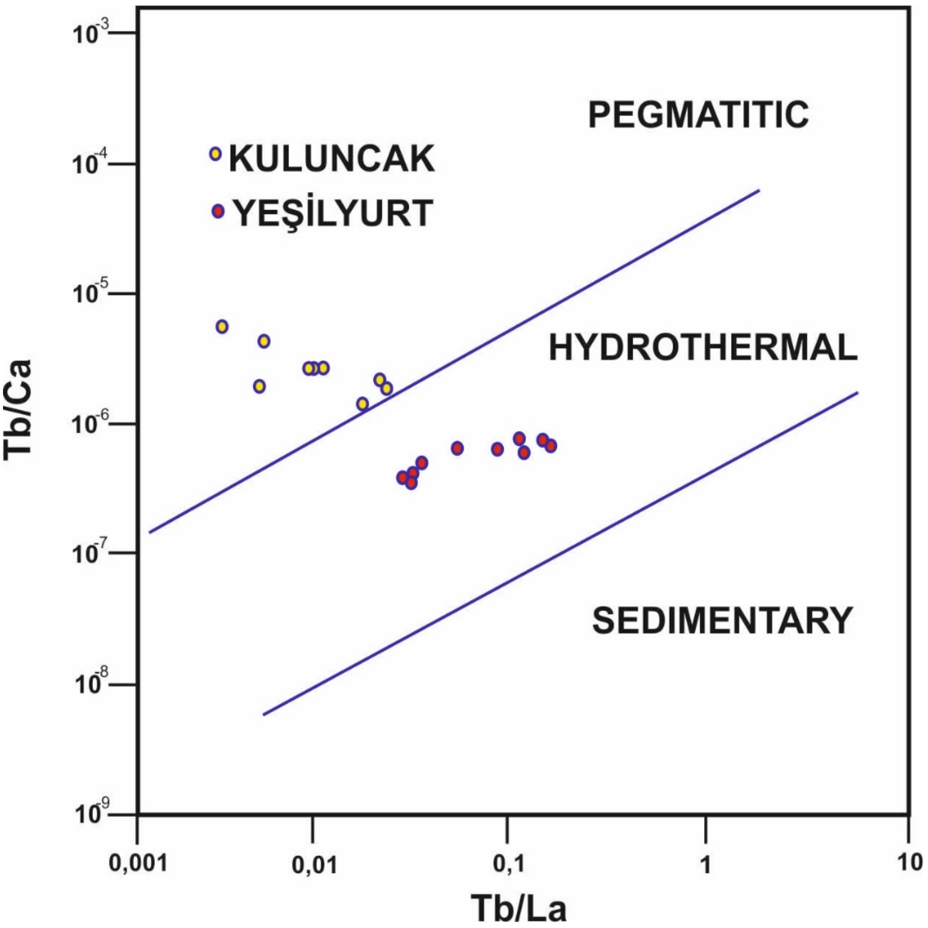

Figure 8. The place of the fluorites in the Tb/La vs. Tb/Ca diagram (Möller and Morteani, 1983)

Table 1. % F, Sr and rare earth element contents of the Yeşilyurt fluorites

Sr (ppm)	37,6	36,4	31,3	32,3	24,2	37,0	38,4	38,8	39,9	35,8
F%	21,69	12,2	13,05	14,09	18,8	35,8	20,00	19,88	20,5	19,78
La (ppm)	3,4	5,1	4,6	4,2	4,9	5,3	2,8	2,6	3,7	2,3
Ce (ppm)	6,0	8,2	6,0	7,0	7,5	5,1	5,3	6,4	5,6	6,2
Pr (ppm)	0,97	1,12	0,91	0,82	1,09	0,84	0,85	0,90	0,90	0,84
Nd (ppm)	4,6	4,5	3,8	3,4	3,2	3,9	4,3	4,3	4,3	3,2
Sm (ppm)	1,26	0,84	0,72	0,82	0,71	1,11	1,11	1,29	1,06	1,27
Eu (ppm)	0,32	0,18	0,14	0,12	0,14	0,24	0,27	0,34	0,31	0,31
Gd (ppm)	1,85	0,90	0,75	0,82	0,78	1,44	1,64	1,74	1,53	1,58
Tb (ppm)	0,32	0,15	0,12	0,11	0,12	0,24	0,28	0,33	0,27	0,31
Dy (ppm)	2,02	0,91	0,79	0,64	0,74	1,47	1,60	2,16	1,69	2,12
Ho (ppm)	0,40	0,20	0,18	0,14	0,18	0,21	0,39	0,44	0,38	0,41
Er (ppm)	1,07	0,59	0,38	0,28	0,45	0,71	0,99	1,16	0,95	1,15
Tm (ppm)	0,12	0,05	0,05	0,05	0,06	0,10	0,10	0,12	0,10	0,11
Yb (ppm)	0,66	0,32	0,24	0,34	0,31	0,49	0,58	0,62	0,61	0,59
Lu (ppm)	0,08	0,04	0,03	0,02	0,09	0,07	0,07	0,08	0,07	0,09
Sc (ppm)	1	1	0,1	0,1	0,1	0,1	0,1	0,1	0,1	0,1
Ce\Yb	9,09	25,63	25,00	20,59	24,19	10,41	9,14	10,32	9,18	10,51
Tb \La	0,094	0,029	0,026	0,026	0,024	0,045	0,100	0,127	0,073	0,135
Tb\Ca*10 6	0,0000007 57	0,0000004 97	0,0000003 95	0,0000003 71	0,0000003 89	0,0000006 54	0,0000006 17	0,0000007 30	0,0000006 47	0,0000006 97
Ce\Ce*	0,8	0,8	0,7	0,9	0,8	0,6	0,8	1,0	0,8	1,1
Eu/Eu*	0,6	0,6	0,5	0,4	0,5	0,5	0,6	0,6	0,7	0,6

ΣREE	44,67	32,30	27,11	26,56	28,57	40,22	41,98	45,68	39,97	42,58

The studied samples from Malatya fluorites cover the crystallized region put forward by Hill et al. (2000) in $(Tb/Yb)_N$ vs. $(La/Yb)_N$ diagram. The Yeşilyurt fluorites are located in the region where the New Mexico fluorites are located but Kuluncak fluorites are located in Akdagmadeni area (Figure 9).

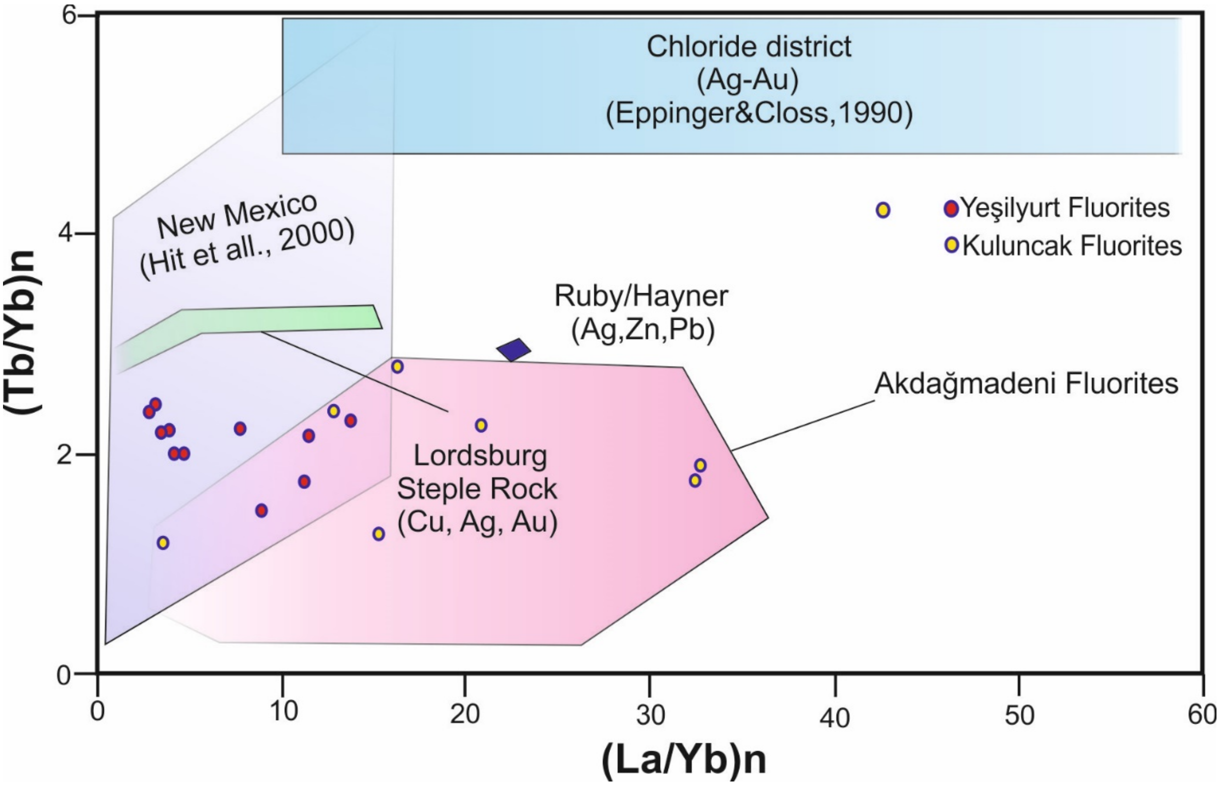

Figure 9. Locations of the studied fluorites in the $(Tb/Yb)_N$ vs. $(La/Yb)_N$ diagram (all values are normalized by comparing (Tb/Yb)n and (La/Yb) The n ratios in Malatya fluorites (Eppinger and Closs, 1990; Hill et al, 2000; Şaşmaz et al, 2005)

Looking at the place of Malatya fluorites within the diagram obtained by comparing the REE results, (La/Yb)n and (Eu/Eu)n ratios, it is observed that Yeşilyurt are located in the same region with the Büyükkızılcık fluorites (Uras and Calışkan, 2014) but Kuluncak fluorites spread in large areas (Fig 10).

Table 2. % F, Sr and rare earth element contents of the Kuluncak fluorites

Sr (ppm)	1432,4	1700,1	1648,8	1781,5	1407,9	2024,9	1603,7	2038,9	1676,4	1485,5
F%	19,33	25,2	25,39	17,1	15,03	17,34	19,37	25,42	18,25	19,86
La (ppm)	105,7	45,4	46,7	380,6	758,7	125,0	43,3	216,8	144,6	138,2
Ce (ppm)	157,6	53,1	56,0	463,7	789,5	178,4	80,9	255,6	203,2	211,1
Pr (ppm)	15,31	6,15	6,19	34,90	56,09	14,46	5,96	18,88	17,29	16,21
Nd (ppm)	46,5	19,8	20,5	91,1	142,6	39,4	17,6	54,1	53,0	50,1
Sm (ppm)	7,64	4,08	3,82	12,18	14,67	5,41	3,41	6,22	7,97	7,65
Eu (ppm)	1,62	0,94	0,89	2,30	2,67	1,28	0,71	1,13	1,54	1,25
Gd (ppm)	8,48	5,19	5,39	10,29	12,93	6,40	3,38	6,54	7,78	6,98
Tb (ppm)	1,41	0,87	0,87	1,68	2,06	1,12	0,64	0,92	1,12	1,09
Dy (ppm)	9,13	5,30	5,57	8,68	11,87	6,86	4,04	5,04	6,59	5,63
Ho (ppm)	1,94	1,24	1,34	1,90	2,65	1,95	0,90	1,31	1,55	1,35
Er (ppm)	5,10	3,42	3,64	5,43	7,30	5,38	3,36	3,84	3,79	3,52
Tm(ppm)	0,59	0,34	0,39	0,70	0,97	0,87	0,38	0,41	0,47	0,41
Yb (ppm)	2,80	1,39	1,63	3,15	5,29	3,98	2,42	2,85	2,81	2,62
Lu (ppm)	0,23	0,12	0,14	0,37	0,62	0,41	0,11	0,18	0,14	0,13
Sc (ppm)	1	0,1	0,1	0,1	0,1	0,1	0,1	0,1	0,1	0,1
Ce\Yb	56,29	38,20	34,36	147,21	149,24	44,82	33,43	89,68	72,31	80,57
Tb \La	0,013	0,019	0,019	0,004	0,003	0,009	0,015	0,004	0,008	0,008
Tb\Ca	0,000000312	0,000001773	0,000001827	0,000003886	0,000005058	0,000002453	0,000001298	0,000001812	0,000002380	0,000002448
Ce\Ce*	1,0	0,8	0,8	1,0	0,9	1,0	1,2	1,0	1,0	1,1

Eu/Eu*	0,61	0,62	0,60	0,62	0,59	0,66	0,64	0,54	0,59	0,52
ΣREE	354,35	194,34	201,27	739,98	1188,82	359,72	167,01	446,82	383,95	382,46

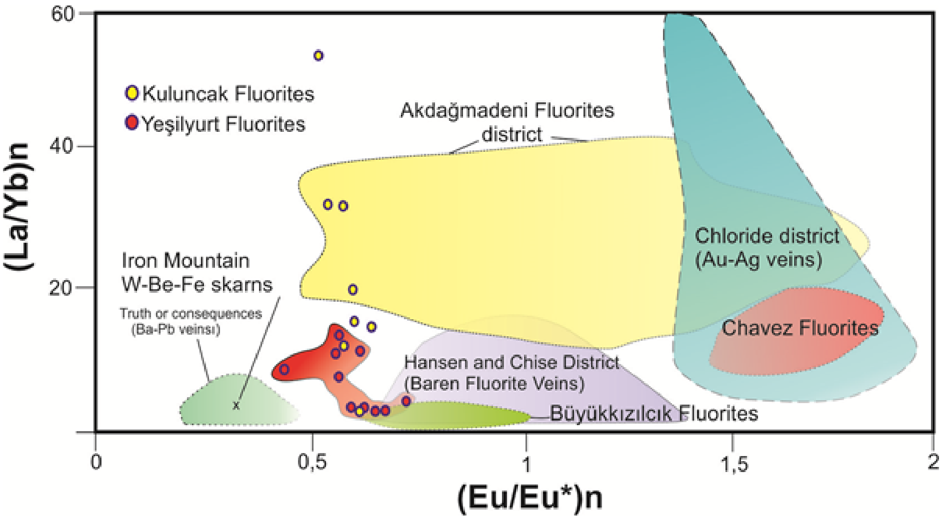

Figure 10. Locations of the Malatya fluorites in the (La/Yb)N vs. (Eu/Eu*)N diagram (Şaşmaz et al, 2005; Uras and Çalışkan, 2004)

In the Sc vs. ∑REE diagram (Şaşmaz et al, 2005), Yeşilyurt fluorites are distributed in a narrow area while Kuluncak fluorites are distributed in large areas (Fig 11).

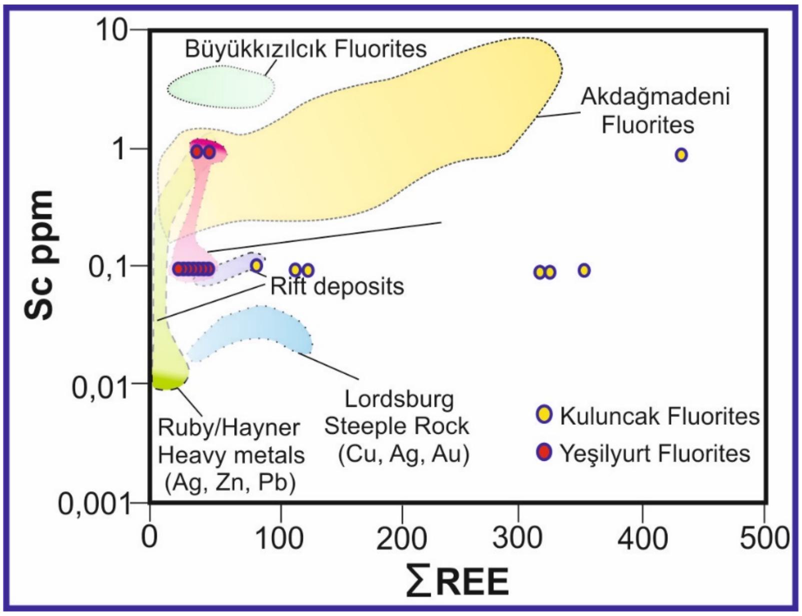

Figure 11. Comparison of Sc vs. ∑REE diagram (Şaşmaz et al, 2005)

The REE compositions of the Malatya fluorites were normalized to Chondrite values and show the light rare earth elements (LREE) are over-rich, as a consequence of continental crust effect, compared to the heavy rare earth elements (HREE) (Fig 12). In normalized diagrams, the positive Ce anomaly of fluorites indicates the presence of low oxygen fugacity at the source of hydrothermal fluids, while the negative Eu anomaly indicates that these conditions also persist in the mineralization environment (Möller and Morteani, 1983; Brookins, 1989).

In this study, rare earth element contents were evaluated by being normalized according to C1-Chondrites (Evensen et al, 1978). It is known that, in case the solutions circulating inside the rock are rich in carbonates, rare earth elements exhibit a more mobilized character compared to the normal aqueous solution (Rollinson, 1993). No significant crystallization has been observed in the normalized rare earth element diagrams of Malatya fluorite samples. With regard to Malatya fluorites, rare earth elements generally present a discordant behaviour during the magmatic crystallization and are enriched in the waste fluid. This presents an enrichment in minerals created in HREE late phase, whereas HREE with small radius also enter in the structure of the minerals created first. Therefore, LREE contents also present enrichment. While LREE contents provide a high value, HREE and LREE values present a lesser enrichment compared to LREE (Figure 12).

The Ce/Ce* and Eu/Eu* ratios provide important data on the oxygen content of the environment (Rollinson, 1993). According to Constantopoulos (1988), if the values of Eu/Eu* are >1, Eu^{+2} transforms into Eu^{+3} by being oxidized (as there is enough oxygen in the atmosphere) and enters into the lattice structures of fluorites. If the Ce/Ce* values are <1, this will cause the Ce to combine with oxygen and precipitate as CeO_2, thus preventing its entry into the structure of fluorites. It causes a negative anomaly to arise for Ce and a positive anomaly to arise for Eu in diagrams normalized with chondritic values (Evensen et al, 1978).

In Eu and Ce anomalies, the fact that Eu presents a negative anomaly and that Ce presents a positive anomaly indicates an environment with low temperature (T) and low oxygen fugacity ($_fO2$). In addition, the negative Eu anomaly is indicative of the presence of Eu^{+2} in the hydrothermal fluid. Ce/Ce* and Eu/Eu* ratios are calculated with $Ce/Ce^*=Ce_n/(La_n \times Pr_n)_{1/2}$ and $Eu/Eu^*=Eu_n/(Sm_n x Gd_n)_{1/2}$ formulas (Constantopoulos, 1988; Palmer and Williams-Jones, 1996; Williams-Jones et al., 2000). Yeşilyurt fluorites are formed under the influence of hydrothermal fluids. The fact that fluorites that are unaffected by a magmatic fluid are poor in terms of High Field-Strength Elements (HFSE) and rare earth elements (REE) indicates that these elements are affected by mineral forming solutions (Yaman, 1985).

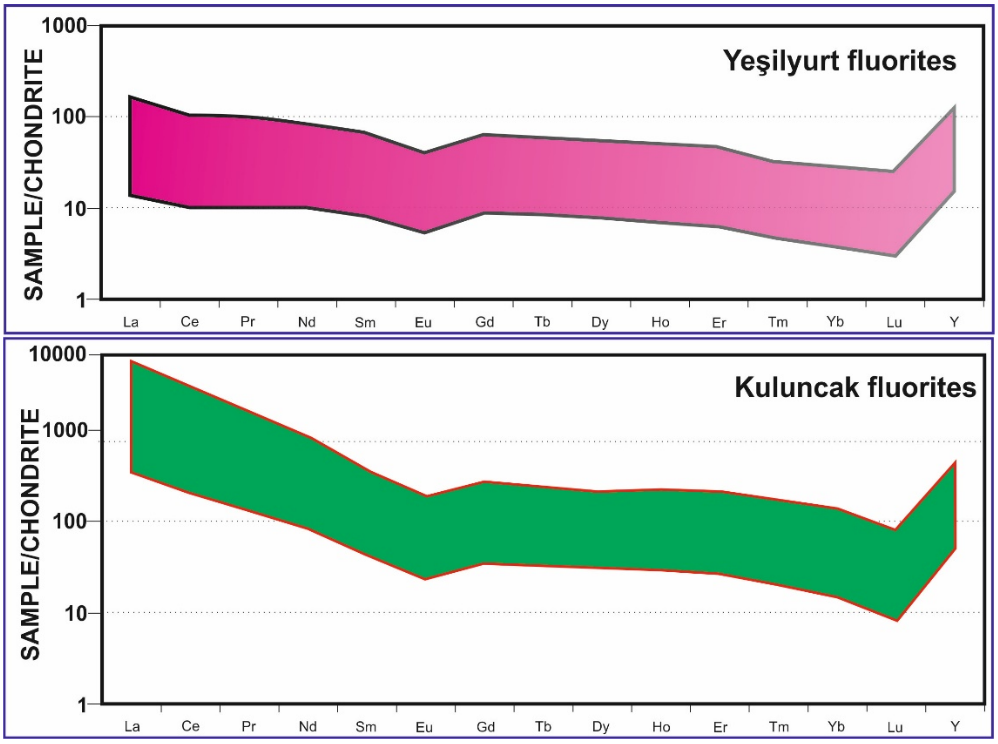

Figure 12. Chondrite- normalized REE spider diagram for (a) Yeşilyurt fluorites and (b) Kuluncak fluorites. (Rare earth element contents were evaluated by being normalized according to C1-Chondrites (Evensen et al, 1978))

DISCUSSION

This study reveals the REE chemical characteristics of Malatya fluorites located in the Eastern Taurus Orogenic belt. The REE contents of the Yeşilyurt fluorites present a poor content. Similar contents were observed in Feke fluorites (Uras, 2002), Büyükkızılcık fluorites (Uras and Çalışkan, 2014) and in Sarıveliler fluorites (Uras et al., 2019). But the REE contents of the Kuluncak fluorites present a rich content.

Altuncu (2009) has been investigated and compared the occurrence of fluorite mineralizations in Turkey and observed the formation environment and origin of fluorites on the Taurus orogenic belts. Coşanay et al. (2017)

demonstrated the microthermometric and geochemical properties of the fluorites observed in the Middle Anatolia. Azizi et al. (2018) examined the fluorites in the Markazi region in Iran and stated that vein type fluorites are poor in REE and dolomite, barite, hematite, goethite and small amount of pyrite are observed in paragenesis.

CONCLUSIONS

As a result; Malatya fluorites where vein type mineralization is seen on Eastern Taurus Orogenic Belt, the formation and geochemical features of Yeşilyurt and Kuluncak fluorites differ from each other. Yesilyurt fluorites are observed as vein type along the plane of unconformity between metamorphic rocks on hydrothermal phase. Kuluncak fluorites are observed in the contacts of alkaline syenites and marbles as vein type which the mineralization occured in the pegmatitic phase. Yeşilyurt fluorites are poor in terms of rare earth element contents but Kuluncak fluorites are rich. All Eu/Eu* values have negative Eu anomaly. This indicates that the fluorite created during the early phase is rich in terms of Eu^{+2} and that there is a presence of low temperature (T) and low oxygen fugacity ($_{f}O2$) in the environment.

REFERENCES

Altuncu, S. (2009). Türkiye Florit Yataklarının Oluşumlarının Karşılaştırmalı İncelenmesi. *Doktora Tezi, İstanbul Üniversitesi, Fen Bilimleri Enstitüsü*, 147 s.

Atabey, E. (2015). Türkiye'de illere göre su kaynakları, potansiyeli ve su kalitesi, 25.11.2016.

Azizi, MR., Alipour, S., Abedini, A., Bagheri, H. (2018). REE geochemical characteristics and fluid inclusion studies of the Bagher-Abad fluorite deposit, Central Iran. *Neues Jahrbuch für Mineralogie-Abhandlungen: Journal of Mineralogy and Geochemistry*, 195(3), 247-263.

Brookins, D. (1989). Aqueous geochemistry of rare earth elements, in geochemistry and mineralogy of the rare earth elements, *Reviews in Mineralogy*, 21: 201-225.

Constantopoulos, J. (1988). Fluid inclusion and rare earth element geochemistry of florite from South-Central Idaho, *Economic Geology*, 83: 626-636.

Coşanay, P., Kirat, E., Cevik, N., Kizilkanat, C., Mutlu, H., Koç, Ş. (2017). Geochemical, microthermometric, and isotopic constraints on the origin of fluorite deposits in central Anatolia, Turkey. *Turkish Journal of Earth Sciences,* 26(3), 206-226.

Eppinger, G.E., Closs, L.G., 1990. Variation of trace elements and rare earth elements in fluorite: a possible tool for exploration. *Econ. Geol*. 85, 1896–1907.

Evensen, N.M., Hamilton, P.J., O'nions, R. K. (1978). Rare Earth Abundances in Chondritic Meteorite, *Geochimica et Cosmochimica Acta*, 42, 1199-1212.

Hill G.T., Campell, A.R., Kyle, P.R. (2000). Geochemistry of Southwestern New Mexico Fluorite Occurrences: Implications for Precious Metals Exploration in Fluorite Bearing Systems. J. *Geochem. Expl*., 68, 1–20.

Ketin, İ. (1966). Anadolu'nun Tektonik Birlikleri. *MTA Dergisi*, 66, 20-34.

Möller, P., Parekh, P.P. and Schneider, H.J. (1976). The Application of Tb/Ca, Tb/la Abundance Ratios to Problems of Fluorspar Genesis. *Min. Deposits*, (11), 111-116.

Möller, P., Morteani, G. (1983). On the Geoehemical Fractination of Rare Earth Elements During the Formation of Ca Minerals and its Application to Problems of the Genesis of Ore Deposits in Augustiths", In: S.S. (Ed)., The Significance of Trace Elements in Solving Petragenetic Problems and Controversies. *Theophrastus Pub*, p. 747-791, Athens.

MTA. (2009). Türkiye Yer Altı kaynakları (illere göre). *Yerbilimleri ve Kültür Serisi-5*, ISBN: 975-605-4075-32-4. Ankara.

Özgenç, İ., Kibici, Y. (1994). Başören Köyü (Kuluncak-Malatya) Britolit Damarlarının Jeolojisi ve Mineralojik-Kimyasal Özellikleri. *Türkiye Jeoloji Bülteni*, Cilt: 37, Sayı 1, S: 77, Ankara.

Özgenc, İ. (1999). Carbonatite-hosted fluorite and britholite mineralization at Sofular area, Malatya, Turkey. In: Stanley CJ (ed) Mineral deposits: processes to processing. *Proceedings of the Fifth Biennial SGA Meeting and the Tenth Quadrennial IAGOD Symposium*, pp 663–666.

Öztürk, H., Altuncu, S., Hanilçi, N., Kasapçı, C., Goodenough, K.M. (2019). Rare Earth Element-Bearing Fuorite Deposits of Turkey; An Overview, *Ore Geology Reviews*, 105, 426-444.

Palmer, DAS., Willams-Jones, A.E. (1996). Genesis of the carbonatite hosted florite deposit at Amba Dongar, India, Evidence from fluid inclusions, stable isotopes and whole rock-mineral geochemistry. *Econ. Geol,* 91: 934–950.

Perinçek, D., Kozlu, H. (1984). Stratigraphic and Structural Relations of the Units in the Afşin-Elbistan-Doğanşehir Region (Eastern Taurus). In Tekeli, O., and Göncüoğlu, M.C. (Eds), *Geology of Taurus Belt*, 181-198, Ankara-Turkey.

Revan, M. (2003). Malatya -Yeşilyurt Altınlı Florit Cevherleşmesinin Oluşumu ve Kökeni. *Yüksek Lisans Tezi, Hacettepe Üniversitesi, Fen Bilimleri Enstitüsü*, s 150.

Revan, M., Genç, Y. (2003). Malatya-Yeşilyurt Altınlı Florit Cevherleşmesi: Toroslarda Paleokarst Tipi Bir Yatak. MTA Gemi Müdürlüğü, Maden EtM Dairesi, 06520, *Jeoloji Mühendisliği Dergisi,* 2.7 (2), Ankara.

Rollinson, H. (1993). Using geochemical data. *Library of Congress Catolog*.

Schneider, H.J., Möller, P. and Parekh, P.P. (1975). Rare Earth Elements Distribution in Fluorites and Carbonate Sediments of the East-Alpine Mid Triassic Sequences in the Nordliche Kalkalpen. *Mineralium Deposita*, vol. 10pp.330-344.

Şaşmaz, A., Yavuz, F., Sağıroğlu, A., Akgül, B. (2005). Geochemical Patterns of the Akdağmadeni (Yozgat, Central Turkey) Fluorite Deposits and İmplications. *J. Asian Earth Sci*., 24, 469-479.

Şengör, A.M.C., Yılmaz, Y., Ketin, İ. (1982). Remnants of a pre-late Jurassic ocean in northern Turkey, Fragments of Permian-Triassic Paleo-Tethys? Reply. *Geol. Soc. America Bull*., 93, 932-936.

Uras, Y. (2002). Feke (Adana) ve Bayındır (Kaman) fluoritlerinin Nadir Toprak Elementlerinin Karşılaştırılması. *Çukurova Üniversitesi Fen Bilimleri Enstütisi Doktora tezi*, 86s.

Uras, Y., Caliskan, V. (2014). Geochemical Patterns of the Buyukkizilcik (Kahramanmaras) Fluorite Deposits. *Geochemistry International*, 52 (12), 1087–1100.

Uras, Y., Yalçın, C., İncediş, Y., Karaman, M. (2019). Orta Toroslarda Karbonatlı Kayaçlar İle İlişkili Sarıveliler (Karaman) Floritlerinin Nadir Toprak Element Jeokimyası, *Fırat Üniversitesi Müh. Bil. Dergisi*, 31(2), 519-528, https://doi.org/10.35234/fumbd.567135.

Yaman, S. (1985). Akçakent (Çiçekdağı-Kırşehir) Yöresi Fluorit Yataklarının Jeolojisi ve Sıvı Kapanım Çalışmaları, *Türkiye Jeoloji Kurumu Bülteni*, 22, 73–78.

ORCID

Yusuf URAS *http://orcid.org/0000-0001-5561-3275*
Cihan YALÇIN *http://orcid.org/0000-0002-0510-2992*
Merve PAKSOY *http://orcid.org/0000-0002-0547-6687*

KSÜ Mühendislik Bilimleri Dergisi, 22, Özel Sayı, 2019 KSU J Eng Sci, 22, Special Issue, 2019
Uluslararası İleri Mühendislik Teknolojileri Sempozyumu (ISADET) Özel Sayısı
International Symposium on Advanced Engineering Technologies (ISADET) Symposium Special Issue
Araştırma Makalesi Research Article

Kahramanmaras Sutcu Imam University
Journal of Engineering Sciences

Geliş Tarihi : 20.07.2019 Received Date : 20.07.2019
Kabul Tarihi : 31.10.2019 Accepted Date : 31.10.2019

DONATILI BETONDA KOROZYON VE ADERANSIN ARAŞTIRILMASI

INVESTIGATION OF CORROSION AND ADHERENCE IN REINFORCED CONCRETE

Ramazan YAVUZ [1], *Osman GÜNAYDIN* [2], *Kadir GÜÇLÜER* [3]

[1,2] Adıyaman Üniversitesi, Mühendislik Fak., İnşaat Müh. Bölümü, Adıyaman, Türkiye.
[3]Adıyaman Üniversitesi, Teknik Bilimler MYO, İnşaat Bölümü, Adıyaman, Türkiye.

*Sorumlu Yazar / Corresponding Author: Ramazan YAVUZ, ramazanyvz02@gmail.com

ÖZET

Betonun hizmet gördüğü süre zarfınca karşılaştığı zararlı etkilere karşı dayanıklı olması önemlidir. Betonun düşük çekme gerilme davranışı, çelik donatı ile geliştirilmektedir. Ancak beton içine gömülen donatının, korozyona uğrama riski bulunmaktadır. Çelik donatının korozyona uğraması, taşıma kapasitesi başta olmak üzere, sistemin tümünün deformasyona uğramasına sebep olur. Bu çalışmada korozyon inhibitörü kullanımının donatı korozyonuna ve beton ile donatı arasında oluşan aderansa etkisi araştırılmıştır. Çalışmada 15 cm kenarlı betonarme küpler üretilmiştir. Beton ile donatı arasındaki aderans kuvveti, kübik betonarme örnek üzerinde test edilmiştir. Çimentonun ağırlıkça % 1' i oranında kalsiyum nitrat bazlı korozyon inhibitörü beton karışımında kullanılmıştır. Numunelere, 20 ±2 °C' de tatlı su kürü uygulanmıştır. Deney örneklerinin aderans özelliklerini belirlemek için çekme-çıkarma deneyi ve korozyon davranışlarını ölçmek için de yarı hücre korozyon potansiyeli ölçümü uygulanmıştır. Yapılan çalışma sonucunda korozyon inhibitörü kullanılan numunelerde kullanılmayan numunelere göre korozyon oluşumunun daha yavaş gerçekleştiği tespit edilmiştir. Korozyon etkisiyle donatı-beton aderansının azaldığı fakat korozyon inhibitörü kullanılan numunelerde aderansın arttığı tespit edilmiştir.

Anahtar Kelimeler: Aderans, Beton, Korozyon, Korozyon İnhibitör

ABSTRACT

It is important that the concrete is resistant to the harmful effects it encounters during its service. The low tensile stress behavior of the concrete is improved by steel reinforcement. However, there is a risk of corrosion of the reinforcement embedded in concrete. Corrosion of the steel reinforcement causes deformation of the entire system, in particular its carrying capacity. In this study, the effect of corrosion inhibitor usage on reinforcement corrosion and the adherence between concrete and reinforcement were investigated. In this study, 15 cm edged reinforced concrete cubes were produced. Bonding Strength between concrete and reinforcement were tested on cubic reinforced concrete specimen. The calcium nitrate-based corrosion inhibitor was used in the mixture of 1% by weight of cement The specimens were cured in two different ways as normal water cure at 20 ± 2 ^{0}C and salt water cure to create a corrosive environment. In order to determine the adherence properties of the test samples, a pull-out test and a semi-cell corrosion potential measurement were applied to measure corrosion behavior. As a result of the study, it was determined that the corrosion formation was slower than the samples not used in the corrosion inhibitor samples. It was determined that the adherence of the reinforcement-concrete decreased with the effect of corrosion but the adherence increased in the samples using the corrosion inhibitor.

Keywords: Adherence, Concrete, Corrosion, Corrosion Inhibitor.

GİRİŞ

İnsanoğlu, var oluşundan bu yana olaylardan ve tehlikelerden korunmak ve hayatını sürdürebilmek için güvenli bir barınağa gereksinim duymuştur. İlk çağlarda malzemeler doğada bulunduğu şekliyle kullanılmaktaydı. Daha sonraki süreçte, malzeme bilimindeki gelişmelere paralel olarak insanlardaki düşünce ve becerilerin gelişimi ile doğadaki malzemeler işlenip şekillenerek kullanılmaya başlandı (Şimşek, 2012). Betonun bulunuşu 18. yüzyılın sonlarına kadar uzanmaktadır. Halen günümüzde de hızla devam eden betonun geliştirilmesiyle ilgili çalışmalarda betonun dayanımı, kalitesi, uzun süredeki davranışı, bakım tekniği, ekonomi, estetik, olumsuz şartlarda beton dökümü, katkılarla özelliklerini geliştirme vb. konularda çalışmalar devam etmektedir (Güner, 1999). Beton, çimento, doğal ve yapay iri agrega, su ve gerektiğinde kimyasal ve/veya mineral katkının karıştırılması ile yapılan ve çimentonun hidratasyonu ile dayanım kazanan malzemedir (TS 11222, 2001 ve TS EN 206-1, 2002). Betonun birçok olumlu özelliğinin yanı sıra çekme dayanımı oldukça düşüktür. Beton elemanın çekme ve eğilme gerilmeleri karşısında çatlayıp kırılmasını önleyebilmek için, çekme gerilmelerinin oluştuğu bölgelere çelik donatılar yerleştirilmektedir. Çekme dayanımı yüksek olan çelik donatılar çekme dayanımı düşük olan betonu desteklemektedirler (Boğa, 2010). Bu çelik donatılar ve betondan oluşan yapı elemanının, betonarme olarak davranabilmesi için çubukların betona kenetlenmesi gerekir. Kenetlenmeyi sağlayan çelik çubukla beton arasındaki kayma gerilmelerine "Aderans" denir (Karakoç, 1985). Donatı-beton aderansı korozyondan olumsuz etkilenir, hatta ileri derecede hasar durumunda aderans tamamıyla yok olur (Baradan vd., 2002). Betonarme yapılarda kullanılan çelik donatılardaki korozyon gelişimi, yapılardan beklenen emniyet ve servis ömrü ile ilgili gereksinimleri büyük ölçüde etkilemektedir (Yiğiter ve Baradan, 2008). Kötü ortam koşullarında betonun hızlı bir şekilde bozulmasını önlemek için yüksek kalitede ve dayanıklılıkta beton üretmek gerekir. Ancak beton içerisine giren zararlı iyonlar çelik donatının yüzeyindeki doğal pasiviteyi bozar ve genellikle betonarme yapılarda donatının korozyonuna neden olur (Baradan vd., 2002; Güneyisi vd., 2005; Yeau ve Kim, 2005; Erdoğdu vd., 2004). Donatının korozyona uğramasıyla betonarme elemanların performansında çeşitli kayıplar olur. Bunlar; pas payı tabakasının çatlamasına bağlı olarak donatının etkili kesit alanlarındaki azalmalar, kesit alanındaki azalmaya bağlı olarak donatıların mekanik performansındaki azalmalar ve donatılı betonların aderans performanslarındaki azalmalardır. Korozyon nedeniyle aderans dayanımlarındaki kayıpları azaltmak için çeşitli önlemler alınmaktadır (Topçu ve Boğa, 2008). Bu önlemlerden bir tanesi korozyon inhibitörü kullanmaktır. Korozyon inhibitörleri betonarme yapılarda donatı çeliğinin korozyonunu yavaşlatabilen veya önleyebilen kimyasallardır. Korozyonu inhibite eden katkılar, betonarmeyi korozyon hasarlarına karşı korumada diğer metotlar arasında koruma mekanizması yönünden eşsizdir ve beton matrisinin ayrılmaz bir parçasıdır (Aydın ve Çizmecioğlu, 2013). Korozyon inhibitörü kullanımı, uygulama kolaylığı, etkin performansı ve ekonomikliği nedeniyle korozyonu önlemede en uygun yöntemlerden biri olarak ele alınmaktadır.

MATERYAL ve METOD

Çalışmada bağlayıcı olarak TS EN 197-1 ile uyumlu CEM I 42,5 R tipte çimento kullanılmıştır. Beton, Çimko hazır beton santralinden temin edilmiş olup su/çimento oranı 0.60 sabit tutularak C30 sınıfında beton kullanılmıştır. Numunelerin hazırlanmasında 0-5 mm 'lik elekler arasında kalan % 59 doğal kum, 5-12 mm 'lik ve 12-22.4 mm 'lik elekler arasında kalan % 41 doğal çakıl kullanılmıştır. Üretilen beton numunelerin hazırlanmasında 16 mm çapında ve 20 cm uzunluğunda nervürlü S 420a betonarme çeliği kullanılmıştır. İnhibitör olarak DCI korozyon inhibitörü kullanılmıştır. DCI, kalsiyum nitrit, su içeren bir solüsyon temelinde likit bir korozyon engelleyicisidir. DCI en az % 35 oranında kalsiyum nitrit içermekte olup özgül ağırlığı yaklaşık olarak 1.28 kg/lt' ye eşittir.

Üretilen betonların mekanik ve dayanıklılık özelliklerini belirlemek amacıyla yarı hücre potansiyeli ve çekme-çıkarma dayanımlarına ait her bir seri için 18 adet, toplamda 4 seri olacak şekilde 72 adet numune hazırlanmıştır. Numuneler 20 cm uzunluğunda ϕ16'lık bir donatının gömüldüğü betonarme eleman şeklinde 15x15x15 cm boyutlarındadır. Numunelerin yüzeyi ile donatının birleştiği kısım epoksiyle kaplanmıştır. Üretilen bu numuneler 7, 28, 90 ve 180 günlük olmak üzere dört farklı kür süresinde tutulmuştur. Betonun mekanik ve dayanıklılık özelliklerinin belirlenmesi amacıyla üretilen numunelere 23 ± 2 ℃ sıcaklığa sahip tatlı su kür havuzunda 7, 28, 90 ve 180 gün boyunca standart kür uygulanmıştır. Şekil 1' de üretilen numunelerde gömülü donatının korozyon aktivitesini tespit etmek amacıyla yarı hücre potansiyel deneyi uygulaması gösterilmiştir. Yarı hücre potansiyel deneyinden sonra ayrıca numuneler çekme - çıkarma deneyine tabi tutularak aderans dayanımları tespit edilmiştir.

Şekil 1. Üretilen beton numuneleri.

Yarı hücre potansiyel korozyon test yöntemi, donatının korozyon potansiyelinin belli bir dönem zarfınca ölçümüne dayanır ve korozyon olasılığı hakkında fikir verir. Yarı hücre potansiyeli ölçüm yöntemi hem yapı üzerinde hem de laboratuvarda olmak üzere en çok kullanılan, hasar oluşturmayan ve elektro-kimyasal tekniklerin uygulama bakımından en basit olanıdır. Bu yöntem betonarme donatısının korozyon aktivitesini tespit etmek amacıyla laboratuvarda betondaki kaplamasız donatıların elektriksel yarı hücre potansiyellerinin tespiti amacıyla kullanılmıştır.

Beton içindeki donatının korozyon potansiyelinin ölçümünde ASTM C 876'ya uygun Şekil 2' de gösterilen deney düzeneğinden yararlanılmıştır. Yarı hücre potansiyeli ölçümünde yüksek empedanslı bir voltmetre aracılığıyla donatı potansiyeli bir referans elektroda göre ölçülmüştür. Kür havuzlarında bekletilen numuneler 7, 28, 90 ve 180 günün sonunda havuzdan çıkartılıp yarı hücre potansiyeli okumaları yapılmıştır.

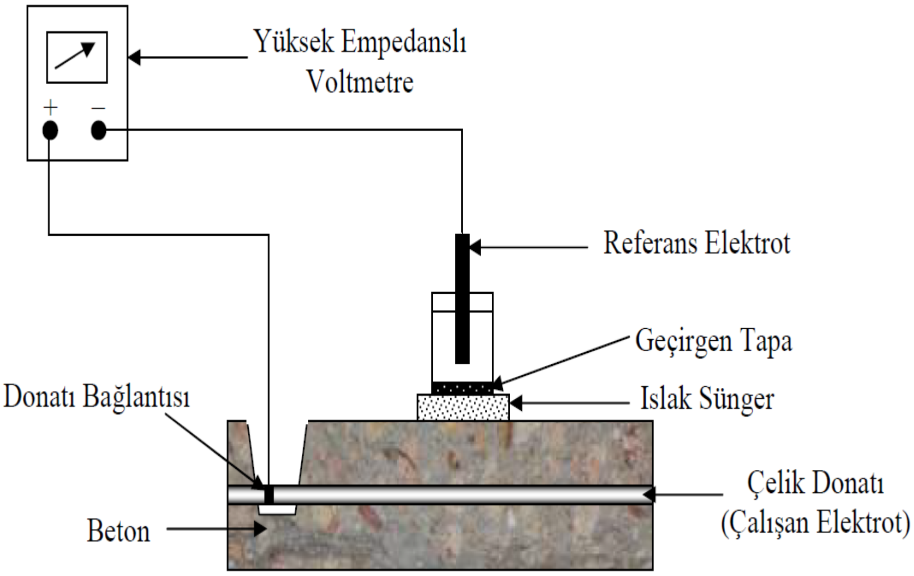

Şekil 2. Yarı hücre potansiyeli ölçüm düzeneği (Boğa, 2010).

Beton içine gömülü donatının potansiyeli, belirli bir yarı hücrenin donatı ile bağlantısı kurularak saptanmıştır. Elektrotun diğer ucu voltmetrenin negatif kutbuna bağlanıp açığa çıkartılan ve pastan temizlenen donatı ise voltmetrenin pozitif kutbuna bağlanmıştır. Bu şekilde devre tamamlanmış ve donatının yarı hücre potansiyeli belirlenmiştir. ASTM C 876'da da belirtildiği gibi referans elektrot olarak $Cu/CuSO_4$ (bakır/bakır sülfat) (CSE) elektrot kullanılmıştır. Deneyler sonucunda elde edilen korozyon potansiyellerinin değerlendirilmesinde Tablo 1 ' de gösterilen ASTM C 876'nın sınır değerlerinden yararlanılmıştır.

Tablo 1. Donatının korozyon potansiyelinin değerlendirilmesi (ASTM C 876-15, 2015).

$Cu/CuSO_4$ mV (CSE)	**Korozyon Riski**
E > -200	Korozyon olasılığı % 10
-200 > E > -350	Korozyon belirgin değil
E < -350	Korozyon olasılığı % 90

E < 500	Şiddetli korozyon

Şekil 3 ’ te görülen tam otomatik, hidrolik çeneli, üniversal çekme cihazı ile çekme çıkarma deneyleri yapılmıştır. Farklı kür koşullarında bekletilen numuneler üzerinde her bir seride 3 numune olacak şekilde toplamda 6 seri yapılarak 7., 28., 90. ve 180. günlerde çekme - çıkarma deneyi ASTM C 234-91-a’ ya uygun olarak yapılmıştır.

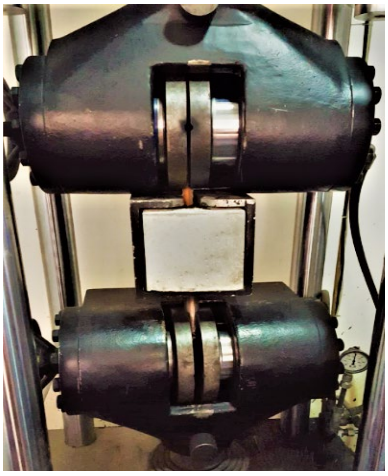

Şekil 3. Aderans Deney Düzeneği

Çekme - çıkarma deneyi sonrasında elde edilen çekme dayanımlarından yola çıkarak aderans kuvveti bulunmuştur. Bulunan aderans kuvveti, aderans gerilmesini belirlemek için formül (1)’de yerine yazılıp aderans gerilmeleri bulunmuştur.

Aderans gerilmesi,

$$\tau = \frac{AderansKuvveti}{\pi \times \phi \times \ell} \tag{1}$$

Bağıntısından hesaplanmıştır (Moetaz, ve Hawary, 1999). Bu formülde;
τ = Aderans gerilmesi
Ø = Donatı çapı
ℓ = Aderans Boyu (Betona gömülü donatı uzunluğu)

BULGULAR ve TARTIŞMA

Şekil 4’ te inhibitörsüz ve inhibitör katkılı betonların içerisindeki donatının yarı hücre potansiyelinin zamanla değişimi verilmektedir. Kutuplaşmayla oluşan potansiyel fark’ın ifade edildiği Yarı Hücre Potansiyeli mV biriminde ölçülüp Tablo 1’ de verilen sınır değerlerine göre donatının korozyon durumu hakkında yorum yapılmıştır.Yarı hücre potansiyelinin ölçüleceği donatılı numuneler, tatlı su küründe bekletilmiştir. Daha sonra bekletilen numuneler 7., 28., 90 .ve 180. günlerde kür havuzlarından çıkarılıp yarı hücre potansiyeli okumaları yapılmıştır.

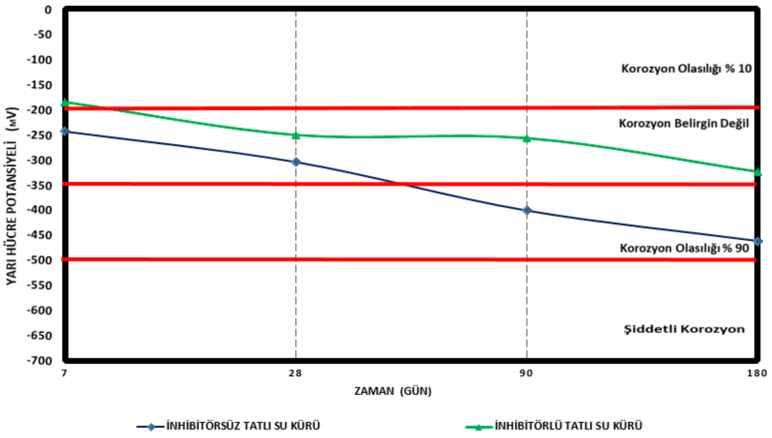

Şekil 4. Beton numunelerin içerisindeki donatının yarı hücre potansiyelinin zamanla değişimi

Şekil 4 incelendiğinde 7 günlük başlangıç kürü uygulandıktan sonra yapılan ilk okumada bütün numunelerin yarı hücre potansiyellerinin –350 mV sınır değerinin üzerinde kaldığı görülmüştür. 7. günün sonunda inhibitörsüz tatlı su kürü ve inhibitörlü tatlı su kürü uygulanan serilerde yapılan okumalarda sırasıyla -244 ve -185 mV değerleri elde edilmiştir ve Tablo 1' deki sınır değerlere göre korozyonun belirgin olmadığı aralıkta olduğu hatta inhibitör ilavesi yapılan tatlı su küründe yarı hücre potansiyeli değerinin daha az negatif değerde kaldığı ve korozyon olasılığının % 10 olduğu aralıkta kaldığı görülmüştür. Serilerde 28., 90. ve 180. günlerin sonunda elde edilen yarı hücre potansiyeli okumalarının gittikçe daha negatif değerler aldığı ancak korozyon inhibitörü kullanılan numunelerin yarı hücre potansiyeli okumalarının daha düşük negatif değerlerde kaldığı görülmüştür. Korozyon inhibitörü kullanımının etkisi 180. günün sonunda özellikle korozyon inhibitörü kullanılan, inhibitörlü tatlı su küründeki numunelere ait yarı hücre potansiyeli okumalarının -350 mV sınır değerinden daha pozitif değerde kaldığı görülmüştür.

Donatılı beton numuneleri ile donatılar arasındaki kenetlenmenin (aderans) korozyon inhibitörü kullanılmasıyla ne derece etkilendiğini incelemek amacıyla yarı hücre potansiyeli deneyi yapıldıktan sonra numunelerdeki donatılar çekip çıkarılmıştır. Deneyler sonucunda (1) bağıntısından yola çıkarak elde edilen aderans kuvveti değerlerinden aderans dayanımları bulunmuştur (Şekil 5).

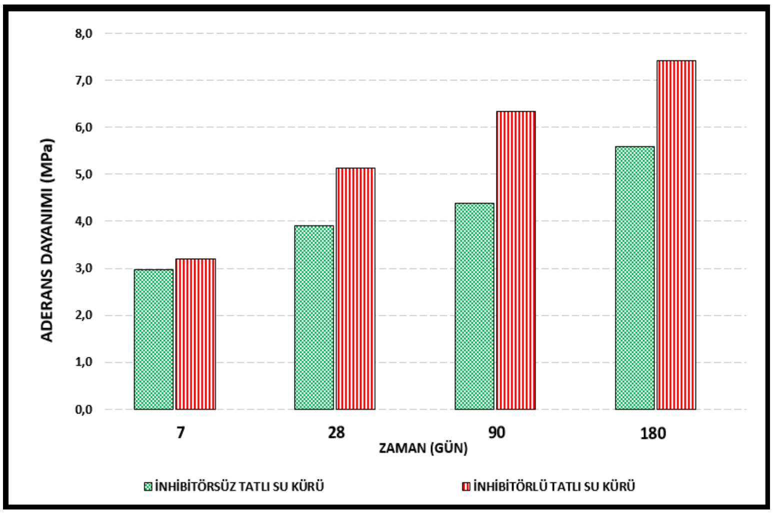

Şekil 5. Numunelerin farklı kür koşulları altında aderans dayanımı değerleri

Çekme – Çıkarma deneyi sonuçlarına göre en yüksek aderans dayanımı değerleri 180 günlük betonlarda, en düşük aderans dayanımı değerleri ise 7 günlük betonlarda tespit edilmiştir. Çekme – Çıkarma deneyi sonuçlarına göre 180. günün sonunda tatlı su kürüne ait inhibitor kullanılan ve kullanılmayan numuneler arasında %33'lük aderans dayanımı artışı bulunmaktadır. Korozyon inhibitörü kullanılan tatlı su kürüne tabi tutulan numunelere bakıldığında ise inhibitörün beton içerisindeki donatının çevresini çözünmez bir tabaka halinde sarıp pas oluşmasını engellemesiyle beraber aderans dayanımlarının inhibitör kullanılmayan numunelerden dört seride de daha yüksek olduğu belirlenmiştir.

SONUÇ ve ÖNERİLER

Korozyon inhibitörü kullanımının beton içerisindeki donatının korozyon performansına ve aderansa etkilerinin deneysel olarak araştırıldığı bu çalışmada; betonlar üzerinde yapılan deneylerden elde edilen sonuçlar ve bunların arasındaki ilişkiler aşağıda maddeler halinde verilmiştir.

- Kür sürelerinin artmasıyla beraber yarı hücre potansiyeli okumalarının gittikçe daha negatif değerler aldığı ancak korozyon inhibitörü kullanılan numunelerin yarı hücre potansiyeli okumalarının daha düşük negatif değerlerde kaldığı sonucuna varılmıştır. 180. günün sonunda tatlı su kürüne ait inhibitor kullanılan ve kullanılmayan numuneler arasında %53' lük yarı hücre potansiyeli okuma farkı bulunmaktadır. Bu sonuçlar aynı zamanda korozyon inhibitörü kullanımının yarı hücre potansiyeli okumalarının daha pozitif değerler almasında önemli olduğunu göstermiştir.

- Numunelerin içinde korozyon etkileri görülmüştür. Betonların içindeki çeliğin korozyona uğraması yalnız çeliğin kaybedilmesi ile kalmamış olup bunun yanında, korozyon sonucu oluşan kimyasal bileşiklerin (Pas), tek başına çeliğe göre daha çok büyük hacim kaplaması nedeniyle beton bünyesinde içsel gerilmeler ve çatlamalara sebep olmuştur.
- Çekme – Çıkarma deneyi sonuçlarına göre korozyon inhibitörü kullanılarak üretilen numunelere ait beton donatı aderansı üzerinde olumsuz bir etki yapmamıştır. 180. günün sonunda tatlı su kürüne ait inhibitor kullanılan ve kullanılmayan numuneler arasında %33' lük aderans dayanımı artışı bulunmaktadır. Bu sonuçlar aynı zamanda korozyon inhibitörü kullanımının aderans dayanımını arttırmada önemli olduğunu göstermektedir.
- Korozyondan kaynaklanan kayıpları en aza indirgemek için; ülkelerin korozyon hakkında kendilerine özgün araştırma geliştirme (Ar-Ge) merkezlerinin kurulması ve bu merkezlerde yapılacak çalışmaların niteliğinin arttırılmasıyla ulusal ve uluslararası eksende yaratılabilecek gelişmeler bilim dünyası açısından faydalı olabilir.

KAYNAKLAR

ASTM C 876-15, (2015). Standart Test Method for Corrosion Potential of Uncoated Reinforcing Steel in Concrete, ASTM International, West Conshohocken, PA.

Aydın, Ö., Çizmecioğlu, Z., (2013). Beton Yapılarda inhibitör kullanımının korozyon önlemedeki etkinliğinin değerlendirilmesi, Anonim, 132s, İstanbul.

Baradan, B.,. Yazıcı H., Ün H. (2002). *Betonarme yapılarda kalıcılık*, Ecem Ofset Matbaacılık, 282s.

Boğa, A. R., (2010). Yüksek fırın cürufu ve korozyon inhibitörü kullanımının beton içerisindeki donatı korozyonuna ve beton özelliklerine etkileri, Doktora Tezi, Eskişehir Osmangazi Üniversitesi Fen Bilimleri Enstitüsü İnşaat Mühendisliği Anabilim Dalı, Eskişehir.

Erdoğlu Ş., Kondratova I. L., Bremmer T. W. (2004). Determination Of Choloride Diffusion Coefficient Of Concrete Using Open- Circuit Potential Measurements. *Cement and Concrete Research*, 34, 603-609.

Güneyisi E, Özturan T., and Gesoğlu, A. (2005). A study on reinforcement corrosion and related properties of plain and blended cement concretes under different curing conditions. *Cement And Concrete Composites*, 27, 449-461.

Güner, M.S., (1999). *Malzeme bilimi - yapı malzemesi ve beton teknolojisi*, Aktif Yayınevi, İstanbul.

Karakoç, C, (1985). Aderans Mekanik Etkileşim Olayı, Doktora Tezi, İstanbul Teknik Üniversitesi Fen Bilimleri Enstitüsü İnşaat Mühendisliği Anabilim Dalı, İstanbul.

Moetaz, M. and Hawary, E. (1999). Evaluation of bond strength of epoxy-coated bars in conc-rete exposed to marine environment, *Construction and Building Materials* 13,357-362.

TS 11222, (2001). Beton- Hazır Beton-Sınıflandırma, Özellikler Performans Üretim ve Uygunluk Kriterleri, Türk Standartları Enstitüsü, Ankara.

TS EN 206-1, (2002). Beton-Bölüm 1: Özellik, Performans, İmalat ve Uygunluk, Türk Standartları Enstitüsü, Ankara.

Topçu, İ.B., Boğa, A. R., (2008). Betonarmede donatı ve beton arasındaki aderansa korozyonun etkisi. *Eskişehir Osmangazi Üniversitesi Müh.Mim.Fak.Dergisi* C.XXI, S.1.

Şimşek, O., (2012). *Beton ve beton teknolojisi*, Seçkin Yayınevi, Ankara.

Yeau K.Y., Kim E. K. (2005). An experimental study on corrosion resistance of concrete with ground granulate blast-furnace slag. *Cement And Concrete Research*, 35, 1391-1399.

Yiğiter H., Baradan B., (2008). "Mineral katkıların donatı donatı korozyonuna etkisinin elektrokimyasal yöntemlerle incelenmesi", http://www.prefab.org.tr/makleler/86-1.pdf, 22 Aralık 2011.

ORCID

Ramazan YAVUZ *http://orcid.org/0000-0002-7069-3231*
Osman GÜNAYDIN *http://orcid.org/0000-0001-7559-5684*
Kadir GÜÇLÜER *http://orcid.org/0000-0001-7617-198X*

KSÜ Mühendislik Bilimleri Dergisi, 22, Özel Sayı, 2019 KSU J Eng Sci, 22, Special Issue, 2019
Uluslararası İleri Mühendislik Teknolojileri Sempozyumu (ISADET) Özel Sayısı
International Symposium on Advanced Engineering Technologies (ISADET) Symposium Special Issue
Araştırma Makalesi Research Article

Kahramanmaras Sutcu Imam University
Journal of Engineering Sciences

Geliş Tarihi : 22.07.2019 Received Date : 22.07.2019
Kabul Tarihi : 17.10.2019 Accepted Date : 17.10.2019

USING DEEP LEARNING ALGORITHM TO DIAGNOSE PARKINSON DISEASE WITH HIGH ACCURACY

PARKİNSON HASTALIĞINI YÜKSEK DOĞRULUKLA TESPİT ETMEK İÇİN DERİN ÖĞRENME ALGORİTMASININ KULLANIMI

Fahriye GEMCI [1*], *Turgay IBRIKCI* [2,]

[1] Kahramanmaras Sutcu Imam University, Department of Computer Engineering, Kahramanmaras, Turkey
[2]Cukurova University, Department of Electrical and Electronics Engineering, Adana, Turkey

*Sorumlu Yazar / Corresponding Author: Fahriye GEMCI, fahriyegemci@ksu.edu.tr

ÖZET

Hem motor hem de motor dışı semptomlarda hayati ve kalıcı hasara neden olan Parkinson hastalığının erken teşhisi, hasta durumunun daha da kötüleşmesini önlemek için çok önemlidir. Bu çalışmada, UCI deposundan alınan Parkinson Hastalığı verileri derin öğrenme mimarisi kullanılarak sınıflandırılmıştır. Çalışmadaki derin öğrenme mimarisi, Python Keras tarafından oluşturulan ileri beslemeli bir sinir ağıdır (İBSA). Çalışmadaki mimari, bir girdi katmanı, iki gizli katman ve softmax fonksiyonunu ReLu (Rectified Linear Units) ile bir çıkış katmanı olarak oluşturulmaktadır. Derin öğrenme mimarisi, Parkinson Hastalığı (PH) veri seti iki sınıfa sahip olduğundan dolayı, ikili veri sınıflandırma problemini çözer. PH veri setini sınıflandırmak için test ve eğitim verisi farklı oranlarda bölünerek birçok test yapıldı. PH veri seti sınıflandırması, % 20'sinde test ve kalan veri eğitim verisi olmak üzere, derin öğrenme algoritması kullanılarak % 100 doğrulukta başarılı oldu.

Anahtar Kelimeler: İkili sınıflandırma, derin öğrenme, ileri beslemeli sinir ağı, parkinson hastalığı (PH), tıbbi tanı

ABSTRACT

Early diagnosis of Parkinson's disease, which causes vital and permanent damage to both motor and non-motor symptoms, is very important to prevent further deterioration of the patient condition. In the present study, Parkinson's Disease data set from UCI repository is classified using deep learning architecture. The deep learning architecture in the study is a feed-forward neural network (FFNN) which is builded by Keras of Python. The architecture in the study composes of an input layer, two hidden layers and softmax function with ReLu (Rectified Linear Units) as an output layer. The deep learning architecture solves binary classification problem since PD data set has two classes. In order to classify the Parkinson Disease (PD) data set, many tests were performed by splitting the test and train data in different ratios. The PD data set classification was succeeded with 100% accuracy using deep learning algorithm splitting in 20 % of the data as the test and the remaining as train data in epoch 30.

Keywords: Binary classification, deep learning (DL), feed-forward neural network (FFNN), parkinson disease (PD), medical diagnosis

INTRODUCTION

In age of various diseases, the transformation from medical big data into meaningful and useful information has rose as a new important field to improve disease diagnosis. Parkinson disease (PD) is one of most common neurodegenerative disorders for people over 60 (Sprenger, F., et all., 2013). PD continues to cause disability reasoned by motor and non-motor symptoms in spite of the therapeutic advances for last 20 years (Sprenger, F., et all., 2013). The disease has many negative effects. The most common of these is shivering; there are many motor symptoms such as slowness, balance problems and many other motor symptoms. There are also problems with many non-motor symptoms such as mood, sleep disorder. Majority patients with Parkinson's disease lose their jobs within 5 years

(Sakar, C. O et all., 2019). For these reasons, early diagnosis and treatment of Parkinson's disease is very important. In recent years, PD has been aimed for early diagnosis using telediagnosis and telemonitoring systems (Sakar, C. O et all., 2019; Sakar C.O., et all., 2009; Min, S., Lee, B., et all., 2017).

In the study, it is aimed to perform new PD diagnosis method, due to PD is latter most common neurodegenerative disease after Alzheimer disease and it is waited to increase widespread of PD. PD diagnosis has performed using the deep neural network classifier with 30 different 10-fold cross-validation techniques containing a stacked autoencoder and a softmax with 93.79 accuracy (Caliskan, A., et all., 2017). Around 90 % accuracy in PD diagnosis is obtained using artificial neural network and support vector machine together for 31 patients which 23 of them are with PD (David Gil, A., et all., 2004). In (Das, R., 2010), four classifiers as Regression, Data Mining Neural, Neural Network and Decision Tree is performed to diagnose PD and Neural network with 92.9 % accuracy rate is performed the most successful classification among them. In (Gharehchopogh, F. S., et all., 2013), two classifiers as d Multi-Layer Perceptron (MLP) with back-propagation learning algorithm and a new algorithm which is built Radial Basis Function (RBF) and ANN (Artificial Neural Network) together is used to diagnose PD for 195 samples. MLP with 93.22 % accuracy is more successful PD diagnosis than the new algorithm with RBF and ANN with 86.44 % accuracy. In (Chen, H. L., et all., 2013), fuzzy k-nearest neighbor (FKNN) is performed to diagnose PD with high accuracy rate. FKNN-based method with 96.07 % classification accuracy by a 10-fold cross validation method outperforms methods such as SVM. In the study, features are reduced by Principal Component Analysis (PCA). FKNN with PCA for PD diagnosis outperforms ANN and SVM. In (Srinivasan, S. M., et all., 2017), ANN with three different preprocessing techniques as discretization, resampling, and smote for success of PD diagnosis is tested. The study successes over 95 % using ANN with preprocessing steps as resampling and smote together by splitting as train in 70 % rate and test in 30 % rate. Hence, it is difficult to obtain results above 95% for PD diagnosis using artificial neural network algorithm or any algorithm of other machine learning algorithms without any preprocessing steps. Hence, the neural network classifier need structural changes. in order to increase succes of neural network for all problems such as parkinson diagnosis as performed in [Badem, H.„ 2017]

Based on these results, the deep learning algorithm is tried, which it is thought it could obtain the most accurate and high results without any preprocessing steps, in the diagnosis of PD in this study. In section 2, PD classification data set is used to classify, deep learning algorithm which are used to classify are introduced. The experimental results of the study such as classification accuracy and preferred epoch number are given in section 3. Conclusion and future work are provided in section 4.

METHOD

Parkinson's Disease Classification Data Set

Parkinson's Disease Classification Data Set used in the study is obtained from UCI Repository (Sakar, C. O., et all., 2019). The data set was collected total 756 samples from 252 people which 188 patients are PD patient and rest of them are healthy. The data set is a binary classification problem since it is composed of two classes as healthy and PD patient. The data set composes of total 754 features which are based on Baseline features, time frequency, mel frequency cepstral coefficients, wavelet transform based features, vocal fold features and the tunable Q-factor wavelet transform (TWQT) features in Table 1 (Sakar, C. O., et all., 2019).

Table 1. Distribution of features of parkinson's disease classification data Set

Feature set	Measure	Number of features
Baseline features	Jitter variants	5
	Shimmer variants	6
	Fundamental frequency parameters	5
	Harmonicity parameters	2
	Recurrence Period Density Entropy (RPDE)	1
	Detrended Fluctuation Analysis (DFA)	1
	Pitch Period Entropy (PPE)	1
Time frequency features	Intensity Parameters	3
	Formant Frequencies	4
	Bandwidth	4
Mel Frequency Cepstral Coefficients (MFCCs)	MFCCs	84
Wavelet Transform based Features	Wavelet transform (WT) features related with F0	182
Vocal fold features	Glottis Quotient (GQ)	3
	Glottal to Noise Excitation (GNE)	6
	Vocal Fold Excitation Ratio (VFER)	7
	Empirical Mode Decomposition (EMD)	6
TWQT features		

Deep Learning

Deep learning has used successfully in many fields such as speech recognition, visual object recognition, object detection, natural language understanding, topic classification, sentiment analysis (LeCun, Y., 2015). Deep learning endeavors to learn data representations with multiple abstraction levels using machine learning techniques with multiple processing layers (LeCun, Y., 2015; Chen, X. W., 2014). Since the data features are extracted from the own data without engineers, deep learning differentiates from other algorithms. Deep learning successfully overcomes complex calculations that artificial intelligence cannot solve in high-dimensional data. It uses the backpropagation algorithm to discover these complex structures. The backpropagation algorithm is used to show the change of parameters which represent information transferred from each previous layer to each subsequent layer (LeCun, Y., 2015). In general, ReLu for deep learning is used as activation function of the hidden layers in deep learning. ReLu takes the penultimate layer activation to learn the classification layer weight parameters using backpropagation. ReLu is used usually with softmax function. When deep learning is used for classification, the softmax function is usually used as the last layer. The softmax function in this last layer assumes the classification task. The softmax function defines a discrete probability distribution according to the number of classes in the problem (Agarap, A. F., 2018). Adam optimization algorithm for deep learning is used to learn weight parameters and the sparse_categorical_crossentrop loss function for deep learning is used in the study.

Feed-forward neural network (FFNN)

FFNN takes substitute for ANN whose neurons between units do not create a directed cycle. As in the human brain, ANN also provides interconnected neurons to exchange messages. FFNN composes of an input layer, an output layer and at least a hidden layer. The hidden layer composes of sigmoid neurons and the output layer composes linear neurons. All relationships between all vectors are extracted with neurons in multiple layers. The values are required the ranging from –1 and +1 are extracted using the network linear output layer. Though, a network outputs extract values ranging from 0 and 1 are fabricated. Therefore, a sigmoid transfer function is used acquiring expected values in the output layer. Log-sigmoid transfer threshold function is calculated to optimize status for FFFN as shown in Figure 1 (Ben-Bright, B., 2017; Beale, M. H., 2010).

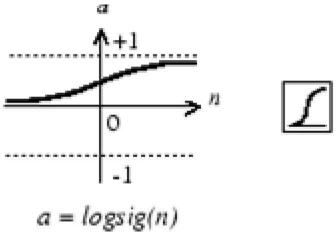

Figure 1. Log-sigmoid Function

EXPERIMENTAL RESULTS

Early diagnosis of Parkinson's disease, which causes vital and permanent damage to both motor and non-motor symptoms, is very important to prevent further deterioration of the patient condition. In the present study, Parkinson's Disease data set from UCI repository is classified using deep learning architecture. The deep learning architecture in the study is a FFNN which is builded by Keras in Tensorflow library of Python. The architecture in the study composes of an input layer, two hidden layers and softmax function with ReLu as an output layer. The deep learning architecture in the study composes of 1 input layer, 2 hidden layers and 1 output layer, ReLu as an activation function, a softmax as a classification function. In addition to four layers, adam function is used as an optimization algorithm and the sparse_categorical_crossentrop is used as a loss function. The deep learning architecture solves binary classification problem since PD data set has two classes. In order to classify the PD data set, many tests were performed by splitting the test and train data in different ratios as shown in Table 2. The highest accuracies of Table 2 are selected as 0.05, 0.20, 0.28, 0.30 and 0.33 test ratios and they are tested again with different epoch numbers as shown in Table 3 and Table 4. PD diagnosis loss and accuracy curves by splitting as 30 % test-70 % train, 20 % test-80 % train, and 10 % test-70 % train are shown in Figure 1, Figure 2 and Figure 3, respectively. The highest performance is obtained by selecting of 0.2 test ratio and 30 epoch number without preprocessing step except for test and train separation and epoch number selection as shown in Table 3 and Figure 2.

Table 2. PD diagnosis classification results using deep learning according to test-train partition.

Rate of Test Data	Rate of Train Data	Percent of Accuracy	Percent of Validation Accuracy
0.05	0.95	100 %	88.30 %
0.10	0.90	100 %	89.89 %
0.15	0.85	100 %	83.33 %
0.20	0.80	100 %	89.87 %
0.27	0.73	99.79 %	91.67 %
0.28	0.72	100 %	85.92 %
0.29	0.71	99.79 %	92.86 %
0.30	0.70	100 %	89.86 %
0.33	0.67	100 %	86.36 %
0.50	0.50	99.39 %	82.00 %
0.66	0.34	98.65 %	85.29 %
0.80	0.20	97.71 %	80.00 %

Table 3. PD diagnosis classification results using deep learning according to epoch number

Rate of Test Data	Rate of Train Data	Epoch Number	Percent of Accuracy	Percent of Validation Accuracy
0.05	0.95	12	100 %	88.30 %
0.05	0.95	20	100 %	89.36 %
0.05	0.95	30	100 %	87.23 %
0.05	0.95	40	100 %	89.36 %
0.05	0.95	45	100 %	90.43 %
0.20	0.80	12	100 %	84.81 %
0.20	0.80	20	100 %	88.61 %
0.20	0.80	30	100 %	93.67 %
0.20	0.80	40	100 %	83.54 %
0.20	0.80	45	100 %	88.61 %
0.28	0.72	12	100 %	84.51 %
0.28	0.72	20	100 %	90.14 %
0.28	0.72	30	100 %	90.14 %
0.28	0.72	40	100 %	90.14 %
0.28	0.72	45	97.71 %	85.92 %
0.30	0.70	12	100 %	88.41 %
0.30	0.70	20	98.70 %	86.96 %
0.30	0.70	30	100 %	91.30 %
0.30	0.70	40	100 %	91.30 %
0.30	0.70	45	100 %	88.41 %
0.33	0.67	12	100 %	86.36 %
0.33	0.67	20	100 %	87.88 %
0.33	0.67	30	100 %	87.88 %
0.33	0.67	40	100 %	90.91 %
0.33	0.67	45	100 %	89.39 %

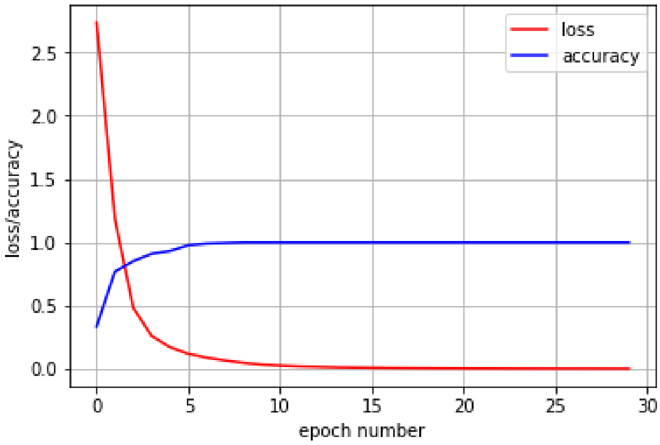

Figure 2. Loss and accuracy curves for PD diagnosis by splitting 30 % test.

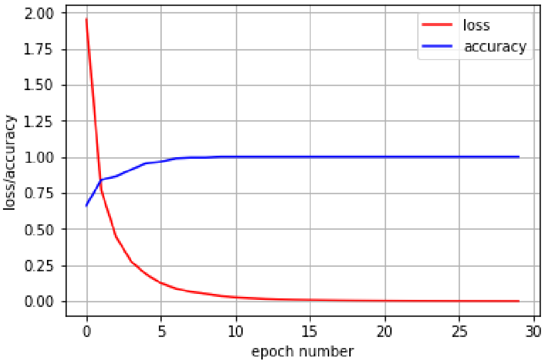

Figure 3. Loss and accuracy curves for PD diagnosis by splitting 20 % test.

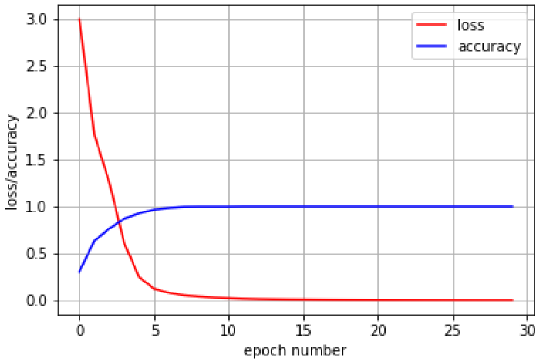

Figure 4. Loss and accuracy curves for PD diagnosis by splitting 10 % test.

Table 4. PD diagnosis classification results using deep learning

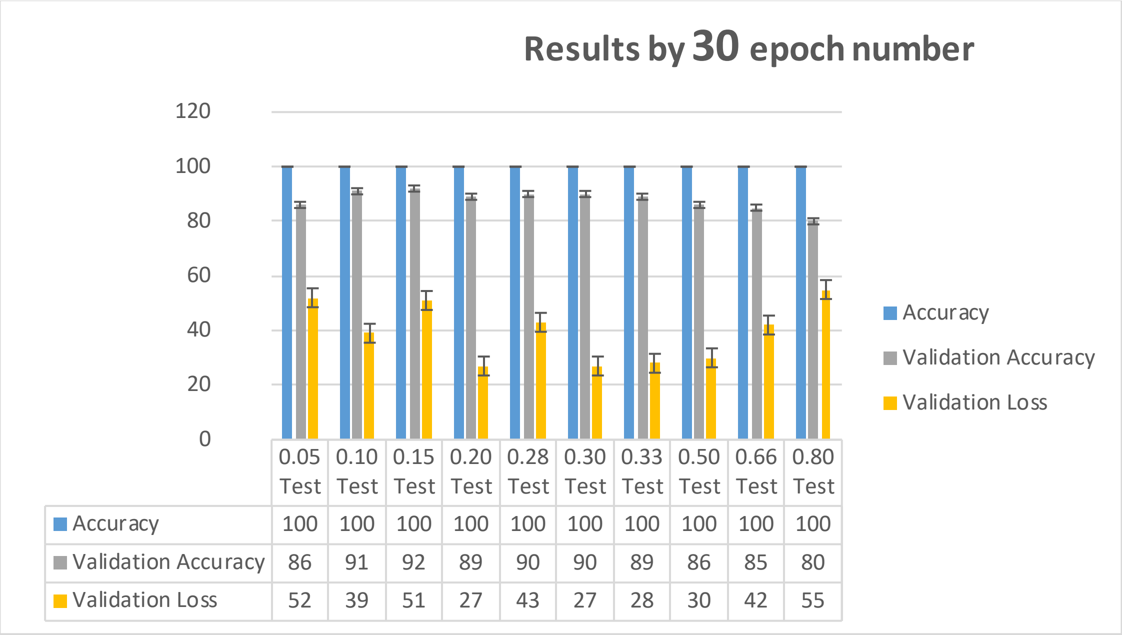

	0.05 Test	0.10 Test	0.15 Test	0.20 Test	0.28 Test	0.30 Test	0.33 Test	0.50 Test	0.66 Test	0.80 Test
🟦 Accuracy	100	100	100	100	100	100	100	100	100	100
⬜ Validation Accuracy	86	91	92	89	90	90	89	86	85	80
🟨 Validation Loss	52	39	51	27	43	27	28	30	42	55

CONCLUSIONS

The proposed method in the study is PD diagnosis using deep learning which is not performed in the literature in Python. Parkinson's Disease data set is classified with 100 % accuracy by 80–20 % train-test data partition and 30 epoch number using Keras API in Tensorflow deep learning library of Python programming language. The method performs PD diagnosis as a binary classification problem, healthy and Parkinson patients. The study for PD diagnosis outperforms previous studies which are performed by ANN and other methods for PD diagnosis, although without any preprocessing steps was performed. In the future works, train-test partition and epoch number selection set for PD diagnosis will be proposed.

REFERENCES

Agarap, A. F. (2018). Deep Learning using Rectified Linear Units (ReLU), *Neural and Evolutionary Computing*, Vol. 1.

Beale, M. H., Hagan, M. T., & Demuth, H. B. (2010). Neural network toolbox. *User's Guide, MathWorks*, 2, 77-81.
Ben-Bright, B., Zhan, Y., Ghansah, B., Amankwah, R., Wornyo, D. K., & Ansah, E. (2017). Taxonomy and a Theoretical Model for Feedforward Neural Networks. *International Journal of Computer Applications*, 975, 8887.

Badem, H., Basturk, A., Caliskan, A., & Yuksel, M. E. (2017). A new efficient training strategy for deep neural networks by hybridization of artificial bee colony and limited–memory BFGS optimization algorithms. Neurocomputing, 266, 506-526.

Caliskan, A., Badem, H., Basturk, A., & Yuksel, M. E. (2017). Diagnosis of the parkinson disease by using deep neural network classifier. Istanbul University-Journal of Electrical & Electronics Engineering, 17(2), 3311-3318.

Chen, H. L., Huang, C. C., Yu, X. G., Xu, X., Sun, X., Wang, G., & Wang, S. J. (2013). An efficient diagnosis system for detection of Parkinson's disease using fuzzy k-nearest neighbor approach. *Expert systems with applications*, 40(1), 263-271.

Chen, X. W., & Lin, X. (2014). Big data deep learning: challenges and perspectives. *IEEE access*, 2, 514-525.

Das, R. (2010). A comparison of multiple classification methods for diagnosis of Parkinson disease. *Expert Systems with Applications*, 37(2), 1568-1572.

David Gil, A., & Maguns Johnson, B. (2004). Diagnosing Parkinson by Using Artificial Neural Networks and Support Vector Machines. *Global Journal of Computer Science and Technology*, 63-71.

Gharehchopogh, F. S., & Mohammadi, P. (2013). A Case Study of Parkinson's disease Diagnosis using Artificial Neural Networks. *International Journal of Computer Applications*, 73(19), 0975 – 8887.

LeCun, Y., Bengio, Y., & Hinton, G. (2015). *Deep learning. nature*, 521(7553), 436-444.

Min, S., Lee, B., & Yoon, S. (2017). Deep learning in bioinformatics. *Briefings in bioinformatics,* 18(5), 851-869.

Okun, M. S. (2012). Deep-brain stimulation for Parkinson's disease. *New England Journal of Medicine*, 367(16), 1529-1538.

Sakar C.O., & Kursun, O. (2009). Telediagnosis of Parkinson's disease using measurements of dysphonia, *J. Med. Syst.,* 34 (4) 591–599.

Sakar, C. O., Serbes, G., Gunduz, A., Tunc, H. C., Nizam, H., Sakar, B. E., Tutuncu,M., Aydin, T., Isenkul, M. E., & Apaydin, H. (2019). A comparative analysis of speech signal processing algorithms for Parkinson's disease classification and the use of the tunable Q-factor wavelet transform, *Applied Soft Computing*, 74, 255-263.

Sprenger, F., & Poewe, W. (2013). Management of motor and non-motor symptoms in Parkinson's disease, *CNS drugs*, 27.4, 259-272.

Srinivasan, S. M., Martin, M., & Tripathi, A. (2017). ANN based Data Mining Analysis of the Parkinson's Disease. *International Journal of Computer Applications*, 168(1).

ORCID

Fahriye GEMCI *http://orcid.org/0000-0003-0961-5266*
Turgay IBRIKCI *https://orcid.org/0000-0003-1321-2523*

KSÜ Mühendislik Bilimleri Dergisi, 22, Özel Sayı, 2019 KSU J Eng Sci, 22, Special Issue, 2019
Uluslararası İleri Mühendislik Teknolojileri Sempozyumu (ISADET) Özel Sayısı
International Symposium on Advanced Engineering Technologies (ISADET) Symposium Special Issue
Araştırma Makalesi Research Article

Kahramanmaras Sutcu Imam University
Journal of Engineering Sciences

Geliş Tarihi : 22.07.2019 Received Date : 22.07.2019
Kabul Tarihi : 14.10.2019 Accepted Date : 14.10.2019

YAZILIM TANIMLI AĞLARDA İZLEME

MONITORING IN SOFTWARE DEFİNED NETWORKS

Hasan ÖZER [*1], *İbrahim Taner OKUMUŞ* [2]

[1] Kahramanmaraş Sütçü İmam Üniversitesi, Biyomühendislik ve Bilimleri Bölümü, Kahramanmaraş, Türkiye
[2] Kahramanmaraş Sütçü İmam Üniversitesi, Bilgisayar Mühendisliği Bölümü, Kahramanmaraş, Türkiye

*Sorumlu Yazar / Corresponding Author: Hasan ÖZER, hozer77@gmail.com

ÖZET

Ağ izleme ve ölçme, ağ yönetiminde çok önemli bir yere sahiptir. Yazılım Tanımlı Ağ (SDN), veri düzlemini ve kontrol düzlemini ayırarak ağ yönetimini kolaylaştırır. OpenFlow protokolü, veri ve kontrol düzlemi arasında güvenli bir kanalla iletişim kuran bir arayüz olarak kabul edilebilir. Aynı zamanda, OpenFlow, veri düzleminden farklı toplama seviyelerinde (örneğin akış, liman ve paket vb.) istatistik toplamamızı sağlar. Bu makalede, port bazında trafik ölçüm istatistiklerinin periyodik olarak ağ cihazlarından nasıl alınacağını ve SDN ortamında bu istatistiklerin ağa getirdiği iş yükünü nasıl hesaplanacağını gösterdik. Test ortamımızda, gerçek zamanlı trafik, periyodik trafik ve SDN'de tahmini trafik arasındaki ilişkiyi karşılaştırmak için farklı zaman aralıklarında toplanan istatistikler kullandık. Farklı zaman aralıklarında gerçekleştirilen ağ sorgulamalarında doğruluk ile ek yük arasında bir ilişki olduğunu gözlemledik. Ayrıca, istatistiklerin daha doğru yorumlanabilmesi için örnek tahmin tasarımı (SPD) ortaya koyduk. İzleme yapmak için Floodlight denetleyicisini kullandık. Sonuçlarımızın geçerliliği, Mininet'teki emülasyonlar yoluyla gösterilmektedir.

Anahtar Kelimeler: Floodlight Denetleyicisi, Mininet, Periodik Port İstatistik Toplama, SDN/OpenFlow, SPD

ABSTRACT

Network monitoring and measurement have a very important place in network management. Software Defined Network (SDN) makes network management easier by separating the data plane and the control plane. The OpenFlow protocol can be considered as an interface that communicates with a secure channel between the data and control plane. At the same time, OpenFlow allows us to collect statistics at different aggregation levels (e.g., flow, port and packet etc.) from the data plane. In this paper, we demonstrate how to get traffic measurement statistics at the port level periodically from network devices and also have calculated the overhead of this traffic measurement statistics in the SDN environment. In our test environment, collected statistics in different time intervals are used to compare relationship between real-time traffic, periodic traffic and predicted traffic in SDN. We have observed that there is a trade-off between accuracy and overhead in the network monitoring performed at different time intervals. A sample predict design (SPD) is introduced to be interpreted more accurately of the statistics. We utilize the Floodlight controller for monitoring. The validity of our results is shown through the emulations in Mininet.

Keywords: Floodlight controller, Mininet and Periodic Port Statistics Collection, SDN/OpenFlow, SPD

INTRODUCTION

Traffic engineering (TE) helps in using network resources effectively by dynamically analyzing, estimating and editing the behavior of the transmitted data (I.F. Akyildiz ve ark.,2014). Traffic Analysis/Characterization is a significant part of mechanisms for Traffic Engineering. Network monitoring and measurement mechanisms are particularly very important for determining traffic behaviors, detecting network errors, and timely intervention of network congestion.

SDN (I.F. Akyildiz ve ark., 2014; Open Networking Foundation, 2012) simplifies control of the network, provides central visibility including global network information and improves network programmability by separating the control plane from the data plane. The control plane generally arranges network states in a centralized or distributed manner through specific network policies. In addition, SDN applications take place in the application panel of SDN architecture. Applications communicate with control plane through Noth-bound APIs. The monitoring istatistics can be used quality of service (QoS), energy usage, resource utilization, security, anomaly detection and many types of network management and measurement. In addition, the data forwarding plane can operate programmable OpenFlow switches through SDN controller, and the switches can communicate with SDN the controller over South-bound Open APIs (e.g., OpenFlow protocol) (Open Networking Foundation, 2014). As a result, thanks to the communication between these planes, the SDN paradigm provides a global and holistic view of complex networks and thus it will allow network resources to be used more easily and efficiently.

OpenFlow (OF) protocol was created in 2008 at Stanford University and was developed under the Open Network Foundation (ONF) in 2008. SDN controller can program the control functionalities of switches on the network by using the OpenFlow protocol. These OpenFlow switches are managed by the policies to generate by the SDN / OF controlers. There are different versions of OpenFlow (OpenFlow Versions, 2016).

The goal of this study is to collect statistics at the port level from the OF switches in SDN environment and to generate a network status information by used this statistics. It is very important that the status information is obtained correctly and on time. Thanks to this information, network resources will be used more efficiently and flexibly. In addition, it was aimed to show the overhead brought to the system via the equations in the SDN environment and calculate them numerically. It is to show whether there is a trade-off between accuracy and overhead. It would helped to develop new network monitoring techniques according to this trade-off. A sample predict design (SPD) is proposed to be interpreted more accurately of the statistics.

RELATED WORK

Generally, network monitoring is both a neglected issue and being very important for network management. There are different approaches in network monitoring. For example, such as host-based latency measures Internet Control Message Protocol (ICMP) or network node-based queries through Simple Network Management Protocol (SNMP) (Marc Hartunga ark., 2017). In most SDN architectures are used existing streaming-based network monitoring tools that are available in traditional IP networks. For example, The most well-known is NetFlow (NetFlow, 2017) from Cisco, which collects sampled traffic statistics and sends them to a central aggregator. It uses probe methods that are installed at switches as special module. Sflow (Sflow, 2017), which uses a time-based sampling to query traffic information, is a different flow sampling method. However, these methods result in a substantial overhead when collecting statistics from an entire network of centralized controls. Therefore, it may not be an efficient solution to implement in SDN architectures.

OpenTM (A. Tootoonchian ve ark., 2010) is a query-based monitoring method that predicts the traffic matrix (TM) by querying a switch for OF networks. It periodically queries the switch on each active stream to collect flow level statistics. This design, despite its high accuracy, brings with it a high overhead. OpenNetMon periodically queries packet counters from the source and destination switches, which is appropriate for end-to-end measurement (N. L. Van Adrichem ve ark., 2104).

FlowSense (C. Yu ve ark., 2013) is a passive push-based monitoring method that uses control messages between controls and switches. It uses control messages for monitoring and calculates network usage without any additional overhead. It uses the PacketIn and FlowRemoved messages to estimate the utilization of the stream on each link. However, FlowSense cannot capture for sudden network fluctuations. This is insufficient in terms of the accuracy and timing of received statistics.

MONITORING IN SDN

To properly provision resources in SDN networks, it is important to monitor resources especially link utilizations to quickly adapt routing rules to changes in workload. There are two different measurement methods: active and passive (V. Mohan ve ark., 2011). In active measurement, agents create probe instructions to perform a network characteristic evaluation. Measurement values can provide instant network behavior information, but if this happens frequently, there is an increase in system load (Overhead). For example, the popular application ping uses ICMP packets to reliably determine end-to-end connection status and compute a paths round-trip time (D. Erickson, 2013).

Passive measurement methods does not generate any traffic to the network. Instead, it provides traffic statistics from network devices. Because the passive approach measures actual network traffic, it does not generate additional test traffic on the network. However, all this information is stored on these network devices, both causing security problems and leads to the installation of in-network traffic monitors that are not suitable for all networks and require large investments.

By using statistics collection mechanisms provided by OpenFlow specification, over a specific network topology, statistics from switches can be obtained. There are two basic types of statistics collection messages provided by OpenFlow:

STATISTICS REQUEST MESSAGE: Message for requesting statistical data for ports, flows, etc. from switches.

STATISTICS REPLY MESSAGE: Message for replying a statistics request by providing requested statistical data for ports, flows, etc.

The monitoring work in SDN is done by connecting the controller to all switches with a secure channel. The controller and switches use this secure channel through a TCP connection. The controller obtains real-time flow statistics from the available switches and combines the raw data by providing interfaces for the applications in the top layer.

An important issue here is how to make monitoring on the SDN environment. Firstly, statistics request messages are sent to the OF switches at fixed intervals, then the statistic reply messages which containing the amount of data and duration on at that time in network are send from OF switches to controller. The amount of data and duration content in statistic reply messages is called as sample. According to these samples from the switches, controller can generate new network status policies for network management. In addition, controller can determine new polling intervals by evaluating samples from switches.

In this study we used these two messages to get port level traffic measurement statistics from switches in an SDN network. In the next section we provide the details of the test environment and measurement setup.

TEST ENVIRONMENT AND EVALUATION RESULTS

Network topology in Fig.2 is used in our study. We used Mininet (The mininet platform, 2106) to setup the network topology with virtual hosts and switches. It is a network emulator which creates a network of virtual hosts, switches, controllers, and links. Its hosts run standard Linux network software, and its switches support OpenFlow for highly flexible custom routing and Software-Defined Networking.

OpenFlow controllers (e.g., Floodlight (Floodlight, 2017), NOX (N. Gude ve ark., 2008), etc.) introduce a platform to write special network applications. Floodlight is one of the popular controller currently used in the SDN environment. In this sample test topology, we used Floodlight as a controller. Floodlight is a Java-based OF controller that supports physical and virtual OF switches. It is based on the Beacon application. Beacon (D. Erickson, 2013) was created by David Erickson at Stanford University.

OpenFlow is the basic SouthBound API of SDN. Nowadays, it is widely used both in the industry and in the academy. OpenFlow is an interface that enables communication between the control plane and the data plane.

Overhead is the additional load that the OF messages used in the SDN environment bring to the network system by queries made at certain time intervals. Overhead is calculated by using topology in Fig. 2. and timing diagram in Fig. 3. Making this calculation will have an important knowledge in developing new inquiry techniques.

To obtain all flow statistics, it is necessary to obtain statistics from the switches for each flow along the path and combine the results. We study is an undirected graph $G=(V,E)$, where $V=\{v_1,v_2,v_2,...,v_k\}$ is the set of switches and E denotes the set of links. Hence $k=|V|$ is the number of switches in the network. In order to calculate the overhead of statistics collection we need to analyze the sizes of statistics request and reply messages. Equation (1) is the size of the reply messages for k flow entry and Equation (2) provides total message sizes for both request and reply for a single switch. Here, $L_{Request}$ represents the size of the flow statistics request message, L_{Rh} represents the length of flow statistics reply message header, L_{Sfe} represents the size of reply message body of a single flow entry, p represent the port numbers of each switch. For a flow statistics reply message with p entries, the whole reply message length $L_{Reply(p)}$ is a linear function:

$$L_{Reply(p)} = L_{Rh} + p * L_{Sfe} \tag{1}$$

$$W_n = k * (L_{Request} + L_{Reply(p)}) \tag{2}$$

According to the OpenFlow specification, size of these messages are as follows: $L_{Request}=$ 122 byte, L_{Rh}= 78 bytes, $L_{Sfe}=$ 96 bytes and n denotes the polling frequency.

Sample Predict Design (SPD):

In network management, accurate measures of network status are needed to aid planning, troubleshooting, and monitoring. For example, it may be necessary to monitor the bandwidth consumption of several hundred links in a distributed system to pinpoint bottlenecks (Edwin A ve ark., 2000).

Nowadays, there are many measurement sampling methods. Sampling techniques are used to examine the behavior of a member population according to a representative subset. In fact, samples are periodically taken at a constant interval. However, as shown in Figure 3, 4 and 5 under some heavy traffic loads, static periodic sampling may not be suitable for the monitoring task. For example, a long sampling interval provides sufficient accuracy when traffic is not dense or there is a low network load. However, in high traffic fluctuations, shorter sampling intervals are required to accurately measure network situations. In this case, it also imposes an excessive overhead on the network. Therefore, there is a need for adaptive inquiry technique that dynamically adjust the interrogation interval based on network fluctuations. Although adaptive inquiry techniques are not studied in this paper, prediction methods that we studied in this paper will provide insights to design efficient adaptive techniques in future studies.

In this section, we present a Sample Predict Design (SPD) to predict the traffic rate of the next sample. The SPD is calculation that is used to select the most representative examples of the population by polling and following the significant fluctuations in the measured variables.

Equations (3) provide the details of sample prediction. Here $S_{Samples}$ denotes past N samples where N is the latest sample received and $S_{Predict}$ denotes the estimated value of the next sample to be received.

$$S_{Samples} = S_1, S_2, S_3, ..., S_N$$

$$S_{Total} = \sum_{i=1}^{N-1} S_i$$

$$S_{Avg} = \frac{S_{Total}}{N-1}$$

$$S_{Predict} = (1-\lambda) * S_N + \lambda * S_{Avg} \tag{3}$$

Where $0 < \lambda < 1$ (e.g., $\lambda = 0.125$) when calculating $S_{Predict}$, by adjusting the value of λ the weight of the most recent sample and average of the previous samples can be changed. Lower λ will increase the weight S_N and decrease the weight of S_{Avg}.

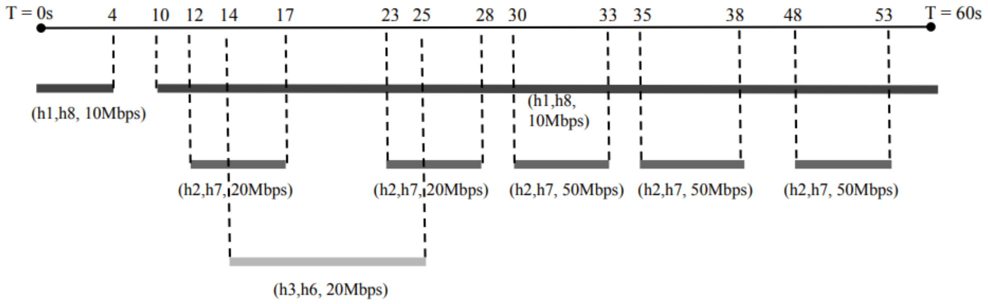

Figure 1. Timing Diagram of Experiment Traffic

To get the analysis results we have created a 3-level tree topology via Mininet and timing diagram shown respectively in Fig. 1 and Fig. 2. which are the same as Payless (S. R. Chowdhury ve ark., 2014) in this analysis. UDP flows for a total duration of 100s between hosts were generated using Iperf (Iperf: TCP/UDP Bandwidth Measurement Tool). Figure 1 shows the timing diagram; start, throughput and end time for each stream. In addition, we have paused traffic at different times between traffic streams to try different scenarios.

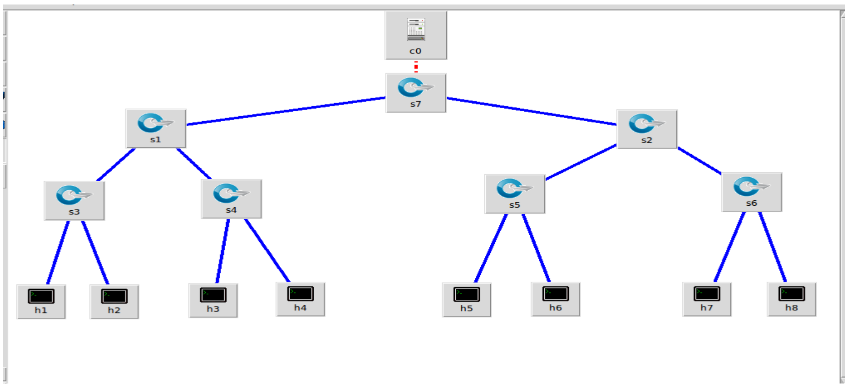

Figure 2. Generated Topology for Experiment

Overhead:

An important issue that needs to be explained here is how inquiries are made and the resulting network overhead (message overhead). OpenFlow defines a flow using fields from different layer (such as, layer 2, 3, 4) header of a package. When a switch receives a stream that does not comply with the rules in the routing table, it sends a PacketIn message to the controller. The control sends a FlowMod message to generate the necessary routing rules for the switches. The controller can specify idle timeout for a routing rule. This is referred to as the prologue of inactivity, after which a routing rule is removed from the switch. When this stream is removed, the switch sends a FlowRemoved message to the controller. This message contains the flow time and the number of bytes that match this flow input in the switch. In addition to these messages, the controller can send a FlowStatisticsRequest message to the switch for information about a particular flow. The switch sends the number of times and bytes for this stream to the controller in a FlowStatisticsReply message.

As shown in Table 1. we have considered the FlowStatisticsRequest message and the FlowStatisticsReply message as overhead. We calculated the overhead of the queries made at different frequencies by using topology created in Figure 2. We used the Equation (1) and (2) when calculating the overhead. The table shows us that the burden on the system is observed to be very high in the monitoring performed at the high interrogation intervals, while it is observed that the load coming to the system is less in the monitoring performed at lesser interrogation intervals.

$$L_{Reply(p)} = L_{Rh} + p * L_{Sfe} \quad (1)$$

$$L_{Reply(p)} = 78 + (96 * 20) = 1998 byte$$

$$W_n = k * (L_{Request} + L_{Reply(p)}) \quad (2)$$

$$W_n = 7 * (122 + 1998) = 14840 byte$$

According to Figure 2, $p = 20, k = 7$.

Table 1. Overhead at Different Time Intervals According to (1) and (2) Equations for Figure 1.

Polling frequency	**Overhead (byte) according to total duration of 100 sec**
1 sec	$W_1 = 14840 * 100 = 1484000 byte$
5 sec	$W_5 = 14840 * 20 = 296800 byte$
10 sec	$W_{10} = 14840 * 10 = 148400 byte$

Figure 1. In the time diagram shown, the UDP stream of 10 mbps between host1 (H1) and host8 (h8), the UDP stream of 20 and 50 Mbps respectively between the host2 (H2) and the host7 (h7), the host3 (H3) and the main host6 (h6) 20 Mbps UDP stream traffic is generated. To see fluctuations in traffic, flows are paused at specific time intervals. The traffic generated according to the timing diagram in Figure 1. is monitored with 1 second, 5 second and 10 second monitoring frequencies. The results are shown in Figure 3, 4 and 5. Different flow times are used to test accuracy and performance.

Figure 3, 4 and 5 show that the overhead in the system is higher in the polling which are done frequently and the effect on accuracy increases. On the other hand, when we conduct polling interval over long time intervals, the overhead it brings to the system is less, but the effect on accuracy is low. This is a situation we don't want. The relationship between the value of the periodic queries and the real-time monitoring value at different time intervals was determined graphically in Figure. 3, 4 and 5. These graphs show us that a high-frequency inquiries in the SDN environment, a close real-time monitoring is seen. On the other hand, the overhead that it brings to the system is observed to increase. As a result, we have observed that there is a trade-off between accuracy and overhead in the network monitoring performed at different time intervals.

According to these analyzes, we need a design that will act according to our traffic density. In this case, if the traffic density is increasing we will need to use frequent query intervals, if not, we should use less query interval. Thus, we can stabilize both the system overhead and the system accuracy. We also think that using the $S_{Predict}$ equation in the SPD can help with these adaptive monitoring designs. As shown in Figures 3, 4 and 5, we have taken close to polling periodically.

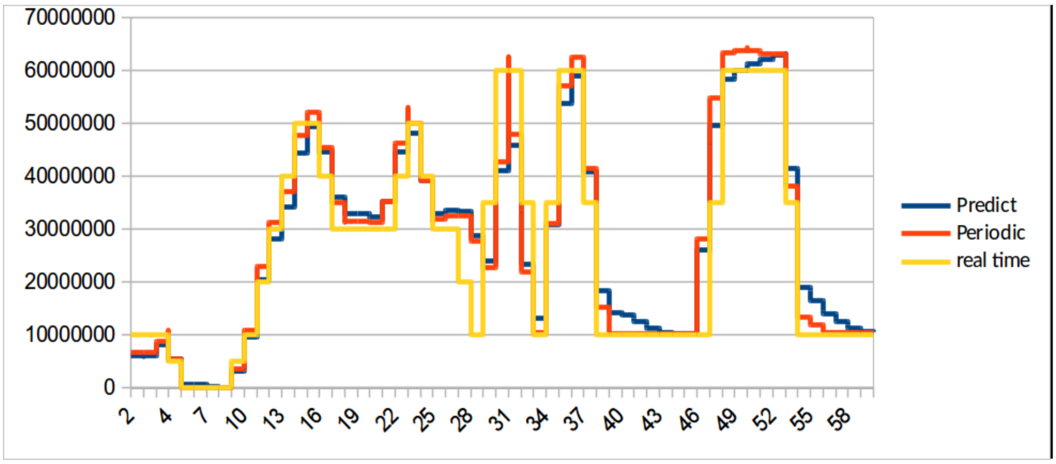

Figure 3. 1 sec Monitoring Frequency

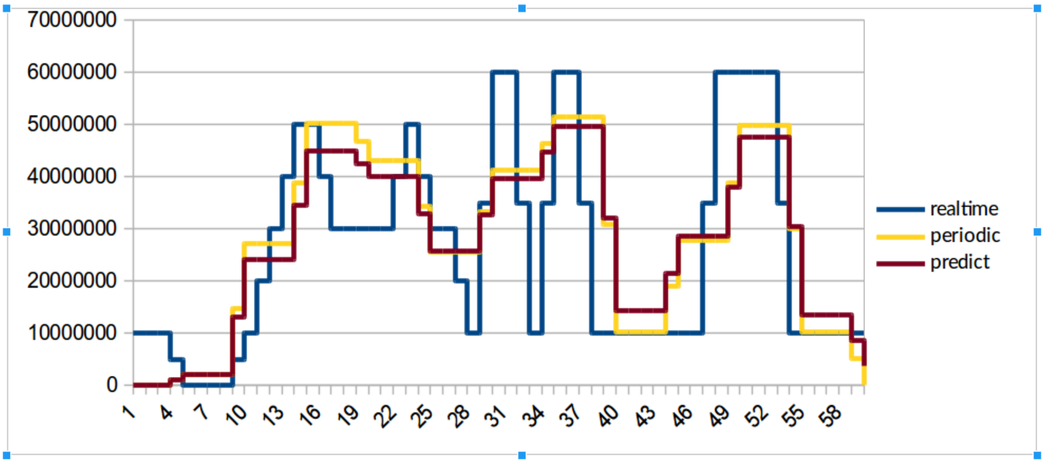

Figure 4. 5 sec Monitoring Frequency

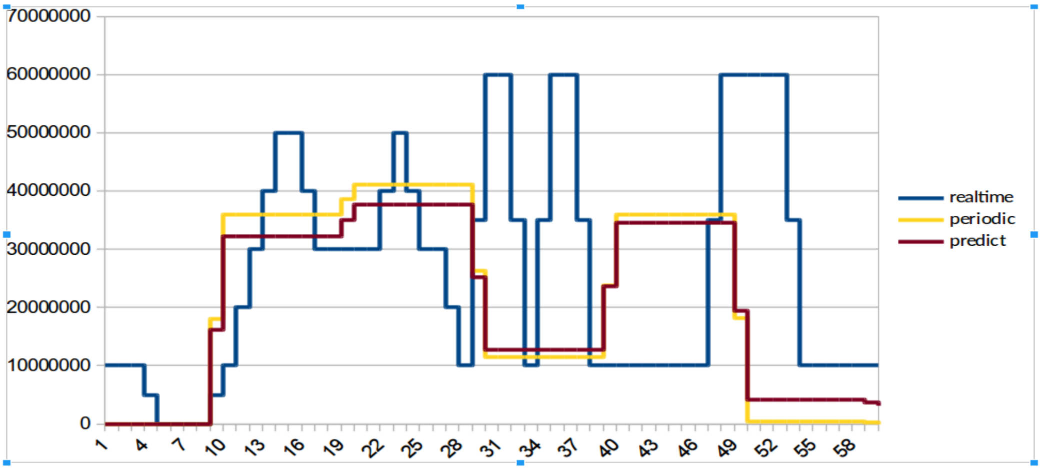

Figure 5. 10 sec Monitoring Frequency

CONCLUSIONS AND FUTURE WORK

In this article, we get periodically traffic measurement statistics at the port level from network devices in an SDN environment. The calculation of the overhead of these monitoring is shown by equations and calculated numerically. As a result of the analysis, we have shown that there is a trade-off between the overhead and the accuracy. At the same time, we present our SPD design, which could help new adaptive monitoring methods.

Our future study is to develop an adaptive inquiry techniques that can be adapted to the intensity of traffic using our SPD design.

REFERENCES

I. F. Akyildiz, A. Lee, P. Wang, M. Luo, and W. Chou, “A roadmap for traffic engineering in SDN-OpenFlow networks,” Computer Networks, vol. 71, pp. 1–30, 2014.

Open Networking Foundation: OpenFlow Switch Specification version 1.5.0 (2014). https://www.opennetworking.org/software-defined-standards/specifications

OpenFlow Versions, updated Apr 26, 2016.
https://floodlight.atlassian.net/wiki/spaces/floodlightcontroller/pages/1343541/Releases+and+Roadmap

Marc Hartunga, Marc K¨ornerb “SOFTmon - Traffic Monitoring for SDN” Procedia Computer Science 110 (2017) 516–523.

Open Networking Foundation: Software Defined Networking: The new norm for networks, White paper (2012).

NetFlow, Mar. 14, 2017. [Online]. Available: http://www.cisco.com/go/netflow

sFlow, Mar. 14, 2017. [Online]. Available: http://www.sflow.org/

A. Tootoonchian, M. Ghobadi, Y. Ganjali, Opentm: traffic matrixestimator for openflow networks, in: Proceedings of the 11thInternational Conference on Passive and Active Measurement,PAM’10, April 2010, pp. 201–210.

N. L. Van Adrichem, C. Doerr, and F. A. Kuipers, “OpenNetMon: Network monitoring in OpenFlow software-defined networks,” in Proc. IEEE Netw. Oper. Manage. Symp., 2014, pp. 1–8.

C. Yu, C. Lumezanu, Y. Zhang, V. Singh, G. Jiang, H.V. Madhyastha,Flowsense: monitoring network utilization with zero measurementcost, in: Proceedings of the 14th International Conference onPassive and Active Measurement, PAM’13, March 2013, pp. 31–41.

V. Mohan, Y. J. Reddy, and K. Kalpana, “Active and passive network measurements: A survey,” Int. J. Comput. Sci. Inf. Technol., vol. 2, no. 4, pp. 1372–1385, 2011.

D. Erickson, The Beacon OpenFlow Controller. In Proceedings of the ACM Workshop on Hot Topics in Software Defined Networks (HotSDN), Hong Kong, China, 12–16 August 2013; pp. 13–18.

The mininet platform, Retrieved March 20, 2016. http://mininet.org/ .

Floodlight, Mar. 14, 2017. [Online]. Available: http://www.projectfloodlight.org/floodlight/

N. Gude, T. Koponen, J. Pettit, B. Pfaff, M. Casado, N. McKeown, and S. Shenker, “NOX: Towards an operating system for networks,” SIGCOMM Comput. Commun. Rev., vol. 38, no. 3, pp. 105–110, 2008.

Edwin A. Hernandez, Matthew C. Chidester, and Alan D. George, “Adaptive Sampling for Network Management,“ journal of Network and Systems Management, Vol.9, No. 4, December 2000.

S. R. Chowdhury, M. F. Bari, R. Ahmed, and R. Boutaba, “PayLess: A Low Cost Network Monitoring Framework for Software Defined Networks,” in NOMS, 2014

Iperf: TCP/UDP Bandwidth Measurement Tool. http://iperf.fr/

ORCID

Hasan ÖZER *http://orcid.org/0000-0002-0729-676X*
İbrahim Taner OKUMUŞ *http://orcid.org/0000-0001-9495-3133*

KSÜ Mühendislik Bilimleri Dergisi, 22, Özel Sayı, 2019 KSU J Eng Sci, 22, Special Issue, 2019
Uluslararası İleri Mühendislik Teknolojileri Sempozyumu (ISADET) Özel Sayısı
International Symposium on Advanced Engineering Technologies (ISADET) Symposium Special Issue
Araştırma Makalesi Research Article

Kahramanmaras Sutcu Imam University
Journal of Engineering Sciences

Geliş Tarihi : 23.07.2019 Received Date : 23.07.2019
Kabul Tarihi : 14.10.2019 Accepted Date : 14.10.2019

VOLTAGE DEPENDENCE OF SOME NEMATIC LIQUID CRYSTALS' ELECTRIC PROPERTIES

BAZI NEMATİK SIVI KRİSTALİN ELEKTRİK ÖZELLİKLERİNİN GERİLİME BAĞLILIĞI

Şükrü ÖZĞAN *[*1], *Hasan ESKALEN* [2]

[1]Kahramanmaraş Sütçü İmam Üniversitesi, Fizik Bölümü, Kahramanmaraş, Türkiye
[2] Kahramanmaraş Sütçü İmam Üniversitesi, Malzeme Bilimi ve Mühendisliği Programı, Kahramanmaraş, Türkiye

*Sorumlu Yazar / Corresponding Author: Şükrü ÖZĞAN, ozgans@gmail.com

ABSTRACT

The nematic liquid crystals that are very important materials, using in the production of display systems and many technological applications. Due to this reason, it is important to investigate the physical and electrical properties of the nematic liquid crystals Voltage dependence of impedance, modulus and loss tangent of hexylcyanobiphenyl (6CB), octlycyanobiphenyl (8CB) pure and E7 coded nematic liquid crystal mixture were investigated at 0-20V DC volts range, room temperature and 1 kHz frequency. Although some electrical properties of mentioned liquid crystals exists in literature, comparison of these three liquid crystals has not been studied before. The real electric modulus of the 6CB and 8CB samples shows a small increase due to the increase in voltage and real modulus values of 8CB is higher than real modulus values of 6CB. The real modulus of the E7 nematic liquid crystal mixture decrease with increasing voltage. The imaginary electric modulus of the samples is decrease with voltage increase. The loss tangent values of the 6CB and 8CB samples decreases after a certain voltage value. Absolute impedance of the 6CB, 8CB samples have wavy behavior and the absolute impedance of E7 approaches zero at all voltage values.

Keywords: Nematic liquid crystals, 6CB, 8CB, E7, modulus, impedance.

ÖZET

Nematik sıvı kristaller, gösterge sistemleri üretiminde ve birçok teknolojik uygulamalarda kullanılan çok önemli malzemelerdir. Bu nedenden dolayı nematik sıvı kristallerin fiziksel ve elektriksel özelliklerinin araştırılması önemlidir. Hexylcyanobiphenyl (6CB), octlycyanobiphenyl (8CB) saf ve E7 kodlu nematik sıvı kristal karışımların empedans, modül ve kayıp tanjantı, oda sıcaklığında ve 1 kHz frekansında, 0-20V DC volt aralığında gerilime bağlı olarak incelenmiştir. Bahsi geçen sıvı kristallerin bazı elektriksel özellikleri ile ilgili bilgiler literatürde bulunmasına rağmen, literatürde bu üç sıvı kristallerin elektriksel özelliklerinin karşılaştırması ile ilgili bir çalışmaya daha önce rastlanmamıştır. 6CB ve 8CB numunelerin gerçek elektrik modülü gerilimdeki artıştan dolayı küçük bir artış gösterir ve 8CB gerçek modül değerleri 6CB gerçek modül değerlerinden daha büyüktür. E7'nin gerçek modülü ise gerilim artması ile azalmaktadır. Numunelerin sanal elektrik modülü voltaj artışı ile azalır. 6CB ve 8CB numunelerin kayıp tanjant değerleri, belirli bir voltaj değerinden sonra azalmaktadır. 6CB ve 8CB numunelerin mutlak empedansı dalgalı davranışa sahiptir ve E7 nin mutlak empedans değeri bütün voltaj değerlerinde sıfıra yaklaşmaktadır.

Anahtar Kelimeler: Nematik sıvı kristaller, 6CB, 8CB, E7, modül, empedans.

INTRODUCTION

Thermotropic liquid crystals are mesophase between the crystalline solid and isotropic liquid. Some organic substances pass through solid, mesopases as semectic, collesteric, nematic liquid crystals (LC's) and isotropic liquid phases due to increase in temperature (Bahadur, 1990; Vill, 1992). Nematic LC's are very important materials for display systems. Due to these important features, LC's have a wide range of applications in technology (Shen & Dierking, 2019). They are used for television, computer, machines display systems, electro-optic filters-lens (Lee, Gau, & Chen, 2005), holography (Chen & Brady, 1992), digital data storage (Matharu, Jeeva, & Ramanujam, 2007) and biosensor.

Due to the increasing importance of liquid crystals, many theoretical as Maier-Soupe and Mean Field theory (Özğan & Keskin, 1995; Wulf, 1976) and experimental researches (Eskalen, Kerli, & Özğan, 2017; Gupta & Kumar, 2019; Nafees, Kalita, & Sinha, 2019; Nimmy, Cherumannil Karumuthil, & Varghese, 2019; Okumus, 2013; Özğan & Okumuş, 2011; Ozgan, Yazici, & Ates, 2011; Sharma, Malik, Dhar, & Kumar, 2019) are carried out. Different types of liquid crystals are needed for different applications. This need is achieved by synthesizing new liquid crystals, mixing in two or more LCs, polymer, nano particles or dyes (Mahalingam, Venkatachalam, Jayaprakasam, & Vijayakumar, 2016; Okumuş, Özğan, Kırık, & Kerli, 2016; Okumuş, Özğan, & Yılmaz, 2014). The physical properties such as thermal, optical, dielectric and optical anisotropy and structural properties of two or more liquid crystal mixtures is investigated (Eskalen, Okumuş, & Özğan, 2019; Eskalen & Özğan, 2014; Özğan; Shiju et al., 2017). Thermal, electro-optical, properties were investigated by mixing zinc oxide, gold, graphene oxide nanoparticles and dyes in nematic liquid crystals (Eskalen, Özğan, Alver, & Kerli, 2015; Eskalen, Özğan, Okumuş, & Kerl, 2019; Okumuş, Eskalen, Sünkür, & Özğan, 2019; Özğan, Eskalen, & Tapkıranlı, 2018; Ye et al., 2016).

Although some electrical properties of 6CB, 8CB and E7 nematic liquid crystals exists in literature, comparison of these three liquid crystals has not been studied before. In this work, voltage dependent some electrical properties as modulus, impedance and lost tangent of hexylcyanobiphenyl (6CB), octylcyanobiphenyl (8CB) and E7 coded mixture nematic liquid crystals is examined under 1 kHz frequency from 0-20V DC volts at room temperature.

MATERIAL AND METHOD

The 6CB and 8CB nematic liquid crystals used in the present study was obtained from Sigma-Aldrich company. The E7 coded eutectic mixture nematic liquid crystal was purchased from Faculty of Advanced Technologies and Chemistry Military University of Technology (Poland). Compose of four different nematic liquid crystals The E7 nematic liquid crystal was obtained by adding different proportions of four different nematic liquid crystals. The E7 liquid crystal compose of 5CB, 7CB, 8OCB and 7CT with proportions 51%,25%,16% and 8% respectively. The molecular structures of the nematic liquid crystals used in this study are shown in Figure 1.

Name	Molecular structure
6CB	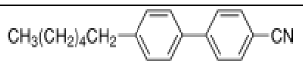
8CB	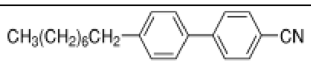
E7 Mixture	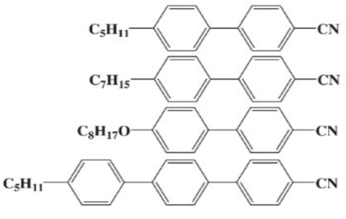

Figure 1. The Molecular Structures of the 6CB, 8Cb and E7 Nematic Liquid Crystals

The planer alignment LC cells with cell gaps 8 μm and 1 cm^2 active area were purchased from Instec, Inc USA. To measurement the electrical properties of the 6CB, 8CB and E7 nematic liquid crystal samples were filled using capillarity method in indium tin oxide (ITO) cells.

Voltage dependence of the modulus, impedance and lost tangent of the 6CB, 8CB and E7 nematic liquid crystal samples were performed by HP 4194A Impedance Analyzer under 1 kHz frequency from 0-20V DC volts at room temperature.

RESULTS and DISCUSSION

The complex electric modulus can be a significantly powerful tool for analyzing dielectric behavior of some material. The complex electric modulus (M^*) is defined as the inverse of the complex dielectric constant (ε^*) and is represented as;

$$M^* = (\varepsilon^*)^{-1}$$
$$M' + iM'' = (\varepsilon' + i\varepsilon'')/(\varepsilon'^2 + \varepsilon''^2) \quad (1)$$

Where M' and M'' are the real and imaginary parts of the electric modulus; $\varepsilon'$and $\varepsilon''$are the real and imaginary parts of the dielectric constant respectively.

The variation of the real electric modulus of the 6CB, 8CB and E7 samples depend on voltage is shown in Figure 2. The Figure 2 is obtained between 1-20V DC voltage range at 1 kHz frequency and the room temperature.

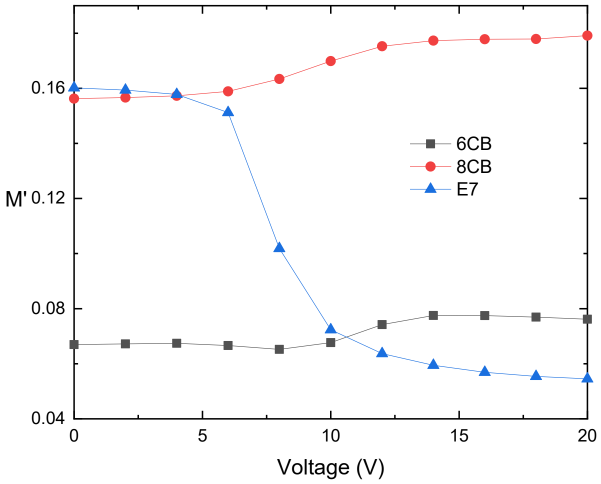

Figure 2. The Real Electric Modulus of The 6CB, 8CB and E7.

The real electric modulus of the 6CB and 8CB samples have a behavior as fixed at low voltages, then they increase with increase in voltage. The values of 8CB modulus are higher than 6CB modulus at all voltages. The values of E7 modulus are big at low voltages and they are small at high voltages. E7 modulus has a damping of around 7 volt.

The variation of the imaginary electric modulus of the 6CB, 8CB and E7 samples depend on voltage is shown in Figure 3. The Figure 3 is obtained between 0-20V voltage range at 1 kHz frequency and the room temperature. The imaginary electric modulus of the 6CB and 8CB samples have a behavior as fixed at low voltages, then they decrease with increase in voltage. The imaginary electric modulus value of 8CB liquid crystal is greater than 6CB and E7 modulus value at all voltages. The values of E7 modulus have a wavy behavior with increase in voltage.

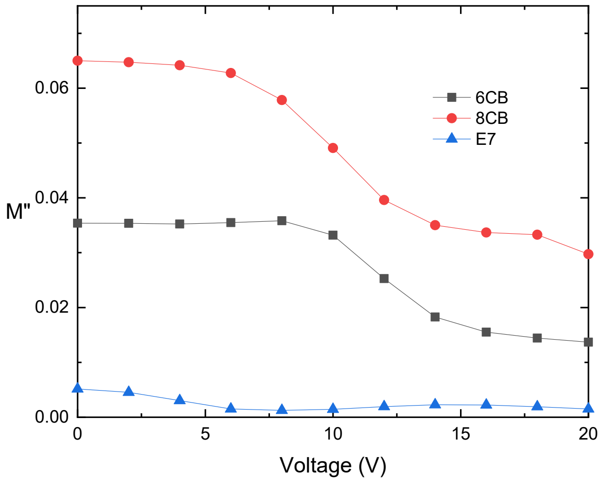

Figure 3. The Imaginary Electric Modulus of the 6CB, 8CB and E7.

The imaginary part of the dielectric constant is known as the loss tangent and calculated by the equation;

$$\varepsilon'' = \varepsilon' tan\delta \tag{2}$$

where $\delta = 90 - \phi$ and ϕ is the phase angle. Variation the loss tangent($tan\delta$) of the 6CB, 8CB and E7 samples with voltage are given in Figure 4.

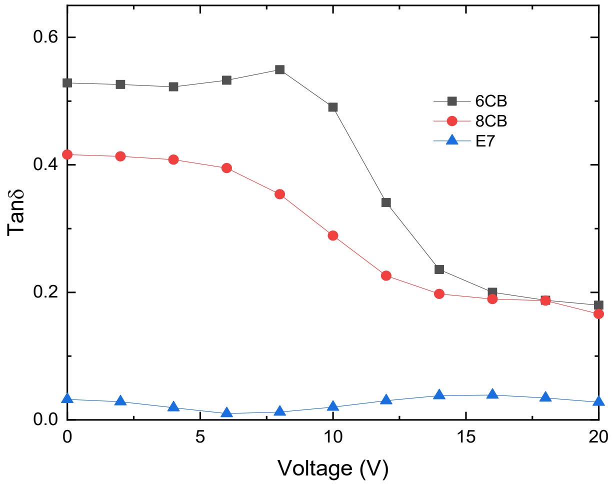

Figure 4. The Loss Tangent of the 6CB, 8CB and E7.

The loss tangent of the 6CB and 8CB samples have a behavior as fixed at low voltages, then they decrease with increase in voltage. The loss tangent value of 8CB liquid crystal is greater than 6CB and E7 modulus value at all voltages. The values of E7 loss tangent are low and having a wavy behavior with increase in voltage.

The variation of the impedance of the 6CB, 8CB and E7 samples depend on voltage is shown in Figure 5. The Figure 5 is obtained between 1- 20V voltage range at 1 kHz frequency and room temperature. Absolute impedance of 6CB sample has wavy behavior ranging from 108-116 kΩ. Absolute impedance of 8CB sample increases with increase in voltage from 250-270 kΩ. The impedance value of the E7 liquid crystal is zero for all voltages at 1kHz frequency.

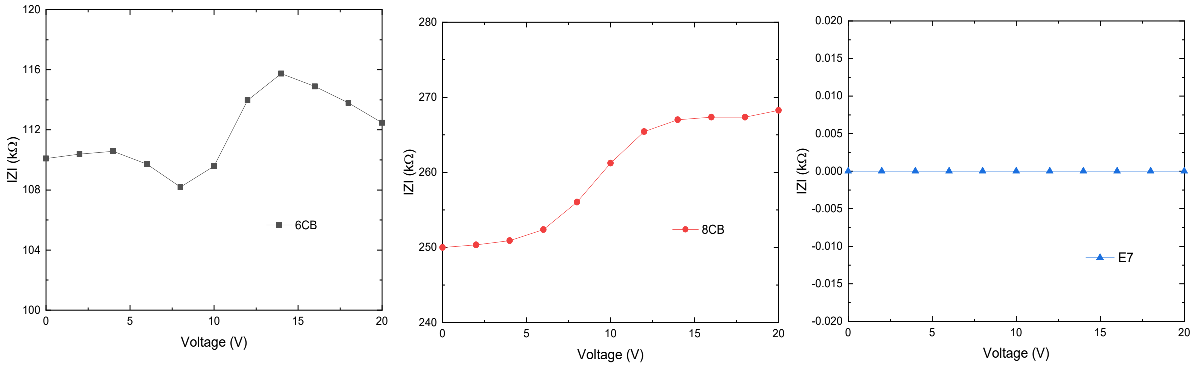

(a) (b) (c)

Figure 5. The Variation of Impedance with Voltage at 1kHz Frequency a) 6CB, b) 8CB and c) E7.

CONCLUSION

The nematic liquid crystals are used display systems and many technological applications. Voltage dependence of the real and imaginary modulus, impedance and lost tangent of hexylcyanobiphenyl (6CB), octylcyanobiphenyl (8CB) and E7 coded nematic liquid crystals as have been investigated under 1 kHz frequency from 0-20V DC volts at room temperature. The 6CB and 8CB real electric modulus have a behavior as fixed at low voltages, then they increase with increase in voltage. The 8CB modulus are higher than 6CB modulus at all voltages. The modulus of E7 is high at low voltages and getting decrease with increasing voltages. The imaginary electric modulus of the 6CB and 8CB samples have a behavior as fixed at low voltages, then they decrease with increase in voltage. The 8CB imaginary electric modulus value is greater than 6CB and E7 modulus value at all voltages. The E7 modulus have a wavy behavior. The loss tangent of the 6CB and 8CB samples have a behavior as fixed at low voltages, then they decrease with increase in voltage. The 8CB loss tangent value is greater than 6CB and E7 modulus value at all voltages. The E7 loss tangent are low and having a wavy behavior. 6CB absolute impedance has wavy behavior ranging from 108-116 kΩ. 8CB absolute impedance increases with increase in voltage from 250-270 kΩ.

REFERENCES

Bahadur, B. (1990). Liquid crystals: applications and uses (Vol. 1): World scientific.

Chen, A. G., & Brady, D. J. (1992). Real-time holography in azo-dye-doped liquid crystals. Optics letters, 17(6), 441-443.

Eskalen, H., Kerli, S., & Özğan, Ş. (2017). Hydrothermally produced cobalt oxide nanostructures at different temperatures and effect on phase transition temperature and threshold voltage of nematic liquid crystal host. Cobalt, InTech, 71-85.

Eskalen, H., Okumuş, M., & Özğan, Ş. (2019). Electro-optical, thermal and dielectric properties of ternary mixture of E7/6CB/6BA liquid crystal mixture complex. Optik, 187, 223-229.

Eskalen, H., & Özğan, Ş. (2014). Altın Nanoparçacıklarla Katkılandırılan Nematik Sıvı Kristallerin İncelenmesi. Düzce Üniversitesi Bilim ve Teknoloji Dergisi, 2(2), 407-414.

Eskalen, H., Özğan, Ş., Alver, Ü., & Kerli, S. (2015). Electro-Optical Properties of Liquid Crystals Composite with Zinc Oxide Nanoparticles. Acta Physica Polonica, A., 127(3).

Eskalen, H., Özğan, Ş., Okumuş, M., & Kerl, S. (2019). Thermal and Electro-optical Properties of Graphene Oxide/Dye-Doped Nematic Liquid Crystal. Brazilian Journal of Physics, 49(3), 341-347.

Gupta, R. K., & Kumar, S. (2019). Effect of functionalised silver nanoparticle on the elastic constants and ionic transport of a nematic liquid crystal. Liquid Crystals, 1-9.

Lee, W., Gau, J.-S., & Chen, H.-Y. (2005). Electro-optical properties of planar nematic cells impregnated with carbon nanosolids. Applied Physics B, 81(2-3), 171-175.

Mahalingam, T., Venkatachalam, T., Jayaprakasam, R., & Vijayakumar, V. (2016). Optical, thermal studies on binary and ternary hydrogen-bonded liquid crystal complexes. Brazilian Journal of Physics, 46(3), 273-281.

Matharu, A. S., Jeeva, S., & Ramanujam, P. (2007). Liquid crystals for holographic optical data storage. Chemical Society Reviews, 36(12), 1868-1880.

Nafees, A., Kalita, G., & Sinha, A. (2019). Effect of titanium dioxide nanoparticles on the dielectric and electro-optical properties of bent-core liquid crystals. Journal of Molecular Liquids, 274, 592-597.

Nimmy, J. V., Cherumannil Karumuthil, S., & Varghese, S. (2019). Nano P (VDF-TrFE) doped polyimide alignment layers for twisted nematic liquid crystal devices. Liquid Crystals, 1-6.

Okumus, M. (2013). Investigation of the phase transition and absorption properties of liquid crystal hexylcyanobiphenyl/octylcyanobiphenyl mixtures. Asian Journal of Chemistry, 25(7), 3879.

Okumuş, M., Eskalen, H., Sünkür, M., & Özğan, Ş. (2019). Mesogenic properties of PAA/6BA binary liquid crystal complexes. Journal of Molecular Structure, 1178, 428-435.

Okumuş, M., Özğan, Ş., Kırık, İ., & Kerli, S. (2016). Thermal and optical characterization of liquid crystal 4′-hexyl-4-biphenylcarbonitrile/4-hexylbenzoic acid mixtures. Journal of Molecular Structure, 1120, 150-155.

Okumuş, M., Özğan, Ş., & Yılmaz, S. (2014). Thermal and optical properties of some hydrogen-bonded liquid crystal mixtures. Brazilian Journal of Physics, 44(4), 326-333.

Özğan, Ş. Investigating of dielectric anisotropy and birefringence of binary liquid crystal mixtures. International Journal of Chemistry and Technology, 1(1), 1-6.

Özğan, Ş., Eskalen, H., & Tapkıranlı, Y. (2018). Thermal and electro-optic properties of graphene oxide-doped hexylcyanobiphenyl liquid crystal. Journal of Theoretical and Applied Physics, 12(3), 169-176.

Özğan, S., & Keskin, M. (1995). A Theory of Melting of Molecular Crystals III. The Liquid Crystalline Phase. Molecular Crystals and Liquid Crystals Science and Technology. Section A. Molecular Crystals and Liquid Crystals, 270(1), 147-157.

Özğan, Ş., & Okumuş, M. (2011). Thermal and spectrophotometric analysis of liquid crystal 8CB/8OCB mixtures. Brazilian Journal of Physics, 41(2-3), 118.

Ozgan, S., Yazici, M., & Ates, K. (2011). Conductance and Dielectric Anisotropy Properties of 4'-Hexyl-4-biphenylcarbonitrile and 4'-Octyloxy-4-biphenylcarbonitrile Liquid Crystals and Their Composite. Asian Journal of Chemistry, 23(7), 3247-3251.

Sharma, A., Malik, P., Dhar, R., & Kumar, P. (2019). Improvement in electro-optical and dielectric characteristics of ZnO nanoparticles dispersed in a nematic liquid crystal mixture. Bulletin of Materials Science, 42(5), 215.

Shen, Y., & Dierking, I. (2019). Perspectives in Liquid-Crystal-Aided Nanotechnology and Nanoscience. Applied Sciences, 9(12), 2512.

Shiju, E., Arun, R., Varma, M. R., Chandrasekharan, K., Sandhyarani, N., & Varghese, S. (2017). Effect of ferroelectric nanoparticles in the alignment layer of twisted nematic liquid crystal display. Optical Materials, 67, 7-13.

Vill, V. (1992). Early history of liquid crystalline compounds. Molecular Crystals and Liquid Crystals Science and Technology. Section A. Molecular Crystals and Liquid Crystals, 213(1), 67-71.

Wulf, A. (1976). Difficulties with the Maier–Saupe theory of liquid crystals. The Journal of Chemical Physics, 64(1), 104-109.

Ye, L., Liu, B., Li, F., Feng, Y., Cui, Y., & Lu, Y. (2016). The influence of Ag nanoparticles on random laser from dye-doped nematic liquid crystals. Laser Physics Letters, 13(10), 105001.

ORCID

Şükrü ÖZĞAN *http://orcid.org/0000-0001-9334-327X*
Hasan ESKALEN *https://orcid.org/0000-0002-4523-6573*

KSÜ Mühendislik Bilimleri Dergisi, 22, Özel Sayı, 2019 KSU J Eng Sci, 22, Special Issue, 2019
Uluslararası İleri Mühendislik Teknolojileri Sempozyumu (ISADET) Özel Sayısı
International Symposium on Advanced Engineering Technologies (ISADET) Symposium Special Issue
Araştırma Makalesi Research Article

Kahramanmaras Sutcu Imam University
Journal of Engineering Sciences

Geliş Tarihi : 24.07.2019 Received Date : 24.07.2019
Kabul Tarihi : 21.10.2019 Accepted Date : 21.10.2019

BENDING STRENGTH AND STRUCTURAL HEALING PROPERTIES OF CARBON/PP(POLYPROPYLENE)/EPOXY COMPOSITES

KARBON/PP(POLİPROPİLEN)/EPOKSİ KOMPOZİTLERİN EĞİLME DAYANIMI VE YAPISAL İYİLEŞME ÖZELLİKLERİ

*Gaye KAYA*and Pınar ÇAM*

Kahramanmaras Sutcu Imam University, Department of Textile Engineering, Kahramanmaras, Turkey

*Sorumlu Yazar/Corresponding Author: Gaye KAYA, gkaya@ksu.edu.tr

ÖZET

Bu çalışmada, karbon/PP(Polipropilen)/epoksi hibrid kompozitlerin eğilme dayanımı ve yapısal iyileştirme özellikleri incelenmiştir. Karbon ve PP lifleri, manuel bir dokuma tezgâhında dokunmuştur. Burada, karbon lifleri yapıya yüksek dayanım kazandırırken, PP lifleri ise tokluk özelliği sağlamaktadır. İki farklı yapısal iyileşme prosesi kullanılmıştır. Önerilen iyileşme proseslerinin etkinliği, hem mekanik hem de mikroskobik olarak değerlendirilmiştir. Sonuçlar, iyileşmiş kompozitlerin eğilme dayanımlarının, hem 0° hem de 90° doğrultuda oldukça azaldığını göstermiştir. Presle iyileştirilmiş kompozitlerin artık eğilme dayanımları, etüvde iyileştirilen kompozitlere kıyasla daha yüksektir. Bunun nedeni, erimiş PP liflerinin boşlukları basınç altında daha etkili bir şekilde doldurmasıdır.

Keywords: Karbon/PP/epoksi kompozitler, karbon lifi, yapısal iyileşme, eğilme dayanımı.

ABSTRACT

In this study, bending strength and structural healing properties of carbon/PP(Polypropylene)/epoxy hybrid composites are investigated. Carbon and PP fibres were woven in a manual loom in which the carbon fibres provide high strength while the PP fibres contribute with their high strain in hybridization. Two different structural healing processes were used. Effectiveness of the proposed healing processes was evaluated by both mechanically and microscopically. The results showed that bending strengths of healed composites incredibly decreased at both 0° and 90° directions. Residual bending strengths of press-healed composites were higher than that of oven-healed composites since the molten PP filled the gaps more influentially under pressure.

Keywords: Carbon/PP/epoxy composites, carbon fibre, structural healing, bending strength.

INTRODUCTION

Carbon fibre reinforced polymeric (CFRP) composites have begun to replace materials such as aluminium and titanium in aerospace applications, with the increase in usage and developments in fibre and matrix. The most important advantages of CFRP composites are to be suitable for mass production in complex geometric shapes, reducing the amount of scrap, improved fatigue strength, design flexibility and improved corrosion resistance. Restrictive aspects are generally material and process costs, low damage tolerance and repair difficulties (Soutis, 2005).

Structural healing and self-healing have an increasing interest in reducing the damage effect on composite materials (Williams et al., 2007). Structural healing aims to re-use of damaged composites which expects to recover the functional properties of the undamaged structures (Gibson, 2010). Use of glass tubes or microcapsules containing healing agents during the production of composite materials is among the methods used. Polymerization of the healing agents in the damaged area increases the mechanical performance of the composite materials (Bleay et al., 2001; Kessler et. al., 2003). Recently, graphene based self-healing materials are used in composites which also contributes to composite performance with their high mechanical, electrical, and thermal properties (Li et. al., 2019). Williams et al. (2007) studied the self-healing properties of resin filled hollow glass fibre implanted carbon/epoxy composites. Flexural strengths of undamaged, damaged and healed composites are investigated. It is stated that the healed samples achieved almost 80% of their undamaged strengths. Ladani et al. (2018) investigated the healing performances Z-fibre reinforced hybrid 3D composites. An incredibly high mode-I fracture toughness up to 2000% is achieved by carbon Z-fibre while EMAA (polyethylene-comethacrylic acid) provides a partial repair of crack of delaminated regions. Mode-II interlaminar fracture toughness of composites increased almost 75% (Ladani et. al., 2019). Dutra et al. (2000) stated that the hybridization of carbon fibre based composites with modified polypropylene fibres increases the impact resistance and thermal properties. Selver et. al., (2015) improved the damage resistance and damage tolerance by hybridisation of glass fibres with thermoplastic fibres and provided healing properties to composite structures.

In recent study, hybridization method is used to provide structural healing on composite structures. Bending properties of carbon/PP/epoxy hybrid composites are investigated before and after healing processes. Carbon and PP fibres were woven in a manual loom in which the carbon fibres provide high strength while the PP fibres contribute with their high strain in hybridization. Different structural healing processes were used to heal damaged composites where the molten PP fibres are expected to heal the damages of composites. Effectiveness of the proposed healing processes was evaluated by both mechanically and microscopically.

MATERIALS AND METHODS

Hybrid fabric and composite production

Carbon/PP hybrid fabric is manufactured by using a manual weaving loom (GARM-55, Gülas Makine, Turkey) in plain weave. Bulk Continuous Filament (BCF) PP fibres (Eruslu Textile, Turkey) are used as warp(90°) while carbon fibres (Aksa, Turkey) are used as weft(0°). Hybrid fabric is layered as $[(0°/90°)]_3$ and consolidated with an epoxy resin system (Hexion MGS L160 resin/Hexion MGS H160 hardener, 100/25 wt.) in vacuum bagging. Curing process is occurred at 80°C for 2h on a hot vacuum table. Hybrid fabric and composite properties are given in Table 1. Thickness of carbon/PP hybrid fabric was measured using portable thickness gauge (SDL Atlas, J200) according to ISO 5084. The thickness of composites was measured by using a digital calliper. The fibre fractions composites were determined as weight based according to ASTM D3171-15. Cross-sectional view of composite is illustrated in Figure 1.

Table 1. Hybrid Fabric and Composite Properties.

Properties		**Fabric**	**Composite**
Yarn sets	**Warp (0°)**	PP (150 tex)	-
	Weft (90°)	Carbon (3K)	-
Fabric density (ends/cm)	**Warp (0°)**	4	-
	Weft (90°)	4	-
Crimp ratio (%)	**Warp (0°)**	4.75	-
	Weft (90°)	1.8	-
Weight (g/m^2)		768	-
Thickness (mm)		1.29	3.44
Fibre fraction (wt., %)		-	Carbon: 45 PP: 10 Total: 55
Composite density (g/cm^3)		-	1.23

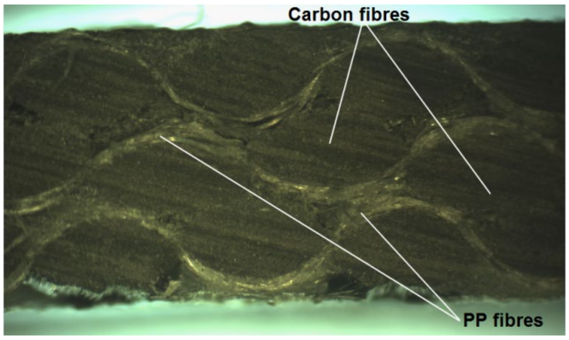

Figure 1. Cross-Sectional View of Composite (x2 Magnification).

Tests

Bending tests are provided on both normal to 0° (PP) and 90° (carbon) directions. Support span length is used as 50 mm on 25×80 mm sample dimension at 1.3 mm/min testing speed. Bending test is performed to undamaged and healed samples. Figure 2 shows the views of composite samples during bending test.

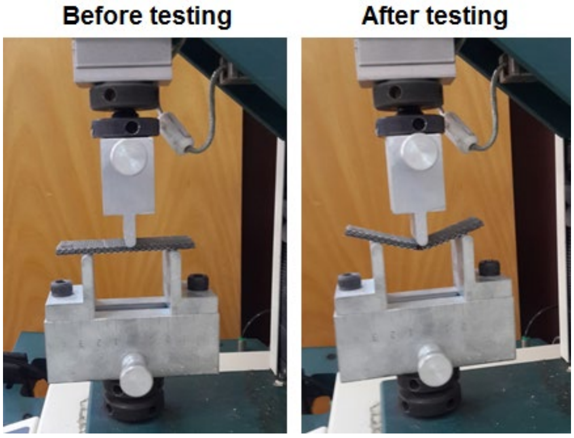

Figure 2. Views of Composite Samples During Bending Test.

Bending strength (1), modulus (2) and strain (3) of composites are calculated according to the formulations of ASTM D790-17.

$$\sigma = 3PL/2bd^2 \tag{1}$$

$$E = L^3 m/4bd^3 \tag{2}$$

$$\varepsilon = 6Dd/L^2 \tag{3}$$

where σ is stress in the outer fibres at midpoint (MPa), P is load at a given point on the load-deflection curve (N), L is support span (mm), b is width of beam tested (mm), d is depth of beam tested (mm), E is modulus of elasticity in bending (MPa), m is slope of the tangent to the initial straight-line portion of the load-deflection curve (N/mm) of deflection; ε is strain in the outer surface (mm/mm), D is maximum deflection of the centre of the beam (mm).

2.3. Healing process

Healing of composites after bending test is performed by using hot-press and oven methods. The process diagram of healing is given in Figure 3. In both hot-press and oven methods, healing process is started at 100°C. Temperature raised to 215°C in 20 min. Samples are subjected to this temperature for 20 min. Process is completed at 50°C. 2 bars pressure is used in hot-press (Wermac®-H501, Turkey).

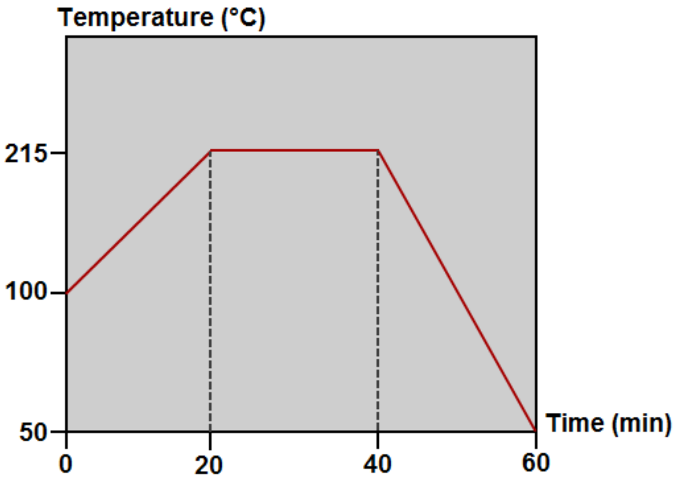

Figure 3. Process Diagram of Healing.

RESULTS AND DISCUSSIONS

Bending test results of undamaged and healed composites are given in Table 2. As seen in Figure 4, stiffness of composites in both healing methods decreased. Bending strength of undamaged composite is 37.77 MPa at 0° direction while the bending strength of undamaged composite is 283.00 MPa at 90° direction. The bending strength at 90° is almost 7.5 times higher than that of 0° since the stiffer carbon fibres are placed at 90° direction. Bending strain of undamaged composite is 7.37% at 0° direction while the bending strain of undamaged composite is 2.39% at 90° direction. This is due to PP fibres which have high strain to failure are placed at 0° and increased the ductility of composite.

Table 2. Bending Test Results of Composite Samples.

Samples	**Flexural strength (MPa)**			**Flexural strain (%)**		
	Undamaged	**Healed**		**Undamaged**	**Healed**	
		Press	**Oven**		**Press**	**Oven**
0°	37.77 ±2.62	13.04 ±2.03	10.17 ±1.07	7.37 ±0.98	3.79 ±1.50	1.52 ±0.30
90°	283.00 ±15.46	24.67 ±2.40	5.96 ±1.45	2.39 ±0.20	5.78 ±0.89	0.82 ±0.33

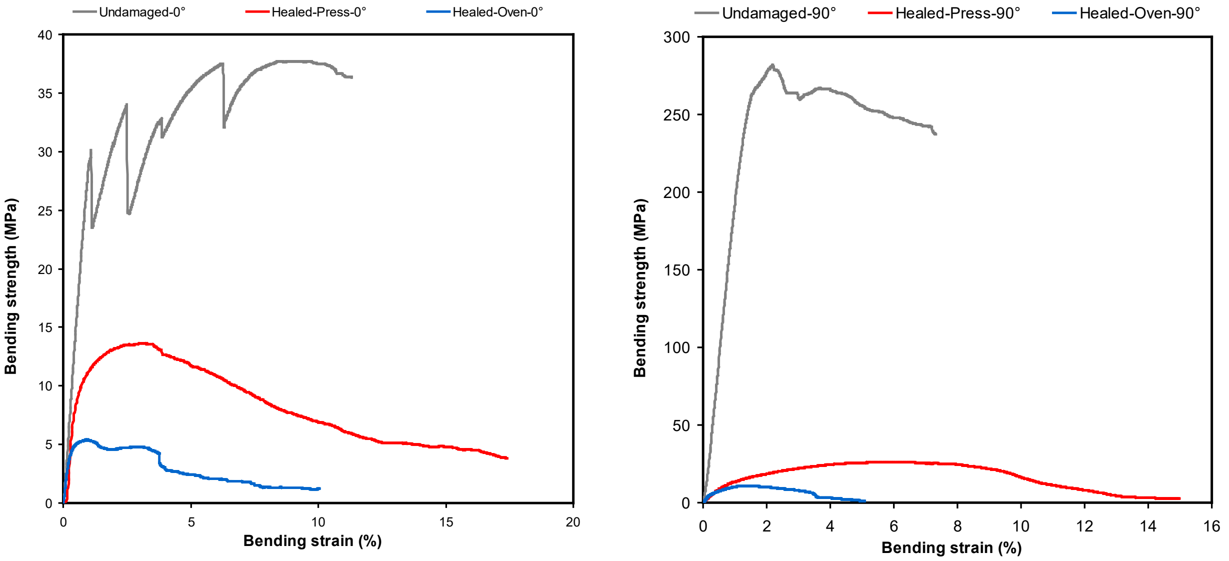

Figure 4. Bending Strength-Strain Curves of Composites.

Thickness results of undamaged and healed composites are also given in Table 3 to compare the effects of oven or press healing process on the thickness values of composites. It can be seen that the healing process has not any effect on the thickness values of composites. Therefore, it can be concluded that the pressure and/or temperature applied during the healing process did not change the fibre volumetric ratio. The pressure and temperature healed composites have better bending properties than the only oven-healed composites. In oven healed composite, PP fibres showed shrinkage under heat without pressure and this caused more gaps within the composite which decreased the bending strength.

Table 3. Thickness Results of Composite Samples.

Samples	**Thickness (mm)**		
	Undamaged	**Healed**	
		Press	**Oven**
0°	3.44 ± 0.10	3.43 ± 0.12	3.44 ± 0.11
90°	3.44 ± 0.04	3.43 ± 0.06	3.43 ± 0.01

Bending strengths of healed composites incredibly decreased at both 0° and 90° directions. However, the decrement at 0° is somehow reasonable. At both directions, the residual bending strengths (Figure 5) of press-healed composites are higher than that of oven-healed composites. This is due to the molten PP filled the gaps more influentially under pressure. Residual flexural strength of press-healed 0° composite is 34.5% while the residual bending strength of oven-healed 90° composite is 28.3%. It can be stated that the healing process is not effective at the bending strength of 90° composites. The bending strains of press-healed and oven-healed 0° composites are lower compare to undamaged composites. These results showed that the molten PP acts more brittle than PP fibres.

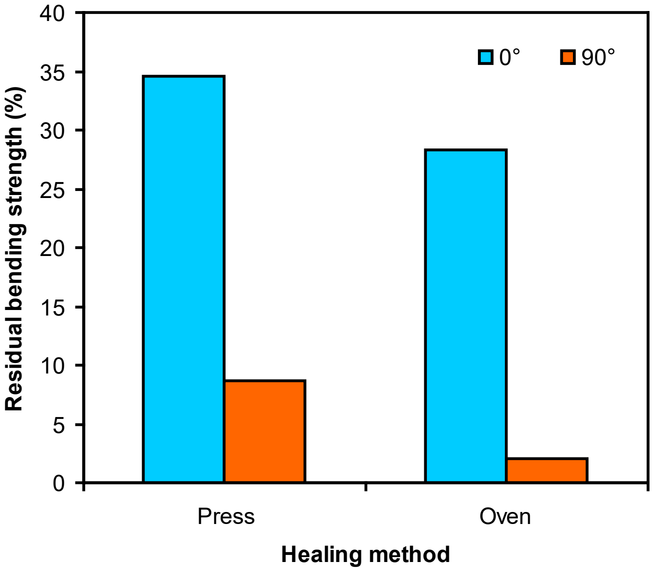

Figure 5. Residual Bending Strengths.

The cross-sectional failure views of composites (Figure 6) showed that both 0° and 90° samples have fibre breakages, fibre-matrix delamination and molten PP fibres. In oven-healing process, there are a lot of gaps are observed between PP and carbon fibres. It can be concluded that the PP fibres showed shrinkage under heat without pressure. Therefore, unpressured samples have more gaps which confirm the lower bending strengths of oven-healed samples.

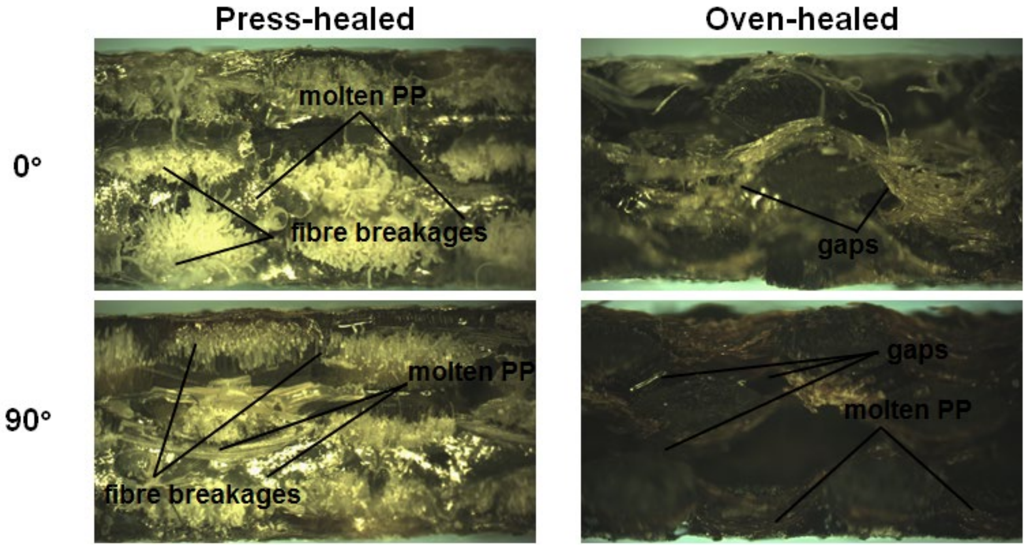

Figure 6. The cross-sectional failure views of composites (x2 magnification).

CONCLUSIONS

Bending strength and structural healing properties of carbon/PP/epoxy hybrid composites are investigated. For this purpose, two different structural healing processes are used. Effectiveness of the proposed healing processes is evaluated by both mechanically and microscopically. The conclusions are:

- The bending strength at 90° is almost 7.5 times higher than that of 0° since stiffer carbon fibres are placed at 90° direction.
- PP fibres increased the ductility of compositesat 0° because of theirhigh strain to failure.
- Bending strengths of healed composites incredibly decreased at both 0° and 90° directions in where the decrement at 0° is somehow reasonable.
- Residual bending strengths of press-healed composites are higher than that of oven-healed composites since the molten PP filled the gaps more influentially under pressure.
- Bending strains of press-healed and oven-healed 0° composites are lower compare to undamaged composites because of more brittle behaviour of molten PP than PP fibres.
- Cross-sectional views of composite samples confirm the lower bending strengths of oven healed samples in which PP fibres showed shrinkage under heat without pressure.

REFERENCES

ASTM D790-17.(2017). Standard test methods for flexural properties of unreinforced and reinforced plastics and electrical insulating materials.

Bleay, S.M. et al. (2001). A smart repair system for polymer matrix composites. *Composites: Part A*, 32, 1767-1776.

Dutra, R.C.L., Soares, B.G., Campos, E.A., & Silva, J.L.G. (2000). Hybrid composites based on polypropylene and carbon fiber and epoxy matrix. *Polymer*, 41, 3841-3849.

Gibson, R.F. (2010). A review of recent research on mechanics of multifunctional composite materials and structures. *Composite Structures*, 92, 2793-2810.

Ladani, R.B., Nguyen, A.T.T., Wang, C.H., & Mouritz, A.P. (2019). Mode II interlaminar delamination resistance and healing performance of 3D composites with hybrid z-fibre reinforcement. *Composites: Part A*, 120, 21-32.

Ladani, R.B., Pingkarawat, K., Nguyen, A.T.T., Wang, C.H., & Mouritz, A.P. (2018). Delamination toughening and healing performance of woven composites with hybrid z-fibre reinforcement. *Composites: Part A*, 110, 258-267.

Li, G., Xiao, P., Hou, S., & Huang, Y. (2019). Graphene based self-healing materials. *Carbon*, 146, 371-387.

Selver, E., Potluri, P., Soutis, C., Hogg, P., (2015). Healing potential of hybrid materials for structural composites. *Composite Structures*, 122, 57-66.

Soutis, C. (2005). Carbon fibre reinforced plastics in aircraft construction. *Materials Science and Engineering*, A, 412, 171-176.

Williams, G., Trask, R., & Bond, I. (2007). A self-healing carbon fibre reinforced polymer for aerospace applications. *Composites: Part A*, 38, 1525-1532.

ORCID

Gaye KAYA *http://orcid.org/0000-0003-1866-4799*
Pınar ÇAM *https://orcid.org/0000-0002-3528-888X*

KSÜ Mühendislik Bilimleri Dergisi, 22, Özel Sayı, 2019 KSU J Eng Sci, 22, Special Issue, 2019
Uluslararası İleri Mühendislik Teknolojileri Sempozyumu (ISADET) Özel Sayısı
International Symposium on Advanced Engineering Technologies (ISADET) Symposium Special Issue
Araştırma Makalesi Research Article

Kahramanmaras Sutcu Imam University
Journal of Engineering Sciences

Geliş Tarihi : 20.07.2019 Received Date : 20.07.2019
Kabul Tarihi : 13.10.2019 Accepted Date : 13.10.2019

LANDSLIDE SUSCEPTIBILITY ASSESSMENT OF AROUND BABADAĞ (DENİZLİ) USING LOGISTIC REGRESSION METHOD

MANTIKSAL REGRESYON YÖNTEMİ İLE BABADAĞ İLÇESİ (DENİZLİ) DOLAYININ HEYELAN DUYARLILIK DEĞERLENDİRİLMESİ

Tolga ÇAN *[*1], *Senem TEKİN* [1]

[1] Department of Geological Engineering, Çukurova University, 01330 Balcalı, Adana, Turkey

* Corresponding Author: Tolga ÇAN, tolgacan@cu.edu.tr

ÖZET

Bu çalışmada, Babadağ ilçesi ve dolaylarını içeren 1133 km^2'lik bölgede, mantıksal regresyon yöntemi ile heyelan duyarlılık çalışması gerçekleştirilmiştir. Toplam alanı 44 km2 olan, 300'e yakın kayma türü heyelan bulunmaktadır. Çalışma alanı içerisinde bulunan yerleşim yerleri, ziraat alanları gibi bölgeler heyelanlardan olumsuz yönde etkilenmektedir. Bölgede yaklaşık 500'e yakın konut boşaltılmıştır. Heyelanları hazırlayıcı faktörler 25 m mekansal çözünürlükte Coğrafi Bilgi Sistemleri ortamında hazırlanmış olup, jeoloji, sayısal yükseklik modeli, yamaç eğimi, kesit, düzlemsel ve teğet yamaç eğrisellikleri, drenaj ağı ve aktif faylara olan uzaklık parametreleri göz önünde bulundurulmuştur. Duyarlılık haritasında yüksek ve çok yüksek duyarlı bölgeler çalışma alanın % 23'üne karşılık gelmekte olup bu bölgelerde heyelanların % 72.13'ü bulunmaktadır.

Anahtar Kelimeler: Babadağ, Heyelan duyarlılık, Mantıksal regresyon

ABSTRACT

In this study landslide susceptibility assessments were evaluated using logistic regression method around the Babadağ town extending to 1133 km^2. Almost 300 slide type landslides corresponding 44km^2 were identified in the area. Some of the residential areas, agricultural lands and lifeline systems has been severely damaged by landslides and more than five hundreds dwellings were evacuated in the region. Among the landslide conditioning factors; elevation, slope, plan and profile curvatures, proximity to faults and rivers and geological maps have been prepared in Geographical Information Systems environment with spatial resolution of 25 m The performance of the susceptibility map when compared to the landslide inventory revealed that high and very high susceptible zones correspond to 23 % of the study area including 72.13 % of the recorded landslides.

Keywords: Babadağ, Landslide susceptibility, logistic regression

INTRODUCTION

Despite the developments in understanding of mechanisms and the availability of a wide variety of mitigation techniques, landslides are still leading to significant casualties and economic losses worldwide. Minimizing the potential damages of landslide hazards requires an integrated approach including inventory, susceptibility, hazard and risk assessments. Landslide susceptibility studies is one of the first stages to help with land management works in landslide prone areas. The landslides susceptibility methods are classified into two main groups: qualitative (inventory-based and knowledge driven methods) and quantitative (data-driven methods and physically based models) (Corominas et al. 2014). Some recent overviews of the methods available for landslide susceptibility assessment can be found in Corominas et al. (2014), Reichenbach et al. (2018); Huang and Zhao (2018). Landslides cause significant problems in and around Babadağ town of Denizli for several decades. Some local landslides in Babadağ settlement using physically based slope stability models and multi-parameter monitoring techniques were studied by Cevik and Ulusay (2005) and Kumsar et al. (2016). Landslide susceptibility assessments has not been studied in the region although the landslides are abundant. In this study, landslide susceptibility assessments were performed using the logistic regression method in the 1133 km^2 area around the Babadağ comprising Karacasu and Sarayköy districts (Figure 1).

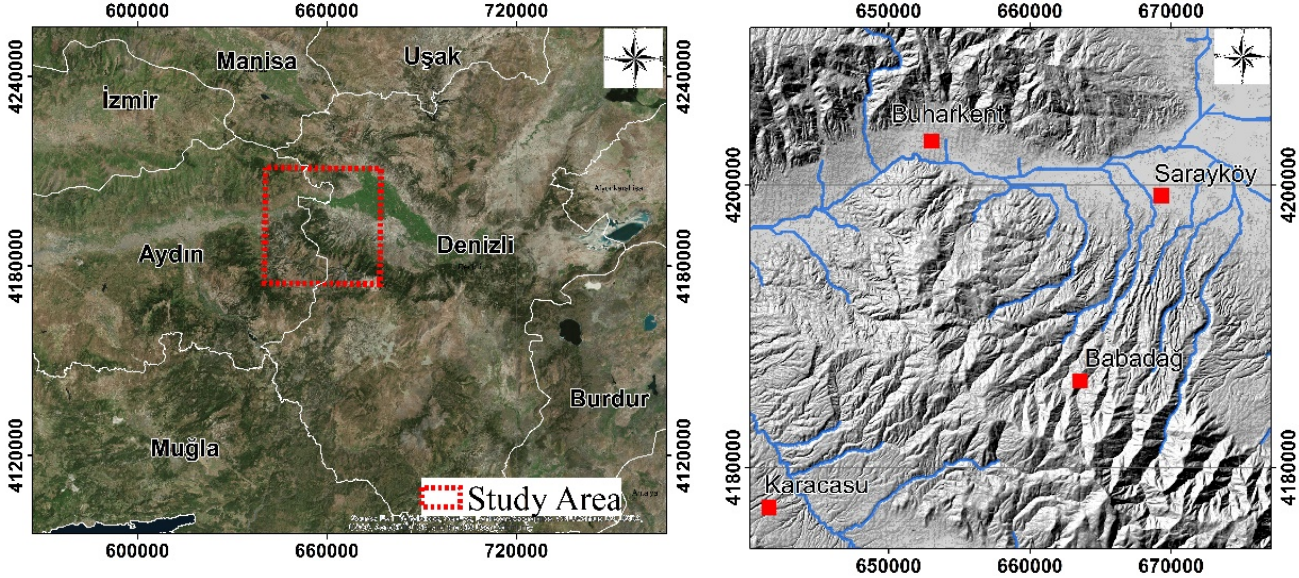

Figure 1. Location map of the study area.

DATA and METHODS

The present geologic and morphotectonic setting of the study area is configured by the Western Anatolian Extensional tectonic regime by means of the horst - graben systems and the E-W trending basins (Westaway 1993). The basement rocks (Ortaköy formation) in the area exposed in the mountainous horst areas composing schists, marbles and gneiss (Bozkurt and Oberhansli 2001). The Neogene cover units (Kızılburun, Sazak, Kolonkaya, and Milet formations) and Quaternary recent deposits overlie uncomformably the basement rocks. Some of the active fault segments related to the Büyük Menderes and Denizli Graben Systems delineated by Emre et al., (2013) are also located in the study area (Figure 2a). A reliable landslide inventory data is essential for quantitative zoning of landslide susceptibility. 300 landslides covering 44 km^2 were identified in the area by Duman et al., 2009 (Figure 2b). Most of the landslides are developed in Neogene cover units (Figure 3a) and numerous deformations are observed in Babadağ downtown (Figure 3b).

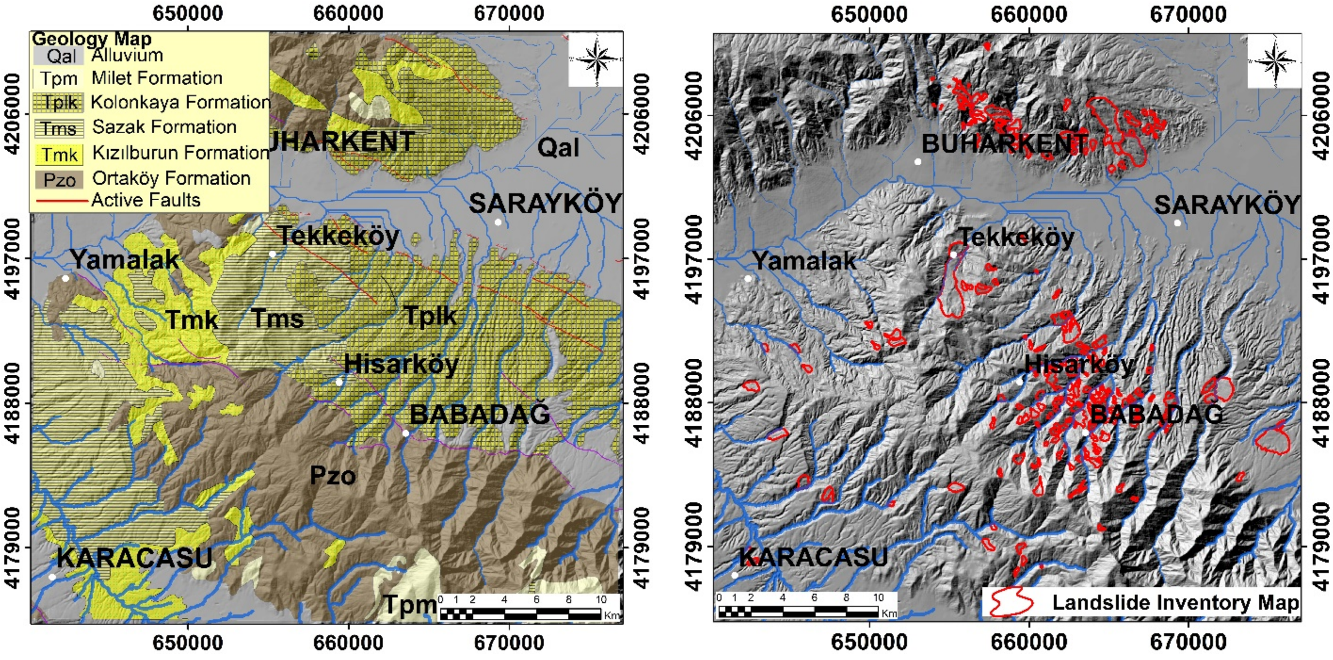

(a) (b)

Figure 2. Geological map (Konak et al., 2002) (a) Landslide inventory (Duman et al., 2009) (b) of the study area.

(a)

(b)

Figure 3. Slide type landslide (a) and landslide induced deformation on dwellings in Babadağ (b).

Accordingly; the landform map was prepared according to Jenness (2006) using the topographic position index (Figure 4)., 7.63% small drainage systems, 14.15% ridges, 14.44% steep slopes, 16.04% lower slope, 20.47% upper slopes, 27.27% gentle slopes classes be made of the study area. Landslides, 8.98 % valley, 8.19% ridges, 19.37% steep slopes, 26.34% lower slope, 21.52% upper slopes, 15.60% gentle slopes are found in the area.

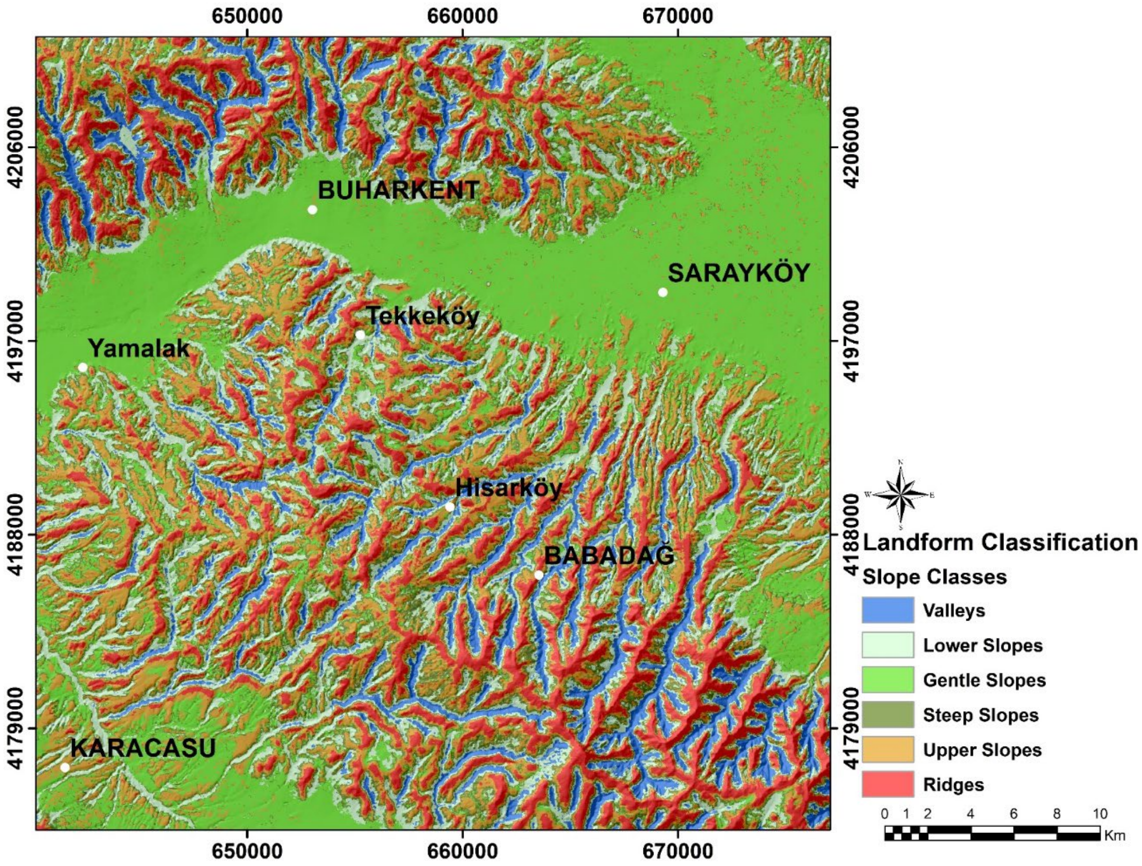

Figure 4. Landform classification.

The mean elevation in the study area is 650 m and the basement rocks constitute the high land areas around Akdağ, where elevation reach up to 2300 m. The lower elevation areas around the Sarayköy plain corresponds to the central part of the Büyük Menderes river where elevation ranges between 84 to 150 m (Figure 5a). The slope ranges between 0-62 degrees with an average of 15 degrees (Figure 5b). Profile and plan curvatures parameters which mainly control the ongoing erosion and deposition processes were also considered (Fig 5c,d). Positive and negative values in the curvature maps indicates convex (≅40%) and concave (≅40%) surfaces and the values close to the zeros (≅20%) are linear surfaces. The maximum distances to active fault (Figure 5e) and distances to stream (Figure 5f) in the study area are 4015 m and 1974 m, respectively.

Geographical Information Systems (GIS) based landslide susceptibility map in the study area was constructed by using logistic regression method. Logistic regression is an efficient multivariate statistical method to investigate the relationship between a binary dependent variable with a set of continuous and / or categorical independent variables. The probability of the observed dependent variable as a function of the independent variables are expressed by the maximum likelihood method and the linear combination of the independent variables $X_1 \ldots X_n$ can be expressed by the following equation (Eq. 1),

$$Z=\beta_0+\beta_1X_1+\beta_2X_2+\ldots\ldots\ldots\ldots\ldots+\beta_nX_n \quad (1)$$

And in order to predict the possibility of landslide occurrences in each grid, the probability was calculated from Eq. 2,

$$P = 1/1 + e^{Z} \quad (2)$$

where P is the probability of landslide occurrence and Z is the weighted linear combination of the independent variables, B_i (i = 0, 1, 2,…,n) is the coefficient estimated from the sample data, n is the number of independent variables and X_i (i = 1, 2, …,n) is the independent variable (Hosmer et al. 2013).

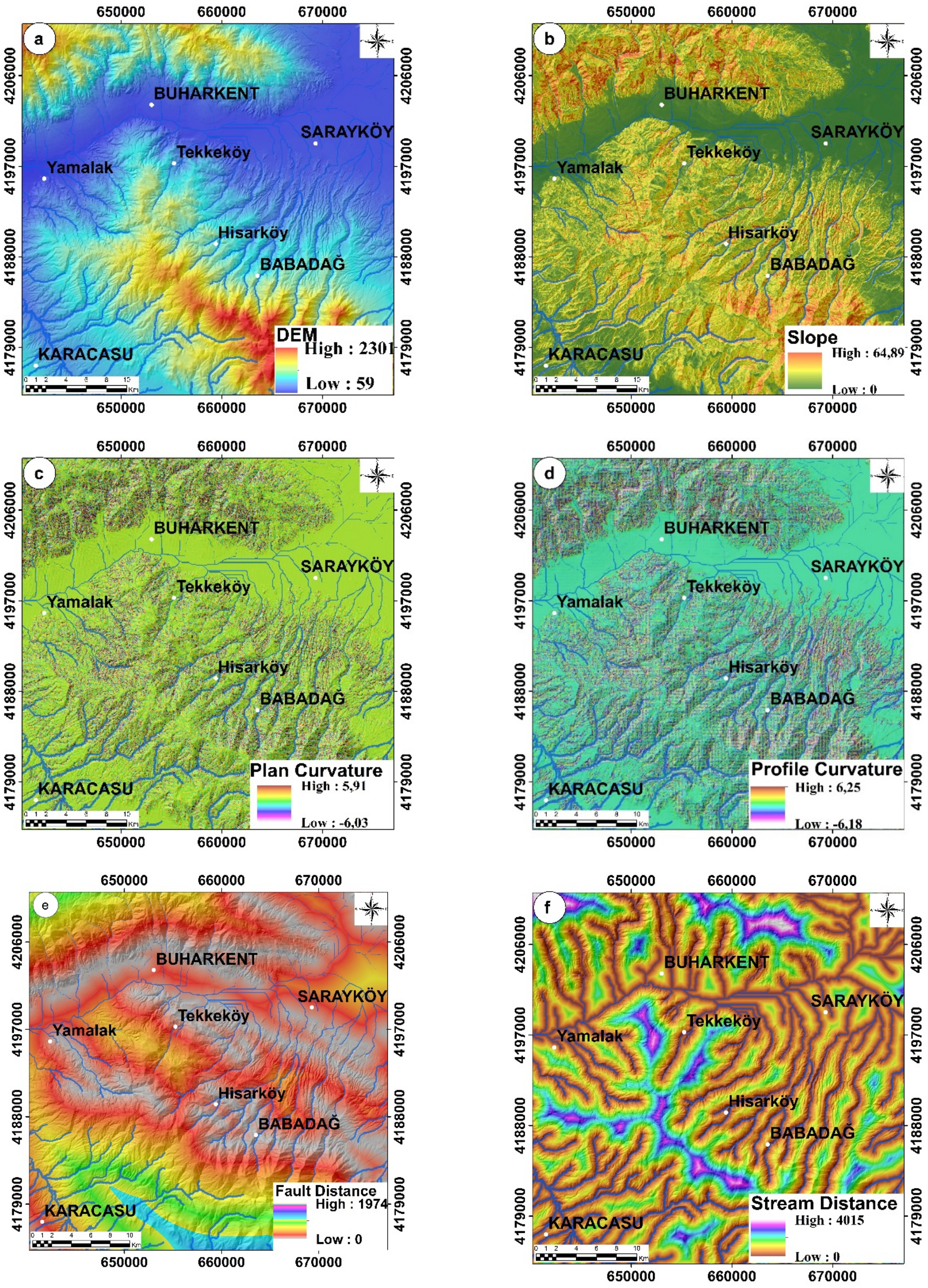

Figure 5. Digital elevation model (a), slope (b), plan curvature (c), profile curvature (d), proximity to faults (e) and proximity to streams (f) maps of the study area.

RESULTS

The grid cell size of 25 m was used for terrain mapping unit where the landslide data set is represented by 67655 grid cells (44 km^2) and the total study area has 2178576 pixels (1133 km^2). Landslide affected pixels were randomly divided into two groups, 80% for the training and 20 % for test data set considering the entire landslide polygons according to the sampling method proposed by Tekin and Çan (2018). The geological map of the study area was converted to raster format and each geological unit was assigned by binary value. Several logistic regression analyses were applied, and the final decision was made by two rules proposed by Can et al. (2005) that first, the majority of the landslides should locate in the high and very high susceptibility classes, and second, the high and very high susceptibility classes should cover the small percentages of the area. The variables entered in the best fit logistic regression model were summarized in Table 1. In regression model DEM and slope were found positively related to the presence of landslides.

Table 1. Beta coefficients and Wald test statistics of the variables in the regression model.

Variable	Beta	Standard error.	Wald	Explanation (B)
Plan Curvature	-,000311	0,014	626,760	0,707
Profile Curvature	-,157886	0,012	169,731	0,854
Dem	,000454	0,000	323,663	1,000
Fault Distance	-,000282	0,000	6308,313	1,000
Slope	,003117	0,001	14,752	1,003
Stream Distance	-,000394	0,000	795,623	1,000
Constant	,590892	0,015	1579,646	1,806

The landslide susceptibility map was given in figure 6a. According to the success and prediction rate curve the 23.06 % of the study area is located within the high – very high susceptibility classes comprising the 61.81% of test, 65.37 % of train 72.13 % of all landslides (Figure 6b). The area under Receiver Operating Characteristics (ROC) curve was found 0.786 indicating acceptable discrimination.

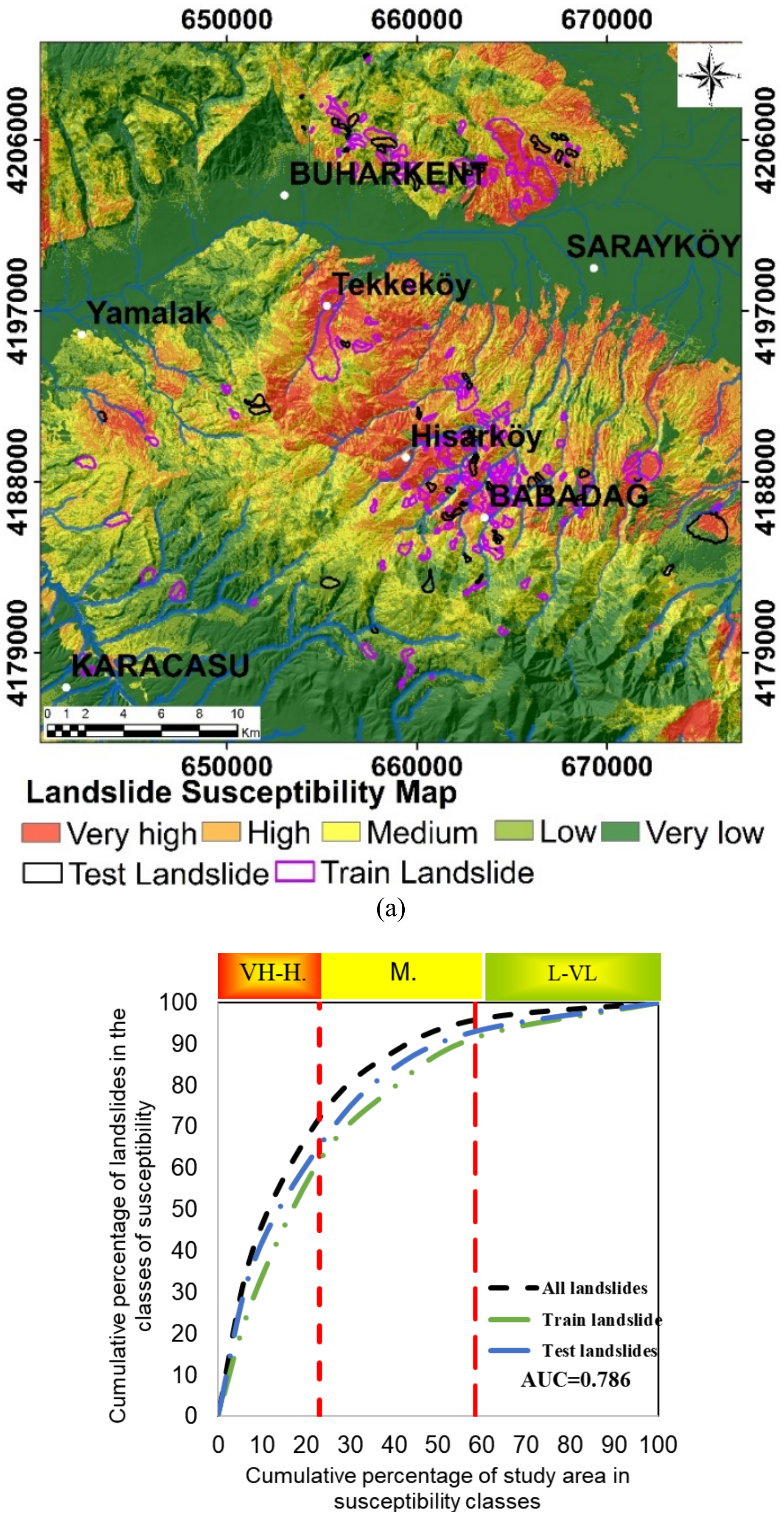

(a)

(b)

Figure 6. Landslide susceptibility map (a), success -prediction curves (b).

CONCLUSIONS

Landslides occur under different geologic, geomorphologic and climatic conditions. Each type of landslides should be studied separately due to their different movement mechanisms. In this study, slide type landslide susceptibility assessment was made around the Babadağ region in the Western Anatolia. Landslides in the Babadağ town cause long-term socio-economic disruption and settlement evacuation. However, there are numerous landslides in the region which have negative effects on natural environment. The results suggest that the landslide susceptibility zonation is sufficient to be used in early land use planning for public safety and site selection studies for engineering structures.

REFERENCES

Bozkurt, E., & Oberhänsli, R., (2001). "Menderes Massif (Western Turkey): Structural, metamorphic and magmatic evolution - A synthesis". International Journal of Earth Sciences. 89. 679-708. 10.1007/s005310000173.

Can, T., Nefeslioglu, H. A., Gokceoglu, C., Sonmez, H., & Duman, T. Y. (2005). Susceptibility assessments of shallow earthflows triggered by heavy rainfall at three catchments by logistic regression analyses. Geomorphology, 72(1-4), 250-271, doi:10.1016/j.geomorph.2005.05.011.

Cevik, S.Y., & Ulusay, R., (2005), "Engineering Geological Assessments of The Repeated Plane Shear Slope Instability Threatening Babadag (Turkey) And Its Environmental Impacts" Environ Geol (2005) 47: 685–701 doi:10.1007/s00254-004-1197-7.

Corominas, J., van Westen, C., Frattini, P., Cascini, L., Malet, J.P., Fotopoulou, S., Catani, F., Van Den Eeckhaut, M., Mavrouli, O., Agliardi, F., Pitilakis, K., Winter, M.G., Pastor, M., Ferlisi, S., Tofani, V., Hervas, J. & Smith, J.T. (2014). Recommendations for the quantitative analysis of landslide risk. Bulletin of Engineering Geology and the Environment, 73, 209-263, doi: 10.1007/s10064-013-0538-8.

Duman, T.Y., Olgun, Ş. Çan, T, Nefeslioğlu, H.A., Hamzaçebi, S., Durmaz, S., & Çörekçioğlu, Ş., (2009). "Türkiye Heyelan Envanteri Haritası-1:500.000 ölçekli Denizli Paftası", MTA Özel Yayınlar Serisi-21, 22 s. Ankara.

Emre, Ö., Duman, T.Y., Özalp, S., Elmacı, H., Olgun, Ş., & Şaroğlu, F., (2013). Active fault map of Turkey with an explanatory text 1:1,250,000 scale. General Directorate of Mineral Research and Exploration, Special Publication Series 30.

Jenness, J. (2006). Topographic Position Index (tpi_jen.avx) extension for ArcView 3.x, v. 1.3a. Jenness Enterprises. http://www. jennessent.com/arcview/tpi.htm.

Konak, N., Şenel, M., A.Arbas, A.Ayhan, M.Y.Barkut, E.Başkan, J.P.Bassaget, H.Baş, E.Başarır, T.Bilgiç, Z.R.Bilgin, A. Bilgin, A.Boray, A.S.Bölükbaşı, B.Can, O.Candan, B. Coşkun, M.H. Çakır, A. Çağlayan, A.Çakmakoğlu, E. Çörekçioğlu, E. Deveciler, M.A.Dinçer, O.Ö. Dora, E.Durukan, E. Elibol, B.Erakman, T. Ercan, A.Erdoğan, E.Ergül, Ş. Ersoy, T.Eşder, E. Gökalp, F.Göktaş, M.Z. Gözler, P.de.Graciansky, M.A. Gül, N.Gültekin, E. Günay, Y.Günay, H.Y. Hakyemez, M.N.Hepşen, İ. Iğdır, G.Kadınkız, A.Kara, T. Karaman, İ.H. Karamanderesi, M.Kastelli, E.Kerey, B. Keskin, H. Keskin, N. Konak, B.Korkmazer, N.Kun, G.P. Lozej, D. Maitre, H. Mengi, M.Meşhur, Y.Metin, O.Monod, T.Öngür, H. Öcal, M.Önalan, & İ.Özkan, (2002). 1/500000 Ölçekli Türkiye Jeoloji Haritası Denizli Paftası, Maden Tetkik ve Arama Genel Müdürlüğü.

Kumsar, H., Aydan, Ö., Tano, H., & Çelik, S.B., (2016). "An Integrated Geomechanical Investigation, Multi-Parameter Monitoring and Analyses of Babadağ-Gündoğdu Creep-like Landslide", Rock Mech Rock Eng (2016) 49:2277–2299 DOI 10.1007/s00603-015-0826-7.

Reichenbach, P., Rossi, M., Malamud, B.D., Mihir, M., & Guzzetti, F., (2018). "A review of statistically-based landslide susceptibility models" Earth-Science Reviews 180 (2018) 60–91.

Tekin, S., & Çan, T., (2018) Effects of Landslide Sampling Strategies on the Prediction Skill of Landslide Susceptibility Modellings. Journal of the Indian Remote Sensing, Doi 10.1007/s12524-018-0800-4.

Westaway, R., (1993) Neogene evolution of the Denizli region of western Turkey. J Struct Geol 15(1):37–53.

Zhao, Z., Wang, Y., Feng, Q., Li, J., & Zhao, X., (2018). "Triggering mechanism and deformation characteristics of a reactivated ancient landslide, Sichuan Province, China", Landslides (2019) 16:383–393 DOI 10.1007/s10346-018-1111-0.

ORCID

Tolga ÇAN *http://orcid.org/0000-0001-9940-2832*
Senem TEKİN *http://orcid.org/0000-0001-7734-9700*

KSÜ Mühendislik Bilimleri Dergisi, 22, Özel Sayı, 2019 KSU J Eng Sci, 22, Special Issue, 2019
Uluslararası İleri Mühendislik Teknolojileri Sempozyumu (ISADET) Özel Sayısı
International Symposium on Advanced Engineering Technologies (ISADET) Symposium Special Issue
Araştırma Makalesi Research Article

Kahramanmaras Sutcu Imam University
Journal of Engineering Sciences

Geliş Tarihi : 28.07.2019 Received Date : 28.07.2019
Kabul Tarihi : 17.10.2019 Accepted Date : 17.10.2019

DESIGN OF AN IMAGE PROCESSING SYSTEM FOR FABRIC DRAPE MEASUREMENT

KUMAŞ DÖKÜMLÜLÜK ÖLÇÜMÜ İÇIN GÖRÜNTÜ İŞLEME SISTEMI TASARIMI

H.İbrahim ÇELİK, Elif GÜLTEKİN, Aydın BAŞKAR, Büşra ÖZTÜRK, H.İbrahim DEMİREL*

[1] Gaziantep University, Textile Engineering Department, Gaziantep, TURKEY

*Corresponding Author: Halil İbrahim ÇELİK, hcelik@gantep.edu.tr

ABSTRACT

Fabric drapeability is an important parameter that affects the apparel comfort and appearance of the fabric. Fabric drape measurement is based on calculating the shadow area of the hanged fabric created due to its weight. This measurement is performed manually and therefore a subjective assessment is made. Today, with the developments in image acquisition technology and image processing methods, many measurements and evaluations can be made objectively and accurately by adapting vision systems. In this study, an example prototype system with which fabric drape can be measured by image processing techniques is presented. The designed system consists of machine vision hardware, equipment and image processing software. The system was tested on 12 different types of woven and knitted fabrics. The fabric samples were selected randomly. Drape measurements were performed with developed image processing software. The same samples were also applied bending length and Cusick drapeability tests to confirm the results obtained by image processing (IP) method and the relationship between the three measurements was determined by regression analysis. As a result, 0.92 and 0.84 R^2 values were obtained between IP method and bending length and Cusick drapeablility results respectively.

Keywords: Fabric drape, bending length, image processing, machine vision

ÖZET

Kumaş dökümlülük özelliği kumaşın giyim konforumu ve görünümünü etkileyen önemli bir parametredir. Kumaş dökümlülüğü ölçümü askıdaki kumaşın kendi ağırlığından dolayı oluşturduğu gölgenin alanın hesaplanması prensibine dayanmaktadır. Bu ölçüm manüel olarak yapılmakta ve dolayısı ile sübjektif bir değerlendirme yapılmaktadır. Günümüzde, görüntü alma teknolojisinde ve görüntü işleme yöntemlerinde meydana gelen gelişmeler ile beraber birçok ölçüm ve değerlendirme yapay görüntü sistemlerinin adapte edilmesi ile objektif olarak ve doğru bir şekilde gerçekleştirilebilecektir. Bu çalışmada, kumaş dökümlülüğünün görüntü işleme teknikleri ile ölçülebileceği prototip bir sistem örneği sunulmuştur. Tasarlanan sistem görüntü alma donanımları, ekipmanları ve görüntü işleme yazılımından oluşmaktadır. Sistem 12 farklı dokuma ve örme kumaş numunesi üzerinde test edilmiştir. Kumaş numuneleri rast gele seçilmiştir. Dökümlülük ölçümleri geliştirilen görüntü işleme yazılımı ile gerçekleştirilmiştir. Görüntü işleme yöntemini doğrulamak amacı ile aynı kumaşlara eğilme uzunluğu ve Cusick dökümlülük testleri uygulanmıştır ve her üç ölçüm arasındaki ilişki regresyon analizi belirlenmiştir. sonuç olarak görüntü işleme yöntemi ve eğilme uzunluğu, Cusick dökümlülük sonuçları arasında sırası ile 0.92 ve 0.84 R^2 değerleri elde edilmiştir.

Anahtar Kelimeler: kumaş dökümlülüğü, eğilme uzunluğu, görüntü işleme, yapay görme

INTRODUCTION

One of the important features that affect fabric appearance and comfort is drapeability. It is an important quality parameter that is taken into consideration by the designers especially because of its effect on my garment appearance. The drape is mainly expressed as the bending behavior of the fabric under its own weight. The drape quality of the fabric varies according to the usage area and the design criteria of the product to be produced. Since knitted fabrics are more flexible and higher in drapeability, the products made of knitted fabrics have a body-covering appearance and follow the body lines. On the other hand, since woven fabrics have a stiffer structure, garments made from these fabrics are positioned further away from the body and do not follow body lines. Curtains, tablecloths, women's clothes are preferred high-draped fabrics (Hu, 2008).

The drapeability coefficient is calculated for the purpose of evaluating the stiffness, softness and drape of the fabric. In general, the CUSICK Drapeability Tester is used for the drape measurement. The device consists of a concave mirror and light system. The image formed by the fabric placed on the sample holder due to its own weight is reflected to the upper part of the device by the concave mirror system. The boundaries of the projected image are then determined by drawing on a standard paper. Standard paper is cut and weighed at specified limits. The ratio of the weight of the cut piece to the weight of the standard paper gives the drape coefficient. The higher the drape coefficient, the stiffer the fabric is. On the other hand, the lower the drape coefficient means the flexible and soft fabric. In CUSICK drape measurement method, the determining the drape area and removing this area from the whole reference paper requires experience and attention. Since there will be a variation in measurement accuracy and the results will change from person to person, this method is evaluated as a subjective method. In literature, to perform drape measurement more accurately and objectively, different approaches that use image processing techniques are presented (Platürk, Kılıç, 2014; Tsai et.al, 2009; Behara, Pattanayak, 2008; Kenkare, May-Plumlee, 2005; Erdumlu, Sarıçam, 2015; Al-Gaadi et.al, 2012).

In this study, a prototype machine vision system was developed to automatically measure the drapeability of a fabric by means of image processing techniques. The system was tested on 12 different types of woven and knitted fabric samples. First of the drape coefficients of the samples were determined by using developed image processing algorithm from the image frames taken with the new designed machine vision system. Then, bending length and Cusick drape coefficients of the same samples were determined. The results of the three methods were compared and validation of the image processing method was achieved by applying regression analysis.

MATERIAL AND METHOD

Material

Within the scope of the study, 12 different samples consisting of knitted and woven fabrics were selected (Figure 1). The properties of the samples are shown in Table 1.

Figure 1. Fabric Samples

Table1. Fabric specimen features

	Fabric Type	Thickness (mm)	Weight (g/m^2)
1	Woven	0.12	51.53
2	Woven	0.26	118.10
3	Woven	0.63	290.25

4	Woven	0.19	84.41
5	Woven	0.23	109.90
6	Woven	0.49	194.01
7	Woven	0.38	103.11
8	Knitted	0.47	166.25
9	Knitted	0.20	61.01
10	Knitted	0.91	242.40
11	Knitted	0.88	226.66
12	Knitted	0.68	351.16

Method

Machine vision system design for drape measurement

A machine vision system and image processing algorithm have been developed to determine fabric drape. The prototype system, developed to capture the fabric samples, consists of a closed cabin, lighting unit, camera system, sample holder apparatus and computer (Figure 2). Since the external light sources affect the received image quality and image pixel values, a closed system has been prepared. The interior of the cabinet is covered with matt black paper to remove reflections. On the top of the system, a lighting unit consisting of LED strips is placed. There is space in the center of the lighting unit so that the camera can be placed. The HD web camera is positioned in this empty area. After all this system design has been realized, the design and manufacture of the apparatus where the sample will be placed has been realized. The design of the sample holder apparatus is achieved on the base of CUSICK measurement method. A cylindrical disc with a diameter of 100 mm and a height of 100 mm is manufactured and its center point is marked. A small needle was then adapted to the center of the cylinder for ease positioning of the sample. Circular samples with 300 mm diameter were taken from each fabric to be used in the drape measurement. The fabric samples were placed by attaching to the needle in the cylinder sample holder in order to get an image frame (Figure 2).

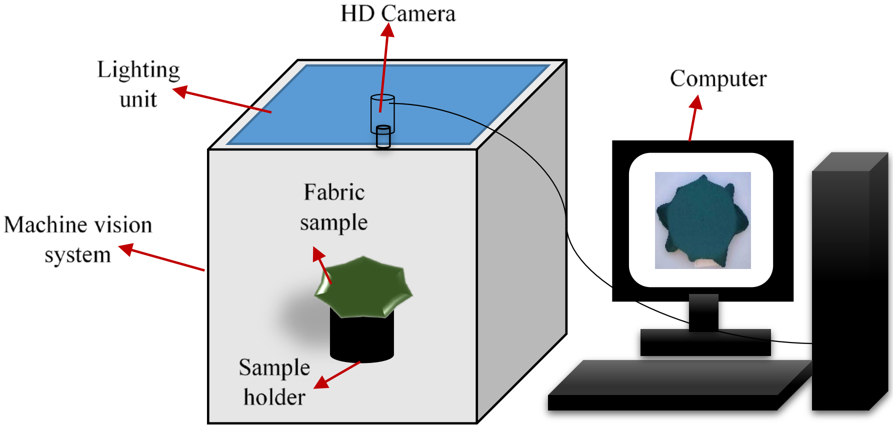

Figure 2. Machine Vision System for Fabric Drape Measurement

Image processing algorithm for drape measurement

In the image processing technique, the quality and characteristics of the image frame have a significant effect on the targeted result. Conditions such as lighting, motion blur, camera resolution, and compression of images taken while storing are factors that affect image quality. Therefore, the images taken with the camera are digitized and transferred to a computer environment and then improved by using various noise cleaning and image enhancement filters (Gonzales & Woods, 2004). Therefore, in the developed algorithm, noise cleaning and enhancement filters were applied on the image before the fabric drape area was calculated.

Image frames taken in RGB format were first converted to gray image format (Figure 3.a). Then Wiener filter (Chen, 2006) was applied to clear the noise (Figure 3.b). A contrast deepening filter was applied to clarify the boundaries of the suspended image of the fabric sample on the cylinder and to distinguish it from the ground texture (Figure 3.c). After all these preliminary operations, the images were converted to binary format consisting of 0 (black) and 1 (white) values (Figure 3.d). Opening and closing morphological operations were used to clarify the fabric boundaries on the binary image and to clear the pattern lines from the image (Figure 3.e). The image results are visualized by selecting the most complex patterns to show how the algorithm is applied. As a result, the ratio of shadow area created due to drape of laid fabric to the whole image frame covered by fabric sample is calculated (Equation 1).

$$\textbf{Drape Coefficients}\ (\%) = \frac{\textbf{Draped fabric area (pixels)} - \textbf{Supporting disc area(pixels)}}{\textbf{Fabric sample area (pixels)} - \textbf{Supporting disc area (pixels)}} \times \textbf{100}$$

(1)

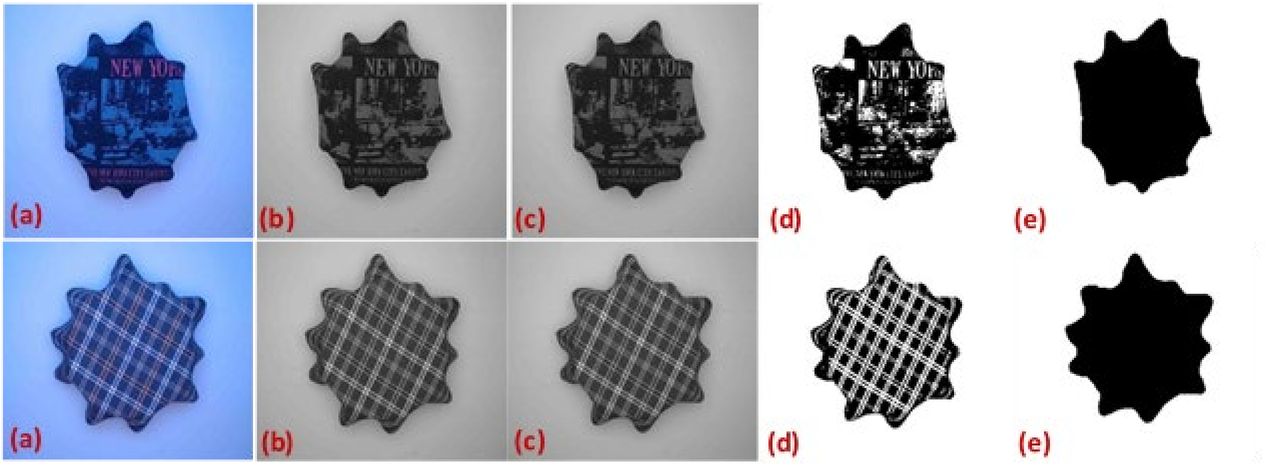

Figure 3. Measurement Algorithm of Fabric Drape. (a) RGB Image (b) Gray Image (c) Contrast Deepened Image (d) Binary Image (e) Morphologically Applied Image

Cusick drape measurement test

CUSICK Drape Tester was used for the drape measurement (Figure 4). The device consists of a concave mirror and light system. The image formed by the fabric placed on the sample holder due to its own weight is reflected to the upper part of the device by the concave mirror system. The boundaries of the projected image are then determined by drawing on a standard paper. Standard paper is cut and weighed at specified limits. The ratio of the weight of the cut piece to the weight of the standard paper gives the drape coefficient. Before testing, all fabric samples were conditioned under standard atmospheric conditions (20 ± 2 ° C temperature and 65 ± 2 relative humidity). The higher the drape coefficient is, the harder the fabric is. On the other hand, the lower the drape coefficient means more flexible and the softer fabric.

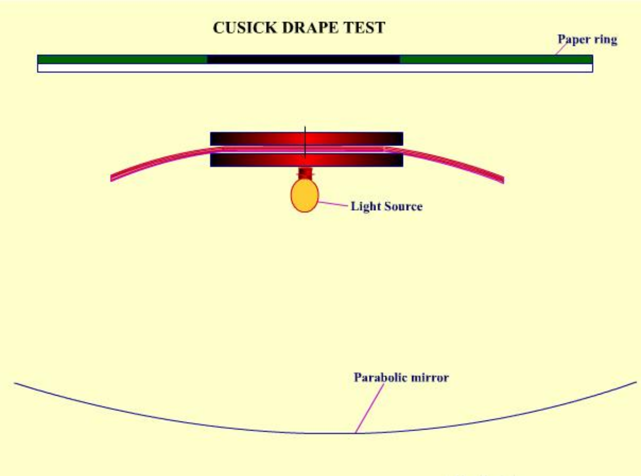

Figure 4. Cusick Drape Measurement Test Device (NPTEL)

Fabric bending strength test

The fabric bending length test was performed using the Prowhite Fabric Hardness tester (Figure 5) in accordance with BS 3356: 1990. A total of 6 samples of 25 mm × 200 mm weft / course and warp / wale directions were prepared from each fabric. A total of 4 measurements were made at both ends of the front and back sides of each sample. As a result, 24 bending lengths, 12 for weft / course and 12 for warp / wale, were measured for each fabric sample.

Before testing, all fabric samples were conditioned under standard atmospheric conditions (20 ± 2 ° C temperature and 65 ± 2 relative humidity). Using the obtained bending length values, mean bending length values were calculated for weft/course and warp/wale directions.

Figure 5. Fabric Bending Length Tester

RESULTS AND DISCUSSION

The fabric parameters that effect the drapeability performance have been investigated in many previous studies. According to findings from these studies, the drapeability property of fabrics is known to be directly related to yarn density, yarn twist, weft and warp density, type of weaving or knitting structure (Al-Gaadi et.al, 2012). It is known from the literature that high drape coefficient is obtained in fabrics where yarns containing the same direction twist are used in weft and warp way, since slip and stretching deformation will be more difficult. When examined as fabric type, the drape coefficients of twill fabrics are lower than plain fabrics. This is due to the fact that the yarns move more easily in the fabric architecture, as there are fewer connection points in the twill weave structure (Özgüney A.T. et.al, 2009).

Because of the difficulties that come from the manual drapeability tests, some attempts were made to automatically and sensitively perform drapeability test. These attempts were generally based on image processing approaches. In similar studies, the results between fabric drapeability and bending property obtained with the test applied to randomly selected fabrics were statistically compared and the difference between them was determined. The success level (high correlation coefficients 0.86-0.99) of the method proposed in similar studies in the literature has been demonstrated in this way (Platürk, Kılıç, 2014; Tsai et.al, 2009; Behara, Pattanayak, 2008; Kenkare, May-Plumlee, 2005; Erdumlu, Sarıçam, 2015; Al-Gaadi et.al, 2012, Süle, G. 2012). There is a study in the literature about determination of drape measurement using image processing technique by Kenkare, May-Plumlee, 2005, it was stated that a correlation coefficient of 0.99 R^2 demonstrate between digital image processing method and conventional cut and weight technique.

In our study, the results obtained from the developed machine vision system, bending length test and Cusick drape test were presented in Table 2. The mean of the bending length values for weft/course and warp/wale directions and drape measurements were compared with the drape coefficient values obtained from the developed machine vision system. The relationship between the drape coefficient values and the bending length were discussed with regression analysis in Figure 6. As flowed from Figure 6, there is high regression with 0.92 R^2 value was reached between image processing (IP) drapeability results and Cusick drapeability test results. This result reveals that the developed image processing method provides high accuracy in comparison to reference Cusick method. The regression value between IP drapeability and bending length was obtained as R^2=0.84. According to the obtained results, we can say that the average bending length increases when the drapeability increases in the fabric and the average bending length decreases when the drapeability coefficient decreases. As a result, it can be stated that the proposed method gives reliable and accurate results for fabric drape measurement.

Table 2. Bending Length and Drape Coefficient Values

	Bending Length (cm)			**IP Drape Coefficient (%)**	**Cusick Drape Coefficient (%)**
Sample No	**Warp / Wale**	**Weft / Course**	**Average Length**		
1	4.88	4.72	4.80	65.10	35.61
2	4.13	4.30	4.21	48.46	35.00
3	4.07	3.47	3.77	33.88	29.95
4	2.23	2.88	2.55	18.51	22.55
5	2.82	1.83	2.33	20.61	22.80
6	1.98	3.61	2.79	31.60	28.04
7	1.80	3.02	2.41	17.53	22.22
8	4.55	7.26	5.90	66.55	35.90
9	2.67	4.59	3.63	18.67	22.09
10	2.64	2.75	2.70	27.62	26.21
11	1.57	2.52	2.04	14.77	19.50
12	2.37	2.25	2.31	19.29	21.95

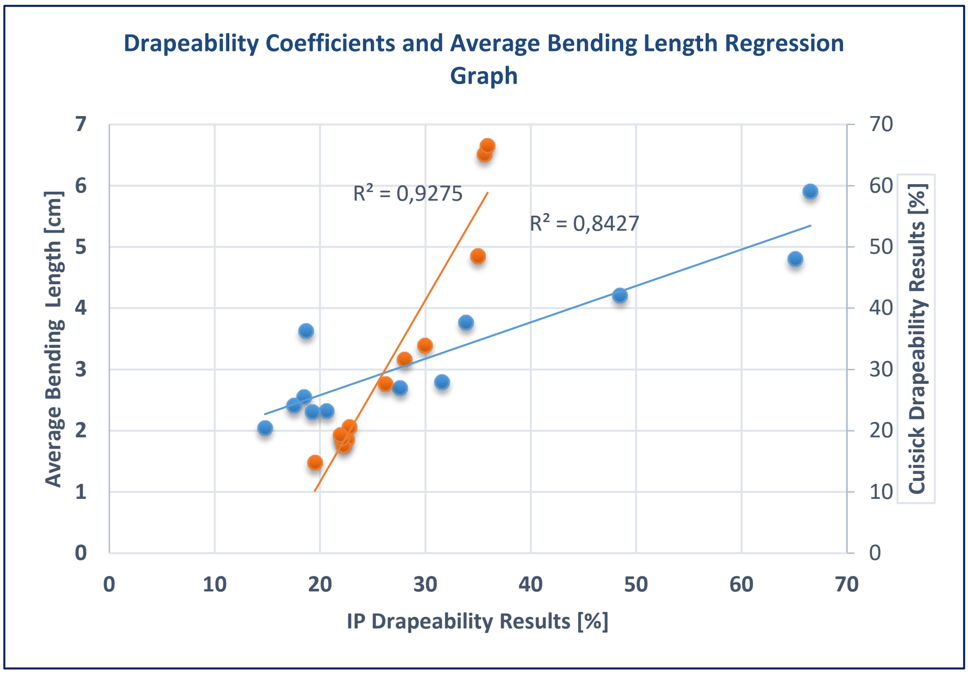

Figure 4. Regression Between Drape Coefficients and Bending Length

CONCLUSION

In this study, the relationship between developed fabric drape measurement with image processing, average bending length and traditional drape test (Cusick Drapeability) were evaluated. The presented study belongs to a prototype system at the initial stage. By applying regression analysis between the three method results, it was proofed that the developed image processing system have high accuracy and sensitivity for fabric drape measurement. On the other hand, the proposed method is easier and takes shorter time than other two methods; bending length and Cusick drape measurement.

Nowadays, developments in artificial intelligence and industry 4.0 provide important advantages in manufacturing and so they are rapidly taking place in the textile sector. Since the image processing technique provides an objective assessment of the quality control tests as well as determining the drapability properties of the fabrics, the manually applied processes can be performed both in a shorter time and with high accuracy. Image processing techniques and machine vision systems can be successfully adapted to industrial application. As a result, this modified method was recommended for reasons such as saving paper, reducing user errors, archiving images and especially reducing the testing time drastically. The manual test method (Cuisck test device) each sample takes half an hour to measure, while in image processing technique each sample is measured in less than one minute. This means a significant saving of time during the test measurement.

REFERANCES

Al-Gaadi, B., Göktepe, F., Halász, M. (2012). A new method in fabric drape measurement and analysis of the drape formation process. *Textile Research Journal*, 82(5), 502-512.

Behera, B. K., & Pattanayak, A. K. (2008). Measurement and modeling of drape using digital image processing. *Journal of Fibre & Textile Research*, 33, 230-238.

BS 3356:1990. Method for determination of bending length and flexural rigidity of fabrics

Chen, J., Benesty, J., Huang, Y., Doclo, S. (2006). New insights into the noise reduction Wiener filter. *IEEE Transactions on audio, speech, and language processing*, *14*(4), 1218-1234.

Erdumlu, N., Sarıçam, C. (2015). Metal Tel Sarımlı Hibrid İplik İçeren Dokuma Kumaşların Dökümlülüğünün Görüntü Analizi Yöntemi İle Ölçülmesi. *Tekstil Ve Mühendis*, *22*(100).

Gonzalez, R. C. In *Digital Image Processing Using Matlab-Gonzalez Woods & Eddins* 2004, pearson

Hu, J. (Ed.). (2008). Fabric testing. *Elsevier.*

Kenkare, N., May-Plumlee, T. (2005). Fabric drape measurement: A modified method using digital image processing. *Journal of Textile and Apparel, Technology and Management*, *4*(3), 1-8.

Plattürk, G. G., Kiliç, M. (2014). Kumaş Dökümlülüğünün Görüntü Analizi Temelli Yöntemlerle Ölçülmesi. *Tekstil ve Mühendis*, *21*(94).

Tsai, K. H., Tsai, M. C., Wang, P. N., Shyr, T. W. (2009). New approach to directly acquiringe the drape contours of various fabrics. *Fibres & Textiles in Eastern Europe*, (3 (74)), 54-59.

NPTEL:Textile Engineering, Textile Testing, Drape https://nptel.ac.in/courses/116102029/53 Accessed 26.07.2019.

Özgüney, A. T., Taşkin, C., Özçelik, G., Ünal, P. G., & Özerdem, A. (2009). Handle properties of the woven fabrics made of compact yarns. *Tekstil ve Konfeksiyon*, 19(2), 108-113.

Süle, G. (2012). Investigation of bending and drape properties of woven fabrics and the effects of fabric constructional parameters and warp tension on these properties. *Textile Research Journal*, 82(8), 810-819.

ORCID

Halil İbrahim ÇELİK *https://doi.org/0000-0002-1145-6471*
Elif GÜLTEKİN *https://orcid.org/0000-0003-4910-4081*
Aydın BAŞKAR………………Undergraduate Student
Büşra ÖZTÜRK……………. Undergraduate Student
H.İbrahim DEMİREL………Under-graduate Student

KSÜ Mühendislik Bilimleri Dergisi, 22, Özel Sayı, 2019 KSU J Eng Sci, 22, Special Issue, 2019
Uluslararası İleri Mühendislik Teknolojileri Sempozyumu (ISADET) Özel Sayısı
International Symposium on Advanced Engineering Technologies (ISADET) Symposium Special Issue
Araştırma Makalesi Research Article

Kahramanmaras Sutcu Imam University
Journal of Engineering Sciences

Geliş Tarihi : 02.08.2019 Received Date : 02.08.2019
Kabul Tarihi : 04.11.2019 Accepted Date : 04.11.2019

ELEKTRİKLİ BİR ARACIN BATARYA SİSTEMİNİN MODELLENMESİ

MODELING THE BATTERY SYSTEM OF AN ELECTRIC VEHICLE

Ümit ÖZBALCI [1]*, *Erdal KILIÇ* [1]

[1] Kahramanmaraş Sütçü İmam Üniversitesi, Elektrik Elektronik Mühendisliği Bölümü, Kahramanmaraş, Türkiye

*Sorumlu Yazar / Corresponding Author: Ümit ÖZBALCI, umitozbalci@ksu.edu.tr

ÖZET

Giderek artan yakıt maliyetleri ve fosil yakıtlı araçların emisyon problemi nedeniyle otomotiv sektörü büyük bir değişim döneminden geçiyor. Bu nedenle hibrit ve elektrikli otomobiller üretilmeye başlandı. Elektrikli araçların maliyet, maksimum hız düşüklüğü, yüksek şarj süresi gibi dezavantajları ise henüz tam olarak çözüme kavuşturulmuş değildir. Lityum tabanlı bataryaların geliştirilmesi ile elektrikli araçlarda depolama bataryaları olarak kullanılmaya başlanmıştır. Bu bataryalar performans, dayanıklılık, güvenlik ve maliyet avantajları açısından günümüzde elektriksel sistemlerin enerji ihtiyacını karşılamak için tercih edilmektedir. Bu çalışmada, elektrikli bir araçta kullanılan batarya ve şarj sisteminin benzetim modeli kullanılarak batarya paketinin akım, gerilim ve şarj durumu grafiği elde edilmiştir.

Anahtar Kelimeler: Elektrikli araç, batarya paketi, batarya modelleme

ABSTRACT

The automotive sector is undergoing a major change due to the increasing fuel costs and the emission problems of fossil fuel vehicles. For this reason, hybrid and electric cars started to be produced. The disadvantages of electric vehicles such as cost, maximum speed decrease, high charging time are not yet fully resolved. Along with the development of lithium-based batteries, have being used as energy storage units in electric vehicles. These batteries are preferred to meet the energy requirements of electrical systems in terms of performance, durability, safety and cost advantages. In this paper, the current, voltage and state of charge graphs of a battery pack is obtained by using the simulation model of the battery and charging system used in an electric vehicle.

Keywords: Electrical vehicle, battery pack, battery modelling

GİRİŞ

Günümüzde enerji ve çevre sorunları nedeniyle yeni enerji teknolojileri geliştirilmektedir. Otomotiv endüstrisi de bu teknolojiler ile donatılan araçların üretimine ivme kazandırmıştır. Yeni enerji araçlarından hibrit, bataryalı ve yakıt hücreli elektrikli araçlar gelecekteki otomotiv enerji güç sistemleri için önemli gelişim teknolojileri olarak kabul edilmektedir. Elektrikli araçlar (EA) geleneksel fosil yakıtlı araçlara kıyasla daha verimli, daha temiz ve sürdürülebilir bir ulaşım alternatifi sunduklarından dolayı dünyadaki önde gelen otomotiv üreticilerinin stratejik öncelikleri haline gelmiştir (Jiang ve ark., 2015).

EA, bataryalarda depolanan gücü kullanarak elektrikli bir motorla çalışan araçtır. EA daha az hareketli parçaya sahip olduklarından bakımları minimum düzeydedir ve daha fazla enerji tasarrufu sağlamaktadırlar. EA, birçok avantajlarının yanında maliyet, hız düşüklüğü, yüksek şarj süresi, batarya ömrü gibi dezavantajları da bulunmaktadır. Elektrikli araç güç aktarma organlarının temel bir bileşeni olan batarya paketleri gerçek zamanlı kontrol ve izleme gerektirir (Ahmed, 2014). Bu batarya paketleri genellikle kurşun-asit, nikel kadmiyum, nikel metal hidrat ve lityum-iyon pil hücrelerinden meydana gelmektedir. Lityum-iyon bataryalar tipik olarak yüksek güç, enerji yoğunluğu ve uzun hizmet ömrü nedeniyle tercih edilen batarya çeşididir (Zhang ve ark., 2018).

Batarya yönetim sistemi, bir bataryadaki şarj durumu, sağlık durumu, kalan faydalı ömür gibi kritik parametrelerin doğru şekilde izlenmesinden ve denetiminden sorumludur. Batarya şarj durumu, bataryadan geri alınabilen mevcut batarya kapasitesini temsil etmektedir. Bu parametre batarya yaşlanma etkilerini azaltacak şekilde bataryayı çalıştırmak ve performansını iyileştirmek için bir bataryada izlenmesi gereken en önemli durumlardan biridir (Chen ve ark., 2017).

Şarj durum tahmini için uygulanan sezgisel veya deterministik matematiksel araçların kullanıldığı çok çeşitli yöntemler bulunmaktadır. Coulomb sayma yöntemi veya amper-saat (Ah) yöntemleri gibi standart ölçüm tabanlı tahmin yaklaşımlarının yanı sıra açık devre voltajı ve empedans ölçüm yöntemleri daha sezgisel ve güvenilir bir tahmin vermektedir (Gandalfo ve ark., 2015; Guo ve ark., 2018; Gadoue ve ark., 2018). Yapay sinir ağı ve bulanık mantık gibi makine öğrenmeye dayalı tahmin yöntemleri şarj durumu ile onu etkileyen faktörler arasındaki doğrusal olmayan ilişkiyi tanımlayarak genelde iyi bir şarj durumu tahmini vermektedir. Ancak öğrenme süreci oldukça hesaplamalı bir şekilde ağır olan bu yöntemlerin tahmin modelleri çevrimdışı oluşturulmaktadır (Zhou ve ark., 2011; Qian ve ark., 2015; Hannan ve ark., 2018). Kalman filtresi kullanan durum uzay modeli temelli tahmin yöntemleri kapalı döngü, çevrimiçi olma ve dinamik bir şarj durumu tahmin hata aralığının mevcut olması avantajları nedeniyle çok popüler bir yöntemdir (Sepasi ve ark., 2015; Zeng ve ark., 2018).

Bu çalışmada, mevcut elektrikli bir araçta kullanılan nominal gerilimi 115,2 V ve toplam kapasitesi 3525 Wh olan batarya paketinin eşdeğer devre modeli elde edilmiştir. Daha sonra batarya paketi ve şarj sisteminin modeli MATLAB/Simulink ortamında oluşturulmuştur. Bu model kullanılarak yapılan benzetim çalışmasıyla batarya paketinin akım, gerilim ve şarj durumu grafiği elde edilmiştir.

BATARYA MODELLEME

Sağlıklı bir şarj durum tahmini, yüksek kalitede bir batarya modeli gerektirir. Batarya modeli, batarya özelliklerini gerektiği kadar doğru yakalamalı, pratik olarak tanımlanabilir model parametrelerine sahip olmalı, seçilen batarya kontrol algoritmasına uygun olmalı ve hesaplama açısından verimli olmalıdır (Ahmed ve ark., 2015; Tong ve ark., 2013).

Batarya modelleri genel olarak eşdeğer devre bazlı modeller, elektrokimyasal modeller, deneysel modeller, yapay sinir ağı ve bulanık mantık tabanlı modeller olarak sınıflandırılabilirler. Eşdeğer devre bazlı modellerde bir bataryanın şarj ve deşarj davranışını modellemek için kapasitör ve direnç gibi elemanlar kullanılır. Bu modeller parametre ve model tanımlaması açısından basit ve hesaplama yönünden verimlidir. Elektrokimyasal modeller elektrolit ve her iki elektrot içindeki lityum birleşmesini modellemek için kısmi diferansiyel denklemleri kullanır. Elektrokimyasal modeller genellikle karmaşık olmalarına rağmen batarya kimyasına fiziksel bir bakış açısı sağladıklarından, batarya sağlık durumu tahmininde ve batarya bozulmasının izlenmesinde tercih edilirler. Deneysel veya davranışsal modeller batarya hücrelerinin davranışını tanımlamak için deneysel fonksiyon ve formüller kullanırlar. Daha az parametre kontrolü ile uygulanması kolaydır ve bir batarya yönetim sistemindeki gerçek zamanlı uygulamalarda kolayca kullanılabilmektedir. Yapay sinir ağı ve bulanık mantık tabanlı modeller doğrusal olmayan ve karmaşık girdi-çıktı ilişkilerini belirleyebilen modellerdir. Bu modelleme türü deneysel eğitim verilerine ihtiyaç duyduğundan gerçek zamanlı uygulamalar için yüksek hesaplama gücü ve zaman gerektirirler (Ahmed, 2014).

Direnç ve kondansatörlerden oluşan eşdeğer devre modelleri bir bataryanın gerilim-akım davranışının benzetimi için yaygın kullanılmaktadır (Xia ve ark., 2015). Bu çalışmada lityum-iyon pillerin modelleme ve benzetimi için Şekil 1'de verilen birinci dereceden bir RC eşdeğer devre modeli kullanmıştır (Zhang ve ark., 2017). Burada kontrollü gerilim kaynağı VOC lityum-iyon pilin açık devre voltajını, R_0 omik direncini, Rl polarizasyon direncini, C_1 polarizasyon kapasitansını ve U ise terminal gerilimi belirtmektedir. R_1 ve C_1 değerleri batarya şarj durumuna ve akımına bağlıdır. Batarya modelinin gerilim değeri şarj durumu, açık devre gerilimi, R_0, R_1 ve C_1 değerleri ile kontrol edilmektedir.

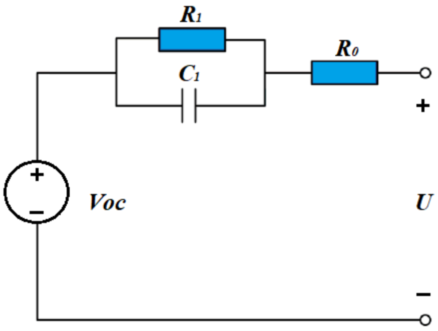

Şekil 1. Birinci derece RC model

Bataryanın parametreleri bataryanın akım ve gerilim değerlerinden faydalanılarak bulunmaktadır. Bu çalışmada kullanılan batarya modelinin 20°C'deki parametre değerleri Tablo 1'de verilmiştir (Web1; Ehsani ve ark., 2010).

Tablo 1. Batarya Modeli Parametreleri

Şarj Durumu (%)	**R_0**	**R_1**	**C_1**	**V_{OC}**
0	0,0085	0,0029	12447	3,5057
10	0,0085	0,0024	18872	3,5660
25	0,0087	0,0026	40764	3,6337
50	0,0082	0,0016	18721	3,7127
75	0,0083	0,0023	33360	3,9259
90	0,0085	0,0018	18360	4,0777
100	0,0085	0,0017	23394	4,1928

Bir bataryanın şarj durumu, bataryaya giren ve çıkan elektrik akımı miktarı göz önüne alınarak tahmin edilebilir (Ehsani ve ark., 2010).

$$SOC = SOC_0 - \int \frac{i}{Q(i)} dt \tag{1}$$

Burada *SOC* batarya şarj durumunu, *SOC0* batarya başlangıç şarj durumunu, *i* batarya akımını ve *Q* batarya kapasitesini göstermektedir.

BENZETİM ÇALIŞMALARI

Batarya paketinin modelleme ve benzetim çalışmaları elektrikli araç sisteminin ve bileşenlerinin tasarım sürecinde kolaylıklar sağlayacak ve fiziksel prototip üretmekten daha az maliyetli olacaktır. Ayrıca aracın performansı hakkında öngörüde bulunulmasını sağlayacaktır. Elektrikli aracın batarya paketinde hızlı şarj, uzun ömür ve yüksek güç yoğunluğu avantajları nedeniyle lityum iyon piller kullanılmıştır. Batarya paketinin performansını artıracak batarya karakterizasyonu, şarj durumu, batarya sağlık durumu, optimizasyon ve batarya yönetim sistemi üzerine algoritma geliştirmek amacıyla Tablo 2'de parametreleri verilen batarya paketi Matlab/Simulink ortamında modellenmiştir.

Tablo 2. Batarya Paketi Parametreleri

Parametre	**Değeri**
Pil Kapasitesi	3400 mAh
Pil Nominal Gerilimi	3,6 V
Hücre Pil Sayısı	9
Hücre Kapasitesi	30,6 Ah
Hücre Nominal Kapasitesi	110,16 Wh
Batarya Paketi	32 adet
Paket Gerilimi	115,2 V
Toplam Batarya Kapasitesi	3525 Wh

Maksimum Şarj Akımı	6,12 A
Şarj Süresi	5 Saat

Batarya paketi için her birinin kapasitesi 3400 mAh ve nominal gerilimi 3,6 V olan 9 adet lityum-iyon pil paralel bağlanarak batarya hücresi elde edilmiştir. 32 adet batarya hücresi birbirine seri bağlanarak nominal gerilimi 115,2 V ve kapasitesi 3525 Wh olan Şekil 2'de gösterilen batarya paketi oluşturulmuştur.

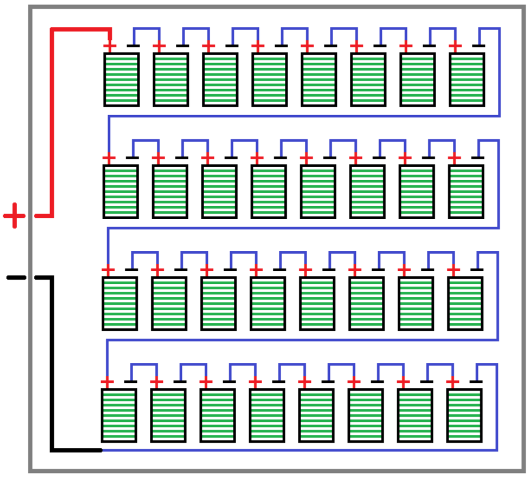

Şekil 2. Batarya paketi

Batarya paketinin şarj ve şarj durum tahmini için benzetim çalışması yapmak amacıyla Şekil 3'te verilen MATLAB/Simulink modeli oluşturulmuştur. Başlangıçta minimum kapasitede olan batarya paketi 6 A sabit akım ile şarj edilmiştir. Batarya paketi maksimum gerilim değeri olan 134,4 V'a ulaşıncaya kadar sabit akımla şarj edilmiştir. Bu gerilim değerinden sonra paket 134,4 V sabit gerilim ile şarj edilmeye devam edilmiştir. Bu durumda batarya paketinin çektiği şarj akımının zamanla azaldığı Şekil 4'te görülmektedir. Akım değeri belirlenen minimum şarj akım değerin altına düştüğünde ise şarj işlemi tamamlanmıştır. Şarj durum tahmini incelendiğinde ise batarya paketinin yaklaşık 4 saatte %90'a yakın ve 5 saatte %100 şarj olduğu görülmektedir.

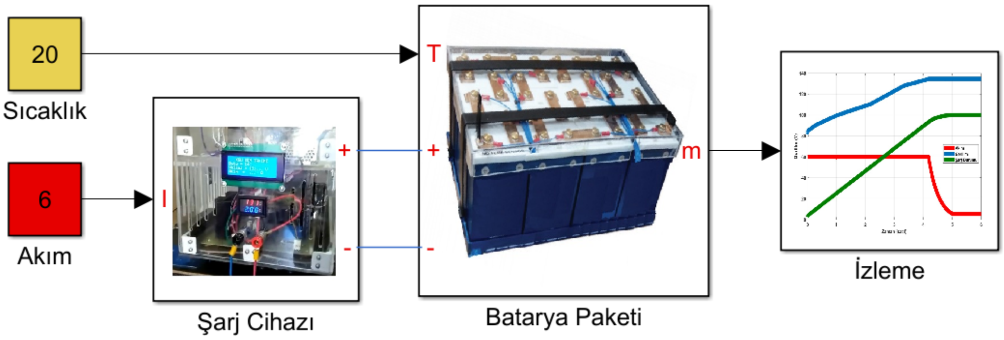

Şekil 3. Batarya paket ve şarj sisteminin simulink modeli

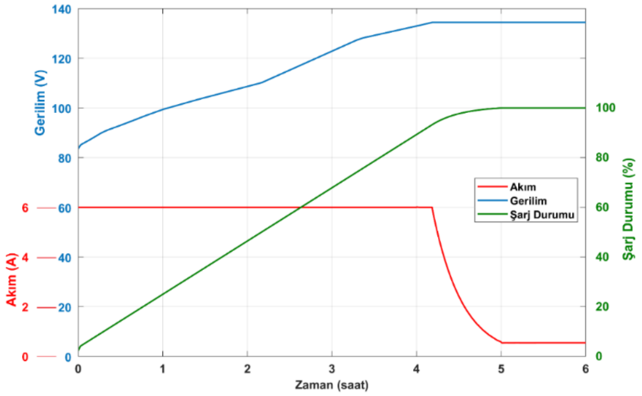

Şekil 4. Batarya paketinin akım, gerilim ve şarj durumu grafiği

SONUÇ

Bu çalışmada elektrikli bir aracın batarya paketi MATLAB/Simulink ortamında modellenmiştir. Batarya paketinin akım, gerilim ve şarj durumu benzetim çalışmalarıyla elde edilmiştir. Batarya paketinin sabit akım-sabit gerilim şarj yöntemiyle yaklaşık 5 saatte tam şarj durumuna ulaşmıştır. Benzetim çalışmalarından elde edilen sonuçların gerçek sistemin nominal değerleri ile örtüştüğü görülmüştür.

Bu çalışma ile batarya paketinin performansını artıracak çalışmaların öncelikle benzetim yoluyla yapılmasına olanak sağlanmıştır. Ayrıca batarya paketi modeli, oluşturulacak bir batarya yönetim sistemi ve araç motor modeliyle entegre edilip araç düzeyinde benzetim çalışmaları yapılabilir.

KAYNAKLAR

Ahmed, R., (2014). Modeling and state of charge estimation of electric vehicle batteries, (Doctoral dissertation, McMaster University).

Ahmed, R., Gazzarri, J., Onori, S., Habibi, S., Jackey, R., Rmezien, K., Tjong, J., LeSage, J. (2015). Model-Based Parameter Identification of Healthy and Aged Li-ion Batteries for Electric Vehicle Applications, *SAE Int. J. Alt. Power*, 4, 2.

Chen, J., Ouyang, Q., Xu, C., Su, H. (2017). Neural network-based state of charge observer design for lithium-ion batteries, *IEEE Transactions On Control Systems Technology*, 26, 1.

Ehsani, M., Gao, Y., Emadi, A. (2010). *Modern Electric, Hybrid Electric, and Fuel Cell Vehicles – Fundamentals, Theory, and Design*, 2nd edition, CRC Press.

Gadoue, S., Chen, K.W., Mitcheson, P., Yufit, V., Brandon, N. (2018). Electrochemical Impedance Spectroscopy State of Charge Measurement for Batteries using Power Converter Modulation, The 9th International Renewable Energy Congress (IREC 2018).

Gandolfo, D., Brandao, A., Patino, D., Molina, M. (2015). Dynamic model of lithium polymer battery e Load resistor method for electric parameters identification, *Journal of the Energy Institute*, 88.

Guo, D., He, L., (2018). A Novel Algorithm for SOC using Simple Iteration and Coulomb Counting Method, IEEE Student Conference on Electric Machines and Systems.

Hannan, M.A., Lipu, M.S.H., Hussain A., Saad, M.H., Ayob, A. (2018). Neural Network Approach for Estimating State of Charge of Lithium-Ion Battery Using Backtracking Search Algorithm, *IEEE Access*, 6.

Huria, T., Ceraolo, M., Gazzarri, J., Jackey, R. (2012). High Fidelity Electrical Model with Thermal Dependence for Characterization and Simulation of High Power Lithium Battery Cells, IEEE International Electric Vehicle Conference.

Jiang, J., Zhang, C. (2015). Fundamentals and Applications Of Lithium-Ion Batteries In Electric Drive Vehicles.

Qian, L., Si, Y., Qiu, L. (2015). SOC estimation of LiFePO4 Li-ion battery using BP Neural Network, EVS28 International Electric Vehicle Symposium and Exhibition.

Sepasi, S., Roose, L.R., Matsuura, M.M. (2015). Extended Kalman Filter a Fuzzy Method for Accurate Battery Pack State of Charge Estimation, *Energies*, 8, 6.

Tong, S., Klein, M.P., Park, J.W. (2013). A Comprehensive Battery Equivalent Circuit Based Model For Battery Management Application, ASME 2013 Dynamic Syst. and Cont. Conf.

Xia, B., Wang, H., Wang, M., Sun, W., Xu, Z., Lai, Y. (2015). A new method for state of charge estimation of lithium-ion battery based on strong tracking cubature kalman filter. *Energies*, 8, 12.

Zeng, Z., Tian, J., Li, D., Tian, Y. (2018). An Online State of Charge Estimation Algorithm for Lithium-Ion Batteries Using an Improved Adaptive Cubature Kalman Filter, *Energies*, 11, 1.

Zhang, C., Allafi, W., Dinh, Q., Ascencio, P., Marco, J. (2018). Online estimation of battery equivalent circuit model parameters and state of charge using decoupled least squares technique, Energy, 142.

Zhang, L., Peng, H., Ning, Z., Mu, Z., Sun, C. (2017). Comparative research on RC equivalent circuit models for lithium-ion batteries of electric vehicles, *Applied Sciences*, 10, 7.

Zhou, Y., Bai, C., Sun, J. (2011). Application of Genetic Neural Network in Power Battery Charging State-of-Charge Estimation, I.J. Intelligent Systems and Applications.

Lithium Battery Model, Simscape Language and Simulink Design Optimization.
https://ww2.mathworks.cn/matlabcentral/fileexchange/36019-lithium-battery-model-simscape-language-and-simulink-design-optimization/ Accessed 26.6.2019

ORCID

Ümit ÖZBALCI *https://orcid.org/0000-0003-2685-156X*
Erdal KILIÇ *https://orcid.org/0000-0002-1572-6109*

KSÜ Mühendislik Bilimleri Dergisi, 22, Özel Sayı, 2019 KSU J Eng Sci, 22, Special Issue, 2019
Uluslararası İleri Mühendislik Teknolojileri Sempozyumu (ISADET) Özel Sayısı
International Symposium on Advanced Engineering Technologies (ISADET) Symposium Special Issue
Araştırma Makalesi Research Article

Kahramanmaras Sutcu Imam University
Journal of Engineering Sciences

Geliş Tarihi : 22.07.2019 Received Date : 22.07.2019
Kabul Tarihi : 04.10.2019 Accepted Date : 04.10.2019

ARITMA ÇAMURU, LÜLE TAŞI (SEPIYOLIT) VE YUMURTA KABUĞU ATIKLARININ POLİMER KOMPOZİT PLAKA ÜRETİMİNDE DEĞERLENDİRİLMESİ

EVALUATION of TREATMENT SLUDGE, SEPIOLITE and EGG SHELLS in THE PRODUCTION of POLYMER COMPOSITE PLATES

İlkay AKGÜRBÜZ [1], *Yağmur UYSAL*[2*]

[1]Atatürk Anadolu Lisesi, Kahramanmaraş, Türkiye
[2]Mersin Üniversitesi Mühendislik Fakültesi Çevre Mühendisliği Bölümü, Mersin, Türkiye

*Sorumlu Yazar / Corresponding Author: Yağmur UYSAL, yuysal@mersin.edu.tr

ÖZET

Bu çalışmada, kağıt fabrikası arıtma tesisinden çıkan atık arıtma çamuru, yumurta kabuğu ve lületaşı tozu atık materyalleri ile birlikte polipropilen (PP) bazlı termoplastik plaka üretiminde değerlendirilmiş ve elde edilen kompozit plakanın radyasyon geçirgenlik ve mekanik dayanım (eğilme direnci, çekme direnci, dinamik eğilme direnci, kopmada uzama ve darbe direnci) özelliklerini belirlenmiştir. Kompozit katkı maddeleri olarak kullanılan atık materyaller kütlece %20-50 oranlarında kompozit levha üretimine katılmış, tüm kompozit plakalar standart sıcak presleme yöntemi ile üretilmiş ve katkı maddeli polimer kompozitlerin özellikleri standart polipropilenden üretilen levha ile karşılaştırılmıştır. Elde edilen sonuçlarda yumurta kabuğu katkılı kompozit levhanın radyasyon geçirgenliğini azalttığı, çekme direncini artırdığı, arıtma çamurunun çekme direncini düşürdüğü ve arıtma çamurunda bulunan liflerin ve lületaşı (sepiyolit) tozunun elastikiyet modülünü artırdığı tespit edilmiştir. Katkı maddeleri kompoziti daha gevrek hale getirerek kopmada uzama ve eğilme direnci modülü değerlerini azaltmıştır. Eğilmede elastikiyet modülü değerleri ise arıma çamuru ve sepiyolit ilavesi ile artış göstermiştir. Çalışma kapsamında üretilen PP kompozitlerin tamamı ASTM D 6662'de istenilen değerlerden daha yüksek eğilme direnci ve eğilmede elastikiyet modülü değerleri sağlamıştır. Çalışmanın sonuçları, arıtma çamuru, yumurta kabuğu ve lüle taşı gibi atık maddelerin "sıfır atık" yaklaşımı ile yeniden değerlendirilmelerinin sağlanarak kompozit levha üretiminde kullanılabileceğini ve ülke ekonomisi açısından faydalı malzeme üretiminin gerçekleştirilebileceğini göstermiştir.

Anahtar Kelimeler: Arıtma çamuru, geri kazanım, kompozit levha, lüle taşı, , yumurta kabuğu

ABSTRACT

The aim of this study is to produce thermoplastic composite plates containing waste materials using additives such as industrial sewage sludge, eggshells and sepiolite, to determine the mechanical properties of these plates and to compare them with commercial polypropylene plates. These fillers were added to the polypropylene (PP) based composite in an amount of 20-50% by weight (dry basis), and all composite plates were prepared using the hot compression molding method. Mechanical properties (tensile strength, tensile modulus of elasticity, flexural strength, elasticity of bending coefficient, elongation and impact strength at break) and radiation permeability of composites were investigated and it was determined that filler type had an effect on mechanical properties significantly. It was found that the addition of egg shells reduced the radiation permeability of the PP-based composites and increased their tensile strength. Addition of sewage sludge to composite production decreased the tensile strength while, it caused to increase elasticity modulus in flexure because of its fibrous structure with sepiolite. In the light of these results, it was determined that PP based polymer composites produced with waste additives provide sufficient mechanical properties than only PP based polymer composite plates.

Keywords: Egg shell, polymer composite, recycle, sepiolite, sewage sludge

GİRİŞ

İki veya daha fazla malzemenin bir araya getirilmesiyle oluşturulan ve yeni özelliklere sahip malzemeler "Kompozit Malzeme" olarak adlandırılmaktadır. Kompozit üretiminde farklı polimerler ve farklı oranlarda lignoselülozik destek elemanı (lif veya un) dolgu maddesi ya da güçlendirici olarak kullanılabilmektedir. Kompozit malzemeler, tasarım gereği, bileşenleri arasındaki ara yüzün kalitesi ile karakterize edilir. Yenilikçi kompozit malzemeler geliştirmedeki ana odak noktalarından biri, takviyeler ve matris arasında uygun bir bağlanma sağlamaktır (Liotier ve ark. 2019). Malzemelerin üretiminde karbon içeriğini azaltma ilgisinin artmasıyla birlikte, biyo-bazlı veya geri dönüştürülebilir malzemeler gibi daha çevre ile uyumlu materyalleri geliştirmek için endüstriyel bir fikir birliği vardır (Boumbimba ve ark., 2017; Hablot ve ark., 2010; Reulier &Avérous., 2015; Reulier ve ark., 2016).

Polipropilen (PP), C_nH_{2n} monomerine sahip lineer yapıda çok yönlü bir termoplastik polimerdir. Ambalaj, inşaat ve diğer endüstriyel uygulamalarda yüksek mukavemet, kimyasal direnç, aşınma direnci ve düşük fiyat gibi geniş kapsamlı kullanışlı özellikleri nedeniyle matris bileşeni olarak yaygın şekilde kullanılır. Bununla birlikte, PP'nin zayıf darbe dayanımı uygulamasını sınırlayan bir özelliktir (Kargarzadeh ve ark., 2018). Bu sebeple, çoğu çalışmalarda üretilen polipropilen bazlı materyallerin özelliklerini iyileştirmek için PP ile uyumlu ajanlar kullanılarak kompozitler halinde kullanımına yönelinmiştir.

Arıtma çamuru; atıksu içerisindeki kendiliğinden çökebilen katılardan ve yine atıksuda bulunan ancak çökemeyen organik ve inorganik askıdaki katı maddelerin kimyasal ilavesi ile ya da biyolojik arıtım ile mikroorganizma flokları halinde çökelmesinden oluşan ve su içeriği yüksek, kokulu ve yüksek hacimli atıklar olarak tarif edilebilir. Endüstri tipine bağlı olarak çıkan atıksu karakterizasyonu da farklılık gösterdiğinden dolayı, arıtma çamuru da asitler, alkaliler, ağır metaller, fenoller, boyalar, hidrokarbonlar, yağlar gibi maddeleri içerebilmektedir. Son yıllarda araştırmacılar endüstriyel işletmelerden çıkan bu arıtma çamurlarının miktarını azaltma veya yeniden kazanmaya yöntemleri geliştirme ile ilgili çalışmalara yönelmişlerdir. Kağıt fabrikası arıtma çamuru, üretilen metrik ton kağıt başına yaklaşık 40-50 kg kuru madde içeren ve bertaraf maliyeti toplam atık su arıtma maliyetinin % 60'ına kadar çıkabilen bir endüstriyel çamurdur (Bajpai, 2015; Mahmood & Elliott, 2006; Son ve ark., 2004). Bu nedenle, kağıt fabrikası arıtma çamurunun geri dönüşümü selüloz ve kağıt endüstrisine ekonomik ve çevresel faydalar sağlayabilecek önemli bir çözüm yöntemidir.

Yumurta kabuğu, karides ve midye kabuğu, mürekkepbalığı iskeleti ve balık pulları gibi kabuk atıkları sadece zengin bir kalsiyum karbonat kaynağı değil, aynı zamanda proteinler, polisakkarit ve kitin gibi diğer organik bileşenleri ihtiva ederler (Ji ve ark., 2009; Nurul ve ark., 2011; Deng ve ark., 2014). Bu kabuk atıkları, mekanik performanslarını geliştirmek ve malzemenin çevre dostu özelliklerini korumak amacıyla biyolojik olarak parçalanamayan polimerler için bir biyo-dolgu maddesi olarak kullanılmaktadır (Mohamad ve ark., 2014; Poompradub ve ark., 2008). Yumurta kabuğu ve karides kabuğu atıkları, gıda endüstrilerinden bol miktarda temin edilebilmektedir. Yumurta kabuğu, % 95 kalsiyum ve % 5 organik bileşenlerden oluşur (Ji ve ark., 2009). Yumurta kabuğu, adsorbent, katalizör, gübre, hayvan yemi için bir katkı maddesi ve kaplama pigmentleri dahil çeşitli uygulamalarda kullanılmaktadır (Cho & Seo., 2010; Tsai ve ark., 2006; Yoo ve ark., 2009). Ayrıca, diğer ticari desteklere göre daha mekanik olarak dirençli oldukları için sürekli işlemlerde kullanım için uygun olduklarını kanıtlanmıştır.

Son yıllarda kil karışımlı polimer nanokompozitlere yönelik çalışmalar artış göstermektedir. Bu kompozitlerin seçilme nedeni, benzerlerine göre mekanik, optik, termal kararlılık ve bariyer özellikleri açısından geliştirilmiş teknik özellikler göstermeleridir. Bu özellikler kullanılan dolgu maddesine bağlı olarak değişim göstermektedir. Kompozit materyallere kil, talk ve kalsiyum karbonat gibi materyallerin eklenmesi ile kırılma, nem içeriği ve eğilme elastikiyet modülü stresi değerlerinde önemli olumlu gelişmelere ulaşılmıştır (Glenn ve ark., 2001; Matsuda ve ark., 2013; Pushpadass ve ark., 2008). Plastik materyallerde mekanik ve termal özellikler kalsiyum karbonat ilavesi ile önemli ölçüde iyileştirilmiştir (Wei ve ark., 2013; Chan ve ark., 2002; Lina ve ark., 2016). Ancak, yapılan önceki çalışmalar kalsiyum karbonatın nişasta/kalsiyum karbonat termoplastik kompozitinin biyodegradasyon hızını geciktirdiğini, aynı zamanda ticari kalsiyum karbonat üretiminin atmosfere CO_2 saldığını ve işlemin karbon ayak izini artırdığını bulmuştur (Klungsuwan ve ark., 2013; Bootklad & Kaewtatip, 2013). Bu sebeple, bu çalışmada polimer kompozit materyale mekanik özelliklerini artırmak amacıyla eklenen kalsiyum karbonatın yumurta kabuklarından temin edilmesi hem atık materyallerin geri kazanımı hem de karbon ayak izi salınım kontrolü açısından büyük önem taşımaktadır. Sepiyolit kil ailesine ait doğal kökenli nano dolgu maddesi olarak kullanılan lifli yapıda magnezyum-silikatlardır. Sepiyolitin kimyasal formülü $Si_{12}O_{30}Mg_8(OH)_4(H_2O).4H_2O$'dur ve iki tetrahedral silika tabakasından oluşan bloklardan ve merkezde magnezyumlu oktahedral levhadan oluşmaktadır. Bu bloklar uzunlamasına kenarları boyunca birbirine bağlanır ve liflerin uzunluğuna paralel doğrultuda uzanan 0.37 x 1.06 nm^2 boyutlarında ince kanalları oluşturur (Nikolic ve ark., 2017). Termoplastik polimerlerle nanokompozitlerde dolgu maddesi olarak sepiyolit kullanımı hakkında az sayıda çalışma vardır. Bu çalışmalarda polipropilen ve sepiyolit nanokompozitleri başarıyla hazırlanmış ve bu nanokompozitler için, sadece yüzey enerjisini azaltan ve sepiyolit dağılımını iyileştiren uyumlulaştırıcı varlığında bile mekanik özelliklerde iyileştirmeler elde edilmiştir (Mohamad ve ark., 2014; Poompradub ve ark., 2008).

Bu çalışmanın amacı, polipropilen bazlı polimer kompozit levha üretiminde kağıt fabrikası arıtma çamuru, yumurta kabukları ve sepiyolit (lüle taşı) atıklarının dolgu maddesi olarak kullanılmasının elde edilen kompozit plakanın fiziksel ve mekanik özellikleri üzerindeki etkisinin araştırılmasıdır. Elde edilen sonuçlar hiçbir katkı maddesinin kullanılmadığı polipropilen bazlı kompozit levhadan elde edilen sonuçlar ile karşılaştırılmıştır.

MATERYAL VE YÖNTEM

Materyal

Bu çalışmada, kompozit üretiminde polipropilen (PP MH 418) polimeri, arıtma çamuru, Lüle taşı (sepiyolit) tozu ve yumurta kabukları kullanılmıştır. Çalışmada dolgu maddesi olarak kullanılan atık arıtma çamuru Kahramanmaraş Kipaş Kağıt Fabrikası'ndan, yumurta kabukları Kahramanmaraş'da faaliyet gösteren bir pastaneden ve lüle taşları Eskişehir'deki lüle taşı üretim atölyesinden temin edilmiştir. Uyumsuzluk giderici ve yağlayıcı olarak toplam kütlenin %3'ü oranında parafin vaks (K.130.1000) ve Çinko stearat kullanılmıştır.

Plastik Kompozitlerin Üretimi

Arıtma çamuru atığı takviyeli polimer kompozitlerin üretimi; boncuk üretimi ve kompozit levha üretimi olmak üzere iki aşamada gerçekleştirilmiştir. Pelet (boncuk) üretimi tek burgulu ekstruder yardımıyla gerçekleştirilirken, levha üretimi pres kalıplama yöntemiyle soğutma özelliğine sahip sıcak preste gerçekleştirilmiştir. Kompozit üretimi Şekil 1'degösterilen iş akışı izlenerek gerçekleştirilmiş ve atık takviyeli PP esaslı kompozit üretiminde kullanılan katkı maddelerinin oranları Tablo 1'de verilmiştir. Atık takviyeli polimer kompozit üretiminde üretim reçetesine bağlı olarak plastik matrisi (PP), atık unları, uyumsuzluk giderici ve vaks yüksek devirli karıştırıcıda (900-1000 devir/dk) homojen bir karışım haline getirilmiştir. Oluşturulan homojen karışım ekstruder içerisinde 170-200 °C sıcaklığında eritilmiştir. Ekstruder içerisinde eritilmiş ve homojen karışım kalıba doğru dakikada 40 dev/dk vida hızı ile itilerek çıkan karışım su banyosunda soğutulmuştur. Soğutulan ekstruder çıktısı kırıcı vasıtasıyla küçük boyutlu peletler haline getirilmiştir (Şekil 2). Ekstrüzyon işlemi pelet haline getirilen malzeme tekrar 103±2°C sıcaklıkta 24 saat bekletilerek kurutulmuş ve kurutulan peletler 4 mm kalınlık çıtası kullanılan teflon bir plaka üzerine serilerek sıcaklığı 200 °C olan soğuma kapasiteli hidrolik preste 250x250x4 mm ebatlarında levhalar haline getirilmiştir (Şekil 2).

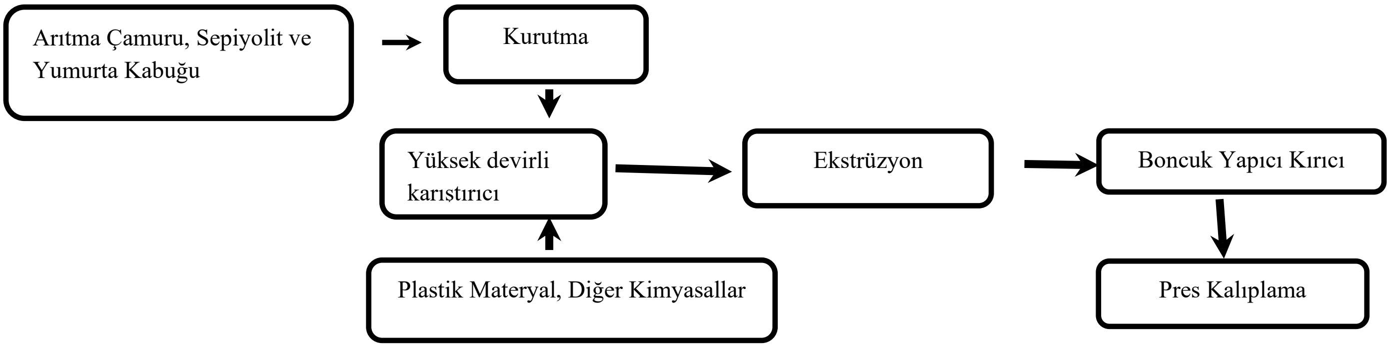

Şekil 1. Levha Üretim Aşamaları

Tablo 1: Arıtma çamuru ile PP karışımlı kompozitlere ait üretim reçetesi (%)

Grup no	Polimer (%)	AÇ (%)	Lületaşı (%)	YK (%)
PP-0	100	0	0	0
PP-1	50	50	0	0
PP-2	50	30	20	0
PP-3	50	30	0	20

Şekil 2. Kompozit Peletler ve Pres Kalıplama İle Üretilen Levhalar

Radyasyon Soğurma Katsayısının Belirlenmesi

Değişik enerjilerde gelen radyoaktif ışınların numunelerden geçerken yüzde kaçının geçip yüzde kaçının soğurulduğu tespit edilerek kompozit malzemenin belirli enerjilerde radyoaktif geçirgenlikleri tespit edilmiştir. Üretilen kompozit levhaların radyasyon geçirgenliğini test etmek için radyasyon kaynağı olarak Am-241 (59,60 KeV) radyoizotop kaynağı ve rezülasyonu 155 eV olan Si (Li) katı hal detektörü kullanılmıştır. Geçirgenlik sonuçları aşağıda verilen eşitliğe (Denk. 1) göre hesaplanmıştır.

$$\mu : \frac{\ln\left(\frac{I_x}{I_0}\right)}{X} \qquad (1)$$

μ: Soğurma katsayısı (1/mm); I_x: numuneden geçen ışın şiddeti (abs); I_0: numune yokken geçen ışın şiddeti (abs); X: numune kalınlığı (mm)

Mekanik Özelliklerin Belirlenmesi

Bu çalışmada üretilen kompozit örneklerin mekanik özellikleri malzeme testlerinde kullanılan Amerikan Standartlarına (ASTM) uygun olarak yapılmıştır. Ahşap biyobozunur plastik kompozitlerin mekanik özelliklerinin belirlenmesi için; eğilme direnci testi (ASTM D 790), çekme direnci testi (ASTM D 638) ve darbe direnci testi (ASTM D 256) uygulanmıştır.

Eğilme Direnci (ED) Testi

Eğilme testleri ASTM D 790'a göre gerçekleştirilmiştir. Test numuneleri 4x13x165 mm boyutlarında kesilmiş ve eğilme direnci ve eğilmede elastikiyet modülü değerlerinin belirlenmesi için her gruptan 5'er tane örnek seçilmiş ve Zwick/Roell z010 Üniversal Test Makinesi kullanılarak deneyler gerçekleştirilmiştir. Deney numunelerinin boyutları 0,01 mm duyarlıkta ölçülerek belirlenmiştir. Deney parçasının yerleştirildiği silindirik mesnetlerin merkezleri arasındaki uzaklık 80 mm olarak ayarlanmıştır. Deneylerde yük parçanın yüzeyine değişmez bir hızla tam ortasından uygulanmış ve deney cihazının yükleme hızı kırılmanın 1,5 ± 0,5 dk gerçekleşmesini sağlayacak şekilde 2 mm/dk olacak şekilde ayarlanmıştır. Kırılma anındaki kuvvet (F_{max}) okunup eğilme direnci (ED) aşağıdaki eşitliğe (Denk. 2) göre hesaplanmıştır.

$$ED = \frac{3.F_{max}.L_s}{2.bh^2} \qquad (2)$$

ED: Eğilme direnci (N/mm^2); Fmax: Kırılma anında uygulanan maksimum yük (N); Ls: Silindirik mesnetlerin merkezleri arasındaki uzaklık (mm); b: Kesit genişliği (mm); h: Kesit yüksekliği (mm)

Elastiklik modülünün belirlenmesinde eğilme direnci numuneleri kullanılmıştır. Elastik deformasyon bölgesinde uygulanan kuvvet farkı (ΔF) ve örnekteki sehimlere ait sonuçların aritmetik ortalamaları arasındaki fark (Δf) kullanılarak, elastiklik modülü (EM), aşağıdaki eşitlikten (Denk. 3) yararlanılarak hesaplanmıştır.

$$E = \frac{\Delta F.L_S{}^3}{4.b.h^3.f} \tag{3}$$

EM: Elastikiyet modülü (N/mm^2); ΔF: Uygulanan kuvvetler farkı (N); Ls: Dayanak noktaları arasındaki açıklık (mm); f: Yer değiştirme miktarı (mm); b: Kesit genişliği (mm); h: Kesit yüksekliği (mm)

Çekme Direnci (ÇD) Testi

Çekme direnci testleri ASTM D 683'e göre gerçekleştirilmiştir. Test örnekleri 4x13x165 mm'lik boyutlarda kesilmiş ve Zwick/Roell z010 Universal test makinesinde 5,0 mm/dk hızında gerçekleştirilmiştir. Deneyden önce, kuvvetin uygulandığı enine kesit alanı (A) 0,01 duyarlıkta ölçülüp, örneklerin çekme dirençleri (ÇD) uygulanan maksimum kuvvet (F_{max}) yardımıyla aşağıdaki eşitlikle (Denk. 4) hesaplanırken, elastikiyet modülü değerleri ise gerilim-eğim eğrisi üzerinden % 0,05 ve 0,2 eğim aralığında hesaplanmıştır.

$$ÇD = \frac{F_{max}}{A} \tag{4}$$

ÇD: Çekme direnci (N/mm^2); F_{max}= Maksimum yük (N); A= Deney parçasının kesit alanı (mm^2)

Dinamik Eğilme Direnci Testi (DE)

Dinamik eğilme direnci testleri ise ASTM D 256'ya göre gerçekleştirilmiştir. Test örnekleri 4x13x64 mm'lik boyutlarda kesilmiş ve test öncesi örnekler üzerinde Polytest RayRan™ cihazı yardımıyla çentik açılmıştır. Çentikleri açılan örneklerin darbe direnci testleri Zwick marka HIT5.5P test makinesinde gerçekleştirilmiştir. Hazırlanan deney numuneleri darbe direnci test makinesine yerleştirilerek deneye başlanmış numunenin kırılması için gerekli enerji (Q) belirlenmiştir. Dinamik eğilme direnci (DE) aşağıdaki eşitliğe göre (Denk. 5) hesaplanmıştır.

$$DE = \frac{Q}{B} \tag{5}$$

DE: Dinamik eğilme direnci (J/m) ; Q: Deney parçasının kırılması için gerekli enerji (J); B: Deney parçasının radyal ve teğetsel yönlerdeki boyutları (m)

BULGULAR VE TARTIŞMA

Kağıt fabrikası arıtma çamuru, Lüle taşı (sepiyolit) tozu ve yumurta kabukları eklenerek üretilen kompozit materyalin radyasyon geçirgenlik ve mekanik dayanım testlerinde elde edilen bulgular aşağıda verilmiştir.

Radyasyon Geçirgenlik Deneyi

Bir radyasyon demeti herhangi bir madde içerisinden geçerken çoğunlukla bir kısmı madde tarafından soğurulduğu için şiddeti azalır. Bu çalışmada, değişik enerjilerde gelen radyoaktif ışınların 4 mm kalınlığındaki numunelerden 500 s süresince geçerken yüzde kaçının geçip, yüzde kaçının soğurulduğu tespit edilerek numunelerin radyoaktif geçirgenlikleri ve lineer soğurma katsayıları tespit edilmiştir. Faklı enerjilerdeki ışınların I_0 (72658-299) numuneden geçen I_X değerleri ölçülerek soğurma katsayıları (μ) (Tablo 2). Geçirgenlik sonuçlarına göre farklı özellikteki kompozit numunelerden PP 3 (%50 PP, %30 AÇ, %20 YK) numunesinin soğurma katsayısının diğer kompozit örneklerine göre daha yüksek olduğu bulunmuştur. Soğurma katsayısının büyük olma durumu radyasyon ışımalarına karşı numunenin az geçirgen olduğunu gösterir. PP 1 (%50 PP, %50 AÇ) ve PP 2 (%50 PP, %30 AÇ, %20 sepiyolit) numuneleri ise istenilen sonuç açısından iyi çıkmakla beraber, PP 3'e göre daha düşük sonuç vermiştir. Geçirgenlik açısından ise PP 3 numunesinin diğerlerine göre az geçirgen olduğu gözlenmiştir.

Tablo 2: Kompozit numunelerin radyasyon geçirgenlik sonuçları

Enerji (keV)	Numune	I_0 (Sayım)	I_x (Sayım)	µ (1/cm)	Geçirgenlik
60 keV	PP 1	72658	66679	0,2146	0,9177
	PP 2		66190	0,2330	0,9109
	PP 3		65291	0,2672	0,8986
26 keV	PP 1	1778	950	1,5669	0,5343
	PP 2		1140	1,1111	0,6411
	PP 3		997	1,4460	0,5607
17,7 keV	PP 1	299	117	2,3456	0,3913
	PP 2		153	1,6750	0,5117
	PP 3		52	4,3729	0,1739
6 keV	PP 1	6740	-	-	-
	PP 2		-	-	-
	PP 3		-	-	-

Mekanik Dayanım Test Sonuçları

Arıtma çamuru, sepiyolit ve yumurta kabuğu katkılı polimer kompozitlerin çekme, eğilme, kopma ve darbe dirençleri gibi mekanik özelliklerinin belirlenmesi amacıyla yapılan testlerden elde edilen sonuçlar Tablo 3'de özetlenmiştir.

Tablo 3: Polimer kompozitlerin mekanik dayanım test sonuçları

Örnek	ÇD (N/mm^2)	ÇEM (MPa)	KU (%)	ED (N/mm^2)	EEM (N/mm^2)	DD (J/m)
PP-0	29,3±0,70	415,5±28,90	17,2±3,90	39,9±4,63	1244,1±135,19	2,7±0,36
PP-1	11,9±0,48	679,7±60,21	2,5±0,30	26,4±1,01	2089,6±61,28	2,1±0,09
PP-2	13,6±0,97	852,6±37,22	2,2±0,27	23,9±1,31	2539,7±107,65	1,7±0,24
PP-3	11,7±0,34	656,9±14,81	2,7±0,26	16,8±2,66	1843,1±97,43	2,0±0,13

Arıtma çamuru, sepiyolit ve yumurta kabuğu takviyeli PP esaslı kompozitlerin çekme direnci değerlerinin önemli oranda azaldığı tespit edilmiştir. Bu çalışmada %3 oranında uyumsuzluk giderici kullanılmasına rağmen istenilen düzeyde bir iyileştirme sağlanamamıştır. Kullanılan polimer tipinin ve takviye malzemelerin kompozit malzemenin çekme direnci üzerinde etkili olduğu tesit edilmiştir. PP esaslı % 30 AÇ-%20 sepiyolitden oluşan kompozitlerin (PP-2) nispeten PP esaslı % 50 AÇ'dan oluşan kompozitlere (PP-1) ve % 30 AÇ-%20 YK'dan oluşan kompozitlere (PP-3) kıyasla daha iyi çekme direnci sonuçları sağladığı tespit edilmiştir. Bu da AÇ oranının atmasının çekme direncini düşürdüğünü bununla birlikte kompozite eklenen sepiyolitin yumurta kabuğuna kıyasla çekme direncini artırdığını göstermektedir.

Üretilen kompozitlerin çekmede elastikiyet modülü değerlerinin kontrole göre önemli düzeyde arttığı tespit edilmiştir. Bu artış, PP-1 ve PP-2 kompozitlerinde daha yüksek bulunmuştur. Çekmede elastikiyet modülü en yüksek bulunan örnek %20 oranında sepiyolit ve %30 AÇ içeren örnektir. Arıtma çamurunda bulunan liflerin elastikiyet modülü değerlerinin saf polimerden elde edilen kompozit plakanınkinden yüksek olmasını ve takviye elemanı olarak kullanılan sepiyolitin de diğer kompozitlere kıyasla daha iyi çekmede elastikiyet modülü değerleri sağladığını göstermektedir. Kopmada uzama değerleri incelendiğinde, kompozitlerin kopmada uzama değerlerinin kontrol örneğine göre önemli düzeyde azaldığı tespit edilmiştir. Polimer matrisi içerisine ilave edilen lignoselülozik malzemelerin kompozitlerin çekmede elastikiyet modüllerini yükselttiği ve kompozit malzemeyi daha kırılgan hale getirdiği diğer çalışmalarda da görülmüştür. Bu çalışmada da AÇ, sepiyolit ve yumurta kabuğu kullanımının üretilen kompozit malzemeyi daha gevrek hale getirdiği ve bu nedenle kopmada uzama değerlerinin azaldığı düşünülmektedir. Mekanik özellik olarak incelenen bir diğer yöntem ise eğilme testleridir. Yapılan analizler sonucunda AÇ oranının azalması ve yumurta kabuğu ile üretilen kompozitlerin, PP esaslı kompozitlerin eğilme direnci değerlerini önemli düzeyde etkilediği tespit edilmiştir. Eğilme direnci modülü en yüksek kontrol örneğinde iken ortama eklenen katkı maddeleri eğilme direnç modülünün azalmasına neden olmuştur.

Eğilmede elastikiyet modülü değerlerine ait etkileşim değerleri incelendiğinde AÇ ve sepiyolit içeren PP esaslı kompozitlerin eğilmede elastikiyet modülü değerlerinin önemli düzeyde arttığı tespit edilmiştir. Bu sonuçlar, karışımı oluşturan lignoselülozik dolgu malzemesi ile polimerin elastikiyet modülü değerlerinin birbirinden farklı ve dolgu maddesinin sepiyolitin elastikiyet modülünün daha yüksek olmasından kaynaklanmaktadır. Bu nedenle de üretilen kompozitlerin nihai elastikiyet modülü değerleri lignoselülozik madde katılım oranındaki artışa bağlı olarak daha yüksek olmaktadır. Kullanılan takviye elemanları (sepiyolit ve yumurta kabuğu) ile üretilen polimer kompozitlerin eğilmede elastikiyet modülü değerleri üzerinde etkili olduğu bulunmuştur. Eğilmede elastikiyet modülü değeri en yüksek örneğin tüm katkı maddelerini içeren örnek olması (PP-2) bunu kanıtlamaktadır. Lületaşı ilavesi eğilmede eladtikiyet modülünde artışa neden olmuştur.Bu çalışmada üretilen polimer kompozitler kullanım alanları bakımından genelde plastik kerestelere alternatif olarak düşünülmektedir. Bu nedenle de bu tip malzemeler için kullanılan ASTM D 6662 standardıyla kıyaslanmıştır. Bu standart, poliolefin (PP ve PP) polimerlerden elde edilen polimerik kerestelerin sahip olması gereken eğilme test sonuçlarını göstermektedir. Eğilme direnci değerlerinin en az 6.9MPa ve eğilmede elastikiyet modülü değerlerinin ise 340 MPa olması istenmektedir. Çizelge7'de görüldüğü üzere çalışma kapsamında üretilen ve test edilen PP kompozitlerin tamamı ASTM D 6662'de istenilen değerlerden daha yüksek eğilme direnci ve eğilmede elastikiyet modülü değerleri sağlamıştır. Darbe direnci değerleri incelendiğinde içerisinde ASÇU, sepiyolit ve yumurta kabuğu takviyeli PP esaslı örneklerin darbe direnci arasındaki fark yok denecek kadar az olmaktadır. Polimerik matris içerisindeki AÇ varlığı darbe direnci değerlerini azaltıp ve kompozitin kırılganlığını artırırken kompozit bileşimine eklenen sepiyolit darbe direncini artırmıştır.

SONUÇ VE ÖNERİLER

Bu çalışmada kağıt fabrikası arıtma çamuru, sepiyolit ve yumurta kabuğu ilavesi ile polipropilen (PP) esaslı polimer kompozitler pres kalıplama yöntemiyle üretilmiştir. Elde edilen kompozitlerin mekanik özellikleri (çekme direnci, çekmede elastikiyet modülü, eğilme direnci, eğilmede elastikiyet modülü, kopmada uzama ve darbe direnci) incelenmiş ve mekanik özellikler üzerinde dolgu maddesi türünün önemli düzeyde etkili olduğu tespit edilmiştir. Dolgu maddesinin türü ile çekme direnci, kopmada uzama, darbe direnci ve eğilme direncinde azalma görülürken çekmede ve eğilmede elastikiyet modülü değerlerinde artış gözlemlenmiştir. Bu sonuçlar ışığında proje kapsamında üretilen PP esaslı polimer kompozitlerin yeterli mekanik özellikleri sağladığı tespit edilmiştir. Radyasyon geçirgenliği üzerinde yumurta kabuklarının etkili olduğu ve yumurta kabuğu katkılı kompozitin radyasyon geçirgenliğini önemli ölçüde düşürdüğü bulunmuştur. Bu sonuçlar, yumurta kabuğu katkılı kompozit malzemelerin özellikle radyoaktif cihazların bulunduğu hastane ve laboratuvarlarda döşeme ve bölme duvarı olarak kullanılabileceğini göstermektedir. Ayrıca, ülkemizin özellikle sepiyolit bakımından zengin yataklara sahip olduğu bilinmekle birlikte son yıllara kadar bu yataklar üzerinde yeterli çalışma yapılmamıştır. Türkiye'nin mevcut sepiyolit yataklarından açığa çıkan atık tozların polimer kompozit üretiminde değerlendirilmesinin ülke ekonomisi açısından önemli faydalar sağlayacağı ve incelenen atıklardan biyobozunur kompozit üretiminin sıfır atık yaklaşımı çerçevesinde alternatif bir yöntem olabileceği ortaya konmuştur.

KAYNAKLAR

Bajpai, P.(2015). Generation of waste in pulp and paper mills, management of pulp and paper mill waste. *Springer International Publishing Switzerland*, p.197.

Bootklad, M. & Kaewtatip, K. (2013). Biodegradation of thermoplastic starch/eggshell powder composites. *Carbohydr. Polym.,* 97, 315–320.

Boumbimba, R.M, Wang, K., Hablot, E., Bahlouli, N., Ahzi S. & Avérous L. (2017). Renewable biocomposites based on cellulose fibers and dimer fatty acid polyamide: experiments and modeling of the stress–strain behavior. *Polym Eng Sci*., 57 (1), 95-104.

Chan, M., Wu, J., Li, X. & Cheung K. (2002). Polypropylene/calcium carbonate nanocomposites. *Polymer,* 43, 2981–2992.

Cho B. & Seo G. (2010). High activity of acid-treated quail eggshell catalysts in the transesterification of palm oil with methanol. *Bioresour. Technol.,* 101, 8515–8519.

Deng, Q., Li, J., Yang, J. & Li, D. (2014). Optical and flexible α-chitin nanofibers reinforced poly (vinyl alcohol) (PVA) composite film: fabrication and property. *Compos. Part A,* 67, 55–60.

Glenn, M., Orts, J. & Nobes, R. (2001). Starch, fiber and $CaCO_3$ effects on the physical properties of foams made by a baking process. *Ind. Crop. Prod.,* 14, 201–212.

Hablot, E., Matadi, R., Ahzi, S. & Avérous L. (2010). Renewable biocomposites of dimer fatty acid-based polyamides with cellulose fibres: thermal, physical and mechanical properties. *Compos Sci Technol*., 70, 504–509.

Ji, G., Zhu, H., Q,i C. & Zeng M. (2009). Mechanism of ınteractions of eggshell microparticles with epoxy resins. *Polym. Eng. Sci.,* 49, 1383–1388.

Kargarzadeha, H., Huang, J., Linb, N., Ahmad, I., Marianoe, M., Dufresnee, A., Thomas, S. & Gałeski A. (2018). Recent developments in nanocellulose-based biodegradable polymers, thermoplastic polymers, and porous nanocomposites. *Progress in Polymer Science,* 87, 197–227.

Klungsuwan, P., Jarerat, A. & Poompradub S. (2013). Mechanical properties and biodegradability of cuttlebone/NR composites. *J. Polym. Environ.,* 21, 766–779.

Lina, Z., Yaodan, M. & Yang N. (2016). Controlled synthesis, characterization and application of hydrophobic calcium carbonate nanoparticles in PVC. *Powder Technol*., 288, 184–190.

Liotier, P.J., Pucci, M.F., Duigou, A., Kervoelen, A., Tirilló, J., Sarasini, F. & Drapiera S. (2019). Role of ınterface formation versus fibres properties in the mechanical behaviour of bio-based composites manufactured by liquid composite molding processes. *Composites Part B Engineering,* 163, 86–95.

Mahmood, T. & Elliott, A. (2006). A review of secondary sludge reduction technologies for the pulp and paper industry. *Water Res.,* 40, 2093-2112.

Matsuda, M., Verceheze, S., Carvalho, M., Yamashita, F. & Mali S. (2013). Baked foams of cassava starch and organically modified nanoclays. *Ind. Crop. Prod.,* 44, 705–711.

Mohamad, N., Latiff, A., Maulod, H., Azam, M. & Manaf M. (2014). A sustainable polymer composite from recycled polypropylene filled with shrimp shell waste. *Polym.-Plast. Technol. Eng.,* 53, 167–172.

Nikolic, M.S., Petrovic, R., Veljovic, D., Cosovic, V., Stankovic, N. & Djonlagic J. (2017). Effect of sepiolite organomodification on the performance of PCL/sepiolite nanocomposites. *European Polymer Journal,* 97, 198–209.

Nurul, I.K., Zuki, B.A.B., Mustapha, N., Mohd, Z.B.H., Norshazlirah, R. &. Eaqub A.M. (2011). Characterisation of calcium carbonate and its polymorphs from cockle shells (*Anadara granosa*). *Powder Technol.,* 213, 188–191.

Poompradub, S., Ikeda, Y., Kokubo, Y. & Shiono T. (2008). Cuttlebone as reinforcing filler for natural rubber. *Eur. Polym.* J., 44, 4157–4164.

Pushpadass, A., Babu, S., Weber, W. & Hanna A. (2008). Extrusion of starch-based loose-fill packaging foams: effects of temperature, moisture and talc on physical properties. *Packag. Technol. Sci.,* 21, 171–183.

Reulier M. & Avérous L. (2015). Elaboration, morphology and properties of renewable thermoplastics blends, based on polyamide and polyurethane synthesized from dimer fatty acids. *Eur Polym, J* 67, 418–27.

Reulier, M., Boumbimba, R.M., Rasselet, D. & Avérous L. (2016). Renewable thermoplastic multiphase systems from dimer fatty acids, with mineral microfillers. *J Appl Polym Sci,* 133(8), 43055-43067.

Son, J., Yang, H.S. & Kim, H.J. (2004). Physico-mechanical properties of paper sludge thermoplastic polymer composites. *J. Thermoplast. Compos. Mater.,* 17, 509-522.

Tsai, T., Yang, M., Lai, W., Cheng, H., Lin, C. & Yeh W. (2006). Characterization and adsorption properties of eggshells and eggshell membrane. *Bioresour. Technol.* 97, 488–493.

Wei, G., Xiaoyu, M., Yan, L., Zichen, W. & Yanchao Z. (2013). Effect of calcium carbonate on pet physical properties and thermal stability. *Powder Technol.,* 244, 45–51.

Yoo, S., Hsieh, J., Zou, P. & Kokoszka J. (2009). Utilization of calcium carbonate particles from eggshell waste as coating pigments for ınk-jet printing paper. *Bioresour. Technol.,* 100, 6416–6421.

ORCID

Yağmur UYSAL http://orcid.org/ 0000-0002-7217-8217
İlkay AKGÜRBÜZ http://orcid.org/0000-0003-2619-2517

KSÜ Mühendislik Bilimleri Dergisi, 22, Özel Sayı, 2019 KSU J Eng Sci, 22, Special Issue, 2019
Uluslararası İleri Mühendislik Teknolojileri Sempozyumu (ISADET) Özel Sayısı
International Symposium on Advanced Engineering Technologies (ISADET) Symposium Special Issue
Araştırma Makalesi Research Article

Kahramanmaras Sutcu Imam University
Journal of Engineering Sciences

Geliş Tarihi : 29.07.2019 Received Date : 29.07.2019
Kabul Tarihi : 22.10.2019 Accepted Date : 22.10.2019

GÜNEŞ ENERJİSİ DESTEKLİ KURUTMA SİSTEMİNDE ÜRÜN NEM ORANININ HESAPLAMALI AKIŞKANLAR DİNAMİĞİ ANALİZİ

COMPUTATIONAL FLUID DYNAMIC ANALYSIS OF PRODUCT MOISTURE RATE'S IN THE SOLAR ENERGY DRYING SYSTEM

Erdem ALIÇ [1,*], *Mehmet DAŞ* [2]

[1] Kahramanmaraş Sütçü İmam Üniversitesi, Makine Mühendisliği Bölümü, Kahramanmaraş, Türkiye
[2] Erzincan Binali Yıldırım Üniversitesi, İliç Dursun Yildirim MYO, Elektrik ve Enerji Bölümü, İliç, Erzincan, Türkiye

*Sorumlu Yazar / Corresponding Author: Erdem ALIÇ, ealic@ksu.edu.tr

ÖZET

Bu çalışmada hava ısıtmalı güneş kollektörlü bir gıda kurutma sistemi tasarlanmıştır. Tasarlanan kurutma sisteminde elma kurutulmuştur. Kurutulan elma dilimlerinin nem içeriği (MCk), kuruma hızı (DR) ve nem oranı (MR) değerleri hesaplanmıştır. Deneylerde kurutulan elma dilimlerinin dehidrasyonu sayısal analiz programı ile simüle edilmiştir. Kurutma analizi için birebir ölçülerde model oluşturulmuştur. İlk durumda elma diliminin çapı 60mm, kalınlığı 14mm ve yüzey sıcaklığı 4°C dir. Kurutma havasının giriş sıcaklığı 56.4°C ve hava hızı 1.6m/s dir. Analiz sonucunda ele edilen kuruma hızı ve zamanı, nem içeriği ve sıcaklık değişimi verileri mevcut deneysel çalışmalar ile karşılaştırılmıştır. Simülasyon sonucu elde edilen değerler ile deneysel çalışmalar sonucu hesaplanan değerler benzerlik göstermiştir.

Anahtar Kelimeler: Hesaplamalı akışkanlar dinamiği, gıda kurutma, nem içeriği, güneş enerjisi

ABSTRACT

In this study, a food drying system with air heated solar collector is designed. In the designed drying system, the apples are dried. Moisture content (MCk), drying rate (DR) and humidity (MR) values of dried apple slices were calculated. In the experiments, dehydration of the dried apple slices was simulated by the numerical analysis program. The model is designed for drying analysis. In the first case, the diameter of the apple slice is 60mm, the thickness is 14mm and the surface temperature is 4°C. The inlet temperature of the drying air is 56.4°C and the air velocity is 1.6 m/s. The velocity and time, moisture content and temperature change data of the dry matter were compared with the available experimental studies. The values obtained as a result of the simulation and the experimental studies were similar.

Keywords: Computational fluid dynamics, food drying, moisture content, solar power

GİRİŞ

Kurutma en önemli ve popüler saklama yöntemlerinden biridir. Isı ve kütle transferi mekanizması ile nemin bir malzemeden uzaklaştırılmasına sebep olur (Hashim vd., 2014). Kurutma, bitkisel, meyveler, otlar, tahıllar, baharatlar, yağlı tohumlar, odun ve yüksek nem içeriğine sahip diğer tarım ürünlerinin nem içeriğini azaltmada yaygın olarak uygulanır (Chen vd., 2015). Literatürde gıda kurutma alanında birçok değerli çalışmalar yapılmıştır. Şahin vd. (2016), konvektif bir kurutucuda kabak dilimlerinin kurutma kinetiğini incelemişlerdir. Deneyleri üç farklı hızda (0.5, 1.0 ve 1.5 m/s) ve üç farklı sıcaklıkta (40, 50 ve 60 °C) gerçekleştirmişlerdir. Artan hız ve sıcaklıkla kütle transfer parametrelerinin arttığı ve kuruma süresinin azaldığı tespit etmişlerdir. Akay vd. (2018) moleküler yapıdaki nem alma özelliğine sahip zeolitler kullanarak iplik kurutmuşlardır. Kurutma sistemi olarak tek iplik bobini kapasiteli kurutma deney düzeneğini kullanmışlardır. Kurutma sistemine iki adet zeolit yatak entegre edilmiş olup, kullanılan zeolit Z10-01 tipinde sentetik zeolit 13X ile doldurmuşlardır. Adsorpsiyon işlemini 19-21 °C ortam sıcaklığında kapalı çevrim olarak gerçekleştirmişlerdir. Adsorpsiyon işlemi sonucunda zeolitin kurutma ve nem alma performansını hesaplamışlardır. Karacabey ve Buzrul (2017), çalışmalarında sıcak havalı kurutucuda armut ürünü kurutmuşlardır. 40, 50, 60, 70 ve 80°C'de armut kurutma verilerini Weibull modeli ile tarif etmişler ve Weibull modelinin şekil parametresinin sıcaklığa bağlı olmadığını gözlemişlerdir. Akpınar (2006), doğal taşınımda direkt güneş altında sekiz farklı tarımsal ürünü (dut, çilek, sarımsak, patates, kabak, patlıcan ve soğan) kurutarak ısı ve kütle transfer katsayılarını tespit etmiştir.

Son yıllarda bilgisayar sistemlerinin gelişmesi ile birçok alanda bilgisayarlı analizler yapılmaya başlanmıştır. Hacıhafızoğlu vd.(2015), çalışmalarında küremsi geometriye sahip mısır tanesi kurutmuşlardır. Mısır tanesi üzerindeki nem içeriği değişimini sayısal olarak göstermişlerdir. Artan sıcaklık ile nem içeriğinin daha hızlı azaldığını ifade etmişlerdir. Reddy vd.(2017), çalışmalarında 1.5 m/s sabit hava hızıyla 55, 60, 65, 70 ve 75°C arasında, farklı sıcaklıklarda ananas kurutma özelliklerini incelemişlerdir. Farklı zaman aralıklarında ürün içerisindeki nem içeriğini karşılaştırmışlardır. Analiz sonuçlarına göre ananas ürünü için en iyi kurutma sıcaklığının 60 ° C olduğunu ifade etmişlerdir. Kumar vd.(2018), çalışmalarında 2-B aksi-simetrik geometride elma ürünü kurutmuşlardır. Çalışmalarında ürün nem içeriği, su buharı dağılımı ve evrimi, sıcaklık dağılımı ve buharlaşma oranını sayısal ve deneysel olarak incelemişlerdir. Sonuç olarak sayısal analiz ile ürün kurutma kinetiğinin hesap edilebileceğini ve ürün kalitesi tahmininde kullanılabileceğini belirtmişlerdir. Defraeye ve Marynenko (2019) çalışmalarında çoklu gıda ürünlerinin elektro hidrodinamik kurutulması üzerine çalışmışlardır. Adrover vd. (2019)'de, hareketli kurutma için izotermal hareketli sınır modeli ile analiz gerçekleştirmişlerdir. Sonuçlarını deneysel çalışmalar ile karşılaştırmışlardır. Sonuçların deneysel çalışmalar ile oldukça uyumlu olduğunu ifade etmişlerdir. Yuan vd.(2019)'de, ısı ve kütle transferi işlemi sırasında elma dilimlerinin kurutma büzülme-deformasyonu üzerine sayısal ve deneysel çalışma gerçekleştirmişlerdir. Nümerik çalışma için 2-D bir model yapmışlardır. Analiz sonuçlarının gıda kurutma büzülme-deformasyonu ile ilgili daha ileri analizler için teorik bir temel olduğunu ifade etmişlerdir. Yukarıda verilen altı çalışmanın da ortak noktası aynı sayısal analiz programı kullanılarak analizlerinin gerçekleştirilmiş olmasıdır. Bu analiz programı gıdalar için ısı ve kütle transferini aynı anda çözebilmektedir. Bu çalışma kapsamında bir güneş enerjisi destekli kurutma sistemi tasarlanmıştır. Tasarlanan kurutma sisteminde Granny Smith cinsi elma kurutulurmuştur. Kurutma işleminin sayısal analizi gerçekleştirilmiştir.

MATERYAL VE METOT

Deneysel Kurulum

Kurutma deney seti, havalı güneş kolektörü (HGK), kurutma kabini ve havalı güneş kollektörüne bağlı radyal fandan oluşmaktadır (Şekil-1). Deneylerde kullanılan HGK'leri 1400mm x 800mm ebatlarında olup, saydam cam örtüden, yutucu siyah mat boyanmış oluklu paslanmaz çelik sac (kalınlık 0.5 mm) plakadan, düz siyah mat boyanmış paslanmaz çelik sac (kalınlık 0.5 mm) plakadan, taş yünü (kalınlık 4 cm) yalıtım malzemesinden ve alüminyum dış kasadan (kalınlık 4mm) meydana gelmektedir (Şekil-2). HGK ise 23.7 ° (yerel enlem 38.4 °) kollektör açısı altında güneye yöneltilip, bu açıda paslanmaz çelik ayak ile sabitlenmiştir. HGK nın hava girişi kısmında bir santrifüj fan, (0.0833 m^3/s, 0.25 kW, 220 V, 50 Hz, 1380 dev/dak) şartlanmış hava sağlamaktadır (hız, 0.4 m/s).

Şekil 1. Havalı güneş kollektörlü kurutma sistemi

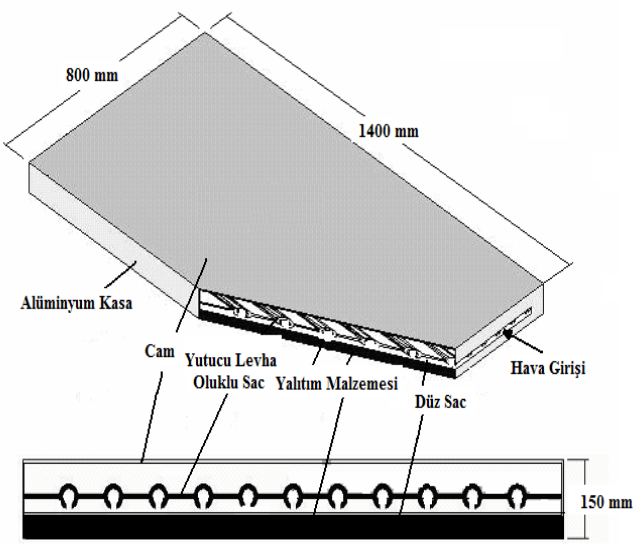

Şekil 2. Havalı güneş kollektörü detayı

Deney setinin kurutma proses şematik gösterimi ve ölçüm noktaları Şekil 3'de gösterilmiştir. Şekil 3'de sıcaklık ölçümleri sensörler yardımıyla, hava hızı ölçümleri anemometre, nem ölçümleri dijital nemölçer, radyasyon ölçümleri piranometre ve ürün tartımları dijital hassas terazi ile ölçülmüştür.

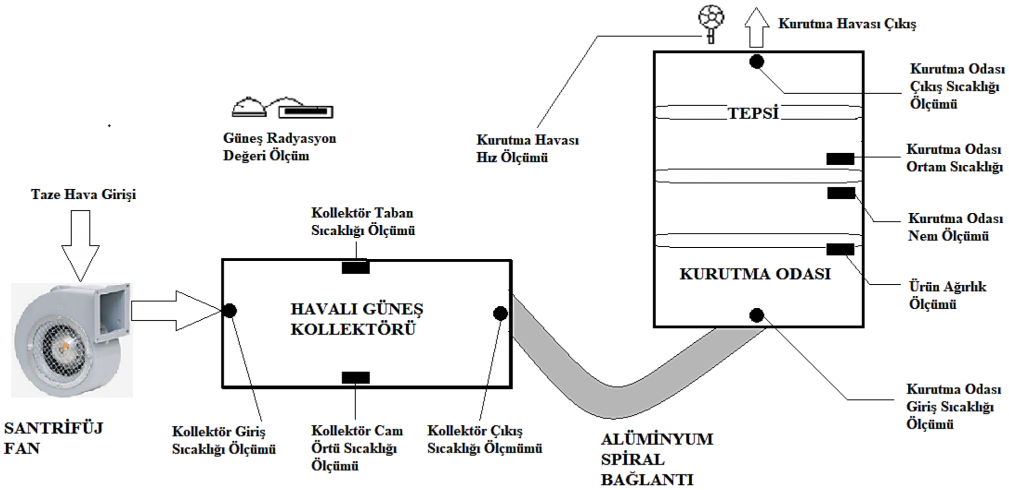

Şekil 3. Deney setinin kurutma prosesi ve ölçüm noktaları

Kurutma deneylerinde kullanılacak Granny Smith tipi elmadır. Kurutma deneyleri açık güneş altında Elazığ'da gerçekleştirilmiştir. Kurutma deneylerinde çevre hava sıcaklığı ve bağıl nem değerleri, güneş kollektör havasının giriş ve çıkış sıcaklıkları, kurutma kabini içindeki havanın nemi ve giriş-çıkış sıcaklıkları, rüzgâr hızları, güneş ışınım değerleri ve kurutma kabininde kurutulan elmaların kütle kaybı değerleri 30 dakika arayla ölçülmüştür.

Kurutma kabini alüminyum malzemeden (kalınlık 2 mm) yapılmış ve dikdörtgen boyutlarında dizayn edilmiştir. (100 cm x 50 cm x 100 cm). Havalı güneş kollektörü ile kurutma kabini arasında ısıtılan havayı aktarmak için bükülebilen alüminyum tip boru kullanılmıştır. Kurutma kabininin hava giriş kısmı, kolektörden gelen sıcak havayı kabine iletmek için davlumbazlı olarak imal edilmişlerdir. Kurutma kabinindeki hava, kabinin üst kısmından açılır kapanır menfez yardımı ile atmosfere çıkmaktadır. Kurutma kabini içine 3 adet gıda kurutmada kullanılan tepsi (90 cm x 40 cm) mevcuttur. Deneylerde gerçekleştirilen ölçümler için kullanılan aletler ve aletlerin hassasiyet değerleri Tablo 1'de gösterilmektedir.

Tablo 1. Ölçüm aletleri ve özellikleri

Parametre	**Ölçüm Aleti**	**Model**	**Hassasiyet**
Sıcaklık	J tipi demir kondansatör ısıl çift	Elimko 6400, İtalya	±0.1°C
Nem	Termo-Higrometre	EXTECH, 444731, Çin	±0.1°C
Hava Hızı	Dijital Anemometre	LUTRON, AM-4201, Tayvan	±0.1 m/s
Kütle	Dijital Tartı	BEL, Mark 3100, İtalya	±0.01 g
Güneş Radyasyon	Pirometre	Kipp and Zonen, İtalya	±0.1 Wm^{-2}
İlk-Son Nem	Nem Analiz Cihazı	Shimadzu MOC3, Japon	±0.001 g

Sistem Analizi

Sistemin kurutma analizlerinde kullanılan bazı genel eşitlikler aşağıda verilmiştir. Elmalardaki kuru esasa göre nem içeriği (*MCk*) ve yaş esasa göre nem içeriği (*MCy*) değerleri için sırasıyla denklem 1 ve denklem 2 kullanılmıştır (Akpinar K., E. 2008)

$$MCk = \frac{Ww - Dw}{Dw} \quad (1)$$

$$MCy = \frac{Ww - Dw}{Ww} x100 \quad (2)$$

Eşitlik (1) ve (2) 'de; *Ww* ıslak ağırlık ve *Dw* kuru ağırlıktır. Boyutsuz nem oranı (*MR*) değerleri Eşitlik (3) kullanılarak hesaplanmıştır.

$$MR = \frac{M - Me}{Mo - Me} \quad (3)$$

Eşitlik (3) ve (4) 'te; *M* nem, *Me* denge nemi, *Mo* ilk nem değerleridir.

COMSOL Analiz Programı

COMSOL programı sonlu elemanlar metodunu kullanarak çözüm yapan bir analiz programıdır. Bu çalışma için analizler COMSOL' da gerçekleştirilmiştir. Sayısal analiz 2b aksi-simetrik olarak gerçekleştirilmiştir. 2b aksi-simetrik analiz yapmanın en önemli avantajı çözümü üç boyutlu olarak alabilmek ve çözümü daha kısa sürede gerçekleştirmektir. Analiz ağ yapısının çarpıklığı 0.85 dir. Bu çarpıklık oranı çözüm için yeterlidir. Çözüm elemanının ağ yapısı Şekil 4'de verilmiştir. Burada tasarlanan güneş destekli kurutma sistemi temel olarak konvektif kurutucu ile aynıdır. Bu yüzden analiz konvektif kurutma şartlarında gerçekleştirilmiştir.

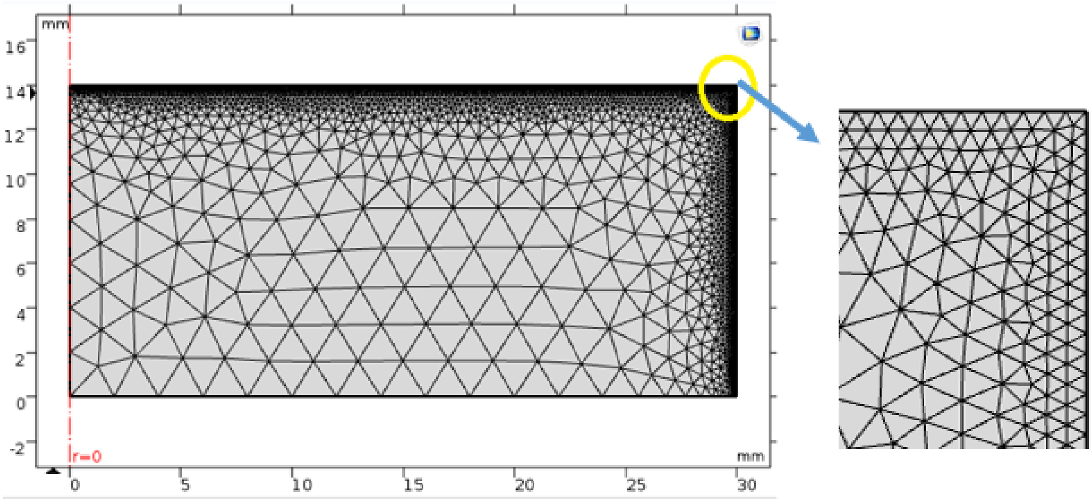

Şekil 4. Analiz ağ yapısı

Analizde kullanılan genel çözüm denklemleri aşağıda yer almaktadır.

*Kütle transfer denklemi

$$\frac{\partial M}{\partial t} = \nabla.\left(D(T)\nabla M\right) \tag{4}$$

*Kurutma havası denklemi

$$\frac{\partial M}{\partial t} + u.\nabla M = \nabla.\left(D_w(T)\nabla M\right) \tag{5}$$

*Süreklilik Denklemi

$$\rho C_p(M)\frac{\partial T}{\partial t} = \rho C_p(M)u.\nabla T = \nabla\left(k(M)\nabla T\right) \tag{6}$$

$$\frac{\partial \rho}{\partial t} + \nabla.(pu) = 0 \tag{7}$$

*Momentum Denklemi

$$\frac{\partial(\rho u)}{\partial t} + \nabla.(puu) = -\nabla p + \nabla.\left[\mu\left(\nabla u + (\nabla u)^T\right)\right] \; -\frac{2}{3}\mu(\nabla.u)I\Big] \tag{8}$$

*Başlangıç koşulları ve sınır şartları

Kurutma havası için;

$$-k\frac{\partial T}{\partial n} = \dot{m}.\lambda \tag{9}$$

Giriş: $T(x,y,z,0) = T_\infty$ (10)

Çıkış: $T(x,y,z,0)=T_0$ (11)

Giriş: $M_\infty = M_e$ (12)

Çıkış: $n.(-D.\nabla M)=0$ (13)

Başlangıç şartları

$$M(x,y,z,0)=M_0 \quad (14)$$

$$T(x,y,z,0)=T_0 \quad (15)$$

*Isı ve Kütle Transfer Katsayısı Denklemi

$$-k\frac{\partial T}{\partial n}=h(T_\infty - T_s) \quad (16)$$

$$h_{sabit}=18.5W(W.m^{-2}.K^{-1}) \quad (17)$$

Şekil 5'te çizilen 2b aksi-simetrik modelin gösterimi yapılmıştır.

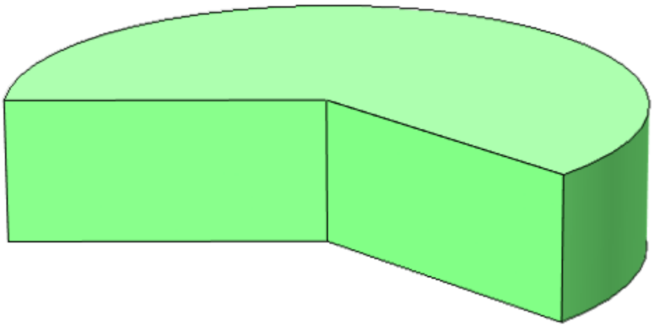

Şekil 5. Kurutulan elmanın 2b aksi-simetrik görünümü

BULGULAR VE TARTIŞMA

Bu çalışmada COMSOL 5.3a sayısal analiz programı kullanılmıştır. COMSOL sayısal analiz programı sıcaklık ve nem dağılımını modelleyebilmiştir. Elde edilen dağılım kontürleri aşağıdaki şekillerde gösterilmiştir. Burada güneş enerjisi destekli bir sistem kullanıldığı için ortam sıcaklığı zaman ile değişmektedir. Bu değişimden dolayı ortam sıcaklığının zamanla değişimini ifade eden bir denklem yazılmıştır. Giriş şartlarında kurutma havası sıcaklığı zamanla değişmektedir. Boyutsuz nem oranı da bu değişimlerden etkilenmektedir. Kurutma kabini içerisinde bulunan tepside kurutulan elma numunelerine ait yüzey ve merkez sıcaklık kontürleri Şekil 6'da gösterilmiştir.

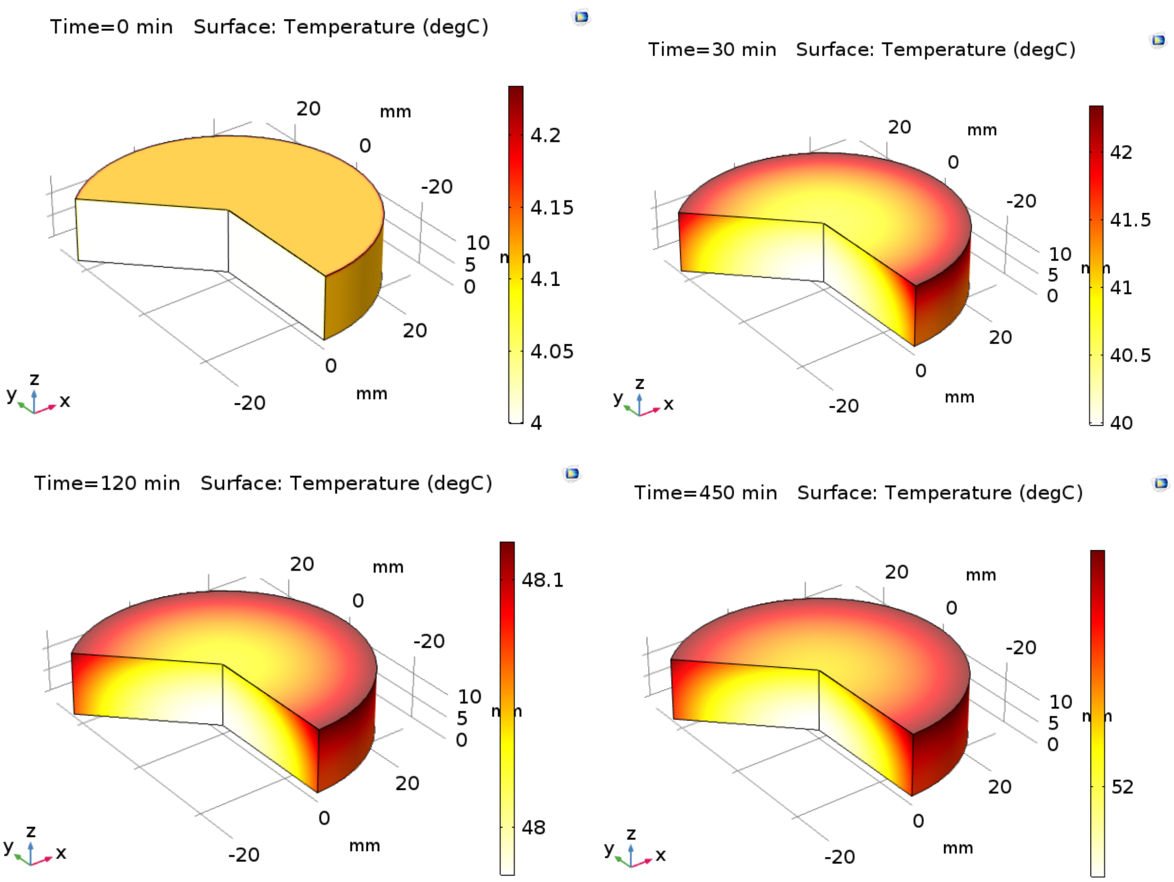

Şekil 6. Sıcaklık dağılım kontürleri

Kurutma deneyleri sonucu elde edilen yaş ve kuru baz nem içerik değerleri Şekil 7-8'de verilmiştir. Şekil 7'de yaş baz nem içeriği değerleri %83.1 ile %20.7 değerleri arasında değişmektedir. Şekil 8'de kuru baz nem içeriği değerleri 4.92-0.3 (gsu\gkmadde) arasında değişim göstermiştir. Elma ürünü kurutma sisteminde 480 dakikada kurumuştur.

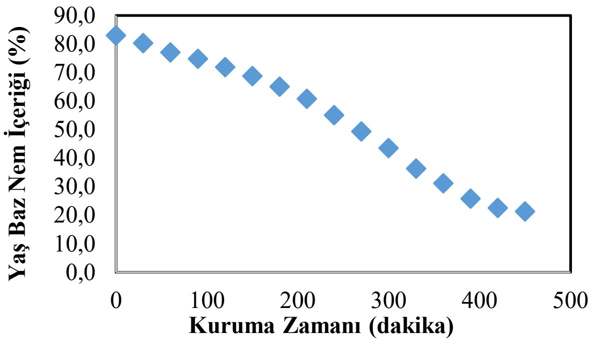

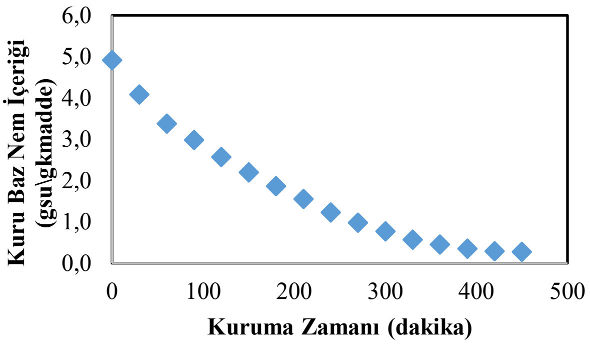

Şekil 7. Yaş baz nem içeriği

Şekil 8. Kuru baz nem içeriği

Comsol analiz programı ile elde edilen nem oranı ve ürün yüzey sıcaklığı değerleri ile deneysel nem oranı ve yüzey sıcaklığı değerleri karşılaştırmalı olarak Şekil 9-10'da gösterilmiştir. ElGamal ve diğ. pirinç tanesi kurutması için gerçekleştirdiği analizlerde de Comsol'un nem konsantrasyonu ve sıcaklık dağılımını başarı ile modelleyebildiğini göstermişlerdir (ElGamal vd. 2014). ElGamal çözüm modeli ile bu çalışmada yer alan çözüm modeli benzerdir. Şekil 9' da elma ürünü üzerindeki sıcaklık dağılım değerleri ile Comsol tarafından modellenen elma ürünü yüzey sıcaklık dağılım değerleri birbirlerine yakındır. Şekil 10'da ise boyutsuz nem oranı (MR) değerleri için deneysel veriler ile Comsol analiz verilerinin 90-270 dakika aralığında birbirlerine yakın değerler olmadığı görülmektedir. Bu farklılığın sebepleri; elma ürünü kurutma odasında oluşan ısı kayıpları ve sıcaklık-nem ölçümlerindeki belirsizlik oranı olarak açıklanabilir.

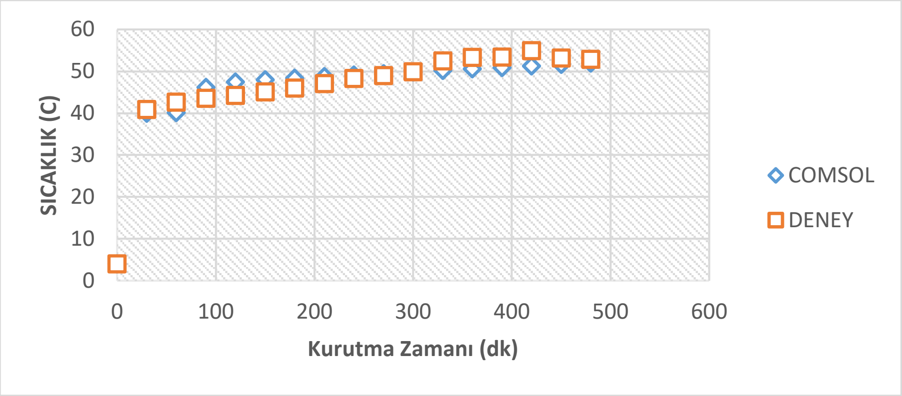

Şekil 9. Sıcaklık zaman eğrileri Comsol analizi ve deney sonuçları karşılaştırması

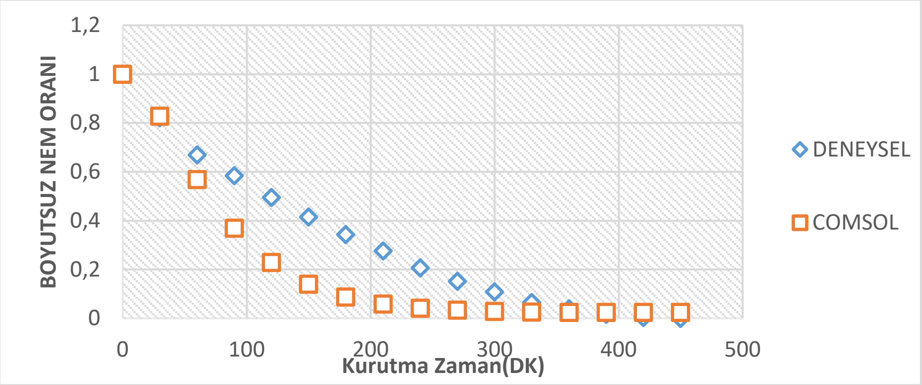

Şekil 10. Boyutsuz nem oranı zaman eğrileri Comsol analizi ve deney sonuçları karşılaştırması

Şekil 11'de nem konsantrasyonunun kontürleri gösterilmektedir. Elma ürünü kurutma başlangıç zamanı (0 dak) ile bitiş zamanı (420 dak) arasındaki nem konsantrasyonu incelendiğinde ürün içerisindeki nemin giderek azaldığı görülmektedir.

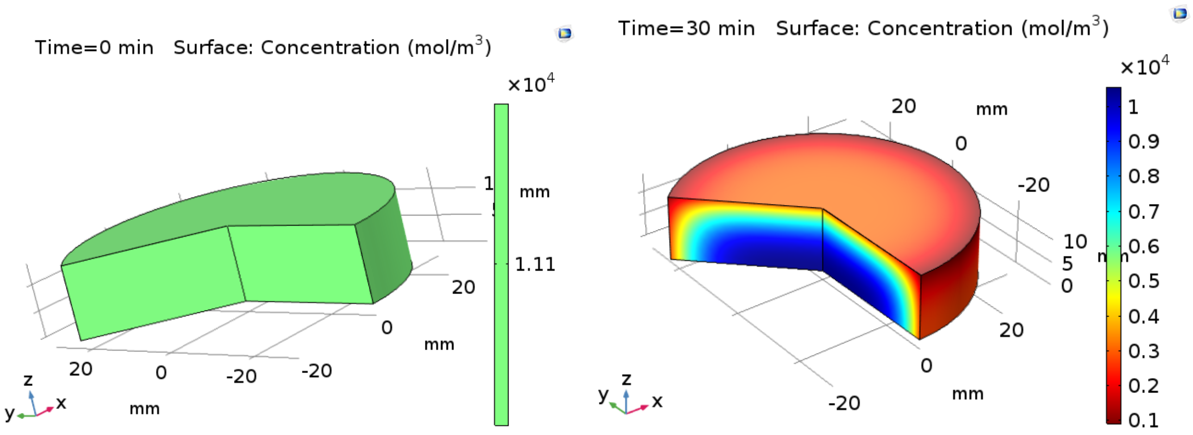

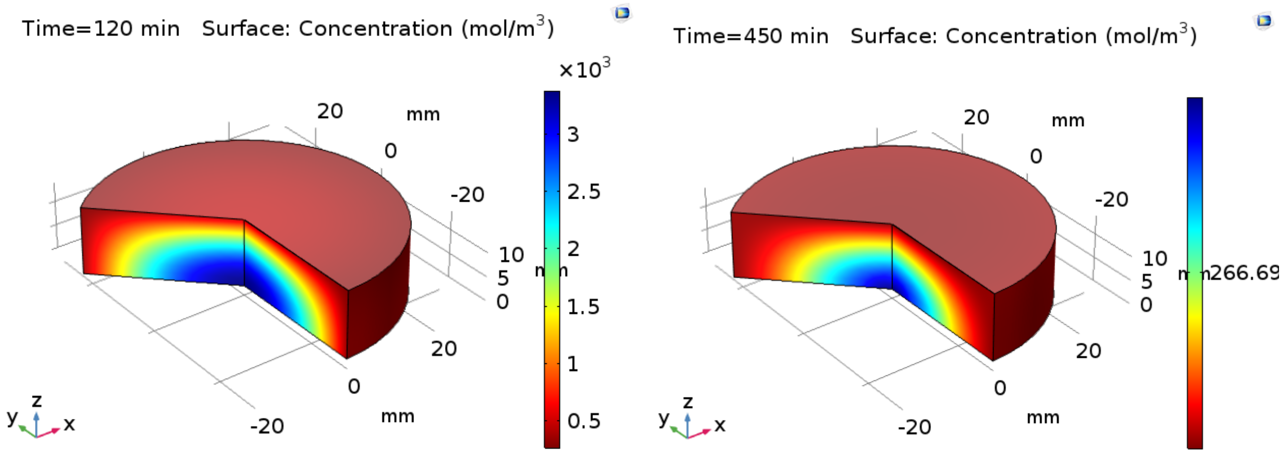

Şekil 11. Nem konsantrasyon dağılımları (mol/m³)

SONUÇLAR

Güneş enerjisi destekli kurutma siteminde kurutulan elma ürünü için yaş ve kuru baz nem içerik değerleri hesaplanmıştır. Kurutma sisteminde elma ürünü 420 dakikada kuruma işlemini tamamlamıştır. Deney şartlarında kurutulan elma ürününe ait nem oranı değeri için sayısal analiz programı kullanılarak aynı deney şartlarında tekrar hesaplanmaya çalışılmıştır. Sayısal analiz programının bulduğu nem oranı değerleri deneysel değerlerle benzerlik göstermiştir. Elma ürününün yaş baz nem içeriği değerleri %83.1 den %20.7 değerine 420 dakikada düşüş göstermiştir. Aynı şekilde kuru baz nem içeriği değeri 4.92 gsu\gkmadde den 0.3 gsu\gkmadde değerine düşüş göstermiştir. Kuruma işlemi süresince elma ürünü yüzey sıcaklık değeri 4-54 °C arasında değişim göstermiştir. Sayısal analiz programı ile elma ürünü yüzey sıcaklığı modellemesi sonucu değerleri 9-51.2 °C arasında değişim göstermiştir. Boyutsuz nem oranı (MR) deneysel olarak değeri 1-0.023 değerleri arasında değişmiştir. Sayısal analiz programı ile nem oranı modellemesi sonucu MR değerleri 1-0.011 değerleri arasında değişmiştir. Deneysel ve sayısal model verilerine göre MR değerleri benzerlik göstermiştir.

Sayısal analiz ile kurutma deneyleri sırasında elma ürününün sıcaklık değerlerinin zamanla değişimini göstermek adına çalışmaya faydalı görsel veriler kazandırmıştır. Sayısal analiz programları ile farklı ürünlerin nem oranları belirlenebilir ve ürün sıcaklıkları hakkında görsel bilgiler elde edilebilir.

KAYNAKLAR

Adrover, A., Brasiello, A., & Ponso, G. (2019). A moving boundary model for food isothermal drying and shrinkage: A shortcut numerical method for estimating the shrinkage factor. Journal of Food Engineering, 244(September 2018), 212–219. https://doi.org/10.1016/j.jfoodeng.2018.09.030

Akay, O. E., Gizlenci, Ö. S., Sönmez, K. (2018). Bir Kurutma Sisteminde Kullanılan Zeolit Kurutma Yatağının Adsorpsiyon Performansının Deneysel Olarak İncelenmesi. Kahramanmaraş Sütçü İmam Üniversitesi Mühendislik Bilimleri Dergisi, 21(1), 100-106.

Akpinar, E. K., & Bicer, Y. (2008). Mathematical modelling of thin layer drying process of long green pepper in solar dryer and under open sun. Energy Conversion and Management, 49(6), 1367-1375.

Akpınar, E.K., (2006). Experimental investigation of convective heat transfer coefficient of various agricultural products under open sun drying. International Journal of Green Energy, 1(4): 429- 440.

Chen, Q., Bi, J., Wu, X., Yi, J., Zhou, L., & Zhou, Y. (2015). Drying kinetics and quality attributes of jujube (Zizyphus jujuba Miller) slices dried by hot-air and short-and medium-wave infrared radiation. LWT - Food Science and Technology, 64(2), 759–766. https://doi.org/10.1016/j.lwt.2015.06.071

Defraeye, T., & Martynenko, A. (2019). Electrohydrodynamic drying of multiple food products: Evaluating the potential of emitter-collector electrode configurations for upscaling. Journal of Food Engineering, 240(July 2018), 38–42. https://doi.org/10.1016/j.jfoodeng.2018.07.011

Elgamal, R., Ronsse, F., Radwan, S. M., Pieters, J. G. (2014). Coupling CFD and diffusion models for analyzing the convective drying behavior of a single rice kernel. Drying Technology, 32(3), 311-320.

Hacıhafızoğlu, O., Susantez, Ç., Kahveci, K., & Akyol, E. (2015). Simulation of Intermittent Drying of Corn. In World Congress on Mechanical, Chemical, and Material Engineering (Vol. 1900, pp. 323-1).

Hashim, N., Daniel, O., & Rahaman, E. (2014). A Preliminary Study: Kinetic Model of Drying Process of Pumpkins (Cucurbita Moschata) in a Convective Hot Air Dryer. Agriculture and Agricultural Science Procedia, 2, 345–352. https://doi.org/10.1016/j.aaspro.2014.11.048

Kamer, M. S., Şahin, H. E., Sönmez, K., İmal, M., Kaya A. (2016). Kabak ve patlıcan dilimlerinin kuruma davranışının deneysel incelenmesi. Kahramanmaraş Sütçü İmam Üniversitesi Mühendislik Bilimleri Dergisi, 19(2), 1-8.

Karacabey, E. and Buzrul, S., (2017). Modeling and Predicting the Drying Kinetics of Apple and Pear: Application of the Weibull Model. Chemical Engineering Communications, 204(5), 573-579.

Kumar, C., Joardder, M. U., Farrell, T. W., Millar, G. J., & Karim, A. (2018). A porous media transport model for apple drying. Biosystems engineering, 176, 12-25.

Reddy, R. S., Ravula, P. R., Arepally, D., Munagala, S. R., & Golla, S. (2017). Drying kinetics and modelling of mass transfer in thin layer convective drying of pineapple. Chemical Science International Journal, 1-12.

Yuan, Y., Tan, L., Xu, Y., Yuan, Y., & Dong, J. (2019). Numerical and experimental study on drying shrinkage-deformation of apple slices during process of heat-mass transfer. International Journal of Thermal Sciences, 136(September 2018), 539–548. https://doi.org/10.1016/j.ijthermalsci.2018.10.042

Zhang, M.G., Li, W.H., Liu, M.Q. (2005). Adaptive PID control strategy based on RBF neural network identification, IEEE International Conference on Neural Networks and Brain, 1854-1857.

ORCID

Erdem ALIÇ *https://orcid.org/0000-0002-2852-0353*
Mehmet DAŞ *https://orcid.org/0000-0002-4143-9226*

KSÜ Mühendislik Bilimleri Dergisi, 22, Özel Sayı, 2019 KSU J Eng Sci, 22, Special Issue, 2019
Uluslararası İleri Mühendislik Teknolojileri Sempozyumu (ISADET) Özel Sayısı
International Symposium on Advanced Engineering Technologies (ISADET) Symposium Special Issue
Araştırma Makalesi Research Article

Kahramanmaras Sutcu Imam University
Journal of Engineering Sciences

Geliş Tarihi : 30.07.2019 Received Date : 30.07.2019
Kabul Tarihi : 31.10.2019 Accepted Date : 31.10.2019

DETERMINATION OF CATCHMENT CHARACTERISTICS OVER BALLIKAYA SUBBASIN IN CEYHAN WATERSHED VIA ARC-GIS ENVIRONMENT

CEYHAN'DAKI BALLIKAYA HAVZASININ KARAKTERISTIK ÖZELLIKLERININ ARC-CBS ORTAMINDA BELIRLENMESI

Muhammet Omer DIS [1*], *Adnan ELAGCA* [1]

[1] Kahramanmaras Sutcu Imam University, Department of Civil Engineering, Kahramanmaras, Turkey

*Sorumlu Yazar / Corresponding Author: Muhammet Omer DIS, momerdis@ksu.edu.tr

ÖZET

Medeniyet göstergesi olan su canlıların yaşam faaliyetlerini sürdürebilmesindeki yegane kaynaklardandır. Mevcut su kaynaklarından faydalanabilme (su kaynaklarının kurumaya karşı kontrol edilmesi, kalitesinin korunumu gibi) veya oluşabilecek fazla suyun risklerini minimize etmek amacıyla (taşkın gibi) havza yönetimi günümüzde büyük rol oynamaktadır. Bu amaçla, doğru bir şekilde havza sınırlarının belirlenmesi ve buna bağlı olarak yağıştan akışa geçiş süreçlerinin simülasyonlarında kullanılmak üzere gelişen teknoloji ile birlikte sayısal yükseklik modelleri (SYM) kullanılmaktadır. Bu çalışmada, Ballıkaya mevkiindeki (Ceyhan Havzası) nehir ağının tanımlanması, akım güzergahının, kümülatif akım haritasının, havza sınırlarının saptanması bunlara ek olarak havza alanı ve eğimi gibi karakteristik özelliklerinin belirlenmesi amacıyla yüksek çözünürlükteki SYM haritalarından faydalanılmıştır. Bu çalışma, SYM verilerinin ve Arc-GIS programının havza analizlerinde ne kadar pratik ve önemli olduğunu ortaya koymaktadır. Elde edilen SYM haritaları Arc-GIS ortamında işlenmiş, bölgede oluşabilecek olası hidrolojik süreçlerin tahmini (yağış-akış hidrografının elde edilmesi, taşkın frekans tahmini gibi) için hazır hale getirilmiştir.

Anahtar Kelimeler: Arc-CBS, Ballıkaya Havzası, Havza Karakteristikleri, SYM

ABSTRACT

Water, an indicator of civilization, is one of the rare resources in which living organisms can continue their life activities. Watershed management plays a major role today in order to benefit from existing water resources (i.e. controlling water resources against drought, maintaining water quality) or to minimize the risks of excess water that may occur (i.e. flooding). For this purpose, Digital Elevation Model (DEM) is used in conjunction with developed technology to accurately determine catchment boundaries and accordingly to be applied in rainfall-runoff simulation process. In this study, high resolution DEM data was implemented to identify the river network in the Ballikaya region (Ceyhan Basin), establish the flow direction, flow accumulation, and basin boundaries in addition to these, to determine the characteristic features such as catchment area, and slope. This study indicates how convenient and important DEM data and Arc-GIS are in watershed implementations. Obtained DEM data was processed in the Arc-GIS environment, and it provides a capability for the prediction of possible hydrological planning over the region (such as obtaining the precipitation-flow hydrograph, flood frequency estimation etc.).

Keywords: Arc-GIS, Ballikaya Basin, DEM, Watershed Characteristics

INTRODUCTION

Due to the importance of water for the life of the various living organisms on the surface of the Earth, it is necessary to protect this natural resource and take all necessary measurements to maintain it. For this reason that human being tried to know the properties, structure, and movement of water in the atmosphere and to identify the dangers that threaten the existence of water resources in nature since ancient times. Watershed management plays an important role today because of increasing demand for water day by day and scarcity of water resources (Ercan and Yuce, 2016).

The watershed is a geographical area that contains common hydrological features and is shared in a single outlet and can contain several small basins called sub-basin and can be a part of large basin (Anonymous, 2019). The identification of basin boundaries is an important step for subsequent studies such as hydrological modeling, water resource management, and determining the nature of vegetation cover and soil type (Sufiyan and Zakariyab, 2018). Previously, the limits of the watershed were determined based on the paper topographic maps (Ercan and Yuce, 2016). Now, as a result of the great evolution of the information technology, man has created computer-based programs that enable us to identify and manage the catchment smoothly and effectively. One of the most important of these programs is Geographic Information Systems (GIS), which process and analyze aerial images taken by satellites and the extraction of the basin boundaries. The GIS is a decision support system by integrating spatial information to solve environmental issues. Data within geographic information systems are divided into two basic types: spatial data that determines the coordinates of the study site on the Earth's surface and non-spatial data describing the quality and characteristics of this data (Dawod, 2012).

Spatial data is represented in the GIS environment through two formats: vector and raster data. Vector data is represented as a point with coordinates (x,y), polyline, or a closed polygon to represent regions. Raster data, on the other hand, is a file format where geographically referenced data is stored in cells of a two dimensional grid; each cell is assigned an attribute value (Irwin et al., 2014).

Digital Elevation Model (DEM) is the basic data required when drawing the boundaries of a catchment using the GIS. The DEM data is a digital file that contains elevation information for the surface of the study area and can be in either a vector or raster format. The DEMs are obtained from the contour maps after being digitized by computer, aerial photos, satellite images or free global models available on the internet. The most common ways to get DEMs are global digital elevation models (i.e. GLOBE, ETOPO2, ASTER, and SRTM) because it's free and covers a wide area of the Earth's surface. The U.S. space agencies have developed SRTM model according to three levels of spatial resolution capacity. The SRTM-30 has low spatial resolution capability, up to 30 seconds (900 m) of latitude and longitude. SRTM-3 and SRTM-1, on the other hand, have finer spatial resolution ability up to 3 seconds (90 m) and 1 second (30 m) for each pixel length, respectively (Dawod, 2012).

The main objective of this study is to derive the boundaries of the basin based on DEM via Arc-GIS environment for the study area located in Gaziantep, Turkey. The obtained high resolution DEM data (30m x 30m) is applied in order to accurately visualize the basin. Additionally, some watershed characteristics (basin area, slope, geomorphology and etc.) are calculated with Arc-GIS based hydrological analysis tool. This can provide an opportunity for the estimation of future hydrological planning over the region.

STUDY AREA AND DATA

Arc-GIS program produced by the American ESRI company, in 1969. The DEM data for the study area was obtained from the U.S. Geological Survey (USGS) with 30 m×30 m horizontal resolution as shown in the following Figure 1. Discharge point coordinates of the watershed obtained from the General Directorate of State Hydraulic Works, in Turkey.

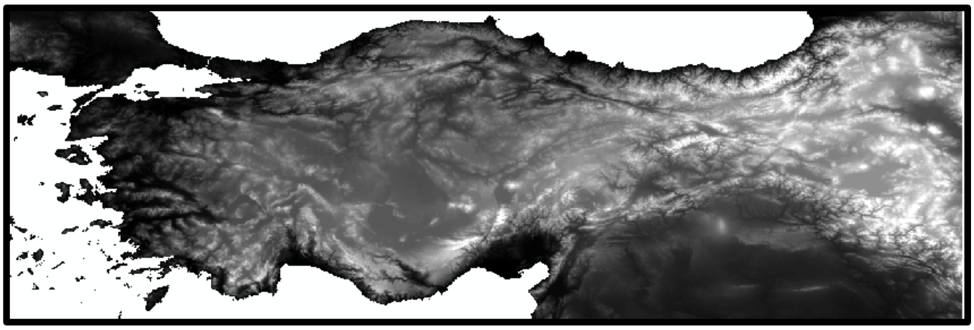

Figure 1. Digital Elevations Model For Turkey (Source: Anonymous, 2018)

In this study, Ballikaya region is selected to acquire basin characteristics such as area, stream, and drainage line. The watershed is located in Gaziantep province, in Turkey (Figure 2). The basin boundary extends between latitudes 37º04'30" N and 37º12'00" N, and longitudes 36º50'00" E and 37º02'30" E with outlet point 37°08'04"N and 36°52'40"E coordinates. The catchment area is approximately 78 square kilometers. In addition, the vegetation cover of the study area is mainly composed of agricultural lands, and forests. Soil type consisting of red Mediterranean, and lime brown forest soil.

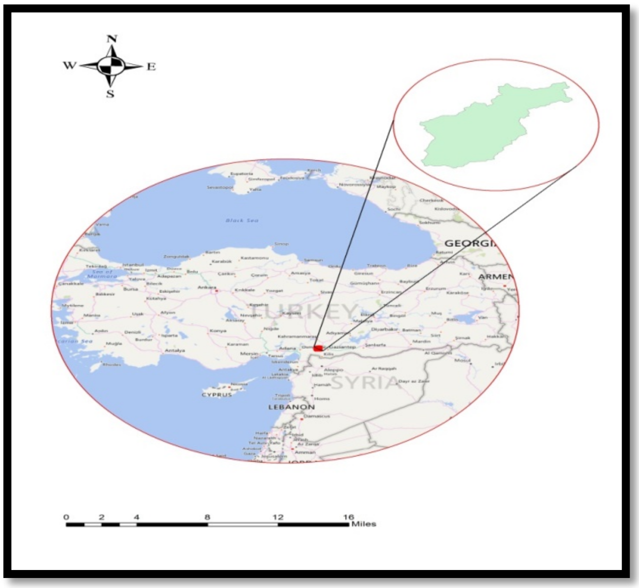

Figure 2. Location of Study Area

METHODOLOGY

Before starting the hydrological analysis process, the Geographic Coordinate System (WGS1984) of the study layer must be converted to the Projected Coordinate Systems (UTM) to avoid errors during measurements. Drawing the boundaries of the watershed using a DEM data is a sequence of steps where the output of each process is used as input for the next process (Ercan and Yuce, 2016).

Terrain Preprocessing

The DEM cells have some errors and abnormal values due to a defect in the model (SRTM) where some cells have high or small elevation values unexpectedly compared to its neighboring cells attribute. Therefore, these must be eliminated by the fill sink tool as shown in Figure 3. The abnormal values in digital elevations can hamper water flow between cells; thus, they have to be removed (Dawod, 2012).

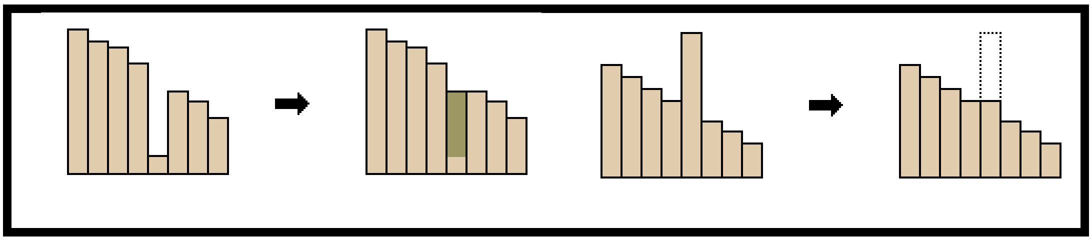

Figure 3. Illustration of Fill Sink (Source: Anonymous, 2019)

Flow Direction And Accumulation

Determination of flow direction is the most crucial step when conducting any hydrological modeling and is considered as input parameter when drawing basins and watershed boundaries (Ercan and Yuce, 2016). The flow direction of each cell is calculated using the corrected DEM produced by fill sink tool. The principle of this tool is to give a number ranging from 1 to 128 for each cell of the DEM data according to the elevation of the cell and adjacent cells (Figure 4a). As it can be seen from the Figure 4a, the number 78 (northwest corner) is accompanied by cells 67, 72, and 74, the lowest adjacent cell (67), because the water always moves in the direction of the steepest slope. From the Figure 4b, the same thing indicated with number 2 (northwest corner) in the way of flow direction instead of elevation. Then, these numbers represent the directions of a river (1-East, 2-South East, 4-south, 8-Southwest, 16-West, 32-northwest, 64-north ,and 128 -northeast) out of each cell of the DEM (Figure 4c). (Dawod, 2012; Anonymous, 2019).

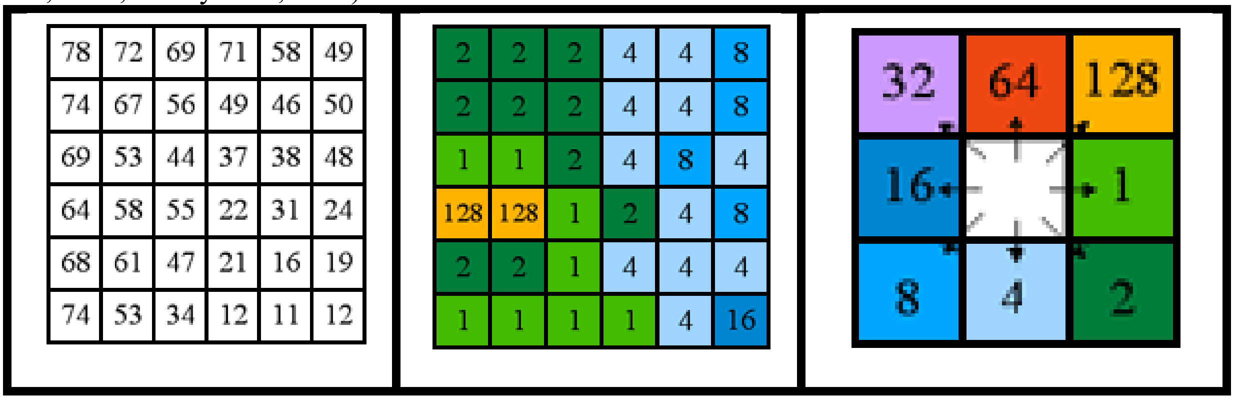

78	72	69	71	58	49
74	67	56	49	46	50
69	53	44	37	38	48
64	58	55	22	31	24
68	61	47	21	16	19
74	53	34	12	11	12

2	2	2	4	4	8
2	2	2	4	4	8
1	1	2	4	8	4
128	128	1	2	4	8
2	2	1	4	4	4
1	1	1	1	4	16

32	64	128
16		1
8	4	2

a) Elevation Surface **b)** Flow Direction **c)** Direction Coding

Figure 4. (Source: Anonymous, 2019)

After calculating the flow direction, the cumulative flow is accounted. This tool figures the cumulative water value in each raster cell and the cumulative values are represented by a number indicating the number of cells that are poured into this cell (Anonymous, 2019). For instance, from the following Figure 5, the cell with the number 11 means that the water flows to it from 11 adjacent cells. Thus, the main stream inside the basin is the cells where the flow values are high and the sub-streams are the cells with relatively lower flow values (Ercan and Yuce, 2016).

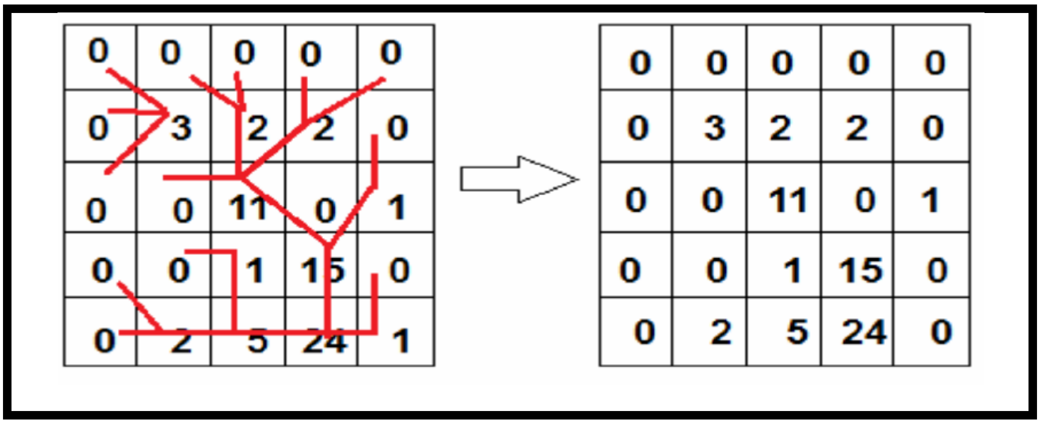

0	0	0	0	0
0	3	2	2	0
0	0	11	0	1
0	0	1	15	0
0	2	5	24	1

0	0	0	0	0
0	3	2	2	0
0	0	11	0	1
0	0	1	15	0
0	2	5	24	0

a) Flow Direction For Each Cell **b)** Flow Accumulation Values In Each Cell

Figure 5. (Source: Dawod, G.M., 2012)

Pour Point And Watershed

Later, the main stream is determined within the basin through the flow accumulation tool, the drainage point of the basin is defined by which the rain water is discharged out of the basin boundary. The pour point of watershed is mostly located on the main stream and then the catchment boundary can be efficiently determined using the watershed tool. If the pour point is adjacent to the main stream then we use the snap pour point tool to match the outlet of watershed on the main stream (Irwin et al., 2014).

RESULTS AND DISCUSSIONS

After transferring the digital elevation model into the Arc-GIS environment, the model is converted from the global geographic projection (WGS1984) to the local metric projection (ED1950). The model is, then, corrected and the errors removed by the fill sink tool in such a way as to ensure the flow of water without any obstacles. From Figure 6, it appears that the white areas represent the high points of the study area and the areas in black are the valleys and the water collection areas.

Figure 6. DEM For Ballikaya Watershed

As a next step, blanks are filled in the DEM data; then, the flow directions are determined in the Ballikaya region. As it can be seen from Figure 7, digital model cells are digitized with numbers varies between 1 to 128.

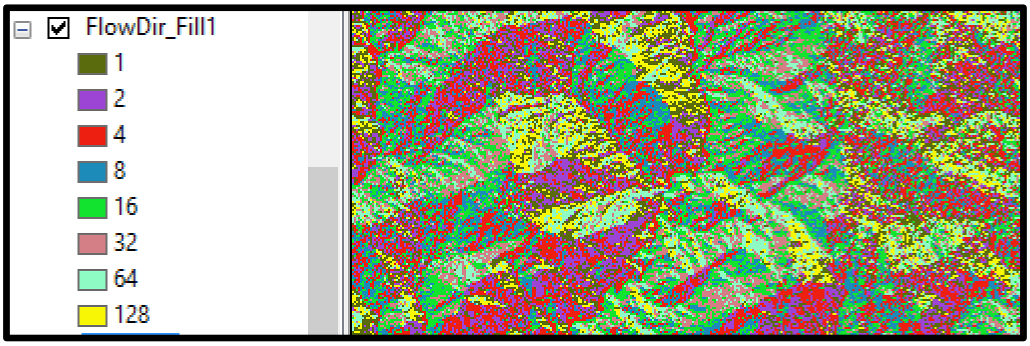

Figure 7. Flow Direction In Ballikaya Watershed

Cumulative flow is calculated based on flow directions and each cell carries a digit indicating the number of cells that flow into it. Cells with the number 0 mean that they are poured into another lower cell. The main stream within the basin consists of cells with high flow values (Figure 8). The discharge point of the basin with the coordinates (37°08'04"N - 36°52'40"E) is designated as a shape file of the type of points with the same type of metric projection (ED1950) to be used as an input to draw the basin boundary. Generally, at the point of drainage of the basin is a station to measure the flow of rain to draw the hydrograph between the flow and time.

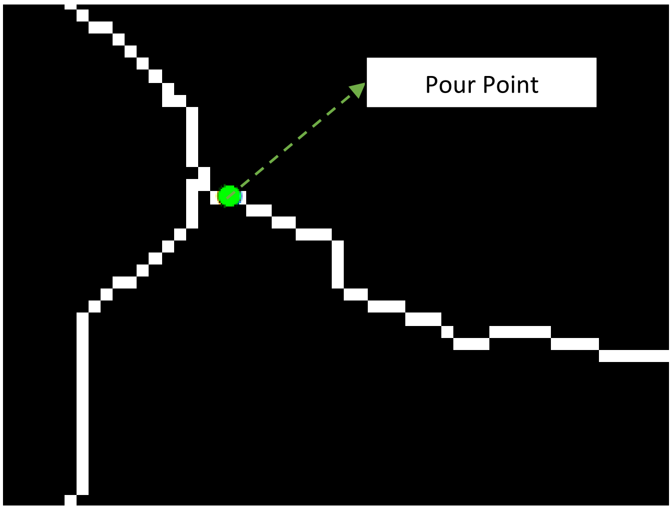

Figure 8. Flow Accumulation And Pour Point In Ballikaya Watershed

Finally, the watershed boundaries is set through the watershed tool based on the discharge point and flow direction. The below drawing of the basin (Figure 9a) is in raster format; however, this figure should be converted from the raster to vector (polygon) format in order to determine the basin area and water stream length (Figure 9b).

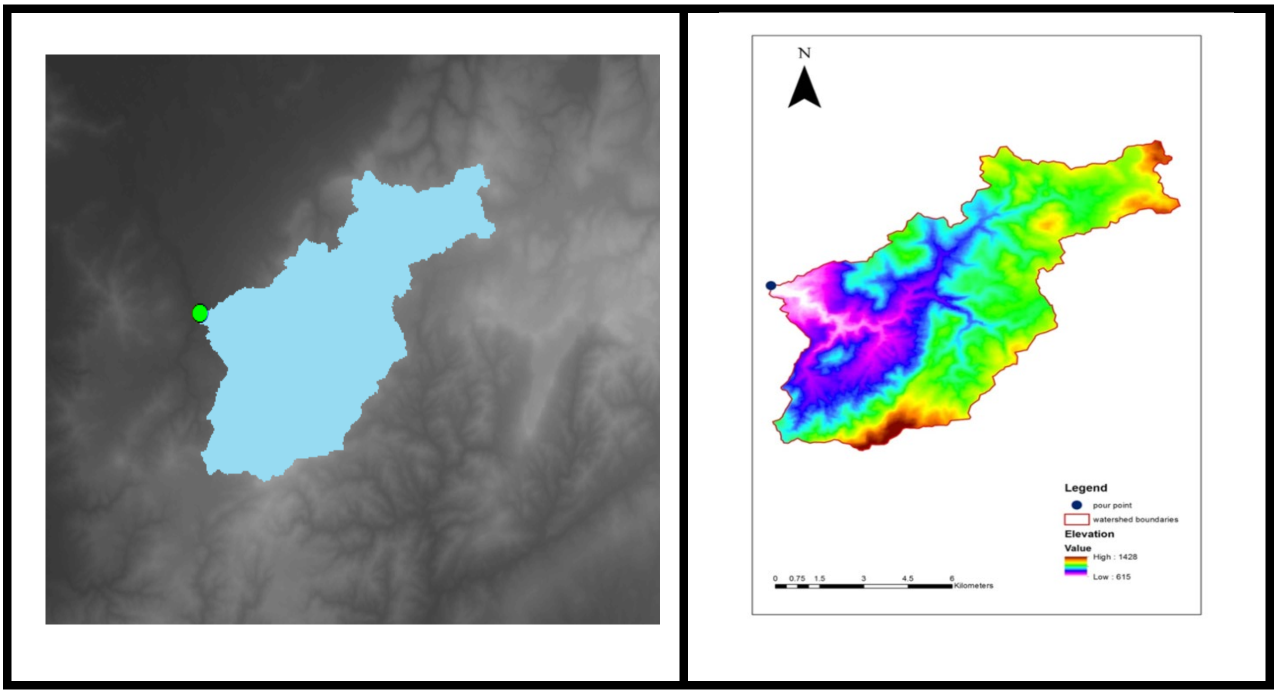

a) Ballikaya Watershed (Raster) **b)** Ballikaya Watershed (Polygon)

Figure 9. Ballikaya Watershed

CONCLUSIONS

Watershed analysis refers to the process of using topographic maps and following water flows to delineate stream networks and watersheds. The development of today's computer and photogrammetry has made it easier and faster to delineate a catchment. Using freely available digital elevation models on the internet and the Arc-GIS program, the boundaries of the watershed can be accurately defined without relying on paper topographic maps. The use of satellite data for processing digital image such as the Digital Elevation Models (DEM) provide visual and high graphics data for topographical analysis (Sanders, 2007 and Srivastava et al., 2011). This study demonstrates how practical and important the DEM data and the Arc-GIS program are in the watershed studies and provides the opportunity for future hydrometeorological studies over the Ballikaya region. This study is the starting point for future studies such as soil type identification, vegetation cover, flood analysis and other hydrological studies of this basin.

REFERANCES

Anonymous, (2018). *Downloaded Geographic (GIS) data website*. URL: http://www.diva-gis.org/gdata. Accessed Date: 25.12.2018

Anonymous, (2019). *Arc-GIS Pro official website*. URL: https://pro.arcgis.com/en/pro-app/help/main/welcome-to-the-arcgis-pro-app-help.htm. Accessed Date: 05.03.2019

Dawod, G.M. (2012). Principles of GIS Spatial Analysis (in Arabic), Holly Makkah, Saudi Arabia.

Ercan, B. and Yuce, M. I., (2016). Delineation of Watershed Boundaries by GIS: Case of the Kizilirmak Basin. *International Conference on Natural Science and Engineering(ICNASE'16.)* March 19-20, Kilis, Turkey.

Irwin, S., Srivastav, R., and Simonovic, S. P., (2014). Instruction for Watershed Delineation in an Arc-GIS Environment for Regionalization Studies. *Department of Civil and Environmental Engineering, Western University, Canada*. May. ISBN: (print) 978-0-7714-3071-8; (online) 978-0-7714-3072-5.

Sanders, B.F., (2007). Evaluation of on-line DEMs for flood inundation modeling. *Advances in Water Resources.* Volume: 30. pg 1831–1843.

Srivastava, P.K., Mukherjee, S., Gupta, M., and Singh, S.K., (2011). Characterizing monsoonal variation on water quality index of River Mahi in India using geographical information system. Water Quality Exposure and Health. Volume: 2. pg 193–203.

Sufiyan, I. and Zakariyab, R. B., (2018). 3D Modeling And Watershed Delineation Of Flood Risk Zones Using GIS And Remote Sensing In Terengganu River. *Journal Of Geology and Geoscience*. Volume 2 (1). pg 1-7.

ORCID

Muhammet Omer DIS https://orcid.org/0000-0002-3347-5112

KSÜ Mühendislik Bilimleri Dergisi, 22, Özel Sayı, 2019 KSU J Eng Sci, 22, Special Issue, 2019
Uluslararası İleri Mühendislik Teknolojileri Sempozyumu (ISADET) Özel Sayısı
International Symposium on Advanced Engineering Technologies (ISADET) Symposium Special Issue
Araştırma Makalesi Research Article

Kahramanmaras Sutcu Imam University
Journal of Engineering Sciences

Geliş Tarihi : 30.07.2019 Received Date : 30.07.2019
Kabul Tarihi : 04.11.2019 Accepted Date : 04.11.2019

GPU ACCELERATED INTUITIONISTIC FUZZY AND OTSU ALGORITHMS FOR FOREIGN LEAF DETECTION IN COTTON

PAMUKTAKİ YABANCI ELYAFLARIN GPU İLE HIZLANDIRILMIŞ SEZGİSEL BULANIK MANTIK VE OTSU ALGORİTMALARI İLE TESBİTİ

Eyup YALCIN[1,*], *Mahit GUNES*[1]

[1] Kahramanmaras Sütçü İmam University, Electrical and Electronics Engineering, Kahramanmaras, TURKEY

*Corresponding Author: Eyup YALCIN, eyalcin@ksu.edu.tr

ABSTRACT

The foreign substances, arising during the production and shaping of wool and cotton raw materials that are used in textile and cotton gin factories or coming from the outside, decrease considerably the quality of the obtained fabric or yarn. Nowadays, a different methods are used to separate foreign substances in the textile sector, most of these methods are not efficient in terms of speed and quality. Computerized vision systems play a vital role in the field of textiles as in other fields. In this study, Intuitionistic Fuzzy Algorithm is used to define the foreign substances in the images that obtained from a camera. CPU (Central Processing Unit) based applications have speed problems due to the structure of the algorithm. For this reason, GPU (Graphics Processing Unit) technology was used to overcome the speed problem. The otsu algorithm generates a dynamic threshold from the numerical values of the image obtained using the Intuitionistic fuzzy algorithm. By this means, the threshold value of each frame obtained from the camera was calculated on real time and implemented on the image timely. These algorithms were accelerated maximum 262 times using NVIDIA GTX 480 GPU supported display card.

Keywords: GPU Programming, Intuitionistic Fuzzy, Otsu, CUDA, Foreign Fibre Detection.

ÖZET

Tekstil, pamuk ve çırçır fabrikalarında kullanılan veya dışarıdan gelen yün ve pamuk ham maddelerinin üretimi ve şekillendirilmesinde ortaya çıkan yabancı maddeler, elde edilen kumaş veya ipliğin kalitesini önemli ölçüde azaltır. Günümüzde tekstil sektöründeki yabancı maddeleri ayırmak için farklı yöntemler kullanılmaktadır, ancak bu yöntemlerin çoğu hız ve kalite açısından verimli değildir. Bilgisayarlı görme sistemleri, diğer alanlarda olduğu gibi tekstil alanında da hayati bir rol oynamaktadır. Bu çalışmada, kameradan elde edilen görüntülerdeki yabancı maddeleri tanımlamak için Sezgisel Bulanık Mantık kullanılmıştır. CPU tabanlı uygulamalar ilgili algoritmanın yapısı gereği hız problemlerine yol açmaktadır. Bu hız problemini gidermek için ise GPU teknolojisi kullanılmıştır. Otsu algoritması kullanarak Sezgisel bulanık mantık algoritmasıyla elde edilen görüntüler için dinamik bir eşik değeri hesaplanmıştır. Bu sayede, kameradan elde edilen her karenin eşik değeri gerçek zamanlı olarak hesaplanmış ve görüntüye aynı anda uygulanmıştır. Bu algoritmalar, NVIDIA GTX 480 GPU destekli ekran kartı kullanılarak maksimum 262 kez hızlandırılmıştır.

Anahtar Kelimeler: GPU Programlama, Sezgisel Bulanık Mantık, Otsu, CUDA, Yabancı Elyaf Tespit Etme.

INTRODUCTION

The different fibre and soil, arising during the production and shaping of wool and cotton raw materials used in textile and cotton gin factories or coming from the outside, decrease the quality of the obtained fabric or yarn considerably.

In general, this filthy in cotton may be caused by black pigment fibres, color which may come from sheep, foreign material and filthy overlooked while picking plants (Yang, 2009).

In modern-day textile business, the methods used to separate these substances are not efficient in terms of speed and quality (Ji, 2010). There are various techniques to clean the foreign fibers in lint. Some of those are ultrasonic-based, sensor-based and machine vision-based inspection (Zhang, 2011). The present day computerized vision systems have affected textile field clearly as well as all other fields. For the first time, Liberman and colleagues built a machine vision system to overcome this problem in textile factories (Liberman, 1998). Tastaswadi and colleagues have developed a real-time system for images taken from cameras has 3D-LUT technology with the help of edge extraction algorithms (Tastaswadi, 1999). Millman and colleagues have designed a system with two options as high resolution / low speed and low resolution / high speed to solve speed problems in these systems (Millman, 2001). However, this system was not quite efficient due to the differences between the chemical and physical characteristics of wool and cotton. The two problems of quality and speed, encountered in other previous studies, are an important distinguishing factor (Wang, 2015), (Chen, 2010). In this study, using GPU technology which can run hundreds of times faster than CPU were tried to solve this speed problem (NVIDIA, 2019).

In the literature, many different algorithms have been used to clean foreign leaf (Zhang, 2014). One of these algorithms, the Intuitionistic Fuzzy Algorithm, is effective for finding the foreign substance in the images using a specified threshold value. However, since the fixed threshold value cannot give the same quality for each frame, it has been observed that the thresholding of the obtained images cannot be performed properly. Otsu method was used determined the threshold value in order to solve this issue. Thus, the threshold value of each frame obtained from the camera was calculated automatically and implemented on the image timely. Afterwards, for only the soiled part to be cleaned, the calculated image was divided into 8 parts. After many trials, using the threshold value method, an average value was calculated for the histogram values of these parts and afterwards, the parts and amount of foreign leaf were determined. After the many experience, it was confirmed that the used methods gave the needed results completely. Besides, in this study, the Intuitionistic Fuzzy Algorithm and Otsu Method were used for the first time together with GPU to process images. Thanks to these methods, unlike in previous studies, the computerized vision system has provided a vital advantage in terms of speed and quality.

The rest of this paper is organized as follows. In section 2, the Intuitionistic fuzzy and edge extraction process which are the basis of the study are explained. In section 3, the experimental results of the study are presented and five examples are given. In the last section, some suggestions are made for future studies.

DEVELOPMENT OF INTUITIONISTIC FUZZY EDGE DETECTION

According to the fuzzy set theory of L.A Zadeh $X = \left\{x_1, x_2, x_3, \ldots, x_n\right\}$ set is mathematically expressed as (Zadeh, 1965):

$$A = \{x, \mu_A(x), \upsilon_A(x) \mid x \in X\} \tag{1}$$

Here in $\mu_A(x)$: X → [0, 1]; is called as membership degree of each x element defined in X set. It is expressed as $\upsilon_A = 1 - \mu_A(x)$ in non- membership degree. Where $\mu_A(x) + \upsilon_A = 1$, fuzzy sets are defined.
In addition to Zadeh's fuzzy set theory, Atanassov added the 3rd parameter hesitation degree (Atanossov, 1986).

$$\pi_A(x) = 1 - \mu_A(x) - \upsilon_A(x) \tag{2}$$

The term indicated by $\pi_A(x)$ are intuitive fuzzy logic index or hesitation value. It was added to the zadeh equation by the Atanasov to minimize user error. Thus, $\pi_A(x)$ is assigned to restrict the real numbers $\mu_A(x), \upsilon_A(x)$.

$$\pi_A(x) = C * \left[1 - \mu_A(x)\right] \tag{3}$$

C is the hesitation constant and should be defined without breaking the equality of Eq. 2. In this study, c value was selected as 0.2.

Intuitionistic Fuzzy Edge Detection

In fuzzy set theory, there are three concepts for establishing relationships between images. These are fuzzy entropy, distance measure and similarity measurement. The relationship between these three concepts are detailed in (Xuecheng, 1992). However, entropy and similarity measurement are applied to images similarly in fuzzy set and based on the divergence calculation between the respective pixels of the two images (Fan, 1999). These relationships are defined following:

$\mu_A\left(a_{ij}\right)$ is the membership of $A \in F\left(A\right)$, $v_A\left(a_{ij}\right) = 1-\mu_A\left(a_{ij}\right)$ is the non-membership of $A^c \in F\left(A\right)$ and c is the complement of A. $d\left(A,B\right)$ is the distance between A and B fuzzy sets. $e\left(A\right)$ is the entropy of A and $s\left(A,B\right)$ is the similarity measurement of the A and B.

The relation between d and s is the $d = 1-s$. The fuzzy entropy defined as:

$$e\left(A\right) = s\left(A,A^c\right) \text{ or } e\left(A\right) = 1-d\left(A,A^c\right) \tag{4}$$

As can be seen from the Eq.4, it can be used by similarity or distance measurement to calculate the entropy. Since $\mu_A + v_A = 1$ in the fuzzy set theory, entropy, distance and similarity measurement calculations can made over these two variables.

Exponential entropy is described by Pal and Pal using Shannon's information entropy (Pal, 1992). $P = \left\{p_0, p_1, \ldots, p_{L-1}\right\}$ is the probability distribution set of image size MxM with L grey level and its exponential entropy is defined as:

$$H = \sum_{i=0}^{L-1} p_i . e^{1-p_i} \tag{5}$$

In fuzzy set theory, Fuzzy entropy of image A having size MxM is defined as:

$$H\left(A\right) = \frac{1}{n\left(\sqrt{e}-1\right)} \sum_{i=0}^{M-1} \sum_{j=0}^{M-1} \left[\left(\mu_A\left(a_{ij}\right) e^{1-\mu_A\left(a_{ij}\right)}\right) + \left(1-\mu_A\left(a_{ij}\right)\right) e^{\mu_A\left(a_{ij}\right)} - 1\right] \tag{6}$$

This entropy was found taking into account the $\mu_A\left(a_{ij}\right)$ degree of membership and the $v_A\left(a_{ij}\right) = 1-\mu_A\left(a_{ij}\right)$ degree of non-membership.

For two image A and B (at the (ij)th pixel), amount of information between $\mu_A\left(a_{ij}\right)$ and $\mu_B\left(b_{ij}\right)$:

$$I_1\left(A,B;ij\right) = \frac{e^{\mu_A\left(a_{ij}\right)}}{e^{\mu_B\left(b_{ij}\right)}} = e^{\mu_A\left(a_{ij}\right)-\mu_B\left(b_{ij}\right)} \tag{7}$$

The fuzzy expected information of image A against the image B (for $\mu_A\left(a_{ij}\right) = 0.5$)

$$I_1\left(A,B\right) = \sum_{i=0}^{M-1} \sum_{j=0}^{M-1} \left(\frac{1}{2} - \left(1-\mu_A\left(a_{ij}\right)\right) e^{\mu_A\left(a_{ij}\right)-\mu_B\left(b_{ij}\right)}\right) \tag{8}$$

Similarly, the fuzzy expected information of image A^c against the image B^c (for $v_A = 0.5$).

$$I_1\left(A^c,B^c\right) = \sum_{i=0}^{M-1} \sum_{j=0}^{M-1} \left(\frac{1}{2} - \left(\mu_A\left(a_{ij}\right)\right) e^{\mu_B\left(b_{ij}\right)-\mu_A\left(a_{ij}\right)}\right) \tag{9}$$

Eq. (8) and Eq. (9) may appear equal. But in general, $I_1(A,B) \neq I_1(A^c,B^c)$. Therefore, the two expected values should be taken into account together.

So, the fuzzy entropy, the total divergence between image A against the image B defined by:

$$I(A,B) = I_1(A,B) + I_1(A^c,B^c) = \sum_i \sum_j \left(1-\left(\left(1-\mu_A(a_{ij})\right)e^{\left(\mu_A(a_{ij})-\mu_B(b_{ij})\right)}\right)-\left(\mu_A(a_{ij})e^{\left(\mu_B(b_{ij})-\mu_A(a_{ij})\right)}\right)\right) \tag{10}$$

Similarly, the total divergence between image of B against the image of A defined by:

$$I(B,A) = \sum_i \sum_j \left(1-\left(\left(1-\mu_B(b_{ij})\right)e^{\left(\mu_B(a_{ij})-\mu_A(b_{ij})\right)}\right)-\left(\mu_B(b_{ij})e^{\left(\mu_A(b_{ij})-\mu_B(a_{ij})\right)}\right)\right) \tag{11}$$

For fuzzy sets A and B, total fuzzy divergence between image of A and image of B can be defined by:

$$I(A,B)+I(B,A) = \sum_i \sum_j \begin{pmatrix} 2-\left(\left(1-\mu_A(a_{ij})+\mu_B(b_{ij})\right)e^{\left(\mu_A(a_{ij})-\mu_B(b_{ij})\right)}\right) \\ -\left(\left(1-\mu_B(b_{ij})+\mu_A(a_{ij})\right)e^{\left(\mu_B(b_{ij})-\mu_A(a_{ij})\right)}\right) \end{pmatrix} \tag{12}$$

As seen Eq. (12) , in fuzzy entropy, the divergence value between A and B is calculated taking into account the degree of membership and non-membership.

In addition to the fuzzy set theory, T. Chaira suggested that should be taken into account the π_A value, which is the hesitation degree in Intuitionistic fuzzy logic theory (Chaira, 2008). This value is added directly to the equation Eq. (12). So, $v_A = 1-\mu_A-\pi_A$ is written instead of $v_A(a_{ij}) = 1-\mu_A(a_{ij})$ in the fuzzy set theory.

In Instuistic fuzzy theory, for the two image of A, B (at the (ij)th pixel) amount of information defined by:

$$I_2(A,B;ij) = e^{\mu_A(a_{ij})+\pi_A(a_{ij})} \,/\, e^{\mu_B(b_{ij})+\pi_B(b_{ij})} \tag{13}$$

Intuitionistic Fuzzy Entropy calculation is the same as Fuzzy Entropy case, so Intuitionistic Fuzzy Entropy can be written directly as follows:

$$\begin{pmatrix} I_2(A,B) \\ +\mathrm{I}_2(B,A) \end{pmatrix} = \sum_i \sum_j \begin{pmatrix} 2-\left(\left[1-\begin{pmatrix} \mu_A(a_{ij}) \\ -\mu_B(b_{ij}) \end{pmatrix}+\begin{pmatrix} \pi_B(b_{ij}) \\ -\pi_A(a_{ij}) \end{pmatrix}\right]e^{\left(\mu_A(a_{ij})-\mu_B(b_{ij})-\left(\pi_B(b_{ij})-\pi_A(a_{ij})\right)\right)}\right) \\ -\left(\left[1-\begin{pmatrix} \pi_B(b_{ij}) \\ -\pi_A(a_{ij}) \end{pmatrix}+\begin{pmatrix} \mu_A(a_{ij}) \\ -\mu_B(b_{ij}) \end{pmatrix}\right]e^{\left(\pi_B(b_{ij})-\pi_A(a_{ij})-\left(\mu_A(a_{ij})-\mu_B(b_{ij})\right)\right)}\right) \end{pmatrix} \tag{14}$$

The overall Intuitionistic Fuzzy Divergence, IFD, between image A and image B.

$$IFD(A,B) = I_1(A,B)+I_1(B,A)+I_2(A,B)+I_2(B,A) \tag{15}$$

$$IFD(A,B) = \sum_i \sum_j \left(\begin{array}{l} \left(\begin{array}{l} 2 - \left(\left[1 - \mu_A(a_{ij}) + \mu_B(b_{ij}) \right] e^{\left(\mu_A(a_{ij}) - \mu_B(b_{ij}) \right)} \right) \\ - \left(\left[1 - \mu_B(b_{ij}) + \mu_A(a_{ij}) \right] e^{\left(\mu_B(b_{ij}) - \mu_A(a_{ij}) \right)} \right) \end{array} \right) \\ + \left(\begin{array}{l} 2 - \left(\left[\begin{array}{l} 1 - \left(\mu_A(a_{ij}) - \mu_B(b_{ij}) \right) \\ + \left(\pi_B(b_{ij}) - \pi_A(a_{ij}) \right) \end{array} \right] e^{\left(\mu_A(a_{ij}) - \mu_B(b_{ij}) - \left(\pi_B(b_{ij}) - \pi_A(a_{ij}) \right) \right)} \right) \\ - \left(\left[\begin{array}{l} 1 - \left(\pi_B(b_{ij}) - \pi_A(a_{ij}) \right) \\ + \left(\mu_A(a_{ij}) - \mu_B(b_{ij}) \right) \end{array} \right] e^{\left(\pi_B(b_{ij}) - \pi_A(a_{ij}) - \left(\mu_A(a_{ij}) - \mu_B(b_{ij}) \right) \right)} \right) \end{array} \right) \end{array} \right) \tag{16}$$

Object Extraction Method

It is defined A={x, $\mu_A(x)$, $\upsilon_A(x)$ |x ε X} and B={x, $\mu_B(x)$, $\upsilon_B(x)$ |x ε X} as intuitive two fuzzy sets. Here in;

A: 3x3 display matrix obtained from the image
B: Sixteen 3x3 matrices including edge templates
In order to use in intuitive fuzzy logic object extraction algorithm, 3x3 matrix including 16 different states is created.

$$\begin{pmatrix} 0 & b & a \\ 0 & b & a \\ 0 & b & a \end{pmatrix} \begin{pmatrix} a & a & a \\ 0 & 0 & 0 \\ b & b & b \end{pmatrix} \begin{pmatrix} a & a & b \\ a & b & 0 \\ b & 0 & 0 \end{pmatrix} \begin{pmatrix} b & b & b \\ 0 & 0 & 0 \\ a & a & a \end{pmatrix} \begin{pmatrix} b & a & a \\ 0 & b & a \\ 0 & 0 & b \end{pmatrix} \begin{pmatrix} b & a & 0 \\ b & a & 0 \\ b & a & 0 \end{pmatrix} \begin{pmatrix} a & 0 & b \\ a & 0 & b \\ a & 0 & b \end{pmatrix} \begin{pmatrix} 0 & 0 & 0 \\ b & b & b \\ a & a & a \end{pmatrix}$$

$$\begin{pmatrix} a & a & a \\ b & b & b \\ 0 & 0 & 0 \end{pmatrix} \begin{pmatrix} a & b & 0 \\ a & b & 0 \\ a & b & 0 \end{pmatrix} \begin{pmatrix} 0 & 0 & 0 \\ a & a & a \\ b & b & b \end{pmatrix} \begin{pmatrix} 0 & a & b \\ 0 & a & b \\ 0 & a & b \end{pmatrix} \begin{pmatrix} b & b & b \\ a & a & a \\ 0 & 0 & 0 \end{pmatrix} \begin{pmatrix} b & 0 & a \\ b & 0 & a \\ b & 0 & a \end{pmatrix} \begin{pmatrix} b & 0 & 0 \\ a & b & 0 \\ a & a & b \end{pmatrix} \begin{pmatrix} 0 & 0 & b \\ 0 & b & a \\ b & a & a \end{pmatrix}$$

Figure 1: Intuitionistic Fuzzy Extraction Sets

The selection of fuzzy extraction sets are very importance. Because, it indicates the type and direction of the edge. These sets expresses examples of the edge and the images also. In the literature there are state matrix applications in different dimensions (Alam, 2013). In general, when the template size increases, the edges are missed and the algorithm is less efficient. However, if the size of the template is reduced, the algorithm takes a lot of time. Therefore, the most suitable template size was chosen as 3x3. *"a", "b"* and *"0"* refer to pixel equivalent of edge samples; *"a"* and *"b"* values are completely found by trial and error method. However, in literature survey, the most convenient estimation is obtained by *a*=0.3 and *b*=0.8 (Chaira, 2008), (Kaushik, 2015). To the center of each fuzzy inference set, it is placed over normalized image to (i, j)th position. IFD (intuitionistic fuzzy divergence) is measured in each pixel (i, j)th position. IFD (i, j)th value is obtained by the same size image with fuzzy inference set and MAX-MIN relationship of fuzzy inference sets from the Eq. (17).

$$IFD(i,j) = \underset{N}{MAX} \left[\underset{r}{MIN} \left(\underset{z}{IFD(A,B)} \right) \right] \tag{17}$$

In Eq. (17), IFD (i, j)th value between A and B is calculated by a_{ij} element of an image matrix and b_{ij} element of B template matrix. N represents the number of sets in fuzzy inference template and r represents the number of elements obtained like 3x3 image matrix. IFD (i, j)th is obtained after processing all pixel positions of the image.

In literature studies, in order to define threshold method, a fixed threshold value is applied by determining trial and error method. The fixed threshold value can't work well because it uses the same value for different images. Therefore, a determination of a dynamic threshold value by the numerical values of image is required. In this study,

it is clear that Otsu method or the calculation method of the automatic threshold value with respect to numerical values of the image is more appropriate to developed system (Otsu, 1979).
In this study, it is aimed to calculate the threshold value in each frame by using the Otsu method instead of using a fixed threshold value. In this way, each frame has its own threshold value.

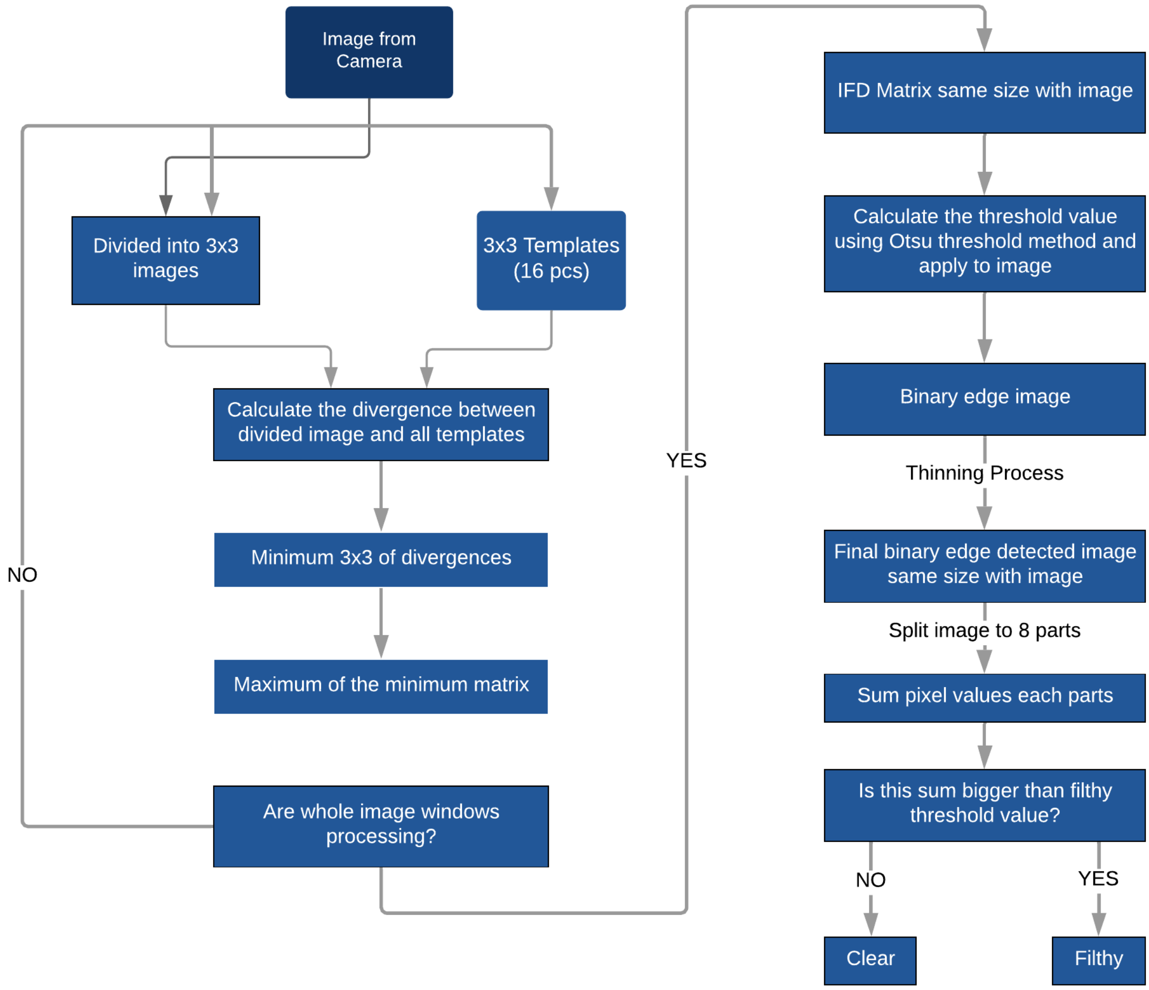

Figure 2: Block Diagram of Intuitionistic Fuzzy Edge Detection

EXPERIMENTAL RESULTS AND DISCUSSION

The obtained images from the camera using OpenCV software system has been applied on two different hardware to measure the difference in speed between the CPU and GPU. In order to measure the difference of speed, NVIDIA GTX 480 GPU-supported graphics card and Intel E5700 Dual Core processor, 12.8 GB / s with a band speed CPU is used.

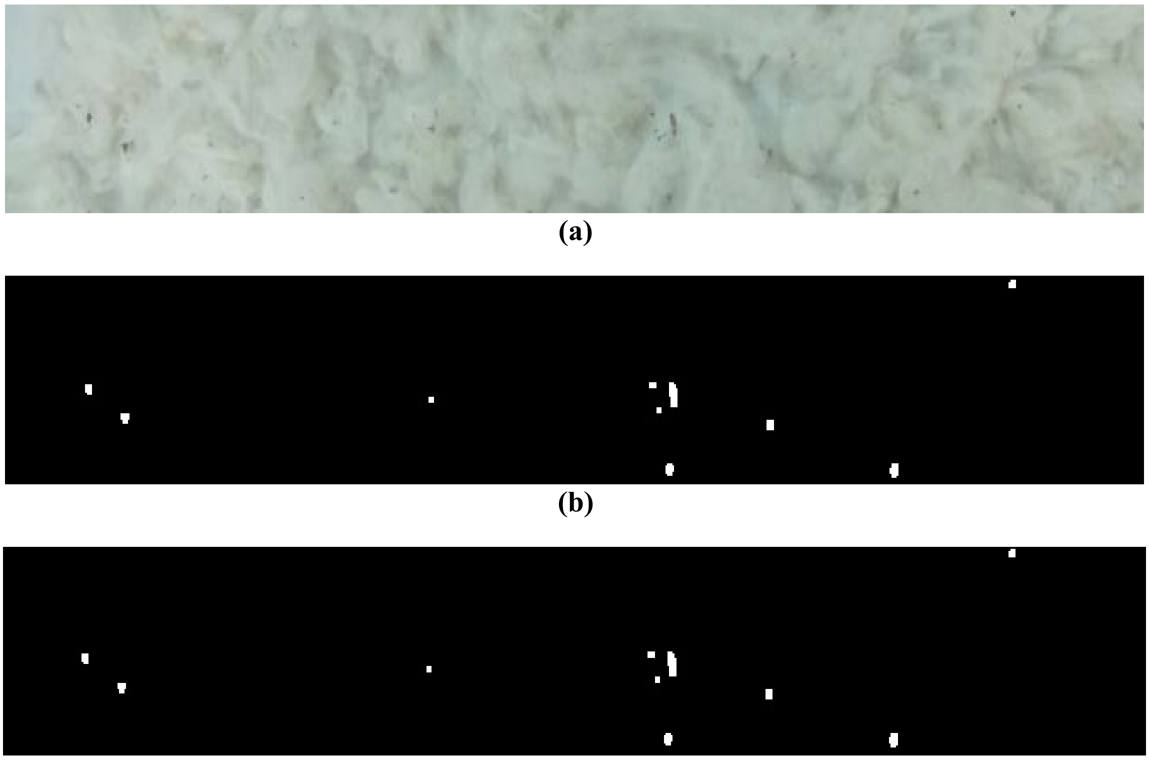
(a)
(b)
(c)

Figure 3: Image 1 taken by Camera (a) Original, (b) CPU output, (c) GPU output.

Table 1: The Speed Comparison of Image 1

Image 1	**640x100**		**1280x200**		**1920x300**	
	CPU	**GPU**	**CPU**	**GPU**	**CPU**	**GPU**
Threshold value	195	195	195	195	195	195
Otsu Method (ms)	0.501	0.14438	2.172	0.427	3.064	0.292
Intuitive Fuzzy Logic (ms)	1682.317	8.685	7458.596	30.874	17992.239	70.932
Total Response Time (ms)	1682.818	8.82938	7460.768	31.301	17995.303	71.224
Foreign Substance Region	NONE	NONE	NONE	NONE	NONE	NONE
Otsu Method Rate (CPU/GPU)	3.475		5.084		10.481	
Intuitive Fuzzy Logic Rate (CPU/GPU)	193.703		241.581		253.654	
Response Time Rate (CPU/GPU)	190.593		238.353		252.656	

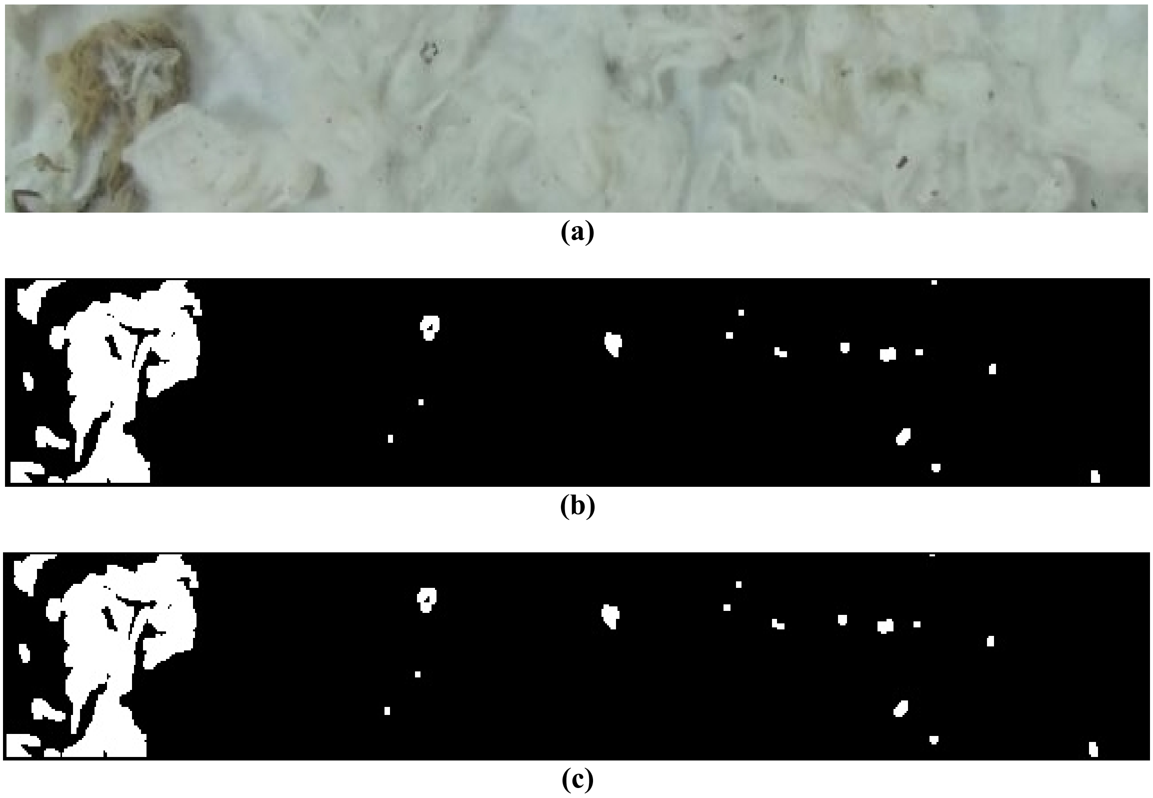

(a)

(b)

(c)

Figure 4: Image 2 taken by Camera (a) Original, (b) CPU output, (c) GPU output.

Table 2: The Speed Comparison of Image 2

Image 2	**640x100**		**1280x200**		**1920x300**	
	CPU	**GPU**	**CPU**	**GPU**	**CPU**	**GPU**
Threshold value	146	146	146	146	146	146
Otsu Method(ms)	0.496	0.098	1.530	0.302	3.040	0.349
Intuitive Fuzzy Logic(ms)	1710.541	8.719	8019.5503	30.736	17517.075	71.069
Total Response Time(ms)	1711.038	8.817	8021.081	31.038	17520.11	71.418
Foreign Substance Region	1-2	1-2	1-2	1-2	1-2-3-5-7	1-2-3-5-7
Otsu Method Rate (CPU/GPU)	5.058		5.059		8.698	
Intuitive Fuzzy Logic Rate (CPU/GPU)	196.185		260.917		246.479	
Response Time Rate (CPU/GPU)	194.058		258.423		245.316	

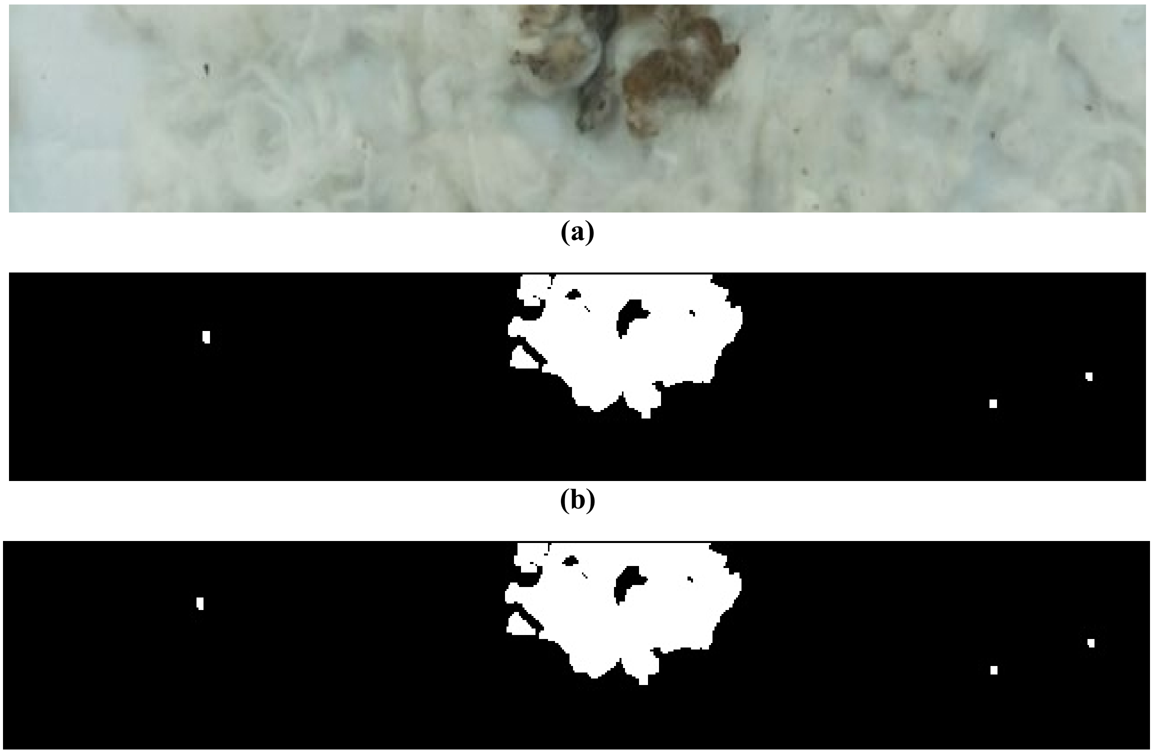

(a)

(b)

(c)

Figure 5: Image 3 taken by Camera (a) Original, (b) CPU output, (c) GPU output.

Table 3: The Speed Comparison of Image 3

Image 3	**640x100**		**1280x200**		**1920x300**	
	CPU	**GPU**	**CPU**	**GPU**	**CPU**	**GPU**
Threshold value	138	138	138	138	138	138
Otsu Method(ms)	0.480	0.098	1.465	0.295	3.043	0.287
Intuitive Fuzzy Logic(ms)	1714.296	8.661	8078.566	30.787	17509.822	70.97
Total Response Time(ms)	1714.777	8.759	8080.032	31.082	17512.8666	71.2573
Foreign Substance Region	4-5	4-5	4-5-6	4-5-6	4-5-6	4-5-6
Otsu Method Rate (CPU/GPU)	4.888		4.966		10.592	
Intuitive Fuzzy Logic Rate (CPU/GPU)	197.932		262.401		246.721	
Response Time Rate (CPU/GPU)	195.766		259.957		245.769	

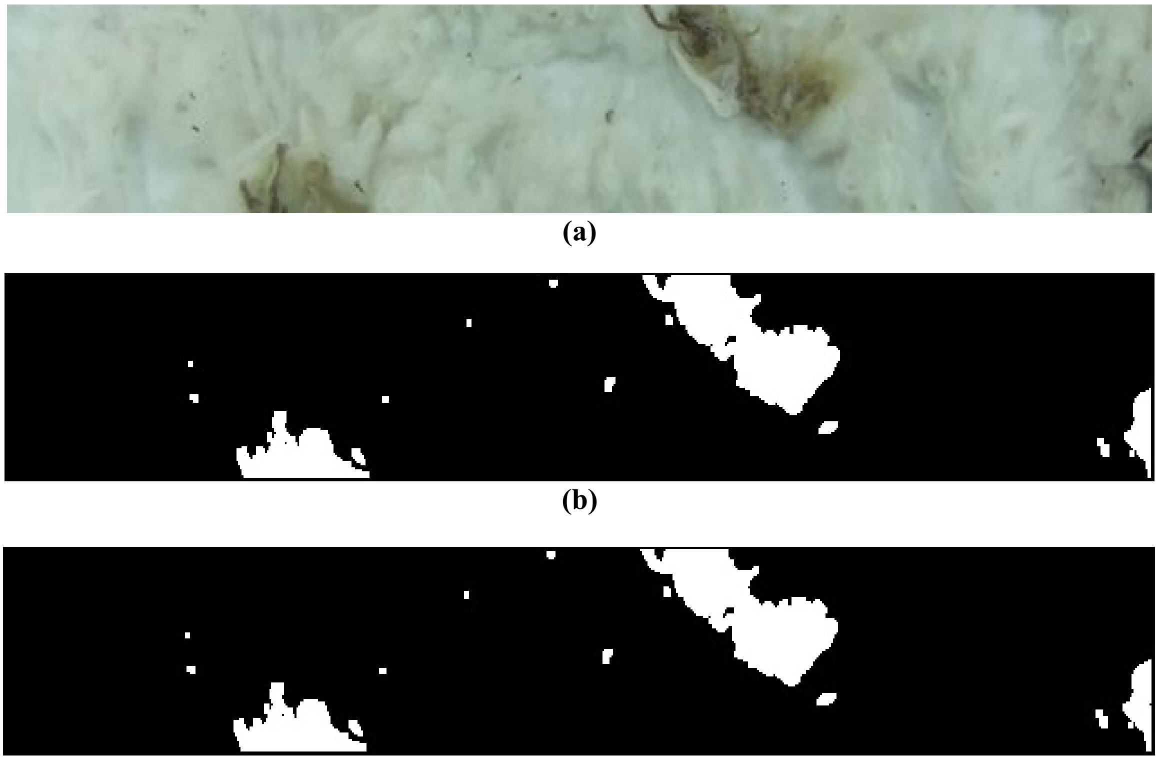
(a)

(b)

(c)

Figure 6: Image 4 taken by Camera (a) Original, (b) CPU output, (c) GPU output.

Table 4: The Speed Comparison of Image 4

Image 4	**640x100**		**1280x200**		**1920x300**	
	CPU	**GPU**	**CPU**	**GPU**	**CPU**	**GPU**
Threshold value	145	145	145	145	145	145
Otsu Method (ms)	0.574	0.098	1.451	0.337	3.061	0.321
Intuitive Fuzzy Logic (ms)	1827.948	9.698	7882.1420	32.417	17517.077	71.125
Total Response Time (ms)	1828.5221	9.796	7883.5936	32.75425	17520.1391	71.44676
Foreign Substance Region	2-3-5-6-8	2-3-5-6-8	2-3-5-6-8	2-3-5-6-8	2-3-5-6-8	2-3-5-6-8
Otsu Method Rate (CPU/GPU)	5.842		4.304		9.516	
Intuitive Fuzzy Logic Rate (CPU/GPU)	188.487		243.148		246.285	
Response Time Rate (CPU/GPU)	186.654		240.689		245.219	

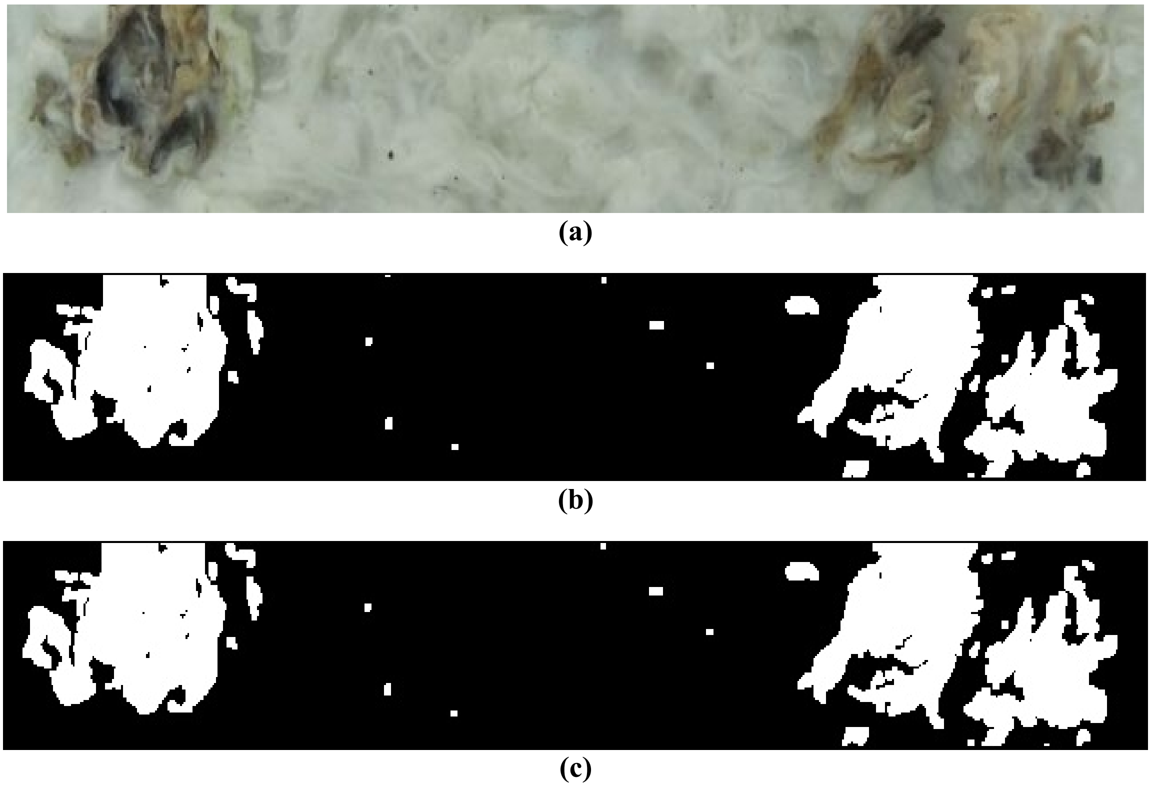

Figure 7: Image 5 taken by Camera (a) Original, (b) CPU output, (c) GPU output.

Table 5: The Speed Comparison of Image 5

Image 5	**640x100**		**1280x200**		**1920x300**	
	CPU	**GPU**	**CPU**	**GPU**	**CPU**	**GPU**
Threshold value	136	136	136	136	136	136
Otsu Method (ms)	0.476	0.0980	1.759	0.302	3.053	0.329
Intuitive Fuzzy Logic (ms)	1.724	8.626	8.018	31.606	17575.31	71.332
Total Response Time (ms)	1724.038	8.724	8019.344	31.908	17578.36	71.662
Foreign Substance Region	1-2-6-7-8	1-2-6-7-8	1-2-6-7-8	1-2-6-7-8	1-2-6-7-8	1-2-6-7-8
Otsu Method Rate (CPU/GPU)	4.861		5.820		9.259	
Intuitive Fuzzy Logic Rate (CPU/GPU)	199.810		253.669		246.384	
Response Time Rate (CPU/GPU)	197.618		251.321		245.293	

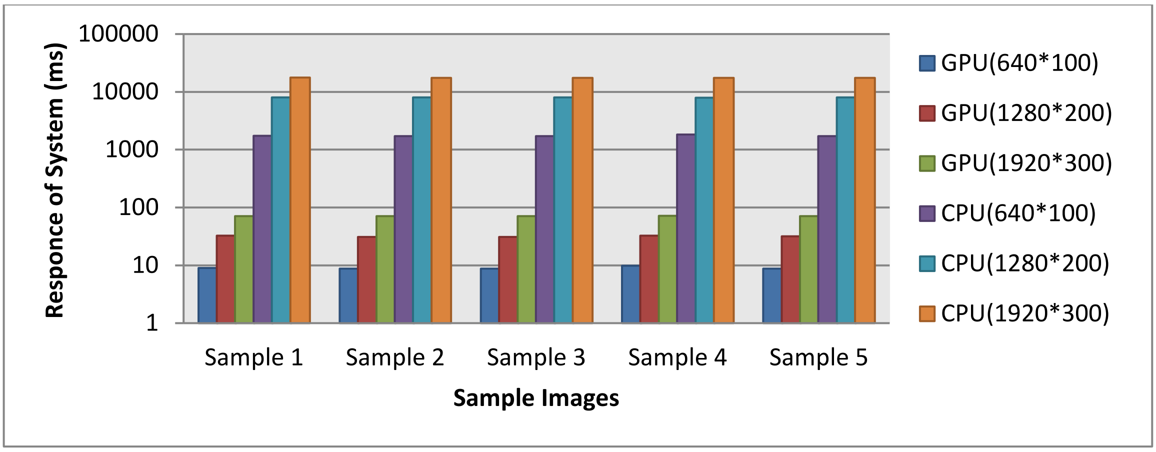

Figure 8: Comparison of Processing Time of Images

In developed algorithm, the aim is to reveal the performance of system by developing either CPU or GPU based application. In result section, when pattern examples in different resolution are analysed, a graphic related to time response of system in Fig. 8 is obtained.

A significant speed difference of GPU based application is seen by analysing the graphic in Fig. 8. The average of results obtained by GPU based application are such like 193 in 640*100 rated images, 249 in 1280*200, 247 times faster in 1920*300. Also, speed ratio in all patterns are obtained between 186 times and 260 times. According to literature studies, the successful systems that hundreds of times accelerated with GPU were found (Bahri, 2017), (Faujdar, 2017), (Gunes, 2016). When 260 times speed is taken into consideration, it is seen that a very successful result is obtained according to the studies in the literature.

CONCLUSION

Nowadays, the used methods to clean filthy in textile sector are not efficient in terms of speed and quality. In recent years, computer vision systems clearly show its effect in textile sector as in other sectors. In this study, intuitive fuzzy logic algorithm developed by Atanossov was preferred in order to determine the impurities within the image taken by camera. In intuitive fuzzy logic algorithm, hesitation error is calculated and subtracted from membership value in order to minimize the professional experience error that does not exist in classic fuzzy logic algorithm. This provides more stable and desired results.

Due to the nature of intuitive fuzzy logic algorithm, some speed problems have been seen in real-time CPU based applications. Therefore, GPU technology was utilized to eliminate the speed problem. In the first stage, intuitive fuzzy object extraction method is applied to the image taken from the camera in grey level of OpenCV. Literature research has shown that a fixed value is used as the threshold value in the intuitive fuzzy logic edge detection algorithm. Because of each frame taken from camera will occur in different values, the algorithm was not to perform desired results. In this study, it is first time, dynamic threshold value obtained by Otsu method was used integrally with heuristic fuzzy logic. In this way, the threshold value of each frame from the camera was calculated in real time and currently applied to the image. While the system is developed, by using examples with different resolutions from taken images in study, it was observed that the most appropriate resolution value in terms of either performance or quality is 640*100 rate. This image was divided into 8 equal region with ratio of 80*100. In each region, whether impurity material exists or not is determined by summation of numerical values of related region of the image. Using this summation, a threshold value was defined to determine whether there is any impurity in related region according to negligence availability levels.

In the used algorithms, minimum 168 maximum 262 times faster speed difference is obtained in pattern samples with different resolutions using NVIDIA GTX 480 GPU supported graphics card. At the end of the trials, it is seen that the methods completely provide desired results. Unlike previous methods of removing filthiness from cotton, textile studies in literature, computerized vision system provided much more important advantage due to these methods.

REFERENCES

Alam, I. J. (2013). Detecting Edge in an Image with the Help of Fuzzy Parameters. *11th International Conference on Frontiers of Information Technology*, (pp. 19-24). Islamabad, Pakistan.

Atanossov, K. (1986). Intuitionistic Fuzzy Sets. *Fuzzy Sets and Systems, 20*, 87-96.

Bahri, H. S. (2017). Image feature extraction algorithm based on CUDA architecture: case study GFD and GCFD. *IET Computers & Digital Techniques, 11*(4), 125-132.

Chaira, T. R. (2008). A new measure using intuitionistic fuzzy set theory and its application to edge detection. *Applied Soft Computing, 8*(2), 919–927.

Chen, Z. X. (2010). A New High-Speed Foreign Fiber Detection System with Machine Vision. *Mathematical Problems in Engineering, Article ID 398364*, 15 pages.

Fan, J. X. (1999). Distance measure and induced fuzzy entropy. *Fuzzy Sets and Systems, 104*, 305-314.

Faujdar, N. G. (2017). A practical approach of GPU bubble sort with CUDA hardware. *7th International Conference on Cloud Computing* (pp. 7-12). Noida: Data Science & Engineering.

Gunes, M. B. (2016). Detecting Direction of Pepper Stem by Using CUDA-Based Accelerated Hybrid Intuitionistic Fuzzy Edge Detection and ANN. *Journal of Sensors*, 11 pages.

Ji, R. L. (2010). Classification and Identification of Foreign Fibers in Cotton on the Basis of a Support Vector Machine. *Mathematical and Computer Modelling, 51*, 1433-1437.

Kaushik, R. B. (2015). On Intuitionistic Fuzzy Divergence Measure with Application to Edge Detection. *Procedia Computer Science, 70*, 2-8.

Liberman, M. A. (1998). Determining gravimetric bark content in cotton with machine vision. *Textile Research Journal, 68*(2), 94-104.

Millman, M. P. (2001). Computer vision for textured yarn interlace (nip) measurements at high speeds. *Mechatronics, 11*(8), 1025-1038.

NVIDIA, C. (2019). *CUDA C Programming GUIDE*. Retrieved from 9th Edition: https://docs.nvidia.com/cuda/cuda-c-programming-guide/

Otsu, N. A. (1979). Threshold Selection Method from Gray-level Histograms. *IEEE Transactions on Systems, Man and Cybernetic, 9*(1), 62-66.

Pal, N. R. (1992). Some Properties of the Exponential Entropy. *Inform. Sci., 66*, 119-137.

Tastaswadi, P. V. (1999). Machine vision for automated visual inspection of cotton quality in textile industries using color isodiscrimination contour. *Computer Industrial Engineering, 37*(1-2), 347-350.

Wang, X. Y. (2015). A fast image segmentation algorithm for detection of pseudo-foreign fibers in lint cotton. *Comput. Electr. Eng., 46*, 500-510.

Xuecheng, L. (1992). Entropy, distance measure and similarity measure of fuzzy sets and their relations. *Fuzzy Sets and Systems, 52*, 305-318.

Yang, W. Z. (2009). A new approach for image processing in foreign fiber detection. *Computers and Electronics in Agriculture, 68*(1), 68-77.

Zadeh, L. A. (1965). Fuzzy sets. *Information and Control, 8*(3), 338–353.

Zhang, H. L. (2014). Applications of computer vision techniques to cotton foreign matter inspection: A review. *Computers and Electronics in Agriculture, 109*, 59-70.

Zhang, X. L. (2011). A fast Segmentation Method for High-Resulation Color Images of Foreign Fibers in Cotton. *Computers and Electronics in Agriculture, 78*, 71-79.

ORCID

Eyup YALCIN *http://orcid.org/0000-0002-4057-6069*
Mahit GUNES *http://orcid.org/0000-0002-1552-3889*

KSÜ Mühendislik Bilimleri Dergisi, 22, Özel Sayı, 2019 KSU J Eng Sci, 22, Special Issue, 2019
Uluslararası İleri Mühendislik Teknolojileri Sempozyumu (ISADET) Özel Sayısı
International Symposium on Advanced Engineering Technologies (ISADET) Symposium Special Issue
Araştırma Makalesi Research Article

Kahramanmaras Sutcu Imam University
Journal of Engineering Sciences

Geliş Tarihi : 01.08.2019 Received Date : 01.08.2019
Kabul Tarihi : 10.10.2019 Accepted Date : 10.10.2019

CO-FERMENTATION OF PROCESSED ORANGE WASTES WITH CATTLE MANURE

PORTAKAL İŞLEME ATIKLARININ BÜYÜKBAŞ HAYVAN GÜBRESİ İLE KO-FERMANTASYONU

Ali AYBEK[1,*], *Levent Gürsel ALBAYRAM*[1], *Serdar ÜÇOK*[1]

[1] Kahramanmaras Sütçü İmam Üniversitesi, Biyosistem Mühendisliği Bölümü, Kahramanmaraş, Türkiye

*Sorumlu Yazar / Corresponding Author: Ali AYBEK, aaybek@ksu.edu.tr

ÖZET

Bu çalışmada, büyükbaş hayvan gübresine portakal işleme atıklarının (kabuk ve posa) farklı oranlarda (%25, %50, %75) eklenmesinin biyogaz verimine etkisi, HBT (Hohenheim Batch Yield Test) yöntemi ile belirlenmiştir. Bu kapsamda, büyükbaş hayvan gübresi çiftlikten, portakal işleme atıkları ise meyve suyu işleme tesislerinden alınarak laboratuar ortamında kurutulup öğütülmüş ve beş materyal (%100 portakal işleme atıkları, %100 büyükbaş hayvan gübresi, %25 portakal işleme atıkları + %75 büyükbaş hayvan gübresi, %50 portakal işleme atıkları + %50 büyükbaş hayvan gübresi, %75 portakal işleme atıkları + %25 büyükbaş hayvan gübresi) meydana getirilmiştir. Yapılan araştırma sonucunda en yüksek, ham protein oranı (%12.06) ve ham yağ oranı (%2.30) %100 portakal işleme atıkları materyalinden, kuru madde oranı (%90.75) %100 büyükbaş hayvan gübresi materyalinden, organik kuru madde oranı (%95.56) %100 portakal işleme atıkları materyalinden, ADF oranı (%60.20) %100 büyükbaş hayvan gübresi materyalinden ve NDF oranı (%26.50) %25 portakal işleme atıkları + %75 büyükbaş hayvan gübresi materyalinden elde edilmiştir. Ele alınan materyallerde en yüksek metan üretimi 25 ile 35 günler arasında gerçekleşmiştir. Karışım materyallerinde en yüksek biyogaz (0.70 Nm^3/kg OKM) ve metan (0.37 Nm^3/kg OKM) üretim değerleri, %75 portakal işleme atıkları + %25 büyükbaş hayvan gübresi materyalinden oluşmuştur. Biyogazdaki metan oranı, en yüksek (%53.77) %50 portakal işleme atıkları + %50 büyükbaş hayvan gübresi materyalinden elde edilmiştir. Çalışmada portakal işleme atıklarının büyükbaş hayvan gübresi ile ko-fermantasyonu, metan ve biyogaz üretimini istatiksel olarak önemli düzeyde ($P \leq 0.05$) arttırmıştır.

Anahtar Kelimeler: Portakal işleme atıkları, Büyükbaş hayvan gübresi, Ko-fermantasyon, Biyogaz, HBT

ABSTRACT

In this study, the biogas production using the co-fermentation of processed orange wastes and cattle manure at different ratios (25%, 50%, 75%) was analyzed by been analyzed by Hohenheim Batch Yield Test. Cattle manure collected from the farms and processed orange waste was collected from the fruit base juice companies then dried and ground in the standard laboratory conditions. Five mixtures (100% processed orange waste, 100% cattle manure; 25% processed orange waste+ 75% cattle manure; 50% processed orange waste+50% cattle manure; 75% processed orange waste+ 25% cattle manure) were prepared. As a result of this study, the highest percentage of raw protein (12.06%) and percentage of raw fat (or raw oil) (2.30%) were obtained from from 100% processed orange waste mixture, the highest dry material percentage (90.75%) was obtained from 100% cattle manure mixture, the highest organic dry material percentage (95.56%) was obtained from 100% processed orange waste mixture, the highest ADF percentage (60.20%) was obtained from 100% cattle manure mixture and the highest NDF percentage (26.20%) was obtained from 25% processed orange waste+75% cattle manure mixture. The highest amount of biogas (0.70 Nm^3/kg ODM) and methane (0.37 Nm^3/kg ODM) was produced from the mixture of 75% processed orange waste+ 25% cattle manure. The highest amount of methane (53.77%) in biogas was produced from the mixture of 50% processed orange waste+50% cattle manure. Based on this study, co-fermentation of processed orange waste with cattle manure statistically increased the production of methane and biogas in higher amount ($P \leq 0.05$).

Keywords: Processed orange waste, Cattle manure, Co-fermentation, Biogas, HBT

INTRODUCTION

Energy and energy resources are the decisive indicator values of development of countries (Acaroğlu, 2007; Aybek and Üçok, 2017) are of great importance for the survival of societies (Onurbaş Avcıoğlu et al., 2011). Today, the interest in renewable energy sources is increasing due to the decrease in fossil fuel sources and negative environmental effects (Mansourpoor and Shariati, 2012). Renewable energy sources have been naturally extracted from the energy-flow available in our natural environment (Deublein and Steinhauser, 2008). Biomass (63%) has an important place among the renewable energy sources (Demirbaş and Demirbaş, 2007). Biomass refers to the biological material that can be used for industrial production or fuel in general (Haggerty, 2010). In broader terms, biomass are non-fossilized organic material sources (Klass, 1998). Plant (corn, wheat, barley straw), animal, urban wastes, and food industry wastes constitute an important potential for biomass (Brown, 2003; McGowan, 2009; Üçgül & Akgül, 2010).

Biomass and wastes depending on their properties can be converted to energy or fuel together with other fuels through combustion, gasification, anaerobic digestion (Manyi-Loh et al., 2013). Anaerobic digestion converts biological materials or biomass materials (organic matter) into biogas with hydrolysis, acidogenesis, acetogenesis and methanogenesis stages (Tiehm et al., 2001; Cassidy et al., 2008; Xiao et al., 2010; Ogunleye et al., 2010). Biogas occurs as the result of decomposition in the anaerobic fermentation of organic origin wastes. It is a colorless, odorless, lighter than air, burning with a bright blue flame, and it preserves 40-75% CH_4, 15-60% CO_2, 0-3% hydrogen sulfide (H_2S) with very little ammonia (NH_3), hydrogen (H_2) and nitrogen (N_2) depending on the content of organic matter in the composition (Ryckebosch et al., 2011; Ozturk, 2011; Abbasi et al., 2012; Matuszewska et al., 2016). Anaerobic digestion of animal waste is the most common biogas application in worldwide. At the same time, rich organic fertilizers as useful as biogas is produced. Today, because organic industrial wastes are added to animal waste, it increases gas production and economic inputs of the system. Disposal in biogas plants of organic solids emerging from industries is gradually increasing. Although some of the substances are difficult to digest, they have not any problems by mixing with animal wastes or wastewater sludge. In this way, the fermentation of different wastes at the same time is called co-fermentation (URL, 2017). Biogas potential of fruit pulp (500-660 m^3/ton organic dry matter (ODM), vegetable and fruit waste (400-600 m^3/ton ODM) is about twice as much as organic materials like cattle manure (200-500 m^3/ton ODM) and chicken manure (250-500 m^3/ton ODM) (Calli, 2012). Pulp from fruit juice production is very rich in chemical composition. Evaluating the potential of fruit pulp and wastes in biogas production can make an important contribution to energy production and also prevent environmental pollution. Fruit pulp and wastes, which have more biogas content than organic materials such as cattle manure and chicken waste which have a significant potential in our country are not utilized sufficiently. To eliminate these problems in the evaluation of fruit pulp and wastes as single, some organic residues can be mixed with these wastes and biogas production efficiency can be increased. This will make more attractive the use of fruit pulp and waste.

In this study, it is aimed to obtain biogas and organic fertilizer by adding orange wastes (OW) to cattle manure (CM) in different ratios and to provide data source for environmental protection and to ensure efficiency. In this study, biogas and methane production efficiencies of blends obtained by mixing in different proportions (25%, 50%, 75%) of orange processing wastes (husk and pulp) collected from fruit juice plants with cattle manure were determined by HBT (Hohenheim Batch Yield) Test) method.

MATERIALS AND METHODS

CM (Figure 1a) and OW (Figure 1b) were used as materials. CM was collected from a farm in Gaziantep and OW were obtained from a fruit juice processing plant in Adana. CM was left in the open air until it dries completely and OW were dried in natural drying environment at room temperature for 3 weeks.

The dried materials were milled by an industrial grinder until the standard size (VDI 4630. 2006) of 1 mm. Bacterial culture, which is a mixture of solid + liquid phase was taken from Gaziantep Water and Sewerage Administration (GWSA) waste water treatment plant. Inoculum (Figure 2) was prepared by mixing with a 1:2 buffer solution and filtered through four layers of cheesecloth in order to keep the bacterial culture in a better environment. 500 mL of distilled purified water, 0.1 mL of solution A, 200 mL of solution B, 200 mL of solution C, 1 mL of resazurine (0.1%, w/v) solution C and 40 mL of solution were used for the buffer solution. Solution A; 13.2 g CuCl22H2O, 10.0 g MnCl24H2O, 1.0 g CoCl26H2O, and 8.0 g $FeCl_26H_2O$ were prepared in 100 mL with purified water. Solution B; 35 g of $NaHCO_3$ and 4 g of NH_4HCO_3 were dissolved in distilled water and prepared in 100 mL. Solution C; 5.7 g

Na_2HPO_4, 6.2 g KH_2PO_4 were prepared in 1000 mL by dissolving 0.6 g $MgSO_47H_2O$ in purified water. Solution D; 0.5 g of resazurine were dissolved in distilled water and prepared in 100 ml. Solution E was prepared from 95 mL of purified water, 4 mL of 1 N-NaOH and 625 mg of Na_2S9H_2O.

a) Cattle manure b) Orange processing wastes

Figure 1. Cattle manure (CM) and orange processing wastes (OW)

Figure 2. Inoculum

Before starting the experiment, chemical analyzes of milled waste materials were carried out. These chemical analyzes consist of dry matter content (DM), crude ash (CA) and organic matter content (OM), crude protein content (CC), crude fat content (CF) (AOAC, 1990) and ADF and NDF (Van Soest et al., 1991).

Materials (100% OW, 100% CM, 25% OW+ 75% CM, 50% OW + 50% CM, 75% OW + 25% CM) were prepared for the experiment. Three samples were taken and weighed to 0.2 g in the microbalance and placed in 100 ml glass syringes (Figure 3a). The syringes were placed to the hole in the incubator (Figure 3b). For the comparison group samples, 3 inoculum syringes prepared by using burette to receive 30 mL were also placed to the hole in the incubator. According to the standard (VDI 4630 2006), the syringe plunger was removed before the materials were put into syringes and plastic clips were attached to the silicone hoses at the end of the injectors and used for gas transfer. Vaseline was applied to the pistons of the injectors in order to prevent gas leakage during the experiment. Then, the syringe pistons were inserted and the clips were closed and made ready for use. After placing the inoculum into the syringes, it was placed in the incubator at a temperature of 37 °C. The methane measuring device (methane-sensor "Advanced Gasmitter" D-AGM Plus 1010), which was used to determine the methane content in the incubator was calibrated with a calibration tube (60.5% CH_4). The purpose of the calibration is to verify that the measured gas is at standard conditions (0 °C and 1013 hPa). Measurements (Figure 3c) were performed for 35 days. The measurements were made every 6 hours for the first 2 days, 8 and 12 hours in the following days to determine the methane yield in each sample.

a) Glass syringe b) Incubator c) Methane measurement

Figure 3. Glass syringe, incubator and methane measurement

RESULTS AND DISCUSSION

The chemical properties (CP, CO, DM, ODM, ADF, and NDF), biogas and methane production values of the materials were discussed. The data obtained are presented below.

The chemical properties of the materials obtained from the analysis are given in Table 1.

Table 1. Chemical properties of materials

Materials	**CP (%)**	**CO (%)**	**DM (%)**	**ODM (%)**	**ADF (%)**	**NDF (%)**
% 100 OW	7.78	2.30	88.67	95.56	14.76	20.12
% 100 CM	12.06	1.77	90.75	90.79	60.20	23.30
%25 OW + %75 CM	11.07	2.11	90.12	90.58	52.96	26.50
%50 OW + %50 CM	9.89	2.03	89.70	91.82	39.14	20.92
%75 OW + %25 CM	8.76	2.14	89.26	94.48	37.42	22.19

Materials; CP values were 7.78-12.06%, CO values were 1.77-2.30%, DM values were 88.67-90.75%, ODM values were 90.58%, ADF and NDF values were between 14.76% and 60.20%, respectively. The highest crude protein value was obtained in 100% CM (12.06%), lowest in 100% OW (7.78%). The highest crude oil value was obtained in 100% OW (2.30%), the lowest in 100% CM (1.77%). The highest DM was obtained in 100% CM (90.79%), lowest in 100% OW and the highest ODM was obtained in 100% OW (95.56), the lowest in 25% OW + 75% CM. The highest ADF value was occurred in 100% CM (60.20%), the lowest in 100% OW (14.76%). The highest NDF value was occurred in 25% OW + 75% CM (26.50%), the lowest in 100% OW (20.12%).

Average cumulative specific methane production over time are given in Figure 4 for all the mixture. Average cumulative specific methane, biogas values and methane ratios of biogas materials are given in Table 2. The changes of average cumulative specific methane and biogas production are given in Figure 5. The variance analysis of biogas, methane production and methane ratios of biogas are presented in Table 3.

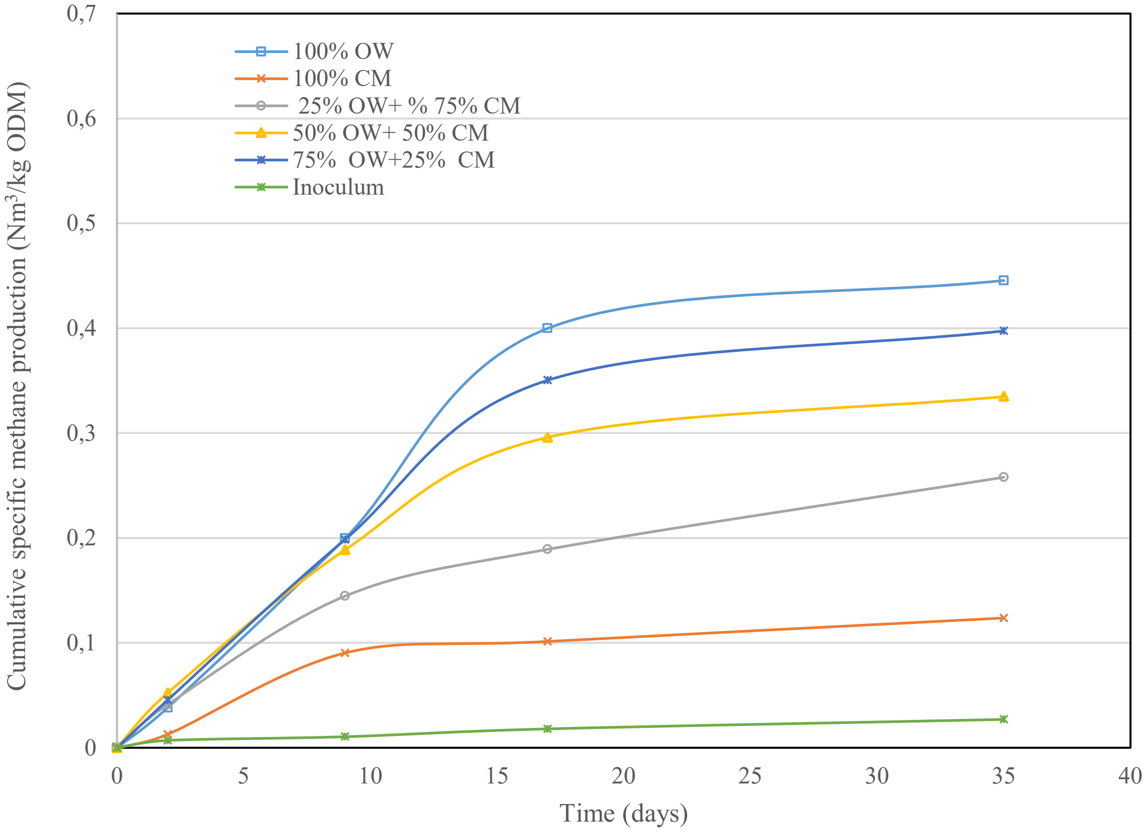

Figure 4. Average cumulative methane production over time of all materials

Table 2. Average cumulative specific methane, biogas values and methane ratios of biogas materials

Materials	**Cumulative specific biogas production (Nm^3/kg OKM)**				**Cumulative specific methane production (Nm^3/kg OKM)**				**Methane ration in biogas**
	Measurements			**Avr.±Std. error**	**Measurements**			**Avr.±Std. error**	**(%)**
	1.	**2.**	**3.**		**1.**	**2.**	**3.**		
% 100 OW	0.82	0.87	0.86	0.85±0.016a	0.41	0.39	0.42	0.41±0.008a	48.42 b
% 100 CM	0.25	0.31	0.24	0.27±0.023d	0.10	0.14	0.10	0.12±0.013d	44.01 c
%25 OW+%75 CM	0.47	0.48	0.49	0.48±0.006c	0.24	0.24	0.25	0.25±0.004c	51.66 ab
%50 OW+ %50 CM	0.63	0.69	0.59	0.64±0.029b	0.35	0.36	0.31	0.34±0.015b	53.77 a
%75 OW + %25 CM	0.75	0.70	0.66	0.70±0.027b	0.39	0.36	0.33	0.37±0.017ab	51.74 ab

$p \leq 0.05$; a, b, c, d,: differences between cumulative specific methane, biogas production and methane ratio averages in biogas indicated by different letters in the same column are important.

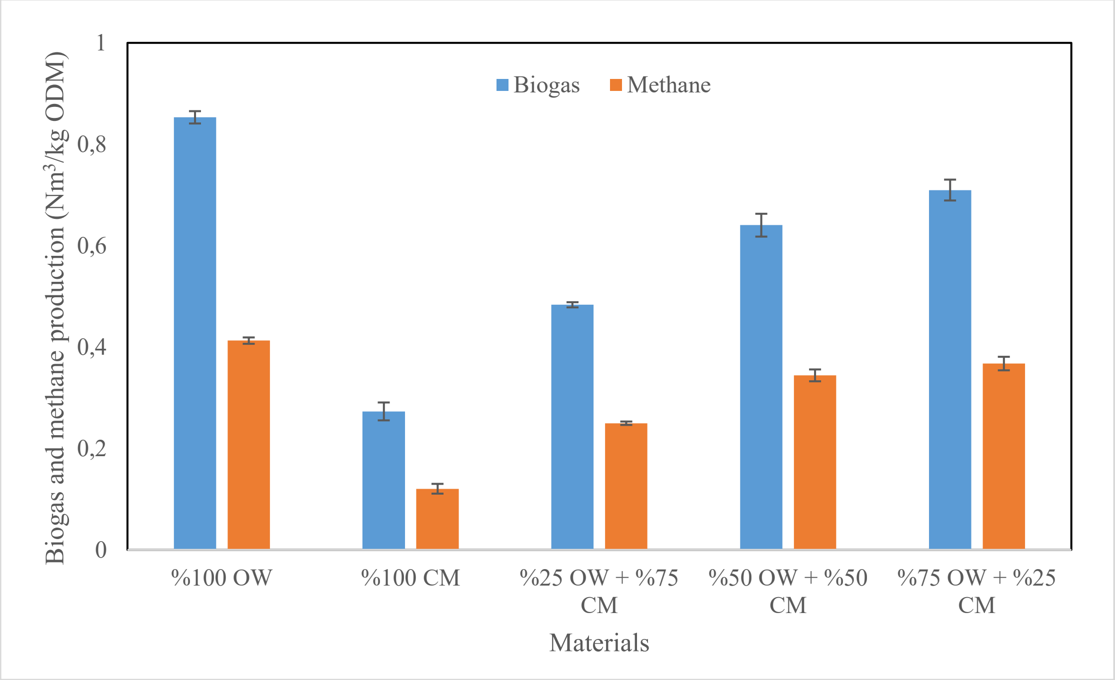

Figure 5. Variation of average cumulative specific methane and biogas production of materials

Table 3. Analysis of variance of biogas, methane production and methane ratios

	Variation source	**DF**	**SS**	**MS**	**F value**	**SEM**	**P value**
Biogas production (m^3/kg ODM)	Between groups	4	0.594	0.148	104.719	0.3074	0.000***
	In Groups	10	0.014	0.001		0.3074	
	Total	14	0.608			0.3074	
Methane production (m^3/kg ODM)	Between groups	4	0.162	0.040	88.146	0.1749	0.000***
	In Groups	10	0.005	0.000		0.1749	
	Total	14	0.166			0.1749	
Methane ratio (%)	Between groups	4	175.152	43.788	17.450	1.2933	0.000***
	In Groups	10	25.093	2.509		1.2933	
	Total	14	200.245			1.2933	

Methane production in all materials starts on the first day and increased rapidly until the 17th day, the rate of increase gradually decreased between 17-35 days and reached maximum value on 35th day (Figure 4). Biogas and methane values in co-fermentation increased, as the proportion of OW in the materials increased. The highest average cumulative biogas values were in 100% OW (0.85 Nm^3 / kg ODM). Biogas values of other materials were determined as 75% OW + 25% CM (0.70 Nm^3 / kg ODM), 50% OW+ 50% CM (0.64 Nm^3 / kg ODM), 25% OW + 75% CM (0.48 Nm^3 / kg ODM), 100% CM (0.27 Nm^3 / kg ODM), respectively (Table 2, Figure 5).

Average cumulative methane production of the materials from the highest to the lowest were determined as 100% OW (0.41 Nm^3 /kg ODM), 75% OW + 25% CM (0.37 Nm^3/kg ODM), 50% OW + 50% CM (0.34 Nm^3/kg ODM), 25% OW+ 75% CM (0.25 Nm^3/kg ODM), 100% CM (0.12 Nm^3/kg ODM), respectively (Table 2, Figure 5).
The methane content of biogas produced by 100% CM, 100% OW and 75% CM+ 25% OW are 44.01%, 48.42 and 51.66-53.77%, respectively. As a result of the statistical comparison, the methane, biogas and methane ratios were found to be significant stage ($P \leq 0.05$) (Table 3).

While Amon et al. (2007) determined methane production of corn silage with animal manure waste as 0.31-0.36 Nm^3/kg ODM- 0.26 Nm^3/kg ODM) in their study, Martin et al. (2010) determined the methane production orange peel as 0.27-0.29 Nm^3/kg ODM). In this study, methane production obtained was found to be different from other studies. These differences may be due to the chemical structure in the material (fat, protein, carbohydrate, C/N ratio, cellulose content, etc.) and initial pH, mixing ratios, electrical conductivity (EC) and animal feed.

The correlation and the main chemical biomasses between biogas and methane production, the fiber particles contained in the biomass confirmed that their chemical composition is essential to predict biogas potential (Angelidaki et al., 1999). Pearson coefficient is used to correlate hemicellulose content in a significant and positive way. Another negative and statistically significant relationship is the biogas production and ADF parameter, especially the degree of fiber lignification with biogas production. Cases that a linear relationship between methane production and cellulose mass content cannot be evaluated, it can be partly explained by the fact that the biomasses tested have different chemical properties (Jimenez et al., 1990). Even if cellulose is digestible by active microorganisms in anaerobic environment, by connecting to the lignin becomes unsuitable for digestion (Dinuccio et al., 2010). In this study, as a result of chemical analysis of materials used, the lowest ADF (14.76) was determined in 100% OW. The highest cumulative specific biogas production was also observed in 100% OW. There was a negative correlation between ADF content and biogas production.

CONCLUSIONS AND RECOMMENDATIONS

The aim of this study was to determine the biogas and methane production efficiencies of the mixtures obtained by mixing OW (husk and pulp) in different ratios (25%, 50%, and 75%) with CM that has an important potential in our country.

The results and recommendations are summarized below.

- While the highest (2.30%) CO values was obtained in 100% OW, the lowest in (1.77%) was obtained in100% CM.
- DM values ranged from 88.67% to 90.75% and ODM values are within the range of 90.58% to 95.56%.
- ADF value was found the highest (60.20%) in 100% CM and the lowest (14.76%) in 100% OW.
- NDF value was found the highest (26.50%) 25% OW + 75% CM, the lowest (20.12%) in 100% OW
- Highest methane production of materials between days 25-35 occurred.
- As the ratio of OW in the mixture materials increased, biogas produced by co-fermentation and methane values in biogas increased.
- Cumulative biogas values was found the highest (0.85 Nm^3 / kg OKM) in 100% OW, the lowest (0.27 Nm^3/kg ODM) in 100% CM
- The highest biogas (0.85 Nm^3/kg OKM) and methane (0.37 Nm^3/kg OKM) values occurred in the mixture of 75% OW + 25% CM.
- Methane content in biogas was obtained from the highest (53.77%) in 50% OW+ 50% CM.
- Methane, biogas and methane content of all materials were statistically significant ($P \leq 0.05$).

Recommendations for this study can be listed as follows.

- Biogas and methane production efficiencies can be increased as a result of co-fermentation of OW with CM.
- As a result of co-fermentation of OW with CM, environmental and natural resources can be protected by eliminating wastes.
- OW are important materials for biogas plants.
- Greenhouse gases (methane and carbon dioxide) to be released to the atmosphere due to the uncontrolled storage of OW and CM will be prevented by the introduction of the biogas process.
- The significant potential of the fruit processing waste and cattle manure waste in Turkey can be utilized based on anaerobic digestion process to acquire the energy.

Acknowledgements

The authors would like to acknowledge the financial support of the Directorate of Scientific Research Projects of Kahramanmaraş Sütçü İmam University (Project No: 2017 / 1-7 YLS).

REFERENCES

Abbasi, T, Tauseef, S. M., Abbasi, S. A., 2012. Biogas and Biogas Energy: An Introduction. *Biogas Energy*, 1-10.

Acaroğlu, M., 2007. Alternatif Enerji Kaynakları. *Nobel Yayın No:* 1253, , ISBN 978-605-395-047-9, 609 p, Ankara

Amon, T., Amon, B., Kryvoruchko, V., Zollitsch, W., Mayer, K., Gruber, L. 2007. Biogas production from maize and dairy cattle manure—influence of biomass composition on the methane yield. *Agriculture, Ecosystems & Environment*, 118 (1-4): 173-182.

Angelidaki, I., Ahring, B. K., 1993. Thermophilic Anaerobic Digestion of Livestock Waste: the Effect of Ammonia. *Applied Microbiology and Biotechnology*, 38: 560-564.

AOAC, 1990. Official Methods of Analysis. 15th ed. *Association of Official Analytical Chemists*, Washington, DC. US.

Aybek, A., Üçok, S., 2017. Determination and Evaluation of Biogas and Methane Productions of Vegetable and Fruit Wastes with HBT Method. International Journal of Agricultural and Biological Engineering, *International Journal of Agricultural and Biological Engineering*, 10 (4): 207-215.

Brown, R.C., 2003. Biorenewable resources : engineering new products from agriculture. Iowa State Press, Ames, Iowa, 286 p.

Cassidy, D. P., Hirl, P. J., Belia, E., 2008. Methane production for ethanol coproduction in anaerobic SBRS. *Water Sci Technol*., 58 (4): 789-93.

Dinuccio, E., Balsari, P., Gioelli, F., Menardo, S., 2010. Evaluation of the biogas productivity potential of some Italian agro-industrial biomasses. *Bioresource Technology*, 101 (10): 3780–3783.

Çallı, B., 2012. Atıklardan Biyogaz Üretimi. Türkiye Kimya Derneği -Genç Kimyacılar Platformu, http://eng.marmara.edu.tr/enve

Demirbaş, A. H., Demirbaş, I., 2007. Importance of rural bioenergy for developing countries. Energy Convers Manage, 48 (8): 2386-2398.

Deublein, D., Steinhauser, A., 2008. Biogas from Waste and Renewable Resources, p.1-450.

Haggerty, A. P., 2010. Biomass crops: production, energy, and the environment. *Nova Science Publisher'*s, Hauppauge, N.Y., 323 p.

Jimenez, S., Cartagena, M. C., Arce, A., 1990. Influence of lignin on the methanization of lignocellulosic wastes. *Biomass*, 21, 43–54

Klass, D., 1998. Biomass for renewable energy, fuels, and chemicals. *Academic Press*, San Diego, USA, 651 p.

Mansourpoor, M., Shariati, A., 2012. Effect of mixture of alcohols on biodiesel properties which produced from waste cooking oils and compare combustion performance and emissions of biodiesels with petrodiesel. *Adv Environ Sci*, 4 (3): 153.

Manyi-Loh, C. E., Mamphweli, S. N., Meyer, E. L., Okoh, A. I., Makaka, G., Simon, M., 2013. Microbial anaerobic digestion (bio-digesters) as an approach to the decontamination of animal wastes in pollution control and the generation of renewable energy. *Int J Environ Res Public Health*, 10 (9): 4390-417.

Matuszewska, A., Owczuk, ., M., Zamojska-Jaroszewicz, A., Jakubiak-Lasocka, J., Lasocki, J., Orlin´ ski, P., 2016. Evaluation of the biological methane potential of various feedstock for the production of biogas to supply agricultural tractors. *Energy Conversion and Management*, 125: 309-319.

McGowan, T., 2009. Biomass and alternate fuel systems: an engineering and economic guide. *John Wiley & Sons Hoboken*, New York, 264 p.

Ogunleye, O. O., Aworanti, O. A., Agarry, S. E., Aremu, M. O., 2016. Enhancement of animal waste biomethanation using fruit waste as co-substrate and chicken rumen as inoculums. *Energy Sources, Part A: Recov. Utiliz Environ Effect*s, 38(11): 1653-60.

Onurbaş Avcıoğlu, A., Türker, U., Demirel Atasoy, Z., Koçtürk, D., 2011. Tarımsal Kökenli Yenilenebilir Enerjiler-Biyoyakıtlar. *Nobel Yayınları, Yayın No*: 72, ISBN 978-605-5426-71-2, 493 p, Ankara.

Öztürk, H. H., 2011. Bitkisel üretimde enerji yönetimi. *Hasad Yayıncılık Ltd. Şti*., ISBN: 978-975-8377-78-7, 248s, Istanbul

Ryckebosch, E., Drouillon, M., Vervaeren, H., 2011. Techniques for transformation of biogas to biomethane. *Biomass Bioenergy*, 35:1633–45.

Tiehm, K. N., Zellhorn, M., Neis, U., 2001. Ultrasonic waste activated sludge disintegration for improving anaerobic stabilization. *Water Res*., 35 (8): 2003-9.

URL, 2017. Biyogaz. http://biyogaz.entmakina.com/biyogaz-nedir/.

Üçgül, İ., Akgül, G., 2010. Biyokütle Teknolojisi. *Journal of YEKARUM*, 1(1): 3-11.

Xiao, W.,Yao, W., Zhu, J., Miller, C., 2010. Biogas and CH4 productivity by co-digesting swine manure with three crop residues as an external carbon source. *Bioresour Technol*., 101: 4042-7.

Van Soest, P.J., Robertson, J.B., Lewis, B.A., 1991. Methods for dietary fiber. neutral detergent fiber and nonstarch polysaccharides in relation to animal nutrition. J. *Dairy Sci*.. 74. 3583–3597.

VDI 4630, 2006. Fermentatıon of Organic Material, Characterisatıon of Substrate, Collectıon of Material Data, Fermentatıon Tests, *VDI Gesellschaft Energietechnik*.

ORCID

Ali AYBEK *http://orcid.org/0000-0003-3036-8204*
Levent Gürsel ALBAYRAM *http://orcid.org/0000-0002-6152-8138*
Serdar ÜÇOK *https://orcid.org/0000-0002-7158-669X*

KSÜ Mühendislik Bilimleri Dergisi, 22, Özel Sayı, 2019 KSU J Eng Sci, 22, Special Issue, 2019
Uluslararası İleri Mühendislik Teknolojileri Sempozyumu (ISADET) Özel Sayısı
International Symposium on Advanced Engineering Technologies (ISADET) Symposium Special Issue
Araştırma Makalesi Research Article

Kahramanmaras Sutcu Imam University
Journal of Engineering Sciences

Geliş Tarihi : 02.08.2019 Received Date : 02.08.2019
Kabul Tarihi : 30.10.2019 Accepted Date : 30.10.2019

INVESTIGATION OF LASER METAL DEPOSITION METHOD BY FINITE ELEMENT ANALYSIS: LASER SPEED EFFECT ON THIN WALLED GEOMETRY BUILDING

LAZERLİ METAL YIĞMA YÖNTEMİNİN SONLU ELEMANLAR ANALİZİYLE İNCELENMESİ: İNCE DUVAR GEOMETRİSİ ÜRETİMİNDE İLERLEME HIZI ETKİSİ

M. İbrahim AŞÇI [1]*, *Mehmet ERMURAT* [1]

[1]Kahramanmaras Sütçü İmam Üniversitesi, Makine Mühendisliği Bölümü, Kahramanmaraş, Türkiye
*Sorumlu Yazar / Corresponding Author: M. İbrahim AŞÇI, mibrahimasci@gmail.com

ÖZET

Lazerli metal yığma yöntemi eklemeli imalat yöntemlerinden biri olarak ortaya çıkmıştır. Özellikle sanayide son ürün çıktısındaki malzeme ürün hassasiyeti ve maliyet açısından yaşanan problemler bu yöntemin geliştirilmesinde ve üzerinde önemle durulmasında önemli bir rol üstlenmiştir. Ancak Lazerli metal yığma yönteminde yöntem gereği uygulanan parametrelerden kaynaklı dezavantajları bulunmaktadır. Bu dezavantajlardan birisi ise artık gerilmedir. Artık gerilme imalat sırasında ısınma ve soğuma hızlarına bağlı olarak, malzeme içerisinde kalan basma-çekme kuvvetlerinin etkisidir. Bu çalışmada Lazerli metal yığma yönteminde kullanılan proses parametrelerinin artık gerilme probleminin giderilmesi ve elde edilecek ürünün kalitesinin artırılması üzerindeki etkileri sonlu elemanlar yöntemiyle analiz edilmiş ve termal sonuçları karşılaştırılmıştır. Çalışma için Simufact programından yararlanılmıştır. 3 boyutlu tasarım modül içerisine aktarıldıktan sonra standart parametreler dışındaki değerler üzerinde değişiklikler yapılarak analizler yapılmakta ve bu analiz değerleri karşılaştırılarak artık gerilme üzerindeki etkileri belirlenmektedir. Bu yöntemde analiz için Simufact programı lazer hızı, katman kalınlığı ve sıcaklık parametrelerinde analizler yapılmasına izin vermektedir. Bu çalışmadaki analizler için yöntem parametrelerinden lazer hızı seçilmiş ve analiz sonucundaki karşılaştırmalar lazer hızının etkisini araştırma adına yapılmıştır. Analiz sonucuna göre, lazer hızının artması ile malzemeye uygulanmış olan enerji miktarı azalmasından dolayı maksimum sıcaklık, deformasyon miktarı ve buna bağlı olarak da gerilmenin azaldığı, ancak katılaşmayan bölge miktarının arttığı gözlenmiştir.

Anahtar Kelimeler: eklemeli imalat, lazerli metal yığma yöntemi, sonlu elemanlar metodu

ABSTRACT

Laser metal deposition method has emerged as one of the additive manufacturing methods. Particularly in industry, the product sensitivity and cost problems in the final product output have played an important role in the development and emphasis of this method. However, there are disadvantages arising from the parameters applied in the method of laser metal deposition. One of these disadvantages is the residual stress. The residual stress is the effect of the tension-compression forces within the material due to heating and cooling speeds during the production. In this study, effects of the process parameters used in laser metal deposition method on the elimination of the residual stress problem and the quality of the product to be obtained have been analyzed by the finite element method and the thermal results have been compared. Simufact program has been used for this study. After being transferred into a 3D design module, changes are made on the values other than the standard parameters d the analyzes are made and the effects on the residual stress are determined. In this method, Simufact program allows analysis of laser speed, layer thickness and temperature parameters. For the analysis of this study, the laser velocity has been chosen from the method parameters and the results of the analysis have been performed to investigate the effect of the laser velocity. According to the results of the analysis, it has been observed that the maximum temperature, the amount of deformation and consequently the stress were decreased due to reducing the amount of energy applied to the material with increasing laser speed, but the amount of non-solidified region was increased.

Keywords: additive manufacturing, laser metal deposition method, finite element method

INTRODUCTION

In Laser Metal Deposition(LMD), powder material is fed to the melting zone simultaneously with the movement of the laser. Powder feeding and laser focusing are carried out by means of the nozzle, concentrically, Figure 1. Since the powder material is not spread over the entire platform, the laser metal deposition technique is particularly advantageous in producing thin wall geometries. With this method, which is actively used in the populer industry such as aerospace and biomedical, the opportunity is provided to obtain physical parts in a short period of time according to the program and part sizes used. Today, companies which use and direct these technologies, develop and make rapid progress in quality, originality and innovation (Ermurat,M 2009).

The most important research topics in methods with high heat input, such as laser metal deposition, have been carried out on the consequences of high heat input on the part. One of the important disadvantages of this method is that residual stresses caused by high heating and cooling which causes faults in the products both during or after manufacturing. In this method, considering the effect area of the laser, a bell-shaped melt pool is formed by the effect of the focused laser beam as seen in Figure 2.

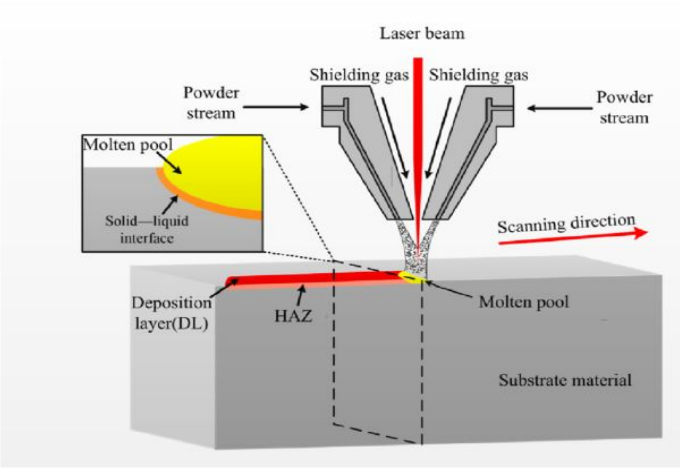

Figure 1. Laser Metal Deposition Process (Zhan, X., et al 2018)

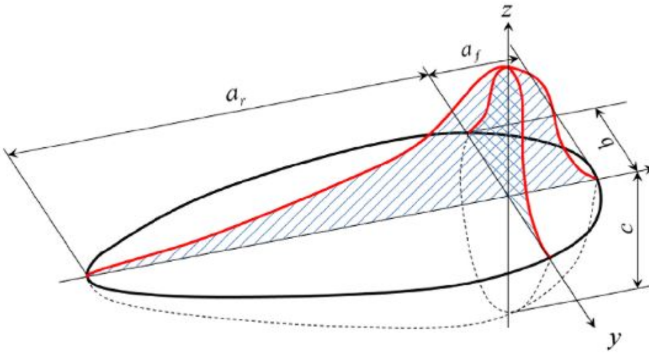

Figure 2. Gaussian Model (Poyraz, Ö. 2018)

This type of melt pool is explained by the Gaussian Dispersion model (Poyraz, Ö. 2018), (Hitz, B. Et al 2001). The laser beam equation that provides the Gaussian density is described below. (Koechner, W. 2006).

$$I(\mathrm{r})=I_0 e^{\left(\frac{-2r^2}{w_0^2}\right)} \tag{1}$$

In equation (1), r is the laser beam radius, $I_{(r)}$ is the intensity of laser beam at the radius of r, I_0 is the intensity of laser beam at midpoint of beam and w_0 is the laser spot radius at the interaction level with material. According to the result of the equation, the maximum energy intensity occurs in the middle axis, that is, $r = 0$ point. (Fathi, A. Et al 2006).

The laser beam reaches the melting area following the conical path after exiting the nozzle. On this route, the energy intensity decreases from the mid-axis to the outer diameter. Therefore, the accumulation capacity increases depending on the laser intensity in the middle axis. The intensity of the laser beam, described by the Gaussian profile, is related to the laser power, radius and standoff distance values. (Poyraz, Ö. 2018).

One of the factors that provide the gaussian distribution is the absorption effect of the material. Some of the laser beam that affects the material is absorbed by the material and some of it is reflected. The absorption coefficient, which varies according to the material, is expressed as the ratio of the energy absorbed by the material to the total energy of the laser as seen in equation (2) (Koechner, W. 2006).

$$A=P_A/P \tag{2}$$

In equation (2), A is the absorption coefficient, P_A is the amount of energy absorbed by the material and P is the total energy of the laser.

If the laser is applied to the material for longer than necessity, it causes an increase in the heat affected zone. Thus, this will have negative effects on the mechanical properties of the part. Repeated melting and solidification cycles can cause defects such as porosity, as well as the use of lasers more than necessity to melt the powder material. In addition, these thermal cycles sometimes cause high residual stresses and shrinkage in the final product (Hitsz, B. Et al 2001). Additionally, excess laser power causes an increase in the surface tension (Agarwala, M. Et al 1995). On the other hand, the increase of the heat-affected zone is directly proportional to the excess effect of the laser, which adversely affects the mechanical properties of the material. (Kathuria, Y.P. 1997).

These conditions depend on some parameters. These parameters may include the laser power, layer thickness, scanning speed, scanning pattern, platform temperature, material type, powder size etc. According to the equation given below (Eq.3), four of these parameters change the volumetric energy density.

$$Evol = P/(Vs \cdot t \cdot d) \tag{3}$$

In equation (3), Evol is the volumetric energy density, P is the laser power, Vs is the scanning speed, t is the layer thickness, and d is the clad width, Inappropriate energy densities applied during this process cause local stresses, gaps and some other defects. (Ermurat, M. 2009).

Higher energy density cause extraordinary thermal effects on the parts which is produced with the laser metal deposition methods and residual stresses, shrinkage and microstructural problems based on this thermal effects. By using thermal and thermo-mechanical analyzes with some software using the Finite Element Method, such problems can be analyzed during part design and design optimization.

Analyzes in this project are carried out in two stages. In the various stages of the process, thermal analysis is performed in which the thermal properties of the part are examined as a result of repetitive heat input in the process zone and the heat affected zone.

In addition, mechanical effects such as stress, deformation, tensile and distortion on the substrate and on the geometry to be produced can be examined by thermo-mechanical analysis.

In this study, thermal and thermo-mechanical effects of laser speed on thin wall geometry by Laser Metal Deposition process have been performed with Simufact Welding software using the Finite Element Method.

MATERIAL-METHOD

Simufact Welding software allows variable parameters to be determined such as the laser speed, type of material, laser area and the volume, ambient temperature, laser power, cooling time and acceleration variables for laser speed. Among the variables mentioned, the laser speed has been studied to investigate its effect on the residual stresses.

A simple geometry without complex structure for the analysis has been designed in 3D. The designed geometry has been subjected to certain pretreatment processes in order to make analysis in Simufact program. The designed geometry is defined layer by layer and mesh assignment is made by applying the necessary mesh structure.

The process inputs of the program have been applied respectively for the geometry transferred into the program . Afterwards, analyzes have been performed by changing the laser speed with all other conditions remaining constant. The results have been obtained in the form of graphs and screenshots and comparisons have been made between them.

The model image on the Simufact software screen is shown in Figure 3 . The geometry shown in the figure in green is a fixture on which the base (substrate) would be placed. The fixture is 15mm X 20mm X 3mm size and it has 3mm element size. Base on which the first layer would be deposited on it, is positioned on the fixture. The base has 5mm X 10mm X 2mm size and it has 0.5mm element size. The geometry has size of 0.2mm X 1mm X 8mm. The metal deposition geometries, which consist of 5 layers and have heights of 0.2mm, are positioned on top of each other and a total geometry height of 1mm is obtained. The metal deposition geometries have a 0.1mm element size.

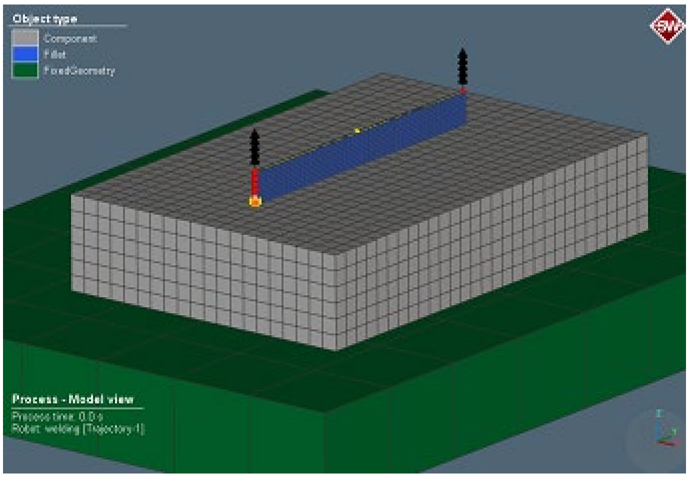

Figure 3. Geometry

Some Important Preliminary Parameters Used in this Study

- Geometry; 0.1mm thickness, 5-layer metal deposition
- Mesh Structure; Hexahedral mesh structure, Apex Program, Simufact Refinement is done.
- Material; Tİ6Al4V (Solidus Temp: 1400C, Melting Temp:1600 C)
- Laser Power; 110W
- Laser Flow Characteristics; Max Radius: 0.15mm, Min Radius: 0.14mm, Conical Depth :0.2mm
- Ambient Temperature; 20 C
- Efficiency; 0,37(Material-Laser Absorbsion Ratio)
- Time Between Layers: 3sn
- Laser Speed Levels: 30mm/sn - 40mm/sn - 50mm/sn

ANALYSIS RESULTS

For the analysis, melting and peak temperature distributions in the cross-sectional area have been examined from the Welding Monitor section of the program. It was observed that as the laser speed increases, the maximum temperature that occurs in each layer decreases. It has also been observed that as the laser speed increases, regions that is away from the center of the laser do not reach the melting temperature haven’t been occurred. Figure 4.

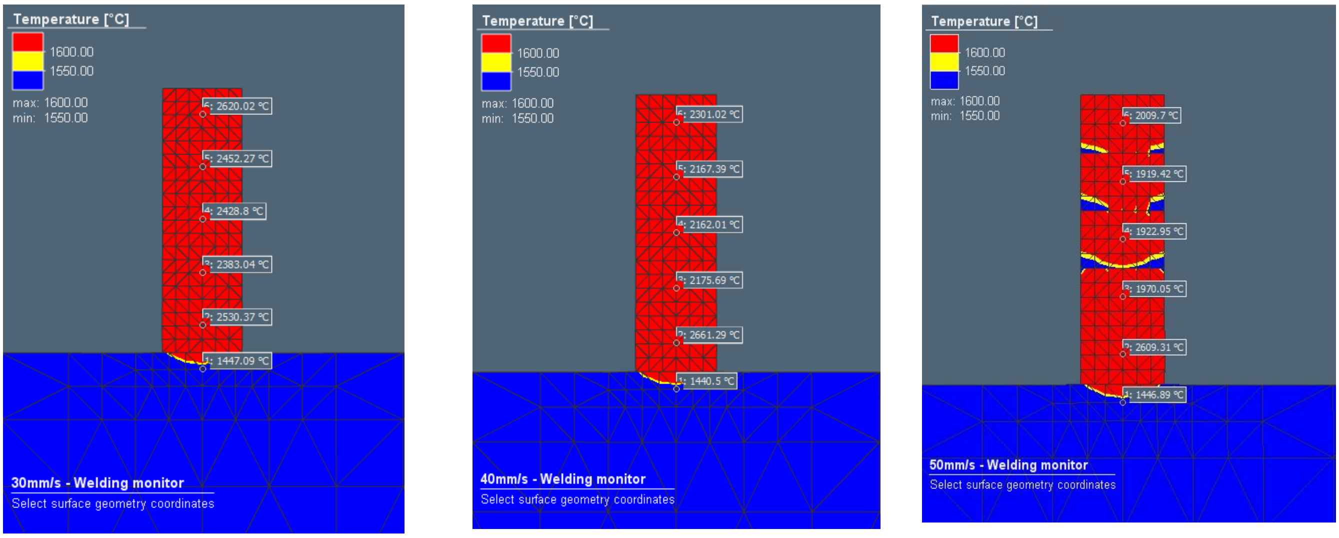

30 mm/sn 40 mm/sn 50 mm/sn

Figure 4. Welding Monitor View (Melting-Solidification Observation)

The maximum temperature level in this analysis provides information on whether or not melting can occur and at what levels the values are exceeded. As a result of the analysis, it has been found that the parameters easily provide the melting temperature of Ti6Al4V material, Figure 5.

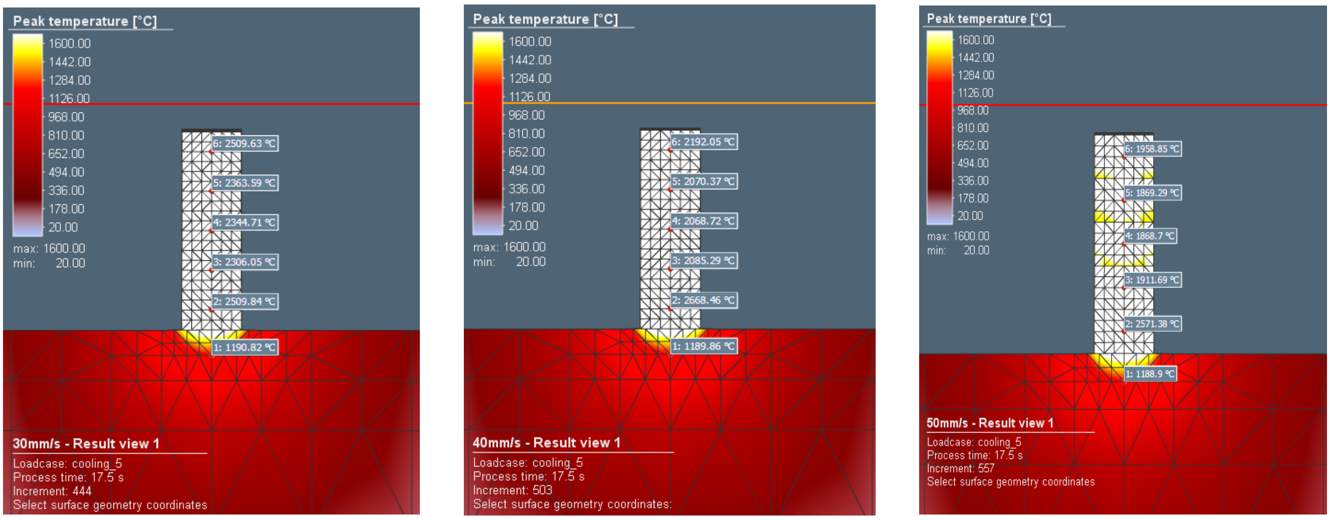

30 mm/sn 40 mm/sn 50 mm/sn

Figure 5. Maximum Temperature Levels

In this process, where repeated high-temperature processes take place, each layer is a cause of the thermal stress. The part subjected to high residual stresses during the heat treatment is deformed after cooling. As a result of this analysis, it has been observed that effective stresses decrease as the laser speed increases, Figure 6.

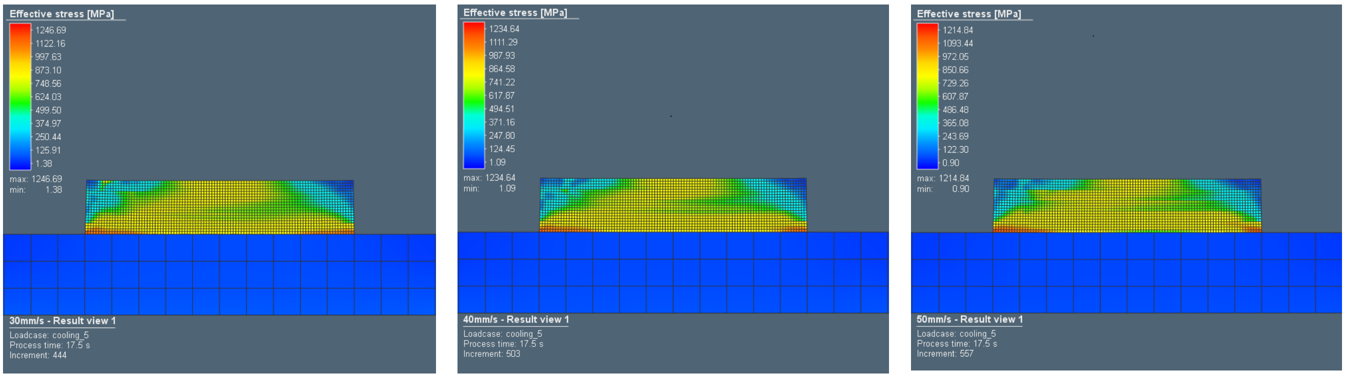

30 mm/sn 40mm/sn 50 mm/sn

Figure 6. Effective Stress (VonMises)

Deformation is one of the inevitable facts in this process involving instantaneous heating and cooling processes. Simufact Welding software is able to calculate the amount of deformation occurred. In this analysis, in the formation of thin wall geometry with the laser source having 110W energy, the maximum deformation in the direction of laser progression occurred approximately 0.03mm and this causes shrinkage of the geometry. It is seen that the deformation amount decreases as a result of the effective stress which decreases with increasing laser speed, Figure 7.

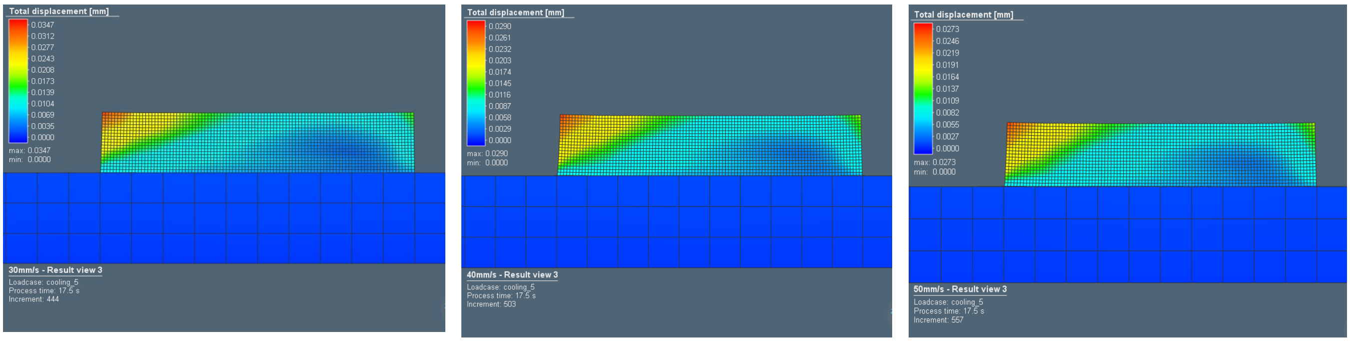

30 mm/sn 40 mm/sn 50 mm/sn

Figure 7. Total Deformation

CONCLUSION

As a result of the analyzes, following conclusions can be made;

- Maximum temperature decreases with increasing the laser speed
- Deformation amount decreases with increasing the laser speed
- Stress decreases with increasing the laser speed
- Non-solidified area in the cross-sectional region increases with increasing the laser speed

According to these results, by using FEM Softwares, a combination of laser power and laser speed can be obtained for optimum part building without any solidified region and the lowest energy input to the part.

Acknowledgement

We would like to thank Netform Engineering for the MSC One Academic license including Simufact Welding.

REFERENCES

Agarwala M, Bourell D, Beaman J, Marcus H, Barlow J, (1995) Direct selective laser sintering of metals, *Rapid Prototyping Journal*, V1, N1,pp 26-36

Dobson, S., Wu, Y., Yang, L. (2018) Material characterization for light weight thin wall structures using laser powder bed fusion additive manufacturing. *Proceedings of the 29th Annual International Solid Freeform Fabrication Symposium – An Additive Manufacturing Conference*

Ermurat, M. (2009). Lazerli doğrudan metal parça imalatı sisteminin geliştirilmesi, üretilen parça özelliklerinin incelenmesi ve sistem optimizasyonu. *Kocaeli Üniversitesi*

Fathi A, Toyserkani E, Khajepour A ve Durali M, (2006) Prediction of melt pool depth and dilution in laser powder deposition, *J. Phys. D: Appl. Phys*. 39 2613–2623

Hitz B, Ewing J J, Hecht J, (2001) Introduction to Laser Technology, *Institute of Electrical and Electronics Engineers Inc*,104-109

Kathuria Y.P:(1997) Laser cladding process: a sutdy using stationary and scanning CO2 laser beams, *Surface and Coatings Technology* 97, pp 442-447

Koechner W., (2006) Solid-State Laser Engineering, *Springer Science Business Media Inc*, 3-4.

Poyraz, Ö. (2018). Metallerin lazer katmanlı imalatında kullanılan proses parametrelerinin etkisinin, modelleme ve simülasyon yöntemleri kullanılarak incelenmesi. *Eskişehir Osmangazi Üniversitesi*

Shao T. M., Lin X. C., Zhou M, (2001) Absorption of some powder materials to YAG laser, *Science in China* (A Serisi), Vol 44

Zhan, x., Lin, X., Gao, Z., Qi, c., Zhou, J., Gu, D. (2018). Modeling and simulation of the columnar-to-equiaxed transition during laser melting deposition of Invar alloy. *Journal of Alloys and Compounds* 755 (2018) 123e134

ORCID

M. İbrahim AŞÇI https://orcid.org/0000-0001-8673-3325
Mehmet ERMURAT *http://orcid.org/0000-0002-5661-2108*

KSÜ Mühendislik Bilimleri Dergisi, 22, Özel Sayı, 2019 KSU J Eng Sci, 22, Special Issue, 2019
Uluslararası İleri Mühendislik Teknolojileri Sempozyumu (ISADET) Özel Sayısı
International Symposium on Advanced Engineering Technologies (ISADET) Symposium Special Issue
Araştırma Makalesi Research Article

Kahramanmaras Sutcu Imam University
Journal of Engineering Sciences

Geliş Tarihi : 02.08.2019 Received Date : 02.08.2019
Kabul Tarihi : 14.10.2019 Accepted Date : 14.10.2019

HEAVY METAL POLLUTION INDEX (HPI) IN SURFACE WATER BETWEEN ALAKIR DAM AND ALAKIR BRIDGE, ANTALYA-TURKEY

ALAKIR BARAJI VE ALAKIR KÖPRÜSÜ ARASINDAKİ YÜZEY SUYUNUN AĞIR METAL KİRLİLİK İNDEKSİ (HPI), ANTALYA-TÜRKİYE

Yasemin LEVENTELI[1*], *Fusun YALCIN*[2]

[1]Akdeniz Üniversitesi, Jeoloji Mühendisliği Bölümü, Antalya, Türkiye
[2]Akdeniz Üniversitesi, Matematik Bölümü, Antalya, Türkiye

*Sorumlu Yazar / Corresponding Author: Yasemin LEVENTELI, leventeli@akdeniz.edu.tr

ÖZET

Nüfus artışına bağlı olarak temiz suya erişimin önemi artmıştır. Söz konusu gereksinim içme ve sulama suyu ile sınırlı değildir; enerji üretimi ve endüstri gelişiminde de önemlidir. Antalya gerek göç alması, gerek tarım ve endüstrideki büyümesi ile en çok su ihtiyacının arttığı iller arasındadır. Kumluca artan nüfusu, önemli tarım alanları ve hemen kuzeyindeki hidroelektrik santralleri ile Antalya'nın önemli ilçelerindendir. Her mevsim tarım yapılmaktadır. Bu çalışmada, artan nüfusun ve tarımın etkilerini anlayabilmek için, ovayı baştanbaşa kesen yüzey sularında ağır metal anomalileri araştırılmıştır. Bunun için Mayıs 2018 tarihinde, sistematik olarak, Alakır Barajı ve Alakır Köprüsü arasındaki 48 lokasyondan numune alınmıştır. Kimyasal analiz sonuçlarında elde edilen veriler HPI istatistiksel analiz yardımıyla yorumlanmıştır. HPI değerindeki anomaliler iki bölgede yoğunlaşmıştır. Bu gruplaşmada üst bölgede barajın, alt bölgede tarımsal faaliyetlerin etkili olduğu düşünülmektedir.

Anahtar Kelimeler: Yüzey Suyu, Ağır Metal, Kirlilik İndeksi, HPI, İstatistik, Alakır.

ABSTRACT

The importance of getting the clean water has increased due to population growth. This requirement is not limited to drinking and irrigation water; it is also important in energy production and industry development. Antalya is one of the provinces with the highest water demand due to its migration, agriculture and industry growth. Kumluca is one of the important districts of Antalya with its growing population, important agricultural areas and hydroelectric power plants just north of it. Agricultural is performed in all season. In this study, in order to understand the effects of increasing population and agriculture, heavy metal anomalies were investigated in surface waters that passes throughout the plain. In May 2018, a systematic sampling was taken from 48 locations between Alakir Dam and Alakir Bridge. The data obtained in the results of chemical analysis was interpreted using HPI statistical analysis. HPI value anomalies were concentrated in two regions. These grouping were considered that because of the dam in the upper region; because of the agricultural activities in the lower region.

Keywords: Surface Water, Heavy Metal, Pollution Index, HPI, Statistics, Alakir.

INTRODUCTION

The importance of water in human health is well known. Therefore, the water pollution, whatever the source, affects adversely human health. On the other hand, it is necessary to know the reason to produce proper and effective solutions. The urbanization, industrial zones, agricultural areas and similar reasons may cause the pollution and they called "anthropogenic" (Fernandez-Luqueno et al., 2013); besides that, sometimes geological factors may cause water pollution. A lot of statistical methods have been developed to measure and evaluate the water pollution (Prasad and Bose 2001; Yalcin et al., 2007; Yalcin et al., 2008; Prasanna et al. 2012; Dadolahi-Sohrab et al. 2012; Yalcin et al., 2017; Cengiz et al., 2017; Bytyçi et al. 2018; Dutta et al., 2018; El-Tohamy et al. 2018; Qu et al. 2018; Leventeli et al. 2019; Singh et al. 2018; Wen et al., 2019; Singh et al. 2019). One of them is heavy metal pollution index (HPI). There are a lot of hydroelectricity power plant (HPP) with small dam, around the country. One of them is Alakir Dam. It is located on the western part of Antalya. The stream flows among greenhouses and settlement areas in the plain; and there is a bridge where it reaches the Mediterranean, Alakir Bridge. The surface water samples have been taken from the locations between Alakir Dam and Alakir Bridge.

MATERIALS AND METHODS

The study area is located on the western part of Antalya Gulf, between Alakir Dam and Alakir Bridge (**Figure 1**). Agricultural and residential areas are common in the region. The samples were collected from 48 locations in May 2018 based on land use properties of the study area. The water samples have been taken by 1 L polythene containers. The samples have been prepared according to EPA 3005A (1992) method (Rohrbough, 1986; ASTM 1985). The Inductively Coupled Plasma – Mass Spectrometer (ICP-MS) device has been used for the experimental studies in the Research Center Laboratory of Akdeniz University. While 43 samples could be analyzed; the rest 5 samples (K1, K2, K4, K12, K19) could not be studied. The heavy metal values (ppb) are given in **Table 1.**

Figure 1. The Location Map of the Study Area.

HEAVY METAL POLLUTION INDEX (HPI)

The geological and anthropogenic factors may cause the accumulation of heavy metals in groundwater. Some trace metals such as cobalt (Cd), copper (Cu), zinc (Zn) and selenium (Se) are essential for humans, but its high level may cause physiological disorders (Kumar et. al., 2019). The heavy metal pollution index (HPI) shows the water quality and is calculated from the concentration of heavy metal in water. Various algorithms have been proposed and used by different researchers to calculate HPI and to determine water quality (Chaturvedi et al., 2018; Horton, 1965; Brown et al., 1970; Dunnette, 1979; CCME, 2001; Mohan et al., 1996; Edet and Offiong, 2002; Prasanna et al., 2012; Tiwari et al., 2015; Islam et al., 2015). The heavy metal pollution index (HPI) is a very useful tool in estimating the overall effects; because, it contains the concentration of all the measured metals. The Heavy Metal Pollution Index (HPI) and the sub-index of each parameter (*Qi*) are calculated using the following correlations (Leventeli et al., 2019).

$$Q_i = \sum_{i=1}^{n} \frac{(M_i - I_i)}{(S_i - I_i)} \text{x}100 \qquad (1)$$

Wi is the unit weight of the *i-th* parameter, and *Qi* is the sub-index of the i-th parameter. *n* is the number of parameters considered. *Mi* is the measured value of the parameter *i*. *Ii* and *Si* give the ideal and standard values of the *i-th* parameter.

$$HPI = \frac{\sum_{i=1}^{n} W_i Q_i}{\sum_{i=1}^{n} W_i} \qquad (2)$$

The analysis results were interpreted based on Nasrabadi (2015).

Table 1. The heavy Metal Values (ppb)

	As	**Mn**	**Ni**	**Cu**	**Pb**	**Fe**	**Sr**	**Cr**		**As**	**Mn**	**Ni**	**Cu**	**Pb**	**Fe**	**Sr**	**Cr**
K3	0,509	14,731	15,054	3,142	0,35	65,734	134,294	1,094	**K29**	0,715	5,73	3,808	0,117	0,191	62,181	223,526	0,334
K5	0,748	10,047	45,716	2,126	0,222	95,871	151,882	1,041	**K30**	0,721	8,214	4,461	0,755	0	76,452	235,509	0,656
K6	0,64	16,885	23,002	5,583	2,914	122,005	149,746	1,366	**K31**	0,764	7,436	7,275	1,787	0	67,098	213,031	0,501
K7	0,654	11,014	32,955	1,914	0	102,467	149,637	0,659	**K32**	0,812	10,534	11,99	6,024	0,466	66,793	200,516	0,851
K8	0,5	11,407	24,433	6,243	0,804	75,561	137,657	1,201	**K33**	0,947	11,249	10,46	3,346	0,208	116,605	237,565	0,575
K9	0,504	10,642	7,482	2,483	0,502	73,493	152,505	1,128	**K34**	0,817	3,118	1,378	0	0	66,605	216,04	0,178
K10	0,513	12,419	12,66	4,469	1,236	84,424	141,689	1,787	**K35**	0,89	9,107	4,907	2,313	1,55	81,968	198,375	0,927
K11	0,539	11,32	11,706	4,634	0,792	88,246	152,474	1,142	**K36**	0,809	7,494	2,578	1,07	0	51,126	168,38	0,131
K13	0,463	4,174	2,082	0	0	68,836	156,381	0,523	**K37**	0,807	8,631	3,432	1,82	0,294	55,298	165,202	0,173
K14	0,493	4,9	1,955	0	0	70,15	152,387	0,633	**K38**	0,77	11,077	4,12	1,817	0	72,565	191,921	0
K15	0,39	6,468	6,658	0,519	0	55,95	144,122	0,285	**K39**	0,645	12,086	5,45	2,434	0	90,173	217,203	0
K16	0,441	3,734	1,773	0	0	60,627	151,296	0,807	**K40**	0,652	15,34	5,256	1,01	0	99,547	253,461	0
K17	0,404	3,636	1,852	0	0	60,171	146,997	0,51	**K41**	0,906	13,403	3,091	0	0	114,033	196,179	0
K18	0,394	3,029	1,571	0	0	56,549	148,155	0,656	**K42**	0,934	17,646	11,171	1,373	0,144	79,979	209,738	0
K20	0,447	5,713	4,705	2,601	0	44,73	145,194	0,234	**K43**	0,924	22,443	4,537	0,6341	0	89,862	224,802	0
K21	0,49	2,824	1,512	0	0	55,379	152,845	0,625	**K44**	1,021	32,975	6,173	1,33	0	106,572	230,234	0,117
K22	0,5	6,276	3,541	0,616	0	60,472	148,079	0,18	**K45**	1,08	42,536	7,399	1,259	0	122,076	232,321	0,217
K23	0,831	6,412	2,541	1,636	0	91,98	195,955	0,458	**K46**	1,136	68,529	4,922	0,535	0	180,711	254,66	0,516
K24	0,684	1,655	0,417	0	0	53,064	215,854	0,772	**K47**	1,202	44,517	11,738	1,691	0	151,272	251,1	0,472
K25	0,71	0,707	0,59	0	0	75,664	264,569	0,719	**K48**	1,117	40,747	34,55	3,812	0,103	155,83	254,868	0,189
K26	3,074	26,46	5,878	0,981	0,585	47,975	86,477	0									
K27	2,473	42,669	9,207	0,683	2,432	134,979	205,535	0									
K28	0,711	8,51	11,457	0,66	1,221	79,078	238,523	0,553									

RESULTS

The results of the HPI anaysis, applied to the results of chemical studies of the samples collected from the study area, show differences among themselves (**Figure 2**). These differences between locations have been changed according to heavy metal content. The highest value has been determined as 85,833 and the lowest value has been identified as 20,7686. As seen from the **Figure 3**, the locations which show anomalies have been concentrated in two areas. The first one is K5 with highest HPI value in the upper area, first sampling locations. The other one is K8 in lower area. The locations between K1 – K11 are located in first or upper area. This region is effective from the downstream of the dam until the K11 location. The source of anomalies of this region can be defined as dam impact. The locations between K13 – K48 are located in second or lower area. External factors affect this region can be considered as different from the dam's factors.

In this case, new research studies can be done about the source of anomalies. The heavy metal consantration of the first area could not be moved to the second area. It is possible to say that the heavy metals are deposeted; could not move along the stream and could not reach the last locations.

All HPI values of the investigated area were below the HPI values in the study by Nasrabadi (2015). According to this study, there is no risk about heavy metal pollution. According to a similar study on the quality of water (Sirajudeen et al., 2014) K6, K7, K8, K28, K32, K33, K46, K47 have "Poor" quality; K5 and K8 have "Very Poor" quality (**Table 2**). The study area has a single location with “very good” quality, which is named as K26. Other locations can be considered as “good” and without any problems.

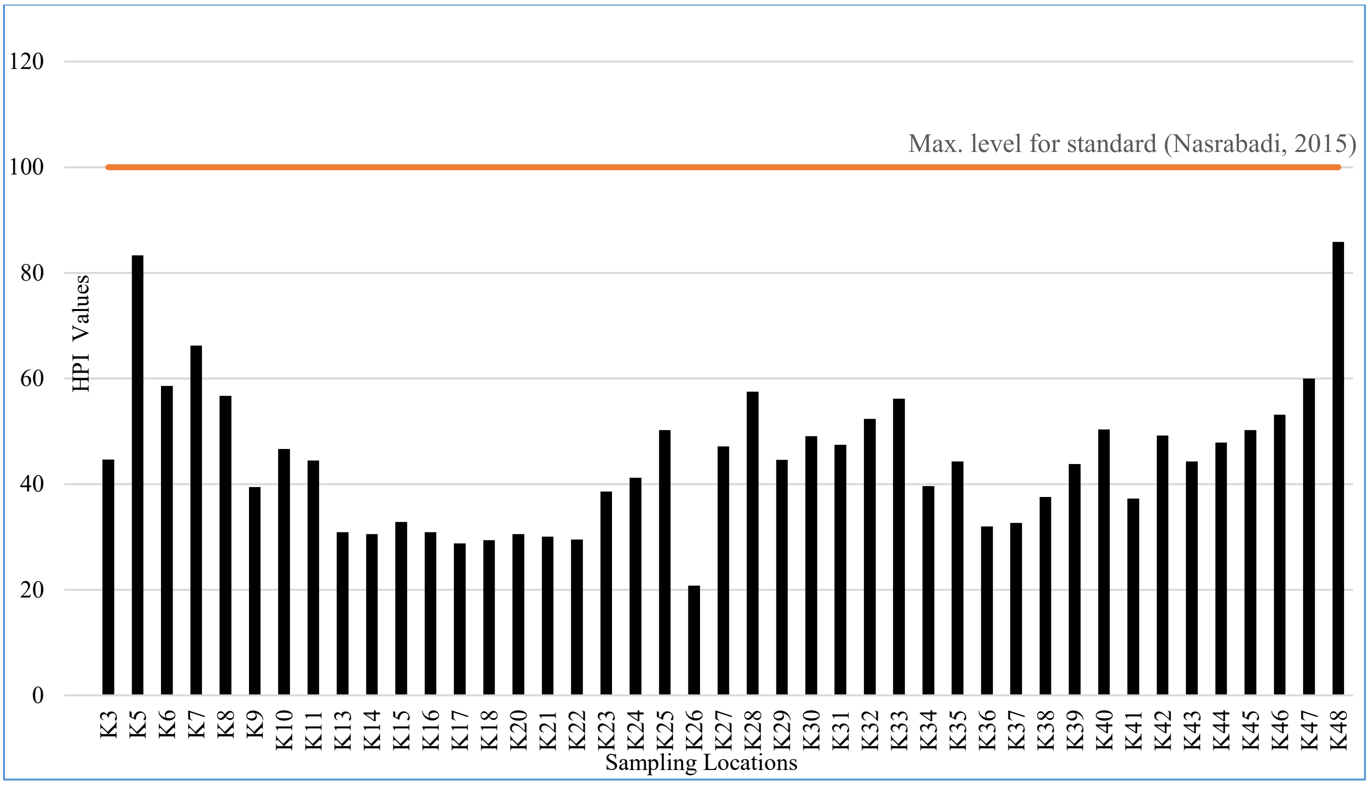

Figure 2. The Values of HPI in Different Locations.

Table 2. Status categories of HPI.

HPI	Quality of water (Sirajudeen et al., 2014)	Stations of study area
0-25	Very good	K26,
26-50	Good	K3, K9, K10, K11, K13, K14, K15, K16, K17, K18, K20, K21, K22, K23, K24, K25, K27, K29, K30, K31, K34, K35, K36, K37,K38, K39, K40, K41, K42, K43, K44, K45
51-75	Poor	K6, K7, K8, K28, K32, K33, K46, K47,
Above 75	Very poor (unsuitable for drinking)	K5,K48

CONCLUSIONS

The maximum anomaly value is 85,833 and it is observed in K48 location. The minimum one is 20,7686 which is measured in K26 location. HPI values of locations generally show two different anomalies in two different regions. HPI values generally show an increasing anomaly in both regions. The highest HPI value in the first region, between K1 and K11, is observed in location K5; and the highest HPI value in the second region, which is between K13 and K48, is K8. The factors that change the HPI value in both regions may be different. While the source of anomalies in first region may be the effects of dam; in second region may be agricultural activities.

The water quality of K6, K7, K8, K28, K32, K33, K46, K47 were determined as “poor”; K5 and K8 as “very poor”. In these locations, it will be useful to avoid using water to avoid heavy metal effects. The water quality in K26 was identified as “very good”; the water quality in the remaining locations were outlined as “good”.

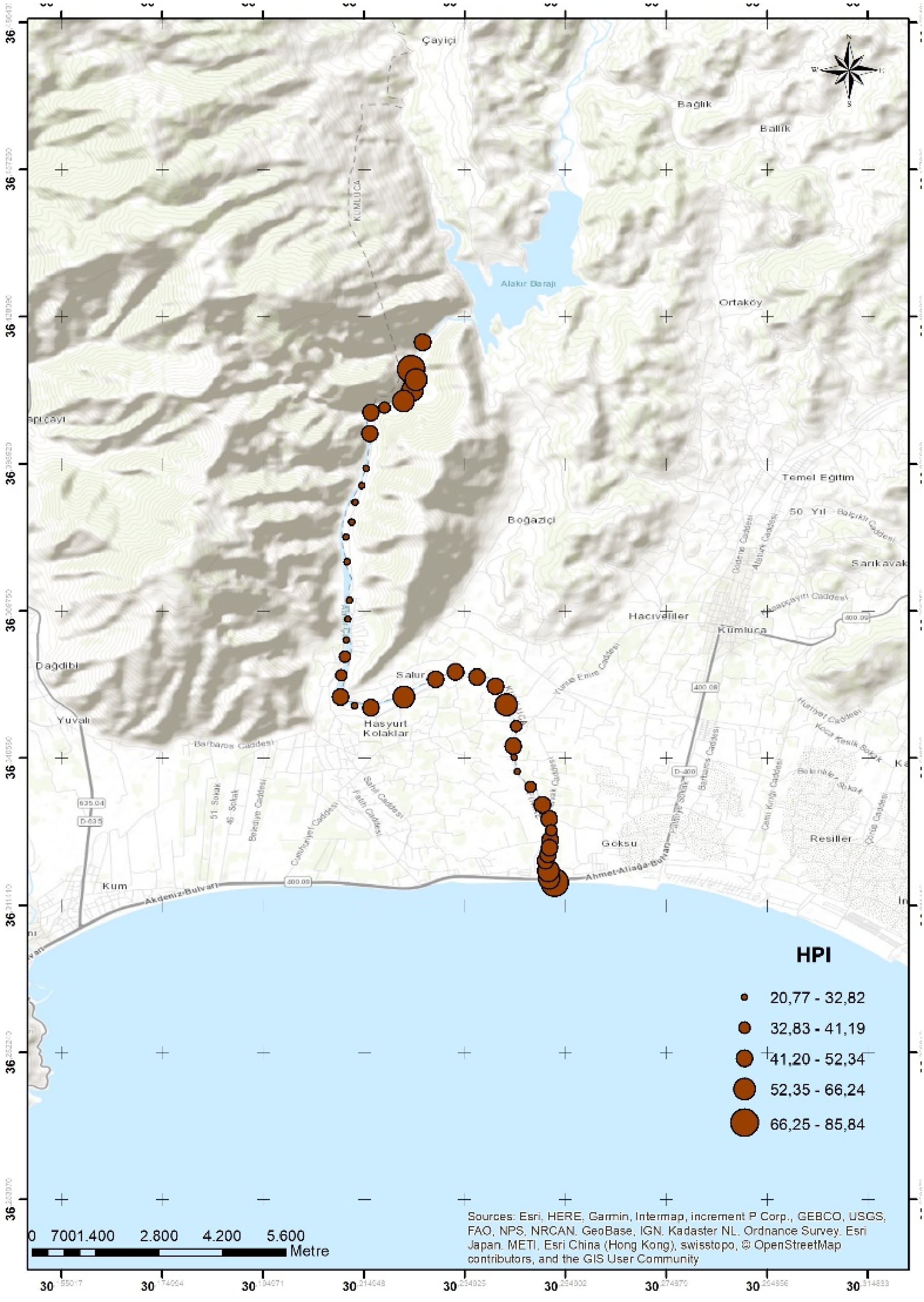

Figure 3. The Distribution of HPI Values.

REFERENCES

ASTM (1985). Standard specification for reagent water. *Annual Book of ASTM Standards* 11(01): D1193-77

Bytyçi, P., Fetoshi, O., Durmishi, B. H., Etemi, F. Z., Çadraku, H., Ismaili, M., & Abazi, A. S. (2018). Status Assessment of Heavy Metals in Water of the Lepenci River Basin, Kosova. *Journal of Ecological Engineering,* 19(5), 19-32.

Brown, R.M., Mc Clelland, N.I., Deininger, R.A., Tozer, R.G. (1970). A water quality index—do we dare? *Water Sewage Works* 117, 339–343 (As noted in Lumb et al.,2011).

CCME, (2001). Canadian water quality guidelines for the protection of aquatic life. CCME water quality index 1.0, *User's Manual 2001* Winnipeg, Manitoba, Canada.

Cengiz MF, Kilic S, Yalcin F, Kilic M , Gurhan Yalcin M. (2017). Evaluation of heavy metal risk potential in Bogacayi River water (Antalya, Turkey). *Environ Monit Assess.*, 189 (6): 248.

Chaturvedi, A., Bhattacharjee, S., Singh, A.K., Kumar, V. (2018). A new approach for indexing groundwater heavy metal pollution. *Ecol. Indic.* 87, 323–331.

Dadolahi-Sohrab, A., Arjomand, F., & Fadaei-Nasab, M. (2012). Water quality index as a simple indicator of watersheds pollution in southwestern part of Iran. *Water and Environment Journal*, 26(4), 445-454.

Dutta, S., Dwivedi, A., & Kumar, M. S. (2018). Use of water quality index and multivariate statistical techniques for the assessment of spatial variations in water quality of a small river. *Environmental monitoring and assessment,* 190(12), 718.

Dunnette, D.A. (1979). A geographically variable water quality index used in Oregon. *J. Water Pollut. Control Fed.* 51, 53–61 (As noted in Lumb et al., 2011).

Edet, A.E., Offiong, O.E. (2002). Evaluation of water quality pollution indices for heavy metal contamination monitoring. A study case from Akpabuyo-Odukpani area, Lower Cross River Basin (southeastern Nigeria). *Geo. J.* 57, 295–304.

El-Tohamy, W. S., Abdel-Baki, S. N., Abdel-Aziz, N. E., & Khidr, A. A. A. (2018). Evaluation of Spatial and Temporal Variations of Surface Water Quality in the Nile River Damietta Branch. *Ecological Chemistry and Engineering* S, 25(4), 569-580.

Fernandez-Luqueno, F., López-Valdez, F., Gamero-Melo, P., Luna-Suárez, S., Aguilera-González, E. N., Martínez, A. I., Pérez-Velázquez, I. R. (2013). Heavy metal pollution in drinking water-a global risk for human health: A review. *African Journal of Environmental Science and Technology*, 7 (7), 567-584.

Horton, R.K. (1965). An index number system for rating water quality. *J. Water Poll. Control Fed.* 37, 300–305.

Islam, M.S., Ahmed, M.K., Raknuzzaman, M., Mamun, M.H.A., Islam, M.K. (2015). Heavy metal pollution in surface water and sediment: a preliminary assessment of an urban river in a developing country. *Ecol. Indic.* 48, 282–291.

Kumar, M., Nagdev, R., Tripathi, R., Singh, V. B., Ranjan, P., Soheb, M., Ramanathan, A.L. (2019). Geospatial and multivariate analysis of trace metals in tubewell water using for drinking purpose in the upper Gangetic basin, India: Heavy metal pollution index, *Groundwater for Sustainable Development*, 8: 122-133.

Leventeli, Y., Yalcin, F., Kilic, M. (2019). An investigation about heavy metal pollution of Duden and Goksu Streams (Antalya, Turkey), *Applied Ecology and Environmental* Research, 17 (2): 2423-2436.

Mohan, S.V., Nithila, P., Reddy, S.J. (1996). Estimation of heavy metals in drinking water and development of heavy metal pollution index. *J. Environ. Sci.* 31 (2), 283–289.

Nasrabadi, T. (2015) An index approach to metallic pollution in river waters. *J. Environ. Res.* 9(1): 385-394.

Sirajudeen, J., Arulmanikandan, S., Manivel, V. (2014). Heavy metal pollution index of groundwater of Fathima Nagar Area near Uyyakondan Channel Tiruchirappalli District, Tamil Nadu, India. *World Journal of Pharmacy and Pharmaceutical Sciences* 4 (1): 967-975.

Rohrbough W.G. (1986). Reagent Chemicals, *American Chemical Society Specifications*, 7th Ed. American Chemical Society, Washington, DC.

Prasad, B., Bose, J. (2001). Evaluation of the heavy metal pollution index for surface and spring water near a limestone mining area of the lower Himalayas. *Environmental Geology*, 41(1-2), 183-188.

Prasanna, M.V., Praveena, S.M., Chidambaram, S. (2012). Evaluation of water quality pollution indices for heavy metal contamination monitoring: a case study from Curtin Lake, Miri City. East Malaysia. *Environ. Earth Sci*. 67, 1987–2001.

Singh, K. R., Dutta, R., Kalamdhad, A. S., & Kumar, B. (2018). Risk characterization and surface water quality assessment of Manas River, Assam (India) with an emphasis on the TOPSIS method of multi-objective decision making. *Environmental Earth Sciences,* 77(23), 780.

Singh, K. R., Dutta, R., Kalamdhad, A. S., & Kumar, B. (2019). An investigation on water quality variability and identification of ideal monitoring locations by using entropy based disorder indices. *Science of The Total Environment*, 647, 1444-1455.

Tiwari, A.K., De Maio, M., Singh, P.K., Mahato, M.K. (2015). Evaluation of surface water qulaity by using GIS and heavy metal pollution index (HPI) model in a coal mining area, India. Bull. *Environ. Contam. Toxicol*. 95, 304–310.

Qu, L., Huang, H., Xia, F., Liu, Y., Dahlgren, R. A., Zhang, M., & Mei, K. (2018). Risk analysis of heavy metal concentration in surface waters across the rural-urban interface of the Wen-Rui Tang River, China. *Environmental pollution*, 237, 639-649.

Wen, X., Lu, J., Wu, J., Lin, Y., & Luo, Y. (2019). Influence of coastal groundwater salinization on the distribution and risks of heavy metals. *Science of The Total Environment*, 652, 267-277.

Yalcin M.G., Ucgun F., Unal B. (2007). Application of an Artificial Intelligence to the Estimation of Water Quality Parameters: Water Quality of Nigde Creek Water, Turkey, *Asian Journal of Chemistry*, 19 (3), 2325-2334

Yalcin M.G., Aydin O., Elhatip H. (2008). Heavy metal contents and the water quality of Karasu Creek in Nigde, Turkey, *Environmental Monitoring and Assessment*, 137, 169–178.

Yalcin F., Ilbeyli N., Aydın O., Yalcin M.G., Leventeli Y., (2017). A Statistical Approach Of Heavy Metal Pollution Index In Creek Surface Water Samples (Nigde, Turkey), *7. International Conference on Medical Geology*, Moskova, Russia, 28 August - 1 September, 82-82.

ORCID

Yasemin LEVENTELI http://orcid.org/0000-0003-3714-4131
Fusun YALCIN http://orcid.org/0000-0002-2669-1044

KSÜ Mühendislik Bilimleri Dergisi, 22, Özel Sayı, 2019 KSU J Eng Sci, 22, Special Issue, 2019
Uluslararası İleri Mühendislik Teknolojileri Sempozyumu (ISADET) Özel Sayısı
International Symposium on Advanced Engineering Technologies (ISADET) Symposium Special Issue
Araştırma Makalesi Research Article

Kahramanmaras Sutcu Imam University
Journal of Engineering Sciences

Geliş Tarihi : 28.08.2019 Received Date : 28.08.2019
Kabul Tarihi : 30.10.2019 Accepted Date : 30.10.2019

LANDFILL LEACHATE TREATMENT USING SEQUENTIAL ANOXIC MOVING BED BIOREACTOR/AEROBIC CONTINUOUS STIRRED TANK REACTOR

ARDIŞIK ANOKSİK HAREKETLİ YATAK BİYOREAKTÖR / AEROBİK SÜREKLİ KARIŞIMLI TANK REAKTÖR KULLANILARAK ÇÖP SIZINTI SULARININ ARTIMI

*Ahmet Duyar[1], Vildan Akgül[2], Serdar Göçer[3], Melike Kozak[3], Gökhan Civelekoğlu[4] and Kevser Cırık[5]**

[1]Department of Environmental Engineering, Suleyman Demirel University, Isparta, Turkey
[2]Department of Bioengineering, Kahramanmaras Sutcu Imam University, Kahramanmaras, Turkey
[3]Department of Environmental Engineering, Cukurova University, Adana, Turkey
[4]Department of Environmental Engineering, Akdeniz University, Antalya, Turkey
[5]Department of Environmental Engineering, Kahramanmaras Sutcu Imam University, Kahramanmaras, Turkey

* Corresponding Author / Sorumlu Yazar: Kevser CIRIK, kcirik@ksu.edu.tr

ABSTRACT

This study was aimed to investigate the performance of sequential anoxic moving bed bioreactor (AnoxMBBR) and aerobic continuous stirred tank reactor (AeCSTR) to remove chemical oxygen demand (COD) and ammonium-nitrogen from landfill leachate. The sequential AnoxMBBR /AeCSTR system was tested at constant hydraulic retention time (HRT) of 48. The performance of this system was evaluated in terms of chemical oxygen demand (COD), ammonium (NH_4^+), nitrite (NO_2^-) and nitrate (NO_3^-) parameters. In AnoxMBBR, nitrate removal (40%) was limited due to low COD removal efficiency. In AeCSTR, COD and ammonium removal efficiencies were obtained as 46% and 71%. Also, partial nitrification in AeCSTR was simultaneously achieved with nitrite accumulation of 1660 mg/L. The results indicated that the AnoxMBBR/AeCSTR system is quite efficient to remove COD and ammonium from landfill leachate, however, the effluent COD and ammonium concentration still did not meet the discharge criteria.

Keywords: continuous stirred tank reactors, denitrification, landfill leachate, nitrification, moving bed bioreactor

ÖZET

Bu çalışmada, çöp sızıntı sularından kimyasal oksijen ihtiyacını(KOİ) ve amonyum-azotu gidermek için ardışık anoksik hareketli yatak biyoreaktörün (AnoxHYBR) ve aerobik sürekli karışımlı tank reaktörün (AeSKTR) performansını araştırmak amaçlandı. Ardışık AnoxMBBR/AeCSTR sistemi, 48'lik sabit hidrolik bekletme süresinde (HRT) test edildi. Bu sistemin performansı, kimyasal oksijen ihtiyacı (KOİ), amonyum (NH_4^+), nitrit (NO_2^-) ve nitrat (NO_3^-)parametreleri açısından değerlendirildi. AnoxHYBR'de, düşük KOİ giderim verimi nedeniyle nitrat giderimi (% 40) sınırlıydı. AeSKTR'de KOİ ve amonyum giderim verimleri sırasıyla % 46 ve% 71 olarak elde edildi. Ayrıca, AeSKTR'de 1660 mg / L nitrit birikimi ile kısmi nitrifikasyon sağlandı. Sonuçlar, AnoxHYBR / AeSKTR sisteminin çöp sızıntı sularından KOİ ve amonyum giderimi için oldukça verimli olduğunu, ancak çıkış KOİ ve amonyum konsantrasyonunun hala deşarj kriterlerini karşılamadığını göstermiştir.

Anahtar Kelimeler: çöp sızıntı suyu, denitrifikasyon, nitrifikasyon, sürekli karışımlı tank reaktör, hareketli yatak bioreaktör

INTRODUCTION

Landfill leachate is usually characterized by high chemical oxygen demand (COD), high ammonia-nitrogen, biological oxygen demand (BOD), BOD_5/COD ratio, heavy metals and strong color (Renou et al., 2008; Luo et al., 2018). Owing to these characterizations, landfill leachate (LFL) are a quite complex wastewater that causes adverse and dangerous effects on aquatic life, soil, sub-soil, groundwater and surface water (Eggen et al., 2010). This wastewater should be treated before directly released into environment, due to the fact that it includes especially a large amount of ammonium and organic matter, which causes eutrophication and dissolved oxygen consumption in natural water (Atmaca, 2009; Wang et al., 2010). Therefore, many researchers used physico-chemical methods and biological methods to remove ammonium-nitrogen and organic matter from LFL (Gkotsis, 2018; Mohajeri et al., 2019). However, the biological treatment is the most cost effective alternative over physico-chemical methods due to its less sludge production and high ammonium/organic matter removal efficiency. Although aerobic, anoxic and anaerobic biological treatment processes are commonly used, these processes alone are insufficient to remove ammonium nitrogen and organic matter from LFL. Therefore, sequential Anoxic/Oxic (A/O) process has been proposed recently and this process was effectively used to treat of the ammonium-nitrogen and organic matter rich wastewater (Zhang et al., 2015; Liu et al., 2018). Especially, this sequential process offers advantages such as saving of added organic carbon for anoxic denitrification and less oxygen consumption for aerobic nitrification. With high COD concentration of leachate, however, microbial population in Anoxic stage of sequential process causes usually inhibition.

The various reactor configurations can be effective on shock loading during operation of A/O systems. Hence, many researchers have been focused on LFL treatment performance of attachment and suspended biological reactor configurations (Chen et al., 2018; Zhang et al., 2018; Xiong et al., 2018; Liu et al., 2017). The CSTR are feasible and eco-friendly technologies in organic carbon and ammonium nitrogen removal. The use of CSTR process to treat LFL can contribute to removal of organic matter and ammonium nitrogen (Ağdağ et al., 2005). Additionally, the MBBR process by using carriers in which microorganism forms biofilm is preferred over other biological reactor configurations due to advantages such as simple construction, low space requirement, low sludge production, high biomass concentration and long sludge residence time (Kawan et al., 2016). In recent years, few researchers have reported that MBBR process is effectively used for nitrification and denitrification of municipal sewage (Malovanyy et al., 2015). However, there are limited studies on LFL treatment using sequential AnoxMBBR-AeCSTR process in literature.

In this context, the main aim of this study was to investigate the effectiveness of sequential anoxic MBBR–aerobic CSTR systems to remove simultaneous organic matter and nitrogen from real LFL.

MATERIAL AND METHODS

Landfill Leachate and Inoculated Sludge

The both bioreactors had already been operated in batch-mode under anoxic and aerobic conditions for more than 80 days. Therefore, the microbial population had already been well acclimated to the heterotrophic denitrification and the aerobic nitrification conditions. Additionally, the mixed liquor suspended solids (MLSS) concentrations of AnoxMBBR and AeCSTR were around 6 g/l and 10 g/L, respectively.

The LFL was monthly taken from landfill site in Kahramanmaras, Turkey. The characteristics of LFL used throughout the study are illustrated in Table 1.

Table 1. Characteristics of the LFL

Parameter	Concentration*
pH	7.98±0.1
COD	10550±350 mg/L
NH_4^+	1620±75 mg/L
NO_3^-	55±5 mg/L
NO_2^-	1±0.1 mg/L

*Values are average of triplicate measurements

Set-up and Operation of Rectors

In this study, the two glass bioreactors (Bioflo 110, New Brunswick Scientific Co, Edison, NJ, USA) with an activate working volume of 5 L were operated as AnoxMBBR and AeCSTR. In anoxic reactor, AnoxKaldnes K1 carrier material was used as biomass carrier with volumetric filling ratio of 40%. The AnoxMBBR was fed with raw LFL and AeCSTR was fed with AnoxMBBR effluent. The influent of the AnoxMBBR was supplemented with about 650 mg/L NO_3^- as the external electron acceptor source of the heterotrophic denitrification process, while organic carbon in LFL was used as electron donor source. The both reactors were mixed via a shaft impeller system. The temperature of AnoxMBBR and AeCSTR were kept at 30±1ºC and 25±2ºC, respectively. In AeCSTR, dissolved oxygen (DO) concentration over 4 mg/L was provided via an air pump (Resun Air Pump LP-60, China). The pH values of AnoxMBBR and AeCSTR were kept at 7.5 and 7.3, respectively. The reactors were continuously operated at hydraulic retention time of 48h. The LFL treatment performance of these reactors was evaluated in terms of COD, NH_4^+, NO_2^- and NO_3^- removal efficiencies.

Analysis

Samples were collected from influent and effluent of the AnoxMBBR as well as effluent of the AeCSTR. Then, samples were immediately centrifuged (Eppendorf, Hamburg, Germany) and filtered using cellulose acetate syringe filters with 0.45µm pore sizes (Sartorius AG, Gottingen, Germany). The COD measurements were carried out according to the dichromate-closed reflux Colorimetric Method described by Standard Methods (Standard Methods, 5220 D). The NH_4^+, NO_2^- and NO_3^- were measured using an ion chromatography (Dionex ICS-3000, Sunnyvale, CA, Japan). The temperature and pH values of both reactors were online measured and recorded in situ daily. In the AeCSTR, DO concentration was measured by a DO meter (Thermo, Orion 4 Star, Indonesia).

RESULTS AND DISCUSSIONS

The COD Removal Performance of AnoxMBBR/AeCSTR

The A/O system has long been used to remove simultaneous nitrogen and COD from municipal and industrial wastewater. It is known that the COD concentration plays an important role in A/O system, which directly affects the reaction rate of denitrification and nitrification. In this part of the study, the continuous AnoxMBBR/AeCSTR system performance was evaluated in terms of COD removal at HRT of 48h. The variations of COD concentrations in this system are presented in Figure 1. The influent COD concentration throughout this study was average 10550±350 mg/L. The COD removal efficiency of both reactors was quite stable. The COD removal was relatively low at AnoxMBBR, corresponding to around 20% removal efficiency and about 8400 mg COD/L effluent concentration.

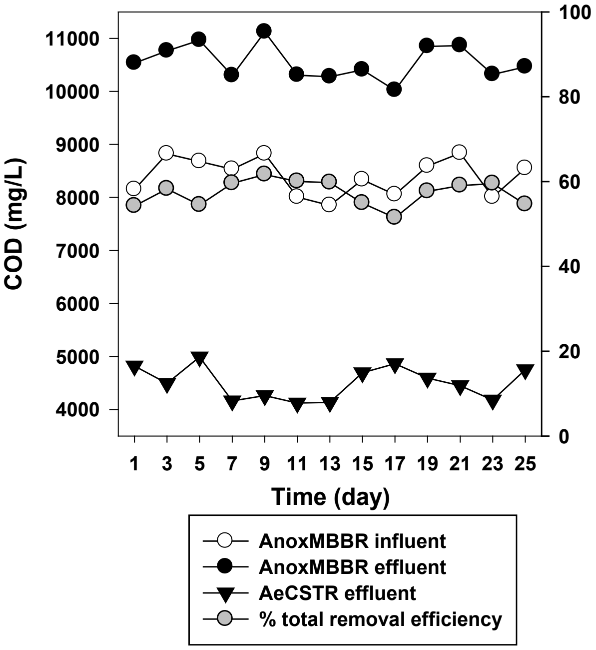

Figure 1. COD Removal Performance of Sequantial AnoxMBBR/AeCSTR

The low COD removal efficiency in AnoxMBBR was due to very high influent COD concentration which caused inhibitions on microbial activities of heterotrophic denitrification (Liang et al., 2015). However, the COD concentration under aerobic conditions decreased sharply and reached 4500 mg/L in the AeCSTR. The increase of COD removal efficiency in AeCSTR can be explained with increasing of microbial activity. Additionally, total COD removal efficiency of this system was about 58 %. Liu et al., (2017), investigated the performance of the two-stage A/O combined membrane bioreactor to remove simultaneous COD and nitrogen from LFL. Similar to our results, they reported that the microorganism in Anoxic zone of first stage A/O showed low COD removal performance while the microbial activity increased in aerobic zone.

The Nitrogen removal performance of AnoxMBBR/AeCSTR

Heterotrophic denitrification process is occurred by reduction-oxidation reactions from nitrate to nitrogen gas via microorganisms under anoxic conditions. The nitrate and organic matter in this process used as electron acceptor and electron donor, respectively. In this study, the influent nitrate concentration was kept constant at 650 mg/L. The denitrification performance of AnoxMBBR during landfill leachate treatment was evaluated in terms of nitrate removal (Figure 2). Similar to COD removal efficiency, the NO_3^- removal was quite stable and nitrate removal efficiency observed as about 40%, corresponding to effluent nitrate concentration of about 390 mg/L. It seems that the nitrate removal rate depends on COD removal performance. The nitrite accumulation was not also observed in the effluent of AnoxMBBR (Figure 2). Additionally, the ammonium removal during anoxic operation can be negligible at ammonium concentration of 55 mg/L, which was probably used for microbial growth

The ammonium conversion under aerobic conditions is carried out in two steps which oxidized to nitrite by ammonium oxidizing bacteria and nitrate by nitrite oxidizing bacteria, respectively, as shown in the following reactions (Eqs. 1-2). The partial nitrification consists of AOB enrichment and NOB washout while complete nitrification consists of NOB enrichment.

$$\mathrm{NH_4^+ + 1{,}5O_2 \xrightarrow{AOB} NO_2^- + 2H^+ + 2H_2O} \tag{1}$$

$$\mathrm{NO_2^- + 0{,}5O_2 \xrightarrow{NOB} NO_3^-} \tag{2}$$

The performance of AeCSTR during landfill leachate treatment using AnoxMBBR/AeCSTR was evaluated in terms of the comple/partial nitrification. AeCSTR was operated at HRT of 48 h and DO concentration over 4mg/L.

Figure 3 shows the ammonium conversion performance of the AeCSTR. The influent NH_4^+ concentration was about 1620±75 mg/L throughout AeCSTR operation.

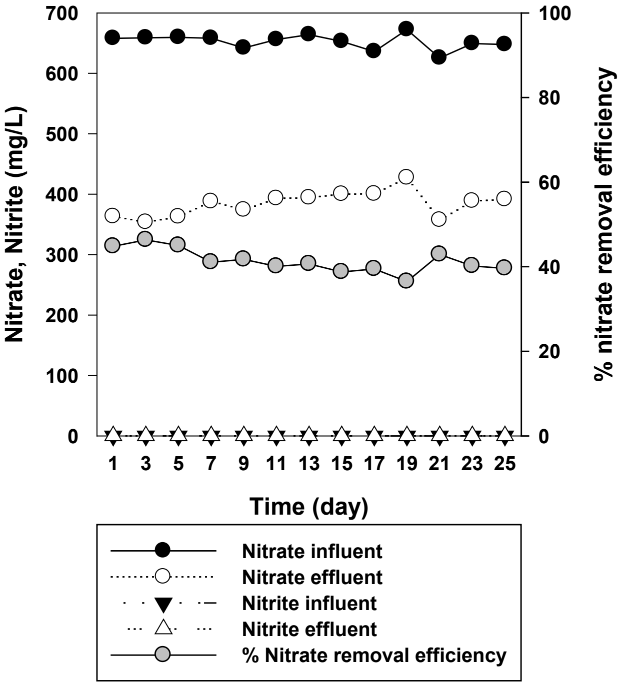

Figure 2. The Nitrate and Nitrite Removal Performance of AnoxMBBR

The NH_4^+ concentrations decreased sharply in AeCSTR, corresponding to 71.5% removal efficiency. Additionally, effluent NH_4^+ concentrations were approximately 463 mg/L. The nitrite accumulation under aerobic conditions was clearly observed and effluent nitrite and nitrate concentrations were 1580 mg/L NO2- and 350 mg/L NO3-, respectively. This indicated that partial nitrification carried out in the reactor. This result was similar that of previous study (Fitzgerald et al., 2015), in which the AOB population during high NH_4^+ oxidation was found to dominant.

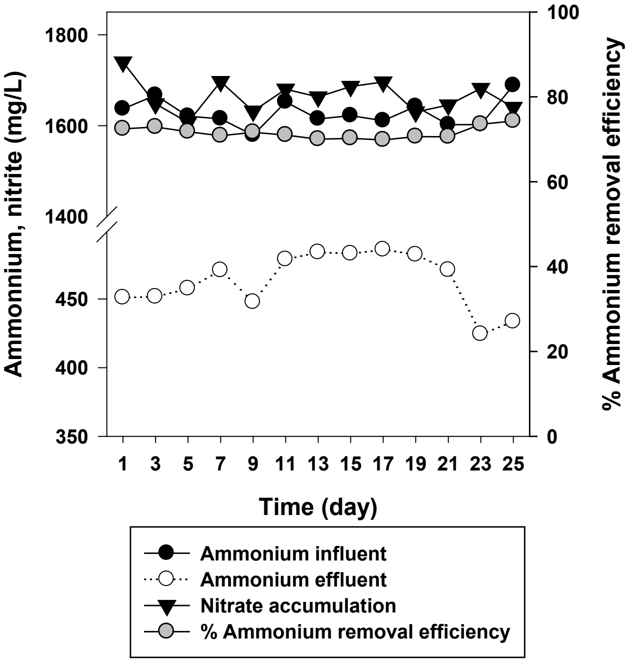

Figure 3. The Ammonium Removal and Nitrite Accumulation Performance of AeCSTR

CONCLUSION

The following conclusions from this study can be drawn:

- The denitrification efficiency of raw LFL in the AnoxMBBR were ineffective due to high COD concentration in influent wastewater
- In AeCSTR, the partial nitrification was observed at HRT of 48-h.
- The AnoxMBBR/AeCSTR system 57% and 74% COD and ammonium removal efficiencies were obtained, respectively.
- This study demonstrates that the AnoxMBBR/AeCSTR system is in favor of LFL treatment.
- However, this study demonstrates that this system still remained insufficient to meet discharge standards and integrated systems are required.

REFERANCES

Ağdağ, O. N., & Sponza, D. T. (2005). Anaerobic/aerobic treatment of municipal landfill leachate in sequential two-stage up-flow anaerobic sludge blanket reactor (UASB)/completely stirred tank reactor (CSTR) systems. *Process Biochemistry*, *40*(2), 895-902.

Atmaca, E. (2009). Treatment of landfill leachate by using electro-Fenton method. *Journal of Hazardous Materials*, *163*(1), 109-114.

Chen, Z., Wang, X., Yang, Y., Mirino Jr, M. W., & Yuan, Y. (2016). Partial nitrification and denitrification of mature landfill leachate using a pilot-scale continuous activated sludge process at low dissolved oxygen. *Bioresource technology*, *218*, 580-588.

Eggen, T., Moeder, M., & Arukwe, A. (2010). Municipal landfill leachates: a significant source for new and emerging pollutants. *Science of the Total Environment*, *408*(21), 5147-5157.

Fitzgerald, C. M., Camejo, P., Oshlag, J. Z., & Noguera, D. R. (2015). Ammonia-oxidizing microbial communities in reactors with efficient nitrification at low-dissolved oxygen. *Water research*, *70*, 38-51.

Gkotsis, P., Tsilogeorgis, J., & Zouboulis, A. (2018). Hydraulic performance and fouling characteristics of a membrane sequencing batch reactor (MSBR) for landfill leachate treatment under various operating conditions. *Environmental Science and Pollution Research*, *25*(13), 12274-12283.

Kawan, J. A., Hasan, H. A., Suja, F., JAAFAR, O. B., & Abd-Rahman, R. (2016). A review on sewage treatment and polishing using moving bed bioreactor (MBBR). *Journal of Engineering Science and Technology*, *11*(8), 1098-1120.

Liang, Y., Li, D., Zhang, X., Zeng, H., Yang, Z., Cui, S., & Zhang, J. (2015). Stability and nitrite-oxidizing bacteria community structure in different high-rate CANON reactors. *Bioresource technology*, *175*, 189-194.

Liu, J., Zhang, H., Zhang, P., Wu, Y., Gou, X., Song, Y., ... & Zeng, G. (2017). Two-stage anoxic/oxic combined membrane bioreactor system for landfill leachate treatment: pollutant removal performances and microbial community. *Bioresource technology*, *243*, 738-746.

Liu, J., Zhang, P., Li, H., Tian, Y., Wang, S., Song, Y., ... & Tian, Z. (2018). Denitrification of landfill leachate under different hydraulic retention time in a two-stage anoxic/oxic combined membrane bioreactor process: Performances and bacterial community. *Bioresource technology*, *250*, 110-116.

Luo, K., Pang, Y., Li, X., Chen, F., Liao, X., Lei, M., & Song, Y. (2018). Landfill leachate treatment by coagulation/flocculation combined with microelectrolysis-Fenton processes. *Environmental technology*, 1-9.

Malovanyy, A., Yang, J., Trela, J., & Plaza, E. (2015). Combination of upflow anaerobic sludge blanket (UASB) reactor and partial nitritation/anammox moving bed biofilm reactor (MBBR) for municipal wastewater treatment. *Bioresource technology*, *180*, 144-153.

Mohajeri, S., Hamidi, A. A., Isa, M. H., & Zahed, M. A. (2019). Landfill Leachate Treatment through electro-Fenton oxidation. *Pollution*, *5*(1), 199-209.

Renou, S., Givaudan, J. G., Poulain, S., Dirassouyan, F., & Moulin, P. (2008). Landfill leachate treatment: review and opportunity. *Journal of hazardous materials*, *150*(3), 468-493.

Wang, C. C., Lee, P. H., Kumar, M., Huang, Y. T., Sung, S., & Lin, J. G. (2010). Simultaneous partial nitrification, anaerobic ammonium oxidation and denitrification (SNAD) in a full-scale landfill-leachate treatment plant. *Journal of hazardous materials*, *175*(1-3), 622-628.

Xiong, J., Zheng, Z., Yang, X., He, J., Luo, X., & Gao, B. (2018). Mature landfill leachate treatment by the MBBR inoculated with biocarriers from a municipal wastewater treatment plant. *Process Safety and Environmental Protection*, *119*, 304-310.

Zhang, G., Jiao, Y., & Lee, D. J. (2015). A lab-scale anoxic/oxic-bioelectrochemical reactor for leachate treatments. *Bioresource technology*, *186*, 97-105.

ORCID

Ahmet Duyar *https://orcid.org/0000-0001-8850-8308*
Vildan Akgül *http://orcid.org/0000-0001-5507-2886*
Serdar Göçer *https://orcid.org/0000-0003-0443-8045*
Melike Kozak *https://orcid.org/0000-0001-6985-3587*
Gökhan Civelekoğlu *https://orcid.org/0000-0001-5508-1918*
Kevser Cırık *https://orcid.org/0000-0002-1756-553X*

KSÜ Mühendislik Bilimleri Dergisi, 22, Özel Sayı, 2019 KSU J Eng Sci, 22, Special Issue, 2019
Uluslararası İleri Mühendislik Teknolojileri Sempozyumu (ISADET) Özel Sayısı
International Symposium on Advanced Engineering Technologies (ISADET) Symposium Special Issue
Araştırma Makalesi Research Article

Kahramanmaras Sutcu Imam University
Journal of Engineering Sciences

Geliş Tarihi : 16.09.2019 Received Date : 16.09.2019
Kabul Tarihi : 30.10.2019 Accepted Date : 30.10.2019

FARKLI BOYUTLARDA KİNOA KEPEK UNU KULLANIMININ KEKLERİN FİZİKSEL, DUYUSAL VE TEKSTÜREL ÖZELLİKLERİ ÜZERİNE ETKİSİ

THE EFFECT OF DIFFERENT SIZED QUINOA BRAN FLOUR USAGE ON THE PHYSICAL, SENSORY AND TEXTURAL PROPERTIES OF CAKES

Hamza ALAŞALVAR [1], *Hakan ERİNÇ* [1], *Abdullah Sinan ÇOLAKOĞLU* [2]

[1]Niğde Ömer Halisdemir Üniversitesi, Mühendislik Fakültesi, Gıda Mühendisliği Bölümü, Niğde, Türkiye
[2] Kahramanmaraş Sütçü İmam Üniversitesi, Elektrik Elektronik Mühendisliği Bölümü, Kahramanmaraş, Türkiye

*Sorumlu Yazar / Corresponding Author: Abdullah Sinan ÇOLAKOĞLU, ascolakoglu@ksu.edu.tr

ÖZET

Tahıl ürünlerinin işlenmesinde sonra kepek kısmı genellikle atık olarak kalmaktadır. Ancak son yıllardaki çalışmalar bu atıkların katma değerli ürünler olduğunu göstermiştir. Bu çalışmada farklı boyutlarda kinoa kepek unu kullanımının keklerin fizikokimyasal, tekstürel ve duyusal özellikleri üzerine etkilerinin incelenmesi amaçlanmıştır. Bu amaçla, farklı boyutlarda kinoa kepek unları değirmende öğütülmüş ve 5 farklı boyutta buğday unundan yapılmış keklere %25 oranında katılmıştır. Elde edilen sonuçlara göre kinoa kepek ununun boyutları küçüldükçe örneklerin kuru madde oranı artış göstermiştir. Yine kepek unu boyutlarının küçülmesi ile kek iç ve dış parlaklık değerlerinde azalma gözlenmiştir. Keklerin tekstür ve duyusal özelliklerinde kinoa katılımı sonucun düşüş belirlenmiştir ve bu olumsuzluk kepek boyutu küçüldükçe daha fazla olmuştur. Bu çalışma kinoa kepek ununun farklı boyutları ile zenginleştirilen keklerin özelliklerinde meydana gelen değişimleri ortaya koymuştur.

Anahtar Kelimeler: kinoa, kek, tekstür profile analizi, zenginleştirme

ABSTRACT

After the processing of cereal products, the bran part is commonly considered as waste. However, recent studies have shown that this waste can be processed into value-added products. The aim of this study was to investigate the effects of quinoa bran flour with different particle sizes on physicochemical, textural and sensory properties of cakes. For this purpose, quinoa bran flours were milled to 5 different particle sizes and added to the wheat flour cakes at a constant level (25% of wheat flour). According to the results, the dry matter contents of the samples increased as the particle size of the quinoa bran flour decreased. Similarly, a decrease in the crumb and crust color values of the cake was observed depending on the bran particle size. The textural and sensory characteristics of cake samples were decreased. This study reveals the changes in the properties of cakes enriched with different sized quinoa bran flour.

Keywords: quinoa, cake, texture profile analysis, enrichment

GİRİŞ

Güney Amerika'ya özgü bir bitki olan kinoa, çevresel faktörlere karşı göstermiş olduğu dirençten dolayı farklı iklimsel koşullara kolaylıkla uyum sağlayabilmektedir (Ruiz *et al*., 2014). Bu özelliği ile kinoa diğer tahıl çeşitlerine kıyasla farklı coğrafyalarda iyi bir alternatif olarak düşünülmektedir (Algosaibi, Badran, Almadini, & El-Garawany, 2017). Farklı şekil, büyüklük, renk ve tane kompozisyonuna sahip kinoa çeşitleri bulunmakta ve kinoa türlerinin sınıflandırılmasında genellikle beyazdan siyaha değişen renk karakteristiklerinden yararlanılmaktadır. Kinoa türlerinin renklerindeki bu farklılık kinoa yapısında yer alan betalainlere atfedilmektedir (Escribano *ve ark.,* 2017).

Besinsel değeri açısından kinoa, esansiyel aminoasitler ve yağ asitlerince zengin bir bitkidir. Özellikle, yüksek miktarda lizin amino asidi içermesi bakımından diğer tahıl çeşitlerinden ayrılmaktadır. Besinsel özelliklerine ilaveten fenolik bileşikler, mineraller, vitaminler ve diyet lifleri gibi sağlık üzerine olumlu etkileri olan maddeleri yapısında bulundurması ile insan sağlığını koruyucu ve artırıcı özelliklere sahiptir (Navruz-Varli ve Sanlier, 2016). Ayrıca, gluten içermediği için karabuğday ve amarant gibi tahıl benzeri gruba dahil edilmektedir. Bu özelliğinden dolayı, glutensiz diyetlerde rahatlıkla kullanılabilmektedir (Alvarez-Jubete *ve ark.,* 2009; Paśko et al., 2009). Son yıllarda, tahılların sebep olduğu alerjik risklere sahip bireyler ile vegan ve vejeteryanların diyetlerinde oldukça tercih edilen yeni bir besinsel ürün haline gelmiştir (Paśko *ve ark.,* 2009).

Kinoa unu makarna, kek, kurabiye ve ekmek gibi tahıl ürünlerinin üretiminde kullanılmıştır (Lorenz ve Coulter, 1991; Caperuto, Amaya-Farfan and Camargo, 2001). Ancak kinoa kepeğinin tahıl ürünlerinde kullanımı ile ilgili sınırlı sayıda çalışma bulunmaktadır (Föste *ve ark.,* 2014). Tahıllardan elde edilen kepekler gıda ürünlerine eklendiğinde besinsel değerini ve biyoaktif özelliklerini geliştirmektedir, Ancak tekstürel açıdan bazı sorunlar meydana gelebilmektedir. Bu sebeple tahıl ürünleri üretiminde kepek kullanımı kısmi olarak gerçekleştirilmesi önerilmektedir.

Kinoa kepeği ekmek, kek ve bebek gıdaları gibi ürünlerin üretimi için kullanılmıştır (Föste et al., 2014). Yüksek kalsiyum, demir, çinko ve magnezyum içeriğinden dolayı, kinoa kepeği farklı hedef popülasyonlar için yüksek besin değeri taşımaktadır (Alvarez-Jubete *ve ark.,* 2009). Özellikle yetişkinler ve çocukların kemik gelişimi için kalsiyum ve kan fonksiyonları için demir ihtiyacı karşılanabilmektedir. Kinoa kepeği, perikarp ve/veya tohum katmanı ve embriyo içeren dış hücreli dokulardan oluşmakta ve kinoa tohumunun yaklaşık %40'ını temsil etmektedir (Kozioł, 1992).

Bu çalışmada, farklı boyutlarda kinoa kepeğinin kek formülasyonlarında kullanılarak ürünlerin fiziksel ve tekstürel özellikleri üzerine etkilerini incelemek amaçlanmıştır. Farklı boyutlarda kinoa kepeği unu ilavesinin kekler üzerinde meydana getirdiği değişimler kontrol örneği ile karşılaştırılarak incelenmiştir.

MATERYAL VE METOT

Materyaller

Kinoa kepeği, Niğde Ömer Halisdemir Üniversitesi, Tarım Bilimleri Fakültesi tarafından Niğde'de yetiştirilmekte olan kinoalardan temin edilmiştir. Hasat edilen kinoalar ön işlemlerden geçirildikten sonra kinoa kepeği elde edilmiş ve daha sonra çeşitli boyutlara öğütülüp kek formülasyonlarında buğday unu yerine sabit oranda ve farklı boyutlarda kullanılmıştır. Kek üretiminde kullanılan un, su, tuz, şeker, yağ, süt tozu, yumurta akı, vanilya ve kabartma tozu Niğde ilindeki yerel marketlerden satın alınmıştır.

Metotlar

Farklı boyutlarda kinoa kepek unlarının üretimi

Bu çalışmada kinoa kepeğinin öğütülme işlemleri 0-500 dev/dk hız aralığında çalışabilen Standart–01 model dikey pinli karıştırmalı değirmende (Union Process, USA) gerçekleştirilmiştir. Öğütme haznesi (0,75 L) seramikten yapılmış olup ürünün ısınmaması için su ceketi ile donatılmıştır. Öğütme işlemin de 4 mm çaplı yoğunluğu 3,6 g/cm^3 olan alümina bilyeler kullanılmıştır. Kinoa kepeği karıştırmalı-bilyeli değirmende öğütüldükten sonra, eleme işlemine tabi tutulmuştur. Bu işlem sırasında 1,18 mm; 0,850 mm; 0,300 mm; 0,212 mm; 0,150 mm; 0,106 mm ve 0,075 mm'lik elekler (İngiliz BS 410) kullanılmış olup sarsıntılı elek makinası (Endecotts-Octagon 200) yardımıyla farklı boyutlarda kinoa kepekleri elde edilmiştir. Eleme süresi 3 dak ile sabit tutulmuştur.

Kek formülasyonlarının üretimi ve pişirilmesi

Kek üretiminde, yumurta ve şeker karıştırma kabına konularak 5 dak çırpılmıştır. Kinoa kepek unu, su, tuz, şeker, yağ, süt tozu, yumurta akı, vanilya, kabartma tozu karıştırma kabına ilave edilerek homojen bir görünüm elde edilene kadar karıştırma işlemine devam edilmiştir. Kek formülasyonlarında kinoa kepek unu miktarı %25 olarak sabit tutulmuştur. Kek formülasyonları Tablo 1'de verilmiştir. Elde edilen kek hamurları 250 g olacak şekilde yağlanmış kek kalıbına konulup 175°C'de 15 dak pişirilmiştir. 300-420, 212-300, 150-212, 106-150 ve 75-106 µm boyutlarında kinoa kepek unu ilave edilen kek formülasyonları sırasıyla Kek 1, 2, 3, 4 ve 5 olarak adlandırılmıştır.

Tablo 1. Farklı boyutlarda kinoa kepek unları ile üretilen keklerin formülasyonları

Girdiler	**Kontrol**	**1. Kek**	**2. Kek**	**3. Kek**	**4. Kek**	**5. Kek**
Un(g)	100	75	75	75	75	75
Kinoa kepeği (g)	-	25	25	25	25	25
Kepek boyutları (µ)	-	850-1180	212-300	150-212	106-150	75-106
Şeker (g)	57	57	57	57	57	57
Yağ (g)	50	50	50	50	50	50
Süt tozu (g)	12	12	12	12	12	12
Yumurta (g)	50	50	50	50	50	50
Kabartma tozu (g)	6	6	6	6	6	6
Tuz (g)	1.5	1.5	1.5	1.5	1.5	1.5
Vanilya (g)	1.5	1.5	1.5	1.5	1.5	1.5
Su (g)	37	37	37	37	37	37

Kuru madde analizi

Kek örneklerinin kuru madde miktarları etüvde 105°C sıcaklıkta örnekler sabit tartıma gelene kadar kurutulması ile gerçekleştirilmiştir.

Renk analizi

Kek örneklerinin iç ve dış renk değerleri (L, a ve b) üzerine farklı boyutlarda kinoa kepek unu ilavesinin etkisi renk ölçüm cihazı (Konica Minolta, Japonya) kullanılarak belirlenmiştir.

Tekstür Profil Analizi

Kek örneklerinin tekstür profil analizi (TPA) analizi, tekstür analiz cihazına bağlanan baskı plakası altında, homojen gıda örneğinin arka arkaya iki kez sıkıştırılması ile gerçekleştirilmiş ve elde edilen verilerden gıdanın tekstürel özelliği hakkında bilgi veren sertlik, kırılganlık, kohezyon, yapışkanlık ve esneklik gibi birincil parametreler elde edilmiştir. Birincil parametreler kullanılarak da sakızımsılık ve çiğnenebilirlik gibi ikincil parametreler hesaplanmaktadır. Kek örneklerinin tekstürel özelliklerinin belirlenmesinde TA-XT2i Texture Analyzer (Stable Mikro Systems Ltd, İngiltere) cihazı kullanılmıştır. Örneklerin TPA' inde P/35 probu kullanılmıştır.

Duyusal Analiz

Kek örneklerinin duyusal değerlendirmesi Niğde Ömer Halisdemir Üniversitesi Gıda Mühendisliği öğretim elemanları ve öğrencilerinden oluşan 16 kişilik panelist grubu tarafından gerçekleştirilmiştir. Analize başlamadan önce panelistlere örnekler hakkında bilgi verilmiştir. Panelistler kek örneklerini renk, tat, ağızda dağılabilirlik, koku, yumuşaklık ve genel kabul edilebilirlik özelliklerine göre 5 puan üzerinden değerlendirmiştir. Örnekler arasında panelistlere su verilerek bir önceki örneğin etkisini ağızlarından kaldırmaları sağlanmıştır.

İstatistiksel Analiz

Elde edilen analiz sonuçlarının istatistiksel değerlendirilmesinde IBM SPSS Statistic 22 programı kullanılmıştır. Sonuçlar üzerine farklı boyutlarda kinoa kepek unu ilavesinin etkisi varyans analizi (One-way ANOVA) ile tespit edilmiş ve Tukey testi ile grup ortalamaları arasındaki farklılıklar %95 güven aralığında belirlenmiştir.

SONUÇLAR VE TARTIŞMA

Bütün kek örnekleri aynı sıcaklık ve süre kullanılarak pişirilmiş olmasına rağmen Kek 5 örneğinde yanma olduğu gözlemlenmiştir. Tekrarlı pişirme işlemleri sonucunda bu durumun kesinliği belirlenmiştir. 75-106 µm aralığında kinoa kepek unu kullanımının keklerin pişme özelliğini olumsuz etkilediği sonucu çıkarılmıştır. Bu sebeple analizlerde Kek 5 örneğine yer verilmemiştir.

Kuru madde

Kek örneklerinin kuru madde analizi sonucu elde edilen veriler Şekil 1' de verilmiştir. Kuru madde analiz sonuçlarına göre kek örneklerine ilave edilen kinoa kepek ununun boyutlarının azalması ile örneklerin kuru madde içeriğinde istatistiksel olarak önemli bir artış meydana gelmiştir ($P<0.05$). İstatistiksel değerlendirme sonucunda en büyük boyutlu kinoa kepek unu içeren Kek 1 formülasyonu kontrol örneği ile aynı kuru madde özelliklerini göstermiştir. Caperuto *ve ark.* (2001), yaptıkları glütensiz spagetti tipi makarnada, kinoa unu eklenmesinin pişirme suyuna geçen kuru madde kaybında azalmaya ve ağırlığında ise artışa neden olduğunu bildirmişlerdir.

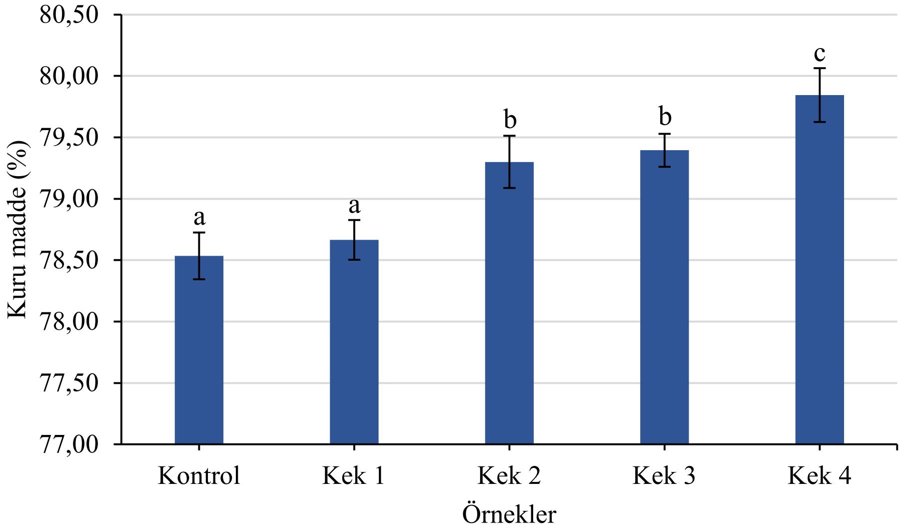

Şekil 1. Kek örneklerinin kuru madde miktarları

Renk Analizi

Gıdaların renk özellikleri gıda tüketilmeden önce tüketici beğenisini etkileyen ve gıda kalitesi hakkında bilgi veren önemli bir parametredir (Biernacka *ve ark.,* 2017). Kek örneklerinin iç ve dış renk özellikleri üzerine kinoa kepek ununun farklı boyutlarının etkisi Tablo 2'de gösterilmiştir. Kinoa kepek ununun boyutlarının azalması ile kek örneklerinin iç L değerlerinde istatistiksel olarak önemli bir azalma gözlenirken, a ve b değerlerinde artış gözlenmiştir ($P<0,05$). Ancak bu artışlar, L değeri için 106-150µ, a ve b değerleri için 212-300µ partikül boyutlarından sonra değişmemiştir ($P>0,05$). Kek dış rengi incelendiğinde, kontrol örneği en parlak (L) ve sarımsı (a), Kek 4 örneği ise en koyu ve daha açık sarı rengi göstermiştir. Alvarez-Jubete *ve ark.* (2010), kinoa ve diğer yalancı tahılların ekmeklerin kabuk renginde önemli derecelerde koyulaşmaya (düşük L değeri) neden olduğunu bildirmişlerdir. Keklere kinoa kepeği katılması kırmızı renk (b) değerlerinde değişime neden olmamıştır (P>0,05). Gerçekaslan ve Hüseyin (2018) tarafından yapılan çalışmada kek örneklerine kakao ikamesi olarak keçiboynuzu unu ilavesi gerçekleştirilmiş ve formülasyonlarda keçiboynuzu unu miktarının artması ile renkte açılma meydana geldiği belirlenmiştir. Bir başka çalışmada ise, farklı oranlarda chia tohumu ilave edilerek keklerin üretimi gerçekleştirilmiş ve keklerin iç ve dış parlaklık değerinde herhangi bir değişim gözlenmemiştir (Özgören *ve ark.,* 2018). Yine aynı çalışmada örneklerin iç a ve b değerlerinin azaldığı ancak dış a ve b değerlerinin değişmediği not edilmiştir. Bu çalışmadan elde edilen veriler ve literatür sonuçları göstermektedir ki zenginleştirme amacıyla keklere ilave edilen materyallerin renk özellikleri, zenginleştirme amacıyla kullanıldığı gıdanın da renk özelliklerini etkilemektedir.

Tablo 2. Keklerin iç ve dış renkleri üzerine farklı boyutlarda kinoa kepek ununun etkisi.

	İç renk			**Dış renk**		
Örnekler	**L**	**a**	**b**	**L**	**a**	**b**
Kontrol	76,63±0,73^{d}	-2,38±0,07^{a}	21,96±0,15^{a}	38,45±3,37^{b}	14,05±0,92^{b}	20,87±3,50^{ab}
Kek 1	65,47±1,00^{c}	1,97±0,34^{b}	24,43±1,25^{b}	34,99±2,70^{ab}	12,07±0,94^{ab}	15,80±0,90^{a}
Kek 2	59,36±1,04^{b}	4,96±0,11^{c}	32,93±0,50^{c}	35,28±2,12^{ab}	11,34±1,99^{a}	16,39±3,36^{a}
Kek 3	56,62±1,34^{a}	5,19±0,11^{c}	33,01±0,53^{c}	34,40±1,20^{ab}	11,43±0,44^{a}	16,32±0,37^{a}
Kek 4	56,23±0,73^{a}	5,14±0,21^{c}	33,43±0,24^{c}	33,36±2,30^{a}	10,55±1,62^{a}	15,44±1,15^{a}

Tekstür Profil Analizi

Kek örneklerine ait tekstür profil analizi sonuçları Tablo 3'de verilmiştir. Kontrol örneği ile kıyaslandığında kek örneklerinin sertliğinin kinoa unu boyutlarına bağlı olarak %3,5-30,4 oranında artığı tespit edilmiştir (P<0,05). Farklı boyutlarda armut posası kullanılarak üretilen kekler üzerine yapılan bir çalışmada, partikül boyutunun azalması ile keklerin sertliğinde artış olduğu rapor edilmiştir (Rocha-Parra *ve ark.,* 2019). Keklerin dış yapışkanlık (adhesiflik), iç yapışkanlık (kohesiflik), ipliksilik ve elastikiyet değerleri, kinoa kepeği katılımı sonucunda azalma göstermiş, ancak bu azalma kepek partikül boyutuna göre istatistiksel olarak değişiklik göstermemiştir (P>0,05). Kek 1, 2 ve 3 arasında ise bir fark olmadığı belirlenmiştir. Kek örneklerinin esneklik değerleri 0.20-028 aralığında değişmiştir. En düşük elastikiyet Kek 2 örneğinde, en yüksek ise kontrol örneğinde belirlenmiştir. Kinoa kepek katımı keklerin çiğnenebilirliğinde düşüşe neden olmuş (P<0,05), ancak, en düşük partikül boyutuna sahip Kek 4 ile kontrol örnekleri arasında farklılık istatistiksel olarak önemsiz bulunmuştur (P>0,05).

Tablo 3. Kek örneklerinin tekstür profil analizi sonuçları

	Tekstürel Özellikler					
Örnekler	**Sertlik**	**Dış yapışkanlık**	**İç Yapışkanlık**	**İpliksilik**	**Elastikiyet**	**Çiğnenebilirlik**
Kontrol	23376,03±1152,52^{a}	-2,76±0,84^{b}	0,63±0,02^{b}	0,87±0,02^{b}	0,28±0,02^{b}	12925,04±1171,72^{b}
Kek 1	24234,17±477,82^{ab}	-4,89±0,48^{a}	0,53±0,01^{a}	0,73±0,03^{a}	0,24±0,01^{a}	9269,02±389,16^{a}
Kek 2	26714,66±1152,27^{bc}	-5,25±1,39^{a}	0,52±0,02^{a}	0,71±0,05^{a}	0,24±0,01^{a}	9719,92±670,16^{a}
Kek 3	28040,17±4313,761^{c}	-4,07±1,79^{a}	0,47±0,03^{a}	0,71±0,03^{a}	0,22±0,02^{a}	9010,65±1581,29^{a}
Kek 4	32123,26±834,16^{d}	-3,81±0,45^{a}	0,50±0,01^{a}	0,75±0,05^{a}	0,25±0,01^{a}	12046,22±1475,16^{b}

Duyusal analiz

Kek örneklerinin duyusal analiz sonuçları Tablo 4'de verilmiştir. Kinoa kepek unu ilave edilen örneklerin rengi panelistler tarafından daha az beğenilmiş, ancak, farklı partikül boyutlarının renk üzerinde farklılık yaratmadığı görülmüştür (P>0,05). Benzer durum tat ve koku özellikleri içinde görülmüştür. Keklerin renk özellikleri bakımından en beğenilen örnek kontrol örneği olmuştur. Ağızda dağılabilirlik açısında en az beğenilen örnek 3.07 ile Kek 3 örneği olmasına rağmen, panelistler tarafından istatistiksel olarak diğer partikül boyutlarından farklı olmadığı şeklinde değerlendirilmiştir. Tekstür profil analizi sonuçlarından farklı olarak duyusal analizde keklerin yumuşaklığının kinoa kepek unu ilavesi ile değişmedi belirlenmiştir. Kek örnekleri genel beğeni puanları incelendiğinde en beğenilen örnek kontrol örneği olmuştur. Lorenz ve Collins (1990), kinoa unlu keklerin, yoğunluk, hacim, tekstür ve genel beğeni özelliklerinin buğday unundan yapılan keklere göre olumsuz etkilendiğini rapor etmişlerdir. Kinoa kepek ununun kullanımı ve farklı boyutlarının kullanımı genel beğeni özelliklerini olumsuz bir şekilde etkilemiştir. Chlopicka *ve ark.* (2012), kinoa, karabuğday ve aramant unları kullanılarak yaptıkları ekmekler yapmışlar ve duyusal özelliklerini incelemişlerdir. Elde ettikleri sonuçlara göre, ekmeklerin renk ve konsistensi özelliklerini, bu yalancı tahıllar içinde en olumsuz etkileyen kinoa unu olmuş, panelistlerin %30'u kinoa unlu ekmeğin tat olarak kabul edilebileceğini, %15'inin ise kabul edilemez olduğunu belirtmişlerdir. Benzer şekilde, kinoa unu katılarak yapılan mısır unlu glütensiz spagetti makarnaların panelistlerin beğenisi orta düzeyde bulunmuştur (Caperuto *ve ark.,* 2001).

Tablo 4. Kek örneklerinin duyusal analiz sonuçları

	Duyusal Özellikler					
Örnekler	**Renk**	**Tat**	**Koku**	**Yumuşaklık**	**Ağızda dağılabilirlik**	**Genel kabul edilebilirlik**
Kontrol	4,33±0,72^{b}	3,80±0,86^{b}	4,20±0,37^{b}	3,87±0,99^{a}	3,60±0,31^{b}	4,33±0,22^{b}
Kek 1	3,53±0,74^{a}	3,13±0,41^{a}	3,47±0,32^{a}	3,53±1,06^{a}	3,47±0,23^{ab}	3,80±0,36^{a}
Kek 2	3,20±0,94^{a}	2,97±0,46^{a}	3,13±0,13^{a}	3,33±1,18^{a}	3,27±0,18^{a}	3,53±0,33^{a}
Kek 3	3,40±0,99^{a}	3,47±0,22^{a}	3,33±0,05^{a}	3,13±1,19^{a}	3,07±0,20^{a}	3,60±0,26^{a}
Kek 4	3,40±1,30^{a}	3,53±0,39^{a}	3,47±0,49^{a}	3,27±1,22^{a}	3,47±0,39^{ab}	3,87±0,22^{a}

SONUÇ

Bu çalışmada, farklı boyutlarda kinoa kepek unu kullanımının keklerin fizikokimyasal, tekstürel ve duyusal özelliklerine olan etkisi incelenmiştir. Elde edilen verilere göre, kinoa kepek unu boyutuna bağlı olarak keklerin karakteristiklerinde değişimler meydana getirmektedir.

KAYNAKLAR

Algosaibi, A. M., Badran, A. E., Almadini, A. M., & El-Garawany, M. M. (2017). The effect of irrigation intervals on the growth and yield of quinoa crop and its components. *Journal of Agricultural Science, 9*, 182-191.

Alvarez-Jubete, L., Arendt, E., & Gallagher, E. (2009). Nutritive value and chemical composition of pseudocereals as gluten-free ingredients. *International Journal of Food Sciences and Nutrition, 60*, 240-257.

Alvarez-Jubete, L., Auty, M., Arendt, E. K. & Gallagher, E. (2010). Baking properties and microstructure of pseudocereal flours in gluten-free bread formulations. *European Food Research and Technology, 230*, 437-445.

Biernacka, B., Dziki, D., Gawlik-Dziki, U., Różyło, R., & Siastała, M. (2017). Physical, sensorial, and antioxidant properties of common wheat pasta enriched with carob fiber. *LWT –Food Science and Technology, 77*, 186-192.

Caperuto, L. C., Amaya-Farfan, J., & Camargo, C. R. O. (2001). Performance of quinoa (*Chenopodium quinoa* Willd) flour in the manufacture of gluten-free spaghetti. *Journal of the Science of Food and Agriculture, 81*, 95-101.

Chlopicka, J., Pasko, Gorinstein, S., Jedryas, A. & Zagrodzkia, P. (2012). Total phenolic and total flavonoid content, antioxidant activity and sensory evaluation of pseudocereal breads. *LWT – Food Science and Technology, 46,* 548-555.

Escribano, J., Cabanes, J., Jiménez-Atiénzar, M., Ibañez-Tremolada, M., Gómez-Pando, L. R., García-Carmona, F., & Gandía-Herrero, F. (2017). Characterization of betalains, saponins and antioxidant power in differently colored quinoa (*Chenopodium quinoa*) varieties. *Food Chemistry, 234*, 285-294.

Föste, M., Nordlohne, S. D., Elgeti, D., Linden, M. H., Heinz, V., Jekle, M., & Becker, T. (2014). Impact of quinoa bran on gluten-free dough and bread characteristics. *European Food Research and Technology, 239*, 767-775.

Gerçekaslan, K. E., & Hüseyin, B. (2018). Keçiboynuzu Unu İlavesinin Kakaolu Kekin Fiziksel, Duyusal ve Tekstürel Özelliklerine Etkisi. *Iğdır Üniversitesi Fen Bilimleri Enstitüsü Dergisi, 8*, 95-101.

Kozioł, M. (1992). Chemical composition and nutritional evaluation of quinoa (*Chenopodium quinoa* Willd.). *Journal of Food Composition and Analysis, 5*, 35-68.

Lorenz, K., & Collins, F. (1990). Quinoa (*Chenopodium quinoa*) Starch - Physico-chemical properties and functional characteristics. *Starch - Stärke*, *42*, 81–86.

Lorenz, K., & Coulter, L. (1991). Quinoa flour in baked products. *Plant Foods for Human Nutrition, 41*(3), 213-223.

Navruz-Varli, S., & Sanlier, N. (2016). Nutritional and health benefits of quinoa (*Chenopodium quinoa Willd.*). *Journal of Cereal Science, 69*, 371-376.

Özgören, E., Kaplan, H. B., & Tüfekçi, S. (2018). Chia Tohumu Kullanilarak Zenginleştirilen Galetalarin Bazi Kimyasal Ve Fiziksel Özellikleri. *FOOD and HEALTH, 4*, 140-146.

Paśko, P., Bartoń, H., Zagrodzki, P., Gorinstein, S., Fołta, M., & Zachwieja, Z. (2009). Anthocyanins, total polyphenols and antioxidant activity in amaranth and quinoa seeds and sprouts during their growth. *Food Chemistry, 115*, 994-998.

Rocha-Parra, A. F., Belorio, M., Ribotta, P. D., Ferrero, C., & Gómez, M. (2019). Effect of the particle size of pear pomace on the quality of enriched layer and sponge cakes. *International Journal of Food Science and Technology, 54*, 1265-1275.

Ruiz, K. B., Biondi, S., Oses, R., Acuña-Rodríguez, I. S., Antognoni, F., Martinez-Mosqueira, E. A., Zurita-Silva, A. (2014). Quinoa biodiversity and sustainability for food security under climate change. A review. *Agronomy for Sustainable Development, 34*, 349-359.

ORCID

Hamza ALAŞALVAR https://orcid.org/0000-0003-3000-7310
Hakan ERİNÇ http://orcid.org/0000-0001-8858-4570
Abdullah Sinan ÇOLAKOĞLU https://orcid.org/0000-0002-5928-3581

KSÜ Mühendislik Bilimleri Dergisi, 22, Özel Sayı, 2019 KSU J Eng Sci, 22, Special Issue, 2019
Uluslararası İleri Mühendislik Teknolojileri Sempozyumu (ISADET) Özel Sayısı
International Symposium on Advanced Engineering Technologies (ISADET) Symposium Special Issue
Araştırma Makalesi Research Article

Kahramanmaras Sutcu Imam University
Journal of Engineering Sciences

Geliş Tarihi : 20.09.2019 Received Date : 20.09.2019
Kabul Tarihi : 10.10.2019 Accepted Date : 10.10.2019

DETERMINATION OF SOME PROPERTIES OF OAT TARHANA AND COMPARISON WITH TRADITIONAL MARAS TARHANA

YULAF KATKILI TARHANALARIN BAZI ÖZELLİKLERİNİN BELİRLENMESİ VE MARAŞ TARHANASI İLE KARŞILAŞTIRILMASI

Nurdan Rana KİŞİ [1], *Bahri ÖZSİSLİ* [1]*
[1] Kahramanmaraş Sütçü İmam University, Department of Food Engineering, Kahramanmaraş, Turkey

*Sorumlu Yazar / Corresponding Author: Bahri ÖZSİSLİ, bozsisli@gmail.com

ÖZET

Çalışmamızda besinsel lif içeriği yüksek, protein, yağ gibi besin maddelerince zengin yulaf ezmesi belirli oranlarda yöresel Maraş tarhanasına ilave edilerek hem yeni bir ürün elde etmek hem de yulafın insan beslenmesinde kullanımına yeni bir alternatif geliştirmek amaçlanmıştır. Bu amaçla geleneksel Maraş tarhanasına dövme yerine yulaf ezmesinden % 10, % 20, % 30, % 40 ve % 50 oranlarında ilave edilmiştir. Yulaf ezmesi katkılı tarhanalar aynı koşullarda üretilen kontrol Maraş tarhanası örneği ile fiziksel, kimyasal ve duyusal açıdan karşılaştırılmıştır.

Bu araştırma sonucunda yulaf ezmesinin geleneksel Maraş tarhanasının kimyasal ve duyusal özelliklerini olumlu yönde etkilediği görülmüştür. Tarhana üretiminde kullanılacak en uygun yulaf ezmesi oranlarının % 40 ve % 50 olduğu belirlenmiştir.

Anahtar Kelimeler: Maraş, tarhana, traditional food, fermented food, dietary fiber, oat

ABSTRACT

In this study, oatmeal which is rich in nutritional compounds such as protein, fat, dietary fiber, were added to the Maras tarhana (Soup with Dried Yoghurt) for the replacement of wheat, as a new product and an alternative of oat use on human nutrition. For this purpose, oatmeal was added to the traditional Maras tarhana at 10%, 20%, 30%, 40% and 50%, and changes in the physical, chemical and organoleptic properties were examined in comparison to the traditional Maras tarhana produced from wheat. As a result of this research, it was found that the ash, fat, protein and cellulose contents increased with the addition of oatmeal, Hunter L values decreased, indicating reduction in the lightness, and Hunter a values increased, indicating increase in the redness. The oatmeal addition affected the organoleptic characteristics of the traditional Maras tarhana positively. It was been determined that the most suitable ratio of oatmeal to be used in tarhana production were 40% and 50%.
Keywords: Maraş tarhana, traditional food, fermented food, dietary fiber, oat

Introduction

Traditional foods are ethnic foods that are formed by the interaction of ecological and sociocultural environment over many years and shaped by factors such as climate, agricultural product composition, nutrition habits, working conditions and religion in the region where societies live in (Şahin and Avşar, 2004; Cayot, 2007). Tarhana, which is a traditional fermented food unique to Turkey and generally used in soup making, is a cereal based fermented food made from a mixture of cereals and yoghurt (Akbaş and Coşkun, 2006). According to the legislation of the European Union (within the framework of regulation 2028/92), traditional food consists of products produced using traditional raw materials or produced by the operating method, which reflects a traditional production type characterized by a traditional composition. Traditional foods explain the culture, history and lifestyle of the region which they belong (Vasilopoulou et al., 2005).

Fermented foods, which are generally produced by traditional methods, play an important role in the daily diet of people (Leroy and De Vuyst, 2004). In the recent years, consumer demands that have been minimally processed, free of preservative chemicals and increased against natural foods have made it necessary to develop alternative food processing and preservation techniques. Among these, fermentation is having a great importance as a biotechnological production and preservation method (Erbaş et al., 2004). Different microorganisms and their enzymes break down food components and changes of the taste, smell, texture, durability and nutritional qualities to create products that are more delightful is called fermentation (Nout and Matarjami 1997). With Fermentation fermented foods with improved aroma, texture, shelf life, nutritional value, reliability and serviceability will be produced (Steinkrauss, 2002).

Food fermentation is one of the oldest known application fields of biotechnology and has reached its current state from natural processes with the use of selected starter cultures from environmental conditions and, more recently, strains developed through gene technology. Lactic acid bacteria, especially Aspergillus and Penicillum species from molds, Saccharomyces species from yeasts are very important microorganisms in the formation of these products (Boyacioglu 1994, Kilic and Yukselci 2004).

Nowadays, there is interest in the consumption of fermented foods by millions of people from different communities and ethnic groups around the world. The reason for this consumers are interest in natural healthy foods. In the future Fermented foods consumption is predicted to increase all over the world. Because fermentation is a very effective preservation method that reduces the need for other food preservation techniques that increase shelf life (Campbell-platt, 1994).

Studies conducted by many researchers have shown that fermentation increases the nutritional value and digestibility of cereals. It has been found that there is a significant increase in the extraction rate and digestibility of cereal proteins after fermentation, in general the starch and fiber content decrease slightly due to the use of microorganisms, but the amount of reducing sugar increases. In addition, carbohydrate digestibility of cereals has been shown to increase after fermentation in various studies. Although no changes have been determined after fermentation in the amount of fat and fatty acid composition of cereals, it has been reported that hydrolytic changes may cause changes in the functional and organoleptic properties of the product. While no change was observed as a result of fermentation in the amount of mineral substances, their digestion and absorption increased because in the amount of phytic acid and tannins is decreased as a result of fermentation is thought to be effective (Özbilgin, 1983; Saldamli, 1983). Flour, which the main raw material in Tarhana, is a food rich in essential amino acids. Yoghurt added to tarhana enriches tarhana in terms of essential amino acids that are also missing in flour (Koca and Tarakçı, 1997). It also increases the amount of low lysine and threonine (Tarakçı et al., 2004).

MATERIAL and METHOD

MATERIAL

Wheat (darıyel), oatmeal (ETİ Lifalif), yoghurt (local village yogurt), thyme, salt (Billur Salt) used in this study were purchased from a local market in Kahramanmaraş. Physical, chemical and organoleptic analyzes were performed in Food Engineering Laboratories of Kahramanmaraş Sütçü İmam University Faculty of Agriculture and Kahramanmaraş Commodity Exchange Private Food Control Laboratory.

METHOD

Formulation and Production of Maraş Tarhana

Tarhana samples were made according to the formulation in Table 3.1. 10%, 20%, 30%, 40% and 50% (w / w) of oatmeal was added for the replacement of to Tarhana formulation. Tarhana samples were produced as given in Figure 1.

Table 2. Tarhana formulation

Rawmaterial	**Quantity (g)**
Wheat	250
Yoghurt	750
Salt	6,25
Thyme	1,5

Table 3. Oatmeal and wheat ratios of oatmeal added tarhanas

Tarhanas	Oat (g)	Wheat (g)
Tarhana with 10% oatmeal added	25	225
Tarhana with 20% oatmeal added	50	200
Tarhana with 30% oatmeal added	75	175
Tarhana with 40% oatmeal added	100	150
Tarhana with 50% oatmeal added	125	125

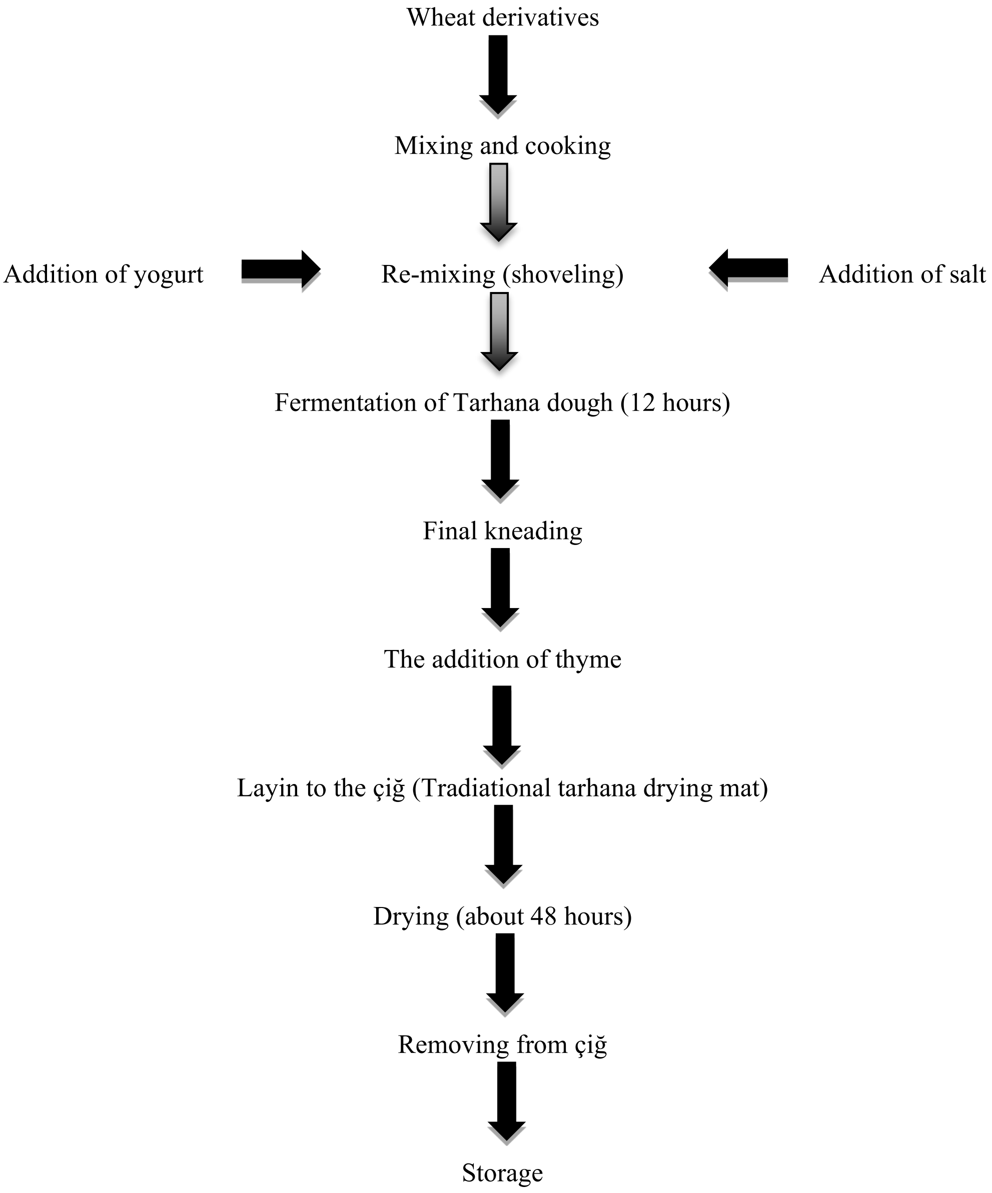

Figure 1. Production flow chart of Maraş tarhana

RESULTS AND DISCUSSION

Raw material properties

The raw material analysis results are given in Table 3. The carbohydrate and moisture content of the wheat which is one of the main components of Maraş tarhana were higher than the oatmeal. However, protein, fat, cellulose and ash ratios of oatmeal are higher than wheat.

Table 4. Properties of wheat and oatmeal

	Moisture (%)	**Ash (%)**	**Protein (%)**	**Fat (%)**	**Cellulose (%)**	**Carbohydrate (%)**
Oatmeal	9.44	1.41	12.6	8.37	1.84	68.18
wheat	10.17	1.09	10.6	1.20	1.20	76.94

Moisture content of tarhana

Tarhana samples produced by adding different amounts of oatmeal had a moisture value between 8.86% and 9.36% (Table 4). The lowest moisture content was found in as 8.86% in the tarhana sample with 20% oatmeal and the highest moisture content was found in the control tarhana sample as 9.36%. TSE 2282 standard states that the amount of moisture in tarhana should be at most 10%. The values found in this study are below the value specified in TSE 2282 standard.

Table 5. Statistical results of moisture content of tarhana samples

Tarhanas	**Control**	**10% oatmeal**	**20% oatmeal**	**30% oatmeal**	**40% oatmeal**	**50% oatmeal**
Tukey	9.36^{a}±1,29	8.90^{a}±0,60	8.86^{a}±0,74	8.97^{a}±0.28	8.93^{a}±0,92	8.93^{a}±0,55
Duncan	9.36^{a}±1,29	8.90^{a}±0,60	8.86^{a}±0,74	8.97^{a}±0.28	8.93^{a}±0,92	8.93^{a}±0,55

Ash content of tarhana

Ash in cereals and cereal products is the residue of the minerals left behind by combustion. The ash contents of tarhana samples are given in Table 5. The ash content of tarhanas produced by adding oatmeal in different ratios were found between 3.19% and 4.27%. The lowest ash content was found in the control tarhana sample as 3.19% and the highest ash content was found in the tarhana sample with 50% oatmeal added as 4.27%.

Table 6. Statistical results of ash content of tarhana samples

Tarhanas	**Control**	**10% oatmeal**	**20% oatmeal**	**30% oatmeal**	**40% oatmeal**	**50% oatmeal**
Tukey	3.19^{a}±0,09	3.49^{a}±0,08	3.55^{ab}±0,21	3.39^{a}±0,71	4.03^{bc}±0,05	4.27^{c}±0,09
Duncan	3.19^{a}±0,09	3.49^{a}±0,08	3.55^{a}±0,21	3.39^{a}±0,71	4.03^{b}±0,05	4.27^{b}±0,09

pH Value

The pH values of tarhanas produced by adding oatmeal in different ratios were found between 4.04 and 4.12. The lowest pH value was found as 4.04 in tarhana sample with 50% oatmeal added, the highest pH value was found as

4.12 in the control tarhana sample and 20% oatmeal added tarhana sample. The results of the analysis are given in Table 6.

Table 7. Statistical results of pH values of tarhana samples

Tarhanas	Control	10% oatmeal	20% oatmeal	30% oatmeal	40% oatmeal	50% oatmeal
Tukey	4.12^{c}±0,03	4.10^{bc}±0,01	4.12^{c}±0,02	4.11^{bc}±0,01	4.09^{b}±0,02	4.04a±0,00
Duncan	4.12^{c}±0,03	4.10^{bc}±0,01	4.12^{c}±0,02	4.11^{c}±0,01	4.09^{b}±0,02	4.04^{a}±0,00

Color Analysis

The Hunter Lab values of tarhana samples are given in Table 7. Hunter L values of the tarhanas produced by adding oatmeal in different ratios were found between 50.77 and 66.06. The lowest L value was found in the tarhana sample with 50% oatmeal added as 50.77 and the highest L value was found in the tarhana sample with 20% oatmeal added as 50.77. The reason of this; It can be explained by the fact that the brightness value of oatmeal used as raw material is lower than the brightness value of wheat.

Hunter a values of the tarhanas produced by adding oatmeal in different ratios were found between 0.87 and 2.01. The lowest a value was found in the tarhana sample with 10% oatmeal added as 0.87 and the highest a value was found in the tarhana sample with 50% oatmeal added as 2.01. The reason of this; It can be explained by the fact that the redness value of oatmeal used as raw material is higher than the redness value of wheat.

Hunter b values of the tarhanas produced by adding oatmeal in different ratios were found between 15.90 and 17.74. The lowest b value was found in the tarhana sample with 10% oatmeal added as 15.90 and the highest b value was found in the tarhana sample with 50% oatmeal added as 17.74. The reason of this; It can be explained by the fact that the yellowness value of oatmeal used as raw material is higher than the yellowness value of wheat.

Table 8 Statistical results of Hunter L, a, and b values of tarhana samples

	Tarhanas	Control	10% oatmeal	20% oatmeal	30% oatmeal	40% oatmeal	50% oatmeal
L	Tukey	62.92^{b}±2,80	65.81^{b}±1,15	66.06^{b}±0,71	60.11^{ab}±1,84	54.60^{a}±4,92	53.77^{a}±0,08
	Duncan	62.92^{bc}±2,80	65.81^{c}±1,15	66.06c±0,71	60.11^{b}±1,84	54.60^{a}±4,92	54.54^{a}±0,08
a	Tukey	1.41^{a}±0,58	$0,87^{a}$±0,41	1.29^{a}±0,33	1.89^{a}±0,54	1.71^{a}±0,25	2.01^{a}±0,19
	Duncan	1.41^{ab}±0,58	$0,87^{a}$±0,41	1.29^{ab}±0,33	1.89^{b}±0,54	1.71^{b}±0,25	2.01^{b}±0,19
b	Tukey	18.85^{a}±2,00	19.24^{a}±0,58	19.69^{a}±1,50	16.48^{a}±4,92	17.01^{a}±1,46	17.74^{a}±0,88
	Duncan	18.85^{a}±2,00	19.24^{a}±0,58	19.69^{a}±1,50	16.48^{a}±4,92	17.01^{a}±1,46	17.74^{a}±0,88

Fat content of tarhana

The fat contents are given in Table 8.The fat content of tarhanas produced by adding different amounts of oatmeal was found between 5.1% and 6.7%. The lowest fat content was 5.1% in 10% oatmeal added tarhana and the highest fat content was 6.7% in 50% oatmeal added tarhana sample.

Table 9 Statistical results of fat content in tarhana samples

Tarhanas	Control	10% oatmeal	20% oatmeal	30% oatmeal	40% oatmeal	50% oatmeal
Tukey	5.72^{ab}±0,04	5.10^{a}±0,02	6.57^{b}±0,24	5.84^{ab}±0,11	6.52^{b}±0,54	6.73^{b}±0,25
Duncan	5.72^{ab}±0,04	5.10^{a}±0,02	6.57^{c}±0,24	5.84^{ab}±0,11	6.52^{c}±0,54	6.73^{c}±0,25

Protein content of tarhana

The results of the protein analysis are given in Table 9.The protein content of tarhanas produced by adding different amounts of oatmeal was found between 15.05% and 15.84%. The lowest protein content was 15.05 % in control tarhana sample and the highest protein content was 15.84% in 50% oatmeal added tarhana sample.

Table 10. Statistical results of protein content in tarhana samples

Tarhanas	Control	10% oatmeal	20% oatmeal	30% oatmeal	40% oatmeal	50% oatmeal
Tukey	15.05^{a}±0,07	15.3^{a}±0,42	15.4^{a}±0,42	15.49^{a}±0,02	15.55^{a}±0,64	15.85^{a}±0,35
Duncan	15.05^{a}±0,07	15.3^{a}±0,42	15.4^{a}±0,42	15.49^{a}±0,02	15.55^{a}±0,64	15.85^{a}±0,35

Organoleptic properties of tarhana

When the results of the organoleptic analysis of tarhanas produced by adding different amounts of oatmeal were examined, the highest score in terms of "color" was obtained from the control tarhana sample. Second highest scored was the tarhana sample with 50% oatmeal added. The lowest score was obtained from tarhana sample with 10% oatmeal added. All results related to organoleptic analysis are given in Table 10.

The highest score in terms of "flavor" was obtained from the control tarhana sample. Second highest scored was the tarhana sample with 50% oatmeal added. The lowest score was obtained from tarhana sample with 10% oatmeal added.

The highest score in terms of "sourness" was obtained from the control tarhana sample. Second highest scored was the tarhana sample with 50% oatmeal added. The lowest score was obtained from tarhana sample with 30% oatmeal added.

In terms of "odor", the highest score was obtained by 50% oatmeal added tarhana and the lowest by 30% oatmeal added tarhana sample. When “Hardness-Brittleness-Fragility” is examined, the highest score is obtained from the control tarhana and with 50% oatmeal added tarhana and also the lowest score was obtained from tarhana with 30% oatmeal added.

The highest score in terms of "General Acceptability" was obtained from the control tarhana sample. Second highest scored was the tarhana sample with 50% oatmeal added. The lowest score was obtained from tarhana sample with 0% oatmeal added.

Table 11. Statistical results of organoleptic analysis in tarhana samples

	Tarhanas	**Control**	**10% oatmeal**	**20% oatmeal**	**30% oatmeal**	**40% oatmeal**	**50% oatmeal**
Appearence	Tukey	4.13^{c}	2.33^{a}	3ab	2.8^{ab}	3.53^{bc}	3.60^{bc}
	Duncan	4.13^{c}	2.33^{a}	3ab	2.8a	3.53^{bc}	3.60^{bc}
Colour	Tukey	4.2^{c}	2.47^{a}	3.6^{bc}	2.87^{ab}	3.47^{bc}	3.73^{c}
	Duncan	4.2^{c}	2.47^{a}	3.6^{bc}	2.87^{a}	3.47^{b}	3.73^{bc}
Flavour	Tukey	3.87^{c}	2.07^{a}	3abc	2.13^{ab}	3.13^{bc}	3.4^{c}
	Duncan	3.87^{c}	2.07^{a}	3b	2.13^{a}	3.13^{b}	3.4^{bc}
Sourness	Tukey	3.47^{b}	2.40^{ab}	2.87^{ab}	1.93^{a}	2.87^{ab}	3.13^{b}
	Duncan	3.47^{c}	2.40^{ab}	2.87^{bc}	1.93^{a}	2.87^{bc}	3.13^{bc}
Odor	Tukey	3.33^{b}	2.80^{ab}	3.33^{b}	2.07^{a}	3.07^{b}	3.47^{b}
	Duncan	3.33^{b}	2.80^{b}	3.33^{b}	2.07^{a}	3.07^{b}	3.47^{b}
Hardness-Brittleness-Fragility	Tukey	4.13^{b}	3.07^{a}	3.47^{ab}	3a	3.80^{ab}	4.13^{b}
	Duncan	4.13^{b}	3.07^{a}	3.47^{ab}	3a	3.80^{b}	4.13^{b}
General Acceptability	Tukey	4b	2.2^{a}	3.13^{ab}	2.67^{a}	3.13^{ab}	3.87^{b}
	Duncan	4d	2.2^{a}	3.13^{bc}	2.67^{ab}	3.13^{bc}	3.87^{cd}

RESULTS

The manufacture techniques of the local tarhana which was produced in Kahramanmaraş was demonstrated. Under laboratory conditions, control (by wheat) and tarhanas 10%, 20%, 30%, 40% and 50% oatmeal added were produced and the chemical and organoleptic properties of the tarhanas were determined and the optimum amount of oatmeal that could be used in tarhana production was determined.

When the analysis results are examined, it is seen that the carbohydrate and moisture content of the wheat which is one of the main components of Maraş tarhana is higher than the oatmeal used as an additive. However, protein, fat, cellulose and ash ratios of oatmeal are higher than wheat.

When the moisture content of Tarhana samples is examined, it is seen that all samples have similar values. It can be said that the small differences observed may be due to the raw material properties in tarhana composition and the weather conditions in which the product is dried.

When the amount of ash was examined, it was observed that the addition of oatmeal generally increased the ash amounts of tarhana.

In Tarhana samples, it was observed that the fat content generally increased with the addition of oatmeal. It can be said that the fluctuations observed may be due to the fat content of yogurt, which is an important fat source for the product.

When the pH analysis results of Tarhana samples were examined, it was observed that the pH value was partially decreased by the addition of oatmeal. Accordingly, titration acidity was partially increased with the addition of oatmeal. However, titration acid values were lower than the standard values. This may be due to the fermentation step does not perform at the desired efficiency due to the cool and rainy days when the tarhana samples are prepared and dried. The acidity may not have developed effectively due to the lack of the desired temperature parameter which significantly affects the fermentation.

The protein content of Tarhana samples increased in direct proportion with the amount of oatmeal. This may be due to the relatively higher protein content of oatmeal than wheat.

The carbohydrate content was decreased due to the increase in the amount of oatmeal. This result may be due to the fact that the wheats' carbohydrate is higher than the oatmeal carbohydrate.

The cellulose content of Tarhana samples was partially increased due to the addition of oatmeal. This may be due to the cellulose content of the oatmeal is higher than the cellulose content of the wheat. Furthermore, this increase in cellulose, which forms the water-insoluble portion of the dietary fiber, may lead us to the conclusion that the total dietary fiber content also increases with the addition of oatmeal.

When the color analysis results of Tarhana were examined, it was observed that the increase in oatmeal ratio decreased the brightness of the products but increased the yellowness and redness values.

When the organoleptic analysis results were examined, control tarhana received the most rating in general. This may be due to its appeal to the palate that has been adopted for years. The increase in oatmeal ratio contributed to the increase in the liking scores of many parameters such as color, odor, hardness-brittleness and fragility.

As a result of our study;

Maraş tarhana is an important traditional food with its unique production, drying method and consumption variety. It is a fermented product with high nutritional value. The amount of raw materials used in Tarhana production will be affects product quality and taste.

Oat is important cereal rich in dietary fiber. Its use in human consumption has become widespread in recent years. Oats, which are consumed especially for weight control, are the main protagonists of a healthy diet. It is a cereal that is rich in vitamin E and regulatory effect of intestinal functions should be included in daily consumption. With the addition of oats bearing these characteristics to the Maraş tarhana, a new product was produced and a new alternative for the use of oats in human nutrition was developed.

As a result of this study, oatmeal added tarhanas were produced by adding certain amounts of oatmeal to Maraş tarhana which was traditionally produced and consumed in a limited region and at homes and the significant differences was found between traditional Maraş tarhana and oatmeal added tarhanas. The addition of oatmeal was found to have a positive effect on the chemical and organoleptic properties of tarhana. When chemical analysis and organoleptic analysis results were examined, it was determined that oatmeal ratios to be used in tarhana production were 40% and 50%.

The production of traditional Maraş tarhana by adding different spices and additives will increase the nutritional quality of our traditional product.

REFERENCES

Akbaş, Ş., Coşkun, H., 2006. *Tarhana Üretimi ve Özellikleri Üzerine Bir Değerlendirme, Bolu, Türkiye, 9. Gıda Kongresi, 703-706.*

Boyacıoğlu, D., 1994, *Geçmişte Ve Günümüzde Gıda Biyoteknolojisi Uygulamaları, II.Gıda Mühendisliği Kongresi, Gaziantep, s194.*

Campell-Platt, G., 1994. *Fermente Foods a World Perspective, Food Research International, 27:253-257.*

Cayot, N., 2007. *Sensory quality of traditional food, Food Chemistry, 102:445-453.*

Erbaş, M., Certel, M., Uslu, M.K., 2004.*Yaş ve Kuru Tarhananın Şeker İçeriğine Fermentasyonun ve Depolamanın Etkisi, Gıda, 29 (4), 299-305.*

Kılıcı Yükselci, A.,2012, *"Yulaf Katkısının Tarhana Kalitesine Etkisi",Yüksek Lisans Tezi, Uludağ Üniversitei Fen Bilimleri Entitüsü, Bursa.*

Koca, A.F., Tarakçı, Z., 1997. *Tarhana Üretiminde Mısır Unu ve Peynir Altı Suyu Kullanımı, Gıda 22 (4), 287-292.*

Leroy, F., De Vusty, L., 2004. *Lactic Acid Bacteria as Functional Starter Cultures for the Food Fermentation Industry, Trends in Food Science and Technology, 15: 67-78.*

Nout, M J.R., Motarjemi, Y., 1997*, Assessment of fermentation as a household technology for improving food safety: a joint FAO/ WHO workshop. Food Control, 8:221-226.*

Steinkrauss, K.H., 2002.*Fermentations in world food processing, Comprehensive Reviews in Food Science and Food Safety I23-30.*

Tarakçı, Z., Doğan, İ.S., Koca, A.F., 2004. *A traditional fermented Turkish soup tarhana, formulated with corn flour and whey, International Journal of Food Science and Technology 39, s. 455-458.*

Özbilgin, S., 1983. *The Chemical and Biological Evaluation of Tarhana Supplemented with Chickpea and Lentil, PhD Thesis, Cornell Uni., Ithaca,*

Pamir,H., 1977, *Fermentasyon Mikrobiyolojisi, Ankara Üni. Zir. Fak. Yayınları No: 639, Ank. Üniv. Basımevi, Ankara.*

Saldamlı, İ., 1983. *Beslenme Açısından Fermente Süt Ürünleri, Gıda 8 (6), 297-311.*

Vasilopoulou, E., Dilis, V., Soukara, S., Trichopolilou, A., 2005. The Systematic *Investigation of Traditional Foods in Europe, İstanbul 1. International Food and Nutrition Congress, TÜBİTAK, Haziran 15.*

ORCID

Bahri ÖZSİSLİ https://orcid.org/0000-0002-4736-4683

KSÜ Mühendislik Bilimleri Dergisi, 22, Özel Sayı, 2019 KSU J Eng Sci, 22, Special Issue, 2019
Uluslararası İleri Mühendislik Teknolojileri Sempozyumu (ISADET) Özel Sayısı
International Symposium on Advanced Engineering Technologies (ISADET) Symposium Special Issue
Araştırma Makalesi Research Article

Kahramanmaras Sutcu Imam University
Journal of Engineering Sciences

Geliş Tarihi : 27.07.2019 Received Date : 27.07.2019
Kabul Tarihi : 25.11.2019 Accepted Date : 25.11.2019

LIFE CYCLE ANALYSIS OF AN EXPANDABLE POLYSTYRENE PRODUCT

BİR GENLEŞEBİLİR POLİSTİREN ÜRÜNÜNÜN YAŞAM DÖNGÜSÜ ANALİZİ

Onur Uludağ [1]*, *Yusuf Uras* [1]

[1]Department of Material Science and Engineering, Kahramanmaras Sutcu Imam University, Kahramanmaras, Turkey

*Corresponding Author: Onur ULUDAĞ, onuruludag81@gmail.com

ABSTRACT

Energy sustainability and efficiency for buildings is of great importance for cities. For this reason, insulation systems are used in buildings. Expandable polystyrene (EPS) is one of these systems. EPS is produced by suspension polymerization. The beads formed in this reaction are coated and packaged. EPS blocks are produced in 3 stages. The first is the pre-expansion and maturation phase. At this stage, steam is applied to the EPS beads and allowed to swell. These swollen particles are then taken into the ripening silos for a certain period of time. In the second step, the matured and inflated beads are taken to the block machine and steam is applied again to obtain the block. The beads fuse together and form blocks in the machine under high temperature and pressure. The third stage is resting and cutting. The EPS blocks are then applied to the building surface to provide good insulation. Storage, recycling (reuse) and recovery (incineration) are the methods of evaluation of EPS wastes. In this study, it is aimed to reduce the environmental impact of each step of EPS life cycle by using Cradle to Grave Life Cycle Analysis. LCA is a very useful method to determine the detailed environmental impacts of the whole process. This analysis consists of 3 steps. The first step is the definition of purpose and scope. The second is inventory analysis. The third step is to assess the environmental impact and the final step is to decide and implement the conservation process. As a result, in this study, the process that causes the most environmental impact is determined by using LCA during the EPS lifecycle and a solution will be developed to reduce this impact as soon as possible.

Keywords: Cradle to Grave, Energy Efficiency, EPS, Environmental Impact, LCA.

ÖZET

Binalar için enerji sürdürülebilirliği ve verimliliği şehirler için büyük önem taşımaktadır. Binalarda bu sebeple yalıtım sistemleri kullanılmaktadır. Genleştirilebilir polistiren (EPS) bu sistemlerden biridir. EPS süspansiyon polimerizasyonu ile üretilir. Bu reaksiyonda oluşan boncuklar kaplanır ve paketlenir. EPS blokları 3 aşamada üretilmektedir. Birincisi ön genişleme ve olgunlaşma aşamasıdır. Bu aşamada buhar, EPS boncuklarına uygulanır ve şişmesi sağlanır. Daha sonra bu şişmiş tanecikler belirli bir süreliğine olgunlaşma silolarına alınır. İkinci aşamada, blok elde etmek için olgunlaştırılmış ve şişirilmiş boncuklar blok makinesine alınır ve tekrar buhar uygulanır. Boncuklar birbirine kaynaşır ve makinede yüksek sıcaklık ve basınç altında blok oluşur. Üçüncü aşama dinlenme ve kesme işlemidir. Daha sonra EPS blokları iyi yalıtım sağlamak için bina yüzeyine uygulanır. Depolama, geri dönüşüm (yeniden kullanma) ve geri kazanım (yakma), EPS atıklarının değerlendirme yöntemleridir. Bu çalışmada, Beşikten Mezara Yaşam Döngüsü Analizi (YDA) kullanarak EPS yaşam döngüsünün her bir adımının çevresel etkisinin azaltılması amaçlanmıştır. YDA, tüm sürecin ayrıntılı çevresel etkilerini belirlemek için çok faydalı bir yöntemdir. Bu analiz 3 adımdan oluşmaktadır. İlk adım, amaç ve kapsam tanımıdır. İkincisi envanter analizidir. Üçüncü adım, çevresel etkinin değerlendirilmesi ve son adım ise karar vermek ve koruma sürecini uygulamaktır. Sonuç olarak, bu çalışmada EPS yaşam döngüsü boyunca YDA kullanılarak en fazla çevresel etkiye sebep olan süreç tespit edilip, bu süreç için mümkün olan en kısa sürede bu etkiyi azaltmak için çözüm geliştirilecektir.

Anahtar Kelimeler: Beşikten Mezara, Enerji Verimliliği, EPS, Çevresel Etki, YDA

INTRODUCTION

Last years, concerns of environment, particularly have been increased the demand for sustainable building and developments. Because of this, for construction industry have been need correct information about environmental impact of used building materials and products. The most suitable way to reach this information has been defined to be the Life Cycle Assessment (LCA) approach. LCA defines environmental impacts of whole processes that includes from production till recycle (cradle to grave).

Expanded polystyrene (EPS) is used in the construction sector, mostly for insulation purposes, and also in the packaging industry. Additionally, it have advantages such as be a cheap, sound and thermal insulator, humidity resistance, easily recyclable [1]

In one of the recent studies, the environmental impacts of insulation materials were evaluated using software, where the environmental impacts of EPS were found to be less for all environmental impact classes than stone wool. In addition, environmental impacts were mostly observed during the production phase. [2]

In the world and in Turkey under study it focused on the intensive use of thermal insulation materials. These materials are Glass wool, Rockwool, Expanded Polystyrene Foam (EPS), Extruded Polystyrene Foam (XPS) and Polyurethane Foam (PUR). In the life cycles of the said insulation materials, waste and emissions released to the environment at different stages such as raw material supply, production, use, transportation and disposal as waste are evaluated. In this context, environmental impact categories mentioned in YDA studies are: global warming, energy consumption, water consumption, acidification, eutrophication and photochemical ozone formation. [3]

In another study, a new approach was developed in which optimum results are obtained by evaluating the life cycle energy consumption, carbon emission and cost of thermal insulation material and optimum insulation thickness. According to the results of the study, XPS and glass wool for Istanbul and Izmir, and stone wool for Erzurum, thermal insulation materials have come to the fore as the materials having optimum life-cycle performance. Furthermore, according to the results of the study, it is recommended that standards for thermal insulation and energy performance in buildings should be revised to take into account the life cycle of the materials. [4]

A life-cycle analysis was performed for a foamed polystyrene (PS) tray used for fresh meat packaging, and the highest environmental impacts were due to PS granule production and electricity consumption. Turning the energy source into a renewable source (for example by building a wind farm) leads to a 14% gain. In this way, the authors documented that there may be alternative ways to improve the global environmental improvement of the analyzed system and thereby improve the environmental sustainability of food packaging systems. [5]

EPS PRODUCTION

EPS (Expandable Polystyrene) is produced by suspension polymerization method and batch process form. In suspension polymerization, the monomer is formed by immersing the monomer in water which is not mixed. The polymer was eluted at 0.01-0.5 cm in aqueous phase. it is dispersed in diameter, ie the suspension of the monomer in water. In order to ensure that the suspension is stable and the formed polymer particles do not adhere to each other, chemicals called stabilizers are added. These suspension-forming substances wrap around the monomer. If necessary precautions are not taken, the particle s are clustered and block. As stabilizers, water-insoluble inorganic compounds such as gelatin, kaolin, powder, bentonite, barium, calcium and magnesium carbonates, aluminum hydroxide are generally used. In addition, mechanical mixing prevents the droplets from sticking together. As initiators of the polymerization, initiators are dissolved in the monomer (organic phase). At the end of the polymerization, the resulting powdered polymer is filtered out of the water and dried. The polymer is produced in granular form. Styrene, methyl methacrylate, vinyl chloride, vinyl acetate can be polymerized by these methods. This type of polymerization is called pearl or grain polymerization by looking at the final product obtained.

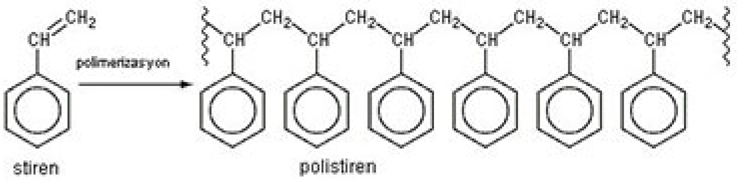

Figure 1: Polymerization reaction of Styrene Monomer

Suspension polymerization is a polymerization method that is very frequently used in industry. During this process, styrene, organic inhibitors, water and solids are added to the reactor. This procedure creates a suspension system that will subsequently form styrene droplets. The droplets polymerize into polystyrene by free radical polymerization. Then the chemical is added to the reactor for the purpose of blowing. The final product is absorbed into the polymer and the expandable polystyrene beads are obtained. After the conversion of the styrene monomer droplets to the expandable polystyrene beads, the reactor is cooled and the particles separated from the water. These particles are then dried, sieved and then separated into different particle fractions and coated with suitable additives according to their size and intended use.

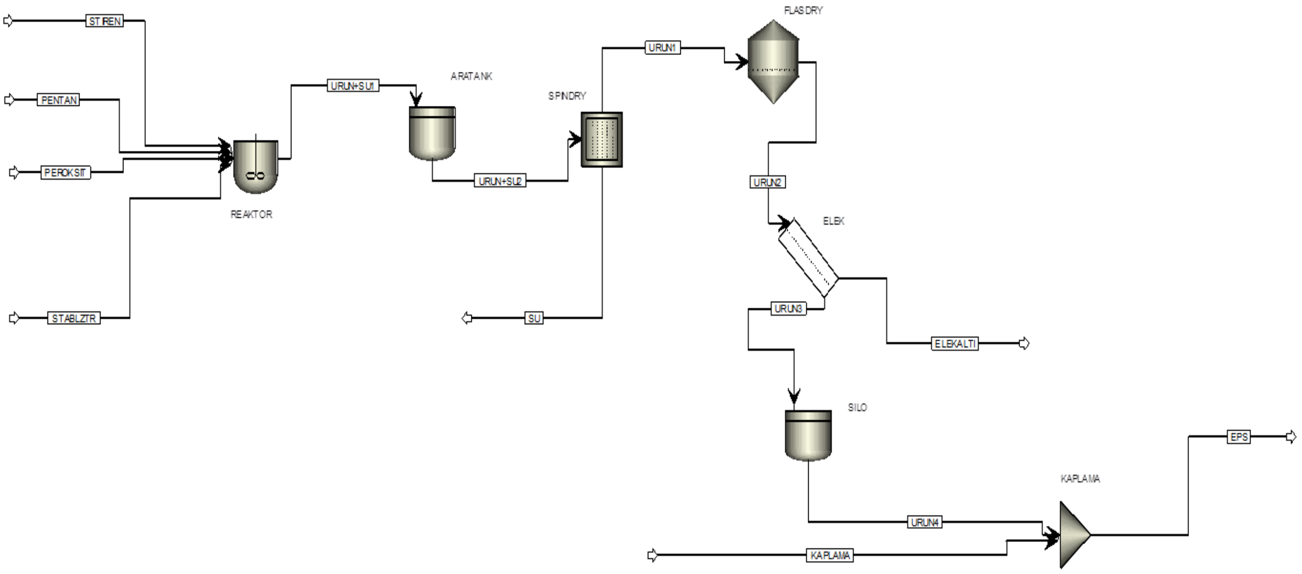

Figure 2: Expandable Polystyrene (EPS) Production Process

Pentane is injected in polystyrene as a blowing agent and then steam is applied to form EPS beads. The beads are then being molded in molding machines to make insulation panels, blocks or special shapes for the building and packaging industry. [1]

The particles are swollen at a temperature of 80-100 ^{0}C. with pentane and subjected to steam. The inflated particles still contain a very small amount of condensed steam and pentane gas. At this stage, when the particles are cooled, the porous structure starts to fill air instead of pentane gas. After pre-inflation, the EPS particles taken into the rest silos are held for 6-12 hours to allow the air - pentane exchange to be at the desired level. The block is molded in order to form a block to EPS and then to obtain a sheet from this block. At this stage, steam is used to maintain the foam shape and to continue the expansion. The use of steam also allows the particles to fuse together. After a short cooling phase, the molded EPS block is shaped by cutting methods. The use of hot wire or by another method is done.

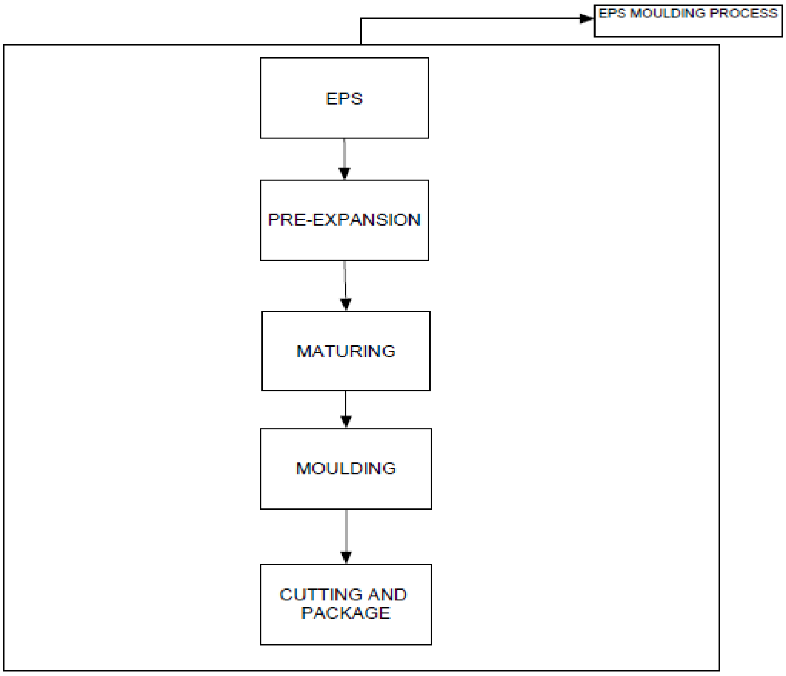

Figure 3: EPS Molding Process

LIFE CYCLE ANALYSIS

Life Cycle Analysis (LCA) is accepted as a scientific method for detailed evaluations and environmental sustainability during whole life cycle of a product from raw material to recycle. This life cycle steps are shown in Figure 4. [6]

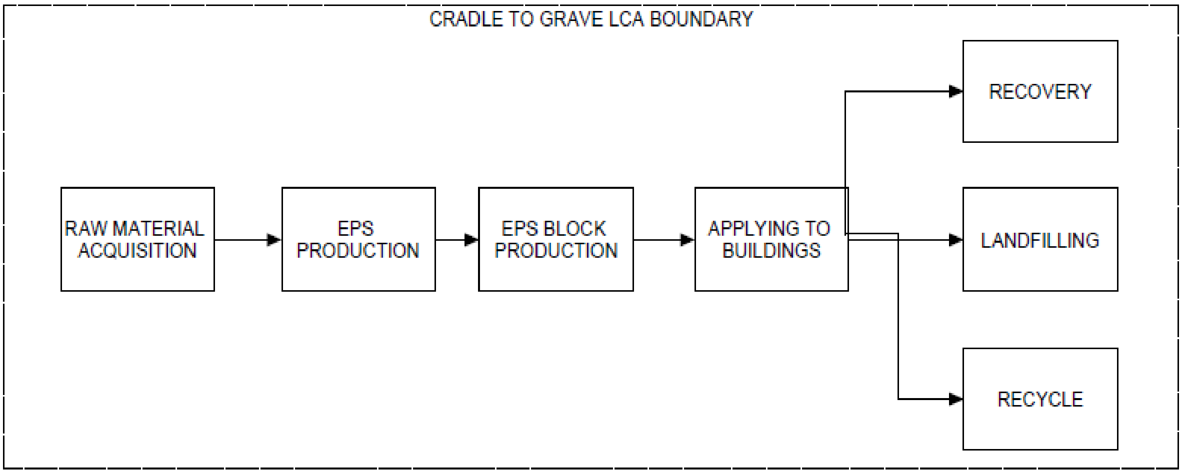

Figure 4: Flow diagram for cradle to grave life cycle of an EPS system

The analysis shows us the environmental impact caused by production steps. Results of LCA can be used for studies that include developing of using resources, environmental impacts of production systems. Also with these results, we can be observing decreasing energy usage and its possible impacts. In this study life cycle inventory (LCI) and life cycle impact assessment gives us evaluations of total energy requirement, energy usage, water consumption, air pollution, water source pollution and solid waste for EPS production. ISO 14040 and ISO 14044 international standards are followed to use methods for LCI and LCIA in this study. The steps of a life cycle assessment (LCA) generally examines , beginning with raw material production, continuing on through material production, product fabrication, use, ends with reuse or recycling. [6]

An LCA consists of four phases:

- Goal and scope definition
- Life cycle inventory (LCI)
- Life cycle impact assessment (LCIA)
- Interpretation of results

In the LCIA phase, the inventory of emissions is classified as different categories which may cause to adverse impacts on human health or the environment. Within each impact category, the emissions are then normalized to a common reporting basis, using characterization factors that express the impact of each substance relative to a reference substance. [6]

LIFE CYCLE ANALYSIS OF EXPANDABLE POLYSTYRENE

Goal and Scope Definition

The aim of this study is to evaluate the environmental impacts caused by all stages of EPS life cycle from cradle to grave, to determine important environmental inputs and outputs and to determine effective points on the basis of environmental impact.

This study includes raw material procurement, industrial production, further processing, packaging, transportation, consumption and waste management processes for the said EPS product. In addition, energy consumption and emissions were evaluated and their potential environmental impacts were examined.

For this purpose, at this stage, the EPS product, assumptions, functional unit, system boundaries, distribution methods and data quality requirements considered within the scope of the case study are defined; decisions are taken regarding critical review and report preparation.

It is a kind of polystyrene which is used extensively in the insulation industry, where pentane is found as a blowing agent in EPS product and it is replaced with 40 times in steam application. Since most of the raw materials in EPS are less than 1%, styrene monomer and pentane are assumed to be active substances. This ratio is 93% styrene monomer and 7% pentane.

For the analysis to be understandable, functional unit definition should be made. The functional unit in this study was determined as 1000 kg EPS product.

Production and supply of raw materials for the production of EPS in the cradle-to-grave life cycle analyzer, production, further processing, use and recovery of the EPS product are the unit operations in this study. The methods used for these processes and the input flows such as material, energy, water in each method and air / water / soil emissions, water based wastes, solid wastes and by-products are the system boundaries in the case study. [7]

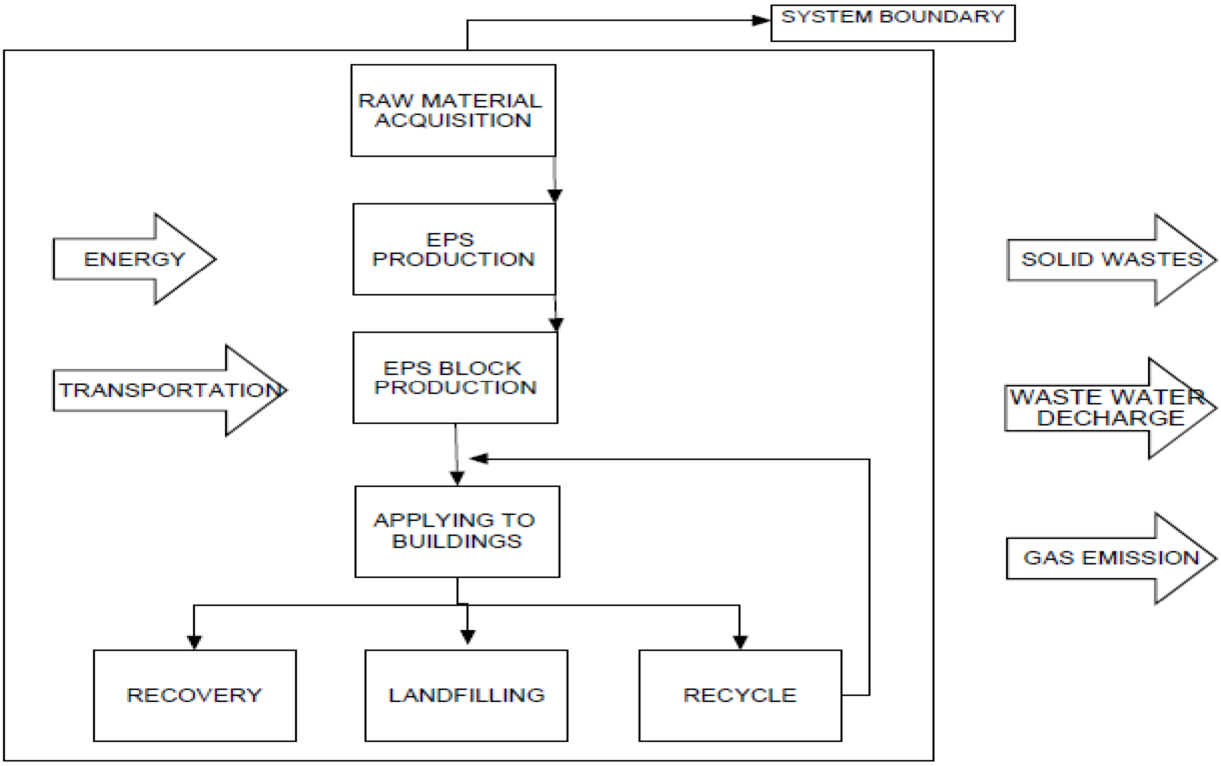

Figure 5: System Boundary for cradle to grave life cycle analysis of EPS

In the case study, mass, energy and exergy balances in unit operations which constitute system boundaries are taken into account when distributing input and output flows to unit operations.

The data quality requirements cover the time, geography and technology variables of the data to be collected for the EPS product. The data obtained and used in the sample study;

- are data that can be calculated and calculated by experience.
- 90% of the primary data and 10% of the literature were obtained and calculated from the literature and databases.
- the data in the last 3 years is current and is currently being implemented.
- are common data in our country and internationally.
- is related to EPS products produced on an international scale and with traditional technology. Secondary data from literature or databases are valid data for current technology.
- represents the system precisely
- Consistent and repeatable.
- Data gaps are filled with database and experience based estimates. [7]

Inventory and Impact Assessment

Results of inventory of this study have been expected to be detailed and long, its mean that is very difficult to evaluate as a short and meaningful. Life cycle impact assessment (LCIA) gives us the opportunity for evaluation of the emissions inventory. LCIA is defined in ISO 14044 Section 3.4 as the "phase of life cycle assessment aimed at understanding and evaluating the magnitude and significance of the potential environmental impacts for a product system throughout the life cycle of the product." In the LCIA phase, the inventory of emissions is firstly classified into categories for impacts on human health or the environment. Each impact category, the emissions are then normalized using characterization factors that give the impact of each substance related to a reference substance. [8,9]

The LCI and LCIA results categories and methods used in this study are given in Table 1. This study includes regional and local impact categories.

Some life cycle inventory (LCI) results:

- Energy demand: this method is not an impact assessment, but it is a total inventory of all kind of energy used for processing , transportation , and feedstock . Energy is also categorized by individual fuel types.
- Solid waste is evaluated as a total inventory values dealing with this category.
- Water consumption is evaluated as a total inventory values dealing with this category **[6]**

Table 1: Summary of LCI/LCIA Impact Categories [6]

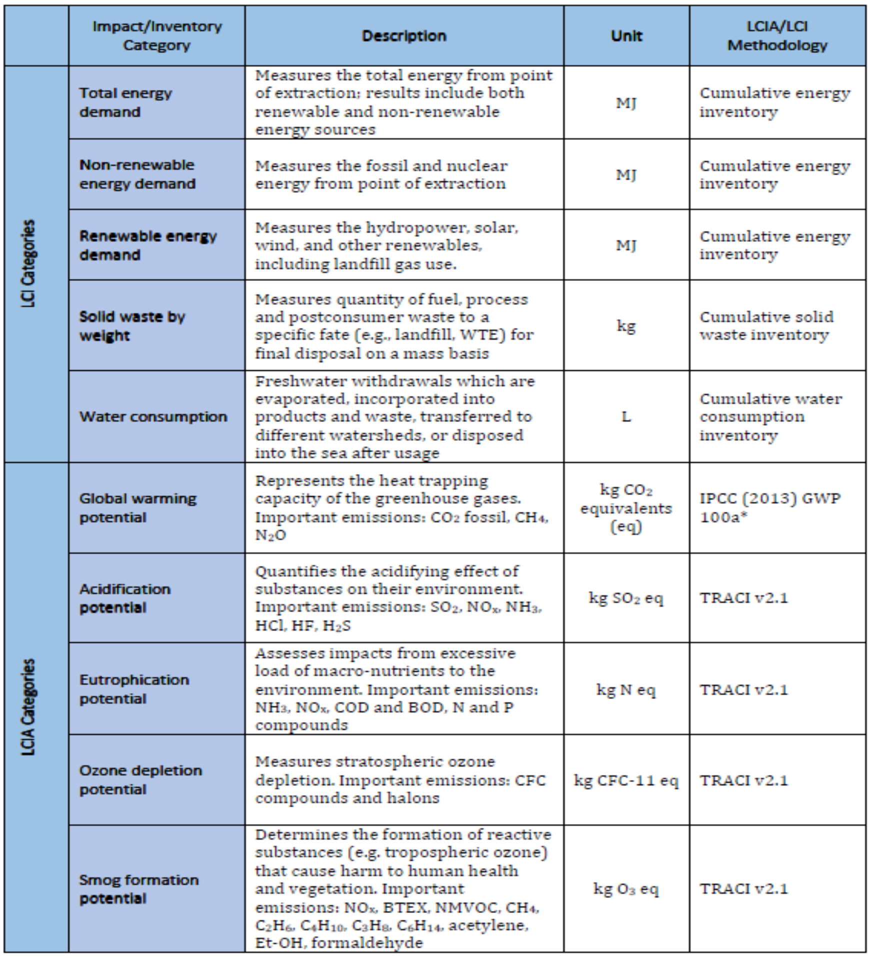

	Impact/Inventory Category	Description	Unit	LCIA/LCI Methodology
LCI Categories	Total energy demand	Measures the total energy from point of extraction; results include both renewable and non-renewable energy sources	MJ	Cumulative energy inventory
	Non-renewable energy demand	Measures the fossil and nuclear energy from point of extraction	MJ	Cumulative energy inventory
	Renewable energy demand	Measures the hydropower, solar, wind, and other renewables, including landfill gas use.	MJ	Cumulative energy inventory
	Solid waste by weight	Measures quantity of fuel, process and postconsumer waste to a specific fate (e.g., landfill, WTE) for final disposal on a mass basis	kg	Cumulative solid waste inventory
	Water consumption	Freshwater withdrawals which are evaporated, incorporated into products and waste, transferred to different watersheds, or disposed into the sea after usage	L	Cumulative water consumption inventory
LCIA Categories	Global warming potential	Represents the heat trapping capacity of the greenhouse gases. Important emissions: CO_2 fossil, CH_4, N_2O	kg CO_2 equivalents (eq)	IPCC (2013) GWP 100a*
	Acidification potential	Quantifies the acidifying effect of substances on their environment. Important emissions: SO_2, NO_x, NH_3, HCl, HF, H_2S	kg SO_2 eq	TRACI v2.1
	Eutrophication potential	Assesses impacts from excessive load of macro-nutrients to the environment. Important emissions: NH_3, NO_x, COD and BOD, N and P compounds	kg N eq	TRACI v2.1
	Ozone depletion potential	Measures stratospheric ozone depletion. Important emissions: CFC compounds and halons	kg CFC-11 eq	TRACI v2.1
	Smog formation potential	Determines the formation of reactive substances (e.g. tropospheric ozone) that cause harm to human health and vegetation. Important emissions: NO_x, BTEX, NMVOC, CH_4, C_2H_6, C_4H_{10}, C_3H_8, C_6H_{14}, acetylene, Et-OH, formaldehyde	kg O_3 eq	TRACI v2.1

Interpretation of Result

The last phase of life cycle assessment is life cycle interpretation. Life cycle interpretations include LCIA data composed from LCI and these data has become a basis of decision making related to goal and scope definitions. So, life cycle analysis starts with goal and scope definition and completes with trusted data interpretation.

CONCLUSIONS

In this study, in general, the data from raw material production to recycling are evaluated in detail. Goals and scopes were identified, functional units were defined and some assumptions were made for life cycle analysis. Inventory analysis has started and the most comprehensive part of this study is this section. The data obtained as a result of inventory analysis will be used in the calculation of environmental impact by using databases within the framework of assumptions. Subsequently, these impacts will be reduced to a single dimension by a common impact factor, and the part with the most environmental impact will be determined in this way. Determined environmental impacts will be evaluated and changes will be made on these points. After this evaluation, the points that need to be changed or improved on the system will be determined and necessary actions will be taken. After the actions to be taken, life cycle environmental impact analysis will be performed again and it will be determined whether there is a decrease in environmental impacts. In previous studies, the life cycle analysis of EPS raw material styrene monomer and packaging materials obtained from EPS were performed. It was seen that the most environmental impact was caused by exergy losses during the production of Styrene Monomer. On the other hand, the most significant environmental impact in EPS packaging is due to the steam and energy consumption in the injection part. Compared to styrene monomer production, the environmental impact in packaging production is lower.

However environmental impact is expected to be highest in EPS polymerization process due to energy losses. In this process, the reactor is heated from 60 ° C to 90 ° C (2 hours) to initiate the polymerization reaction, after which the reaction is cooled for 4 hours to maintain the reactor at constant temperature (exothermic reaction), when the reaction is complete, the reactor is heated to 120 ° C for pentane diffusion. It is allowed to cure at this temperature for 3 hours. After curing, the reactor is cooled to 30 ° C in 3 hours to remove the product from the reactor. Environmental impact analysis is not yet clear, because inventory analysis is in progress. As a result, this study will show us how we can reduce the environmental impact of the EPS production system, especially losses in the polymerization reaction and curing section, and what changes we need to make to reduce certain environmental impacts.

REFERANCES

[1] EUMEPS, (2002), EPS The Environmental Truth – Results of the Life cycle Assessment, *International/non-profit association*, Belgium

[2] C. Çamur, (2010), Environmental Evaluation of Thermal Insulation Materials by Life Cycle Assessment Methodology, *Gazi University Institute of Science and Technology (MSc. Thesis)* , Turkey

[3] E. Alkaya, M. Böğürcü and F. Ulutaş, (2012), Life Cycle Analysis and Implementations for Insulation Materials, *Journal of Environmental, Science and Technology, Version:3 , Volume:4 Page: 261-274*, Turkey

[4] K.F. Çetintaş and A.Z. Yılmaz, (2017), A New Approach for Determining Thermal Insulation Material and Optimum Insulation Thickness for Housing Buildings, *13th National Installation Engineering Congress*, Izmir-Turkey

[5] C. Ingrao, A. LoGiudice, J. Bacenetti, A. M. Khaneghah, A. Sant'Ana, R. Rana and V. Siracus, (2015), Foamy Polystyrene Trays for Fresh-meat Packaging: Life-Cycle Inventory Data Collection and Environmental Impact Assessment, *Book of Food Research International, Volume 76, Part:3, Pages: 418-426*, UK

[6] EPS Industry Alliance, EPS Life Cycle Analysis, http://epsindustry.org/eps-sustainability/life-cycle-analysis, USA

[7] The European Manufacturers of Expanded Polystyrene (EUMEPS) association-Packaging section, (2011), Life Cycle Assessment of the Industrial Use of Expanded Polystyrene Packaging in Europe Case Study: Comparison of Three Fishbox solutions, *EUMEPS – Comparative LCA of fishbox packaging solutions - report-,*France

[8] British Standart Institute, (2018), Environmental management - Life cycle assessment - Requirements and guidelines, *BSI Standards Publication*, UK

[9] Franklin Associates, A Division of ERG, (2016), Cradle to Gate Life Cycle Analysis of an Expanded Polystyrene Resin, *EPS Industry Alliance-Final Report,* USA

ORCID

Onur ULUDAĞ http://orcid.org/ 0000-0003-1080-4128